Amélioration de l'aide à la décision dans la gestion de la biocorrosion des systèmes d'injection d'eau de l'industrie du gaz et du pétrole

Marko Stipaničev

THÈSE

En vue de l'obtention du

DOCTORAT DE L'UNIVERSITÉ DE TOULOUSE

Délivré par :
Institut National Polytechnique de Toulouse (INP Toulouse)

Discipline ou spécialité :

Génie des procédés et de l'environnement

Présentée et soutenue par :
Marko STIPANIČEV

le : mardi 27 août 2013

Titre :

Improved decision support within biocorrosion management
for Oil & Gas water injection systems

Ecole doctorale :
Mécanique, Energétique, Génie civil et Procédés (MEGeP)

Unité de recherche :
Laboratoire de Génie Chimique

Directeur(s) de Thèse :
Régine Basséguy

Rapporteurs :

Sanja Martinez
José Moura

Membre(s) du jury :
Théodore Tzedakis, Professeur, LGC - Université Toulouse III, Président du jury
Sanja Martinez, Professeur, Université de Zagreb, Rapporteur
José Moura, Professeur, Université Nova de Lisbonne, Rapporteur
Damien Féron, Directeur de Recherche CEA, Saclay, Examinateur
Régine Basséguy, Directeur de Recherche au LGC, CNRS- INP Toulouse, Examinateur
Kristian Heen, Ingénieur supérieur Det Norske Veritas, Examinateur

Acknowledgments

Working on Ph.D. and being a member of a BIOCOR ITN has been a unique and quite often overwhelming experience. It is hard to say whether it has been grappling with the topic itself, which has been a real challenging experience, or grappling with how to write papers, make presentations, work on international level, changing flights, stay up until the birds start singing, stay in focus...In any case I am indebted to many extraordinary individuals for enabling me to be in this position, typing last paragraph of my Ph.D. thesis. Not just that, at the same time they made time and work during Ph.D. project an unforgettable roller-coaster ride.

Thereby, I would like to express my gratitude to all the people who contributed in some way to the work described in this thesis.

First and foremost, I thank my academic advisor, Dr. Régine Basséguy, for accepting me as her apprentice, patient handling with my energetic character, making me better scientist and person. I also owe a sincere gratitude to my industrial advisor Dr. Florin Turcu, for guiding me all along this project, for being a teacher and a friend and for unreserved support. During my tenure, both of them, contributed to a rewarding research experience by giving me intellectual freedom in my work, engaging me in new ideas, supporting execution of challenging concepts, and demanding a high quality of work in all my endeavors. I want to thank them for their advice and teachings; their careful revisions of my essays have honed my research and organizational skills and made my writing a little less amateurish. To work with both of you has been a real pleasure and honor to me.

In addition, I have been very privileged to get to know and to work with many other great individuals who became friends over the last two and half years. I learned a lot from all of you about different aspects of life, research, work…You have helped me to develop my own way how to tackle new challenges and how to turn them in my benefit.

I would also like to thank to Dr. Karine Drønen and all the members of olje mikrobiologi scientific group at UiB for opening their laboratory to me and providing basic tools and fundamental knowledge I have been lacking. I want to thank them for always welcoming me with a simile on their face. You made my life easier.

Most of the results described in this thesis were accomplished with the help and support of fellow BIOCOR-mates and collaborators. I owe a debt of gratitude to all the members of BIOCOR ITN. I am awarded that I had a chance to work with the group of such knowledgeably rich and at the same time kind people. I want to thank all of them for helping me to develop intellectually as well as personally in a better individual.

I would like to thank Øystein Birketveit for his interest in my work and general support during this research project. His help and advice have helped me to keep on track and work at a smooth pace, as well as to develop different skills.
Moreover, I want to thank to Professor Iwona B. Beech for being stimulating and supporting at any given moment, for opening new horizons and being herself.
I was lucky enough to had opportunity to discuss with and learn a lot form Dr. Jan Sunner. Thank you very much for all your support.
I am very grateful to Professor Jose Moura for welcoming me each time in Lisbon and UNL laboratory. I am grateful for all your support and kind words that made me keep going on. You made me feel as home in Lisbon.
I would like to thank to Dr. Marie Libert and Marta Schutz for always being accessible and helpful.
Many thanks go to Dr. Renate Killian and Dr. Elmar Schweitzer. It was my pleasure to cooperate with both of them. Thank you for all your support and help.
I am very grateful to all people from LGC in Toulouse for welcoming me in their labs and supporting me during the time I spend with them.
For all nice moment and work conducted during my stay in Aix en Provence I am very grateful to all the members of EcoGeoSafe, especially to Loic Esnault.
I want to thank to Anne Karin Nyhaug and Endy Spriet from Molecular Imaging Center in Bergen for helping me with microscopically analyses.
My deepest gratitude and thanks goes to my colleagues from Det Norske Veritas for supporting me since the first day of my arrival to Norway and for teaching me how to work in industry. I want to thank them for transferring their knowledge, experience and skills to me during this project. Not less important, thank you for giving me advises how to handle with darkness and rain.

Especially I want to thank to my partners in crime, Leonardo Dall'Agnol, Agata Wikiel, Omar Rosas and Magdalena Sztyler, with whom I shared sweet and bitter moments of beautiful research work. Thank you for your friendship, love and unyielding support.

I am indebted to my friends, the new ones and the old ones, who have helped me to overcome hard moments, laughed with me, and made past few years an enjoyable and stimulating experience.

At the end, I would like to thank my family, especially to my parents and my brothers for their infinite support at any given moment and in any given situation.

Funding was received from the European Community's Seventh Framework Programme (FP7/2007-2013).

Improved decision support within biocorrosion management for Oil & Gas water injection systems

Abstract: The objective of this work, achieved in the framework of the BIOCOR European Network, has been to provide the operators of Sea-Water Injection System (SWIS) with improved decision support. The implication of biological component on carbon steel corrosion was explored as well as the possible synergy with other elements (mechanical stress, material properties…). This work showed that biogenic sulphide production, a corrosion threat for steel, can have different origins in seawater. The production rate can determine kinetics and morphology of corrosion attack, which might be governed by the type of microorganisms present. The key parameters are the availability of electron acceptors and the surrounding environment temperature. Sulfate-Reducing Bacteria (SRB) exhibit more vigorous attack compared to sulfidogenic bacteria or genera *Clostridium*, both found in the studied SWIS. Microbial activity also affects the mineralization process naturally occurring on carbon steel surface leading to architectures composed of mixed iron (II) and (III) minerals such as iron sulfides, magnetite, iron oxyhydroxides, chukanovite and green rust (sulfated or carbonated) as well as calcareous deposits. Inner layers of these structures could possibly provide an anaerobic habitat for SRBs, where they can flourish by using sulfate from GR(SO_4^{2-}) as a terminal electron acceptor for their dissimilatory respiration. This enables continuous degradation of steel. Finally, significance of material microstructure and impact of mechanical stress on corrosion processes was also recognized. Grain boundaries and inclusions are playing a role during the initial stage of corrosion attack. This impact can diminish during the immersion time. An elevated bacterial activity coupled with mechanical stress leads to an increase of material deterioration. However, the mechanisms are not different from those usually observed for unstressed steel. Moreover, sulfidogenic microbial activity does not seem to lead to a failure mechanism related to Stress Corrosion Cracking (SCC). In conclusion, the outcomes indicate the possible situations, which may (or may not) lead to breach the safe operating window for a given SWIS.

Keywords: Seawater, Injection System, Microorganisms, Corrosion, Carbon steel, Stress

Amélioration de l'aide à la décision dans la gestion de la biocorrosion des systèmes d'injection d'eau de l'industrie du gaz et du pétrole

Résumé: L'objectif de ce projet, réalisé dans le cadre du réseau BIOCOR, est de fournir aux opérateurs intervenant dans les systèmes d'injection d'eau, un support amélioré d'aide à la décision. L'implication de composants biologiques dans la corrosion de l'acier au carbone ainsi que les synergies potentielles avec d'autres éléments (contrainte mécanique, propriétés intrinsèques du matériau…) ont été étudiées. Les travaux ont montré que la production du sulfure (une réelle menace pour l'acier) par voie biologique avait différentes origines dans l'eau de mer, les différents taux de production pouvant déterminer diverses cinétiques et morphologies de la corrosion. Les paramètres clé sont la disponibilité des accepteurs d'électrons et la température du milieu environnant. Les bactéries sulfato-réductrices (BSR) sont responsables d'attaques plus sévères que les bactéries sulfidogéniques ou du genre *Clostridium*, deux groupes identifiés dans le système étudié. L'activité microbienne affecte également les processus de minéralisation qui ont lieu naturellement à la surface de l'acier doux, conduisant à des architectures composées de minéraux à base de fer II et III, comme le sulfure de fer, la magnétite, les oxy-hydroxydes de fer, la chukanovite et la rouille verte (sulfatée ou carbonatée) ainsi que des dépôts calcaires. Les couches internes de ces structures peuvent constituer un habitat favorable, dans lequel les BSR peuvent se développer en utilisant le sulfate de la rouille verte sulfatée comme accepteur terminal d'électrons pour leur respiration dissimilatrice. Ce processus conduit à la dégradation continue de l'acier. Enfin, l'influence de la microstructure du matériau et l'impact du stress mécanique sur la biocorrosion ont été identifiés : les joints de grains et les inclusions jouent un rôle important dans les premières étapes de la corrosion, qui s'estompe avec le temps d'immersion. Un taux élevé de bactéries couplé à une contrainte mécanique conduit à une augmentation de la détérioration sans toutefois révéler des mécanismes nouveaux par rapport à l'absence de contrainte. De plus, l'activité sulfidogénique des bactéries ne semble pas conduire aux mécanismes de rupture par fissuration (Stress Corrosion Cracking). En conclusion, les résultats de ce travail indiquent les situations qui pourraient (ou non) conduire à s'écarter de la 'fenêtre de sécurité' pour un système donné.

Mots clé: Eau de mer, Système d'injection d'eau, Micro-organismes, Corrosion, contrainte mécanique, acier au carbone.

Za Likija

i Anteicu,

Moju motivaciju

Table of Content

Chapter I

Chapter II

List of Figures and Tables

List of Figures:

Chapter I:

Chapter II:

Chapter III

Introduction:

Article I:

Supplementary information:

Chapter IV

Introduction:

Article II:

List of Tables:

Chapter II

Chapter III

Article I:

Chapter IV

Article II:

Article III:

Chapter V

Article IV:

List of abbreviations

$1/R_p$ – Instantaneous corrosion rate

A – Area

A – Fracture percentage elongation

AC – Alternating Current

AFM – Atomic Force Microscopy

APB – Acid Producing Bacteria

ASAP – As Soon As Possible

ASM – American Society for Metals

ASW – Artificial Sea Water

B – Tafel constant

BCFC – Biofilms removed from steel specimens exposed in the control flow cell (BCFC)

BEFC – Biofilms removed from steel specimens exposed in the experimental flow cell

BFE – The biofilm field enrichment in SRB/2 medium

BHN – Brinell Hardness Number

BLAST – Basic Local Alignment Search Tool

bp – base pair

BP – British Petroleum

BVI – Bioreactor vessel inoculum consisting of pooled re-enrichments as described

C – Capacitance

C_{dl} – Double Layer Capacitance

CE – Counter Electrode

CEA – Commissariat à l'énergie Atomique

CF2 – Casualty Factor 2

CF3 – Casualty Factor 3

CPE – Constant Phase Element

CR – Corrosion Rate

CTRL1 system – specimen immersed in 2.0 % NaCl modified-VMNI (autoclaved – no bacteria)

CTRL2 system – specimen immersed in DSMZ 826 GEOBACTER media (autoclaved – no bacteria)

D – Intender diameter

D_1 – Indentation diameter

DAL system – specimen immersed in 2.0 % NaCl modified-VMNI inoculated with D. alaskensis AL1 culture

DAPI – Dye 6-Diamidino-2-Phenylindole

DC – Direct Current

DDS system – specimen immersed in 3.5 % NaCl modified-VMNI inoculated with D. desulfuricans ATCC 27774 culture

DGGE – Denaturing Gradient Gel Electrophoresis

DNA – Deoxyribonucleic acid

DNV – Det Norske Veritas

DSMZ – Deutsche Sammlung von Mikroorganismen und Zellkulturen

E – Modulus of elasticity

E – Potential

EC – Electric Circuit

ECN – Electrochemical Current Noise

E_{corr} – Corrosion potential

EDX – Energy Dispersive X-ray Spectroscopy

EFM – Electrochemical Frequency Modulation

EIS – Electrochemical Impedance Spectroscopy

EN – Electrochemical Noise

EPN – Electrochemical Potential Noise

EPS – Extracellular Polymer Substance

ER – Electrical Resistance

EW – Equivalent Weight

F – Force

f – Frequency

FCT-UNL – Departamento de Química Faculdade de Ciências e Tecnologia Universidade Nova de Lisboa

FFT – Fast Fourier Transformations

FISH – Fluorescence In-Situ Hybridization

G – Gibbs energy

GBS system – specimen immersed in DSMZ 826 GEOBACTER media inoculated with Geobacter sulfurreducens ATCC 51573 culture

HF – High Frequency

I – Current

I_{corr} – Corrosion current

ICP-AES – Inductively Coupled Plasma-Atomic Emission Spectroscopy

IMS – Integrity Management System

IP1 – Individual Project 1

IPRE – Inconel Pseudo-Reference Electrodes

IRB – Iron Reducing Bacteria

I_{rms} – root-mean-square current value

ISO – International standards organization

IZI – Impedance

K – Constant that defines the units for the corrosion rate

KISCC – Plane strain stress intensity factor

L – Final gauge length

LB – Lysogeny broth

LEIS – Localized Electrochemical Impedance Spectroscopy

LF – low frequency

LGC – Laboratoire de Genie Chimique

LI – Localization Index

L_o – Initial gauge length

LPR – Linear Polarization Resistance

$m_{3,ECN}$ – ECN third central moment

$m_{4,ECN}$ – ECN fourth central moment

MIC – Microbiologically Influenced Corrosion

MOB – Metal Oxidizing Bacteria

MPN – Most Probable Number

MRB – Metal Reducing Bacteria

η – Overpotential

NDT – Non-Destructive Testing

nNRB – heterotrophic Nitrate-Reducing Bacteria

NR-SOB – Nitrate-Reducing Sulfide-Oxidizing Bacteria

O&G – Oil and Gas

OCP – Open Circuit Potential

P&ID – Piping and Instrumentation Diagrams

PC – Personal Computer

PCR – Polymerase Chain Reaction

PFA – Perfluoroalkoxy

PG system – specimen immersed in North Sea seawater inoculated with pigging debris isolate and being under tensile stress

PP – Polypropylene

PRE – Pseudo-Reference Electrode

PVC – Polyvinyl Chloride

PWIS – Produced Water Injection System

Q – 1st parameter of the constant phase element impedance

qPCR – quantitative Polymerase Chain Reaction

R – gas constant

Re – Reynolds number

R_{eH} – Upper yield strength

R_{eL} – Lower yield strength

R_m – Tensile strength

rms – root mean square

R_n – Electrochemical noise resistance

RNA – Ribonucleic acid

R_p – Polarization resistance

$Rp_{0.2}$ and Rp_1 – Proof strength (plastic extension)

R_s – Resistance of the solution

RSGP – Reverse Sample Genome Probing

S – Code name of oil and gas offshore installation located in North Sea

SCC – Stress Corrosion Cracking

SCE – Saturated Calomel Electrode

SEM – Scanning Electron Microscopy

SOC – Super optimal broth with catabolite repression

Sp – Complete analysed spectrum for particular surface area

SP – Sampling Port

SPP – Sulfate Producing Prokaryotes

SRA – Sulfate Reducing Archaea

SRP – Sulfate Reducing Prokaryotes

SSCC – Sulfide Stress Corrosion Cracking

SW – As-received North Sea seawater

SW system – specimen immersed in North Sea water (filter sterilized – no bacteria)

List of abbreviations

SWIS – Sea-Water Injection System

T – Temperature

TOC – Total Organic Carbon

UK – United Kingdom

UoP – University of Portsmouth

USA – United States of America

UV – Ultra Violent

v – Sweeping rate

v – Velocity

W- Warburg element

WE – Working Electrode

WEFC – Water samples from the experimental flow cell (WEFC)

WIS – Water Injection system

wt % - weight fractions

XPS – X-ray Photoelectron Spectroscopy

XRD – X-ray Diffraction

z – Number of electrons

Z – Percentage reduction of area

Z' – Real part of the impedance

Z'' – Imaginary part of the impedance

ZRA – Zero Resistance Ammeter

Z_W – Warburg impedance

α – 2nd parameter of the constant phase element impedance

α – is the factor of symmetry or charge transfer coefficient

β_a – Anodic Tafel slopes angles

β_c – Cathodic Tafel slopes angles

ΔL – Change in gauge length measured with extensometer

ε – Engineering Strain

ρ – Density

σ – Warburg constant

σ – Engineering stress

σ_{ECN} – ECN standard deviation

i_{corr} – *corrosion current*

ω – radial frequency

Chapter I

General introduction

I.1. Introduction

Currently, the involvement of microorganisms in corrosion processes is receiving ever more attention. Their impact on the operational capacity and life cycle of various assets and infrastructures in the Oil and Gas (O&G) industry is increasingly coming into focus. Therefore, building multidisciplinary expertise related to Microbiologically Influenced Corrosion (MIC) in order to manage problems in O&G area is of high importance for operators and vendors.

The objective of this work, achieved in the framework of the BIOCOR European Network, has been to provide the operators of Sea-Water Injection System (SWIS) with improved decision support. Moreover, guiding though all along project has been to generate more knowledge about MIC in offshore O&G systems. This chapter describes the main notions and bibliography to attain these objectives and also the methodology that will be described below.

I.2. The offshore water injection system and integrity management

Produced water, aquifer water, seawater or a mixture of these is frequently injected into wells to achieve additional extraction of oil. For an offshore installation (Fig. I.1.A) and its associated field (Fig. I.1.B), the Water Injection System (WIS) plays a significant role. The main function of the WIS is to create and maintain reservoir pressure by injecting water either directly into the well or via another connected well site. The principle is simple and is based on the balance between gravimetrical and buoyant forces; water floods the well, forcing oil to the top since oil is less dense than water.

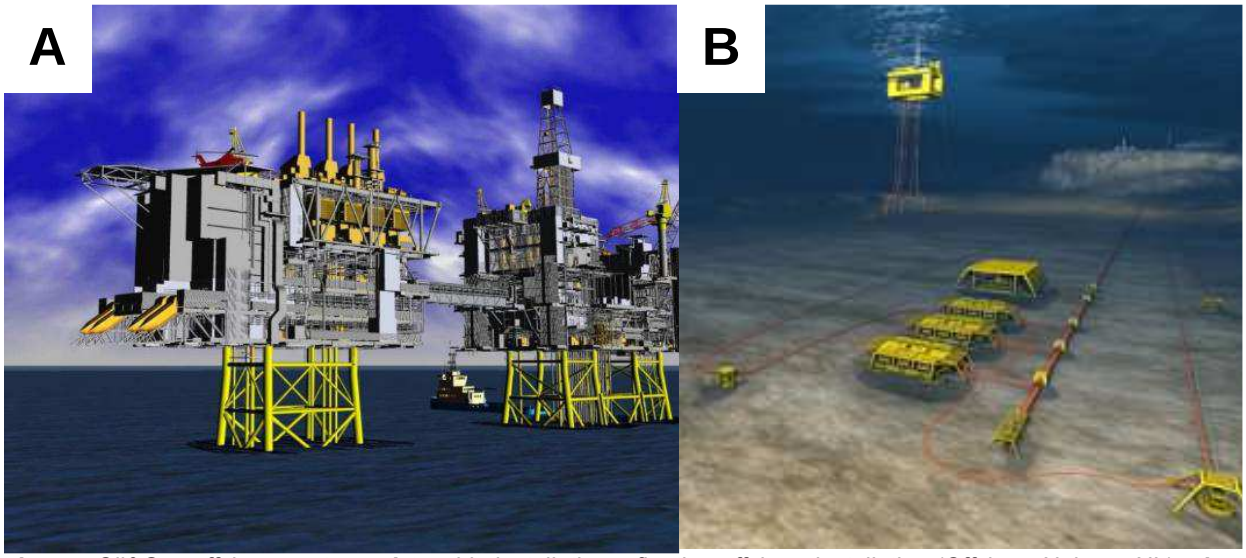

Fig. I.1. Oil&Gas offshore system: **A)** topside installation – floating offshore installation (Offshore Neiuws. NL); **B)** downside – FMC Subsea Water Injection and Compression of well associated to topside installation.

Any disruptions in the water injection process can adversely affect production as well as the integrity of not only the WIS itself but also those systems that receive water from it. Therefore WIS management is a crucial element in oil extraction and production. The establishment of what is termed a "*safe operating window*" is the main goal of the Integrity Management System (IMS). The parameters of the safe operating window are defined via risk assessment based on analyses of data acquired from condition monitoring of the WIS.

On-site, the limits, set in the safe operating window, are part of the "*decision support*" offered to the operators of WIS. Decision support is continually improved through an iterative process facilitated by condition monitoring and updated risk assessment.

The main cause of crude oil production disruption on installations operating by means of water injection is in fact the integrity degradation of the WIS. WISs are mostly constructed out of ferrous alloys e.g. construction carbon steels such as S235JR or St-37. These steels are subject to corrosion if the loads (mechanical stress, biological activity, etc.) and the conditions that are favorable for corrosion development are present. Therefore, in order to establish a suitable safe operation window,

one needs to assess environment, material and different loads (mechanical stress, biological activity, etc.).

As mentioned before, seawater is one of the typical medium used for pressuring wells. Seawater can be very corrosive to carbon steel leading to internal corrosion of Sea-Water Injection Systems (SWIS) and possible failure.

The presence of bacteria increases the probability of corrosion failure. Integrity degradation of WIS is often a consequence of anaerobic corrosion processes occurring due to different loads. Additionally, when combined with certain operating conditions (low flow rates and therefore low hydrodynamic drag) or with high material stresses (i.e. mechanical stress) Microbially Influenced Corrosion (MIC) becomes the most likely cause for system failure.

In order to improve decision support for SWIS operators, it is necessary to better understand the instantaneous interface interactions between bacteria and carbon steels as well as the behavior of carbon steels after long exposure periods in presence of bacteria, as typically experienced by SWIS. Moreover, SWIS simulations with environments containing bacteria on mechanically stressed steel samples could provide a better understanding of the nature of certain failure mechanisms, such as stress corrosion cracking.

I.3. Corrosion of ferrous alloys

Degradation of ferrous alloys is defined as a result of chemical, electrochemical and/or mechanical interactions of a specific ferrous alloy with its surrounding environment that results in material loss. Furthermore, corrosion of ferrous alloys, such as carbon steels, in aqueous environments possesses an electrochemical nature, involving two or more electrochemical reactions taking place on the ferrous alloy surface. The corrosion process of ferrous alloys involves the transfer of iron or some other alloying metals (chromium for example) from a metallic state into a non-metallic or ionic state (I.1).

$$Me^{\circ} \rightarrow Me^{n+} + ne^{-} \qquad (I.1)$$

The products of a corrosion reaction can be dissolved species or solid corrosion products; in either case, the energy of the system is lowered as the metal converts to a lower-energy form. The change in the energy of the system is the driving force for the corrosion process, which behaves according to the thermodynamics laws.

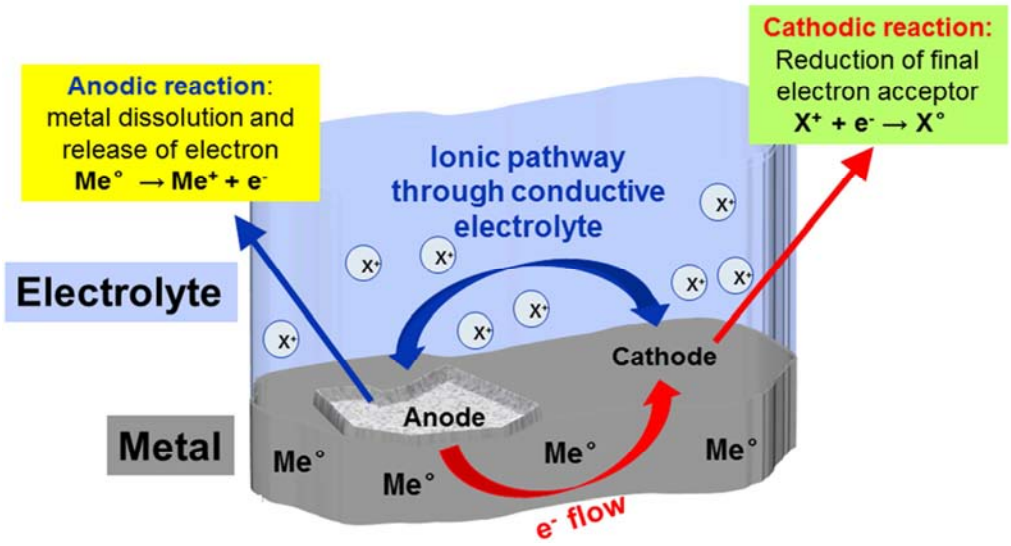

Fig. I.2. Electrochemical corrosion process – formation of a corrosion cell

The precondition for electrochemical corrosion reaction is the simultaneous presence of both anodic and cathodic sites, where anodic and cathodic reactions take place (Fig. II.2). In order to enable electrochemical reaction, an ionic conduction path through an electrolyte needs to be established between electroactive sites (Fig. II.2). Within the electrochemical corrosion process, electrons are

flowing from a metallic component of the ferrous alloy, through a set of electrochemical redox reactions, to a final electron acceptor, located in proximity of the ferrous alloy surface. The magnitude of electron flow corresponds to the oxidation rate of the metallic component to metal ions (anodic site), equal to the reduction rate of chemical species in contact with the ferrous alloy surface (cathodic site).

Anodic and cathodic sites can be physically separated; however, there must always be an electronic contact between the anode and cathode enabling flow of electrons (requirement of Kirchhoff's circuit laws). The most common structures typically involve close proximity between the anodic and cathodic sites, which results in the formation of a "*corrosion cells*". If the equilibrium between the anodic and cathodic reaction in a corrosion cell is disturbed, an elevated flow of corrosion current is established leading to more enhance metal dissolution. Allocations of the corrosion cells will determine the distribution of material loss across the ferrous alloy surface. An uneven allocation of corrosion cells will result with localized corrosion attacks forming pits that can propagate to crevices, depending on circumstances. Conversely, a homogenous distribution of corrosion cells will result in a uniform material deterioration, i.e. general corrosion.

As previously mentioned, the electrochemical corrosion process comprises of two "*half-reaction*", oxidation and reduction. Oxidation is taking place on the anodic site (anodic reaction half-cell) and reduction on the cathodic site (cathodic reaction half-cell), each featured by specific potential. Anodic and cathodic half-cell regions have to balance their charges, and when charges are in equilibrium a particular potential difference is generated and entitled as the corrosion potential (E_{corr}). At such potential, metal it is corroding freely generating corrosion current (I_{corr}). Corrosion current is defining intensity of corrosion process; hence, it is used to calculate corrosion rates. Overpotential (η) is driving force, an extra energy, which forces the electrode reaction to proceed at a particular rate. It can be produced by differences in the atom binding energies within a metal forming "*composition cells*" e.g. "*galvanic cells*". For example, perlite morphology is filled with miniature carbide structures that with surrounding ferrous phase form galvanic couples. Another source of overpotential can be so formation of so called "*stress cells*"; they may exist in a metal where a portion of the metal's microstructure possesses more stored strain energy compared to the rest of the metal, such as grain boundaries or triple points. Besides irregularities in metal structure external factors can be source of overpotential. For example, product of the system environment such as biological deposits, concentration gradients or galvanic couples (formed as a result of scaling process) can generate driving force sustaining elevated corrosion rate.

In general, metal dissolution will be defined by intensity of the oxidation reaction, and therefore corrosion rate will be determined by the magnitude of anodic current. The rule of electric-neutrality dictates that released electrons in oxidation reaction need to be consumed by cathodic reaction. Consequently, kinetics of corrosion reaction and rate of corrosion will be dependent on the cathodic reaction. In electrochemical corrosion, therefore, no matter the form of the oxidizing agent (molecular oxygen and/or hydrogen protons, depending on environment), the rate of corrosion is in direct correlation with the capability of the oxidizing agent (placed in vicinity of metal surface) to accept electrons released during metal oxidation. Enhanced corrosion is associated with the establishment and promotion of kinetically favored reduction pathways that are directly correlated to an increase of an electrode potential, defined as cathodic depolarization. This change leads to an increase of the potential difference between electrode potential and metallic component redox potential; called overpotential (η), and it is correlated to an increase in corrosion rate.

Which one of cathodic reactions will be dominating in a particular corrosion system is mostly determinated with the thermodynamic and kinetic features of the cathodic reactions. In general, oxygen reduction is thermodynamically favored. On the contrary, hydrogen evolution is kinetically favored. Summarized, hydrogen evolution as a dominating cathodic reaction occurs under anaerobic conditions at any pH, while under aerobic conditions, hydrogen evolution will take place only at a low pH. In addition, environment plays a crucial role in determining the prevailing cathodic reaction. Logically, in oxygen depleted environments the role of oxygen as a possible oxidizing agent is excluded.

As mentioned previously, material loss of ferrous alloy can be a result of an action of mechanical forces the surface, such as sheer stress in the case of flowing systems. This type of corrosion is defined as "erosion corrosion". Mechanical action can be a result of impinging liquid, particles suspended in flowing liquid, bubbles, cavitation, etc. The mechanism can be described as follows: on the surface, the mechanical degradation by an erosion process of the material or of the protective (or

passive) oxide or of a layer of some other corrosion products frequently leads to enhance corrosion of the material. In this destructive process the surface chemistry can play a role due to mechano-chemical effects.

Moreover, some other types of mechanical stress can lead to serious corrosion failures, such as Stress Corrosion Cracking (SCC). SCC is the growth of cracks in a corrosive environment as a consequence of aggressive environment and tensile stress, which is often quite below level of material yield and tensile strength. Once a crack is initiated, further crack propagation is caused by a synergetic effect between corrosion and tensile stress.

I.4. Microbially Influenced Corrosion (MIC) of ferrous alloys

Microbially Influenced Corrosion (MIC) is one of the most urgent problems related to the degradation of ferrous alloys, e.g. carbon steels. The economic consequences of the corrosion of iron and its alloys in various industrial sectors, including oil and gas operations, are well documented [Borenshtein *et al*., 1994; Videla, 1996; Heitz *et al*., 1996]. Undisputedly, corrosion causes considerable damage to marine steel infrastructures, such as offshore oil installations and pipeline systems, leading to revenue losses. It has been estimated that nearly 20% of the total corrosion cost is due to MIC, also referred to as biocorrosion [Beech and Sunner, 2004].

The scientific community provides several definitions of microbiologically influenced corrosion; common and emphasized in all definitions is the presence of microorganisms in observed systems where corrosion has occurred. On account of various inputs from different literature [Videla, 1996; Beech and Sunner, 2004], any increased deterioration of metal material due to microbial activity at the metal surface-solution interface is termed MIC.

Occurrence of MIC requires certain favorable conditions [Flemming *et al*., 2000]. Favorable conditions vary from one to another according to the type of microorganisms. Prerequisites for MIC occurrence can be divided into primary and secondary prerequisites. A primary prerequisite for occurrence of MIC obviously is presence of microorganisms. Secondly, in order to be active bacteria need an energy source, a carbon source, an electron donor, an electron acceptor and a conductive medium e.g. water.

From the moment that a ferrous alloy is immersed into a non-sterile solution that supports microbial development, the process of microorganism attachment to material surface is triggered. Planktonic microorganisms become ensconced on the fluid boundary, typically a pipe wall (such as the piping of SWIS) or porous media (such as corrosion product). Attachment of microorganisms leads to formation of biofilms: a structured surface microbial community embedded in an attaching matrix [Madigan *et al*., 2009]. Once cells belonging to microorganisms are attached, they can grow and reproduce, colonizing the surface.

Biofilm formation consists of a sequence of a four steps (Fig. I.3). During the first stage of biofilm formation which commences immediately after the immersion of the ferrous alloy in the solution, a thin film will form on the surface due to deposition of different chemical species (e.g. inorganic ions and organic compound of high molecular mass). At this stage there are still no attached bacteria to the ferrous alloy surface. Nevertheless, the presence of these chemical species at the metal surface can result in electrostatic charges and increase the wettability of the metal surface, promoting bacterial attachment and biofilm development [Videla and Herrera, 2005]. This process is also called "*biofilm conditioning*". Planktonic bacteria actually adhere to this surface film that may have different chemical properties than the non-living surface and/or clean surface [Korber *et al.*, 1995; Marshall *et al*., 1997].

At the second stage, microbial colonization starts with transport of microorganisms form the bulk electrolyte to conditioning layer by diffusive transport due to Brownian motion or by convective transport due to the liquid flow and active movement of motile bacteria near the interface. Microorganisms that reach the surface may or may not attach to it. Initial attachment of microorganisms on a conditioned surface is occurring as a result of electrostatic, van der Waals or simple hydrostatic forces [McCoy, 1987]. At this stage, some bacteria reach the conditioning layer, secret Extracellular Polymer Substances (EPS) and attach to the surface while others may continue to revolve [Marshall, 1988]. This phase is referred to as the "*reversible attachment stage*". During reversible attachment, the rate of surface colonization and the dynamic of the microorganism's attachment are dependent on hydrodynamics. Planktonic microorganisms are transported through

medium to the proximity of the metal surface by diffusion. In flowing systems the diffusion transport is replaced by convective transport.

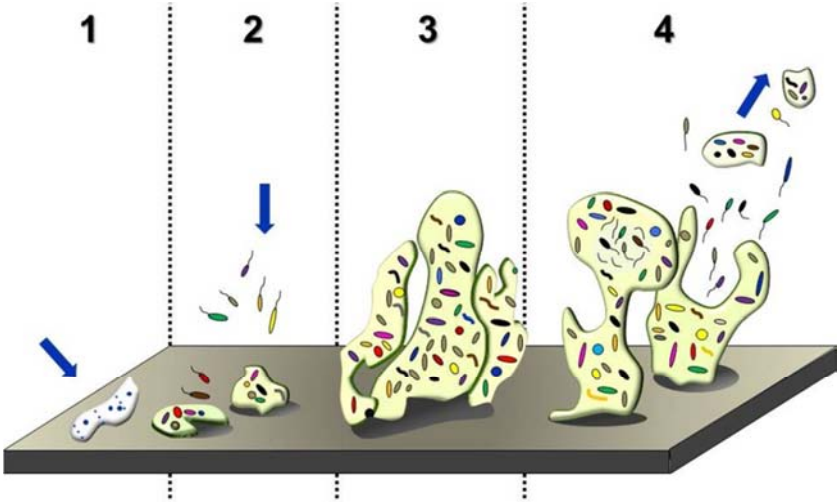

Fig. I.3. Four stages of biofilm formation: (1) Surface conditioning, (2) Reversible attachment, (3) Irreversible attachment, (4) Detachment.

At the third stage, microorganisms use their motility to sustain contact with the surface while searching for a suitable location [Korber *et al*., 1995]. Quantity of EPS on steel surface increases when more microorganisms attach to surface. EPS functions as a "cement" or "glue" that traps microorganisms (bacteria), their metabolic products and all other chemical species (e.g. corrosion products, inorganic precipitates from the bulk medium) within the biofilm. EPS consists of a complex mixture of cell-derived polysaccharides, proteins, lipids and nucleic acids [Wingender *et al*., 1999; Beech and Gaylarde, 1999]. EPS production combined with microbial growth will alter the surface (increases surface irregularity) and propagate biofilm development. This results in increasing available surface area for microorganisms attachment, reducing the influence of fluid sheer stress and increasing convective mass transport in the formed initial layer of biofilm near the steel surface [Bouwer, 1987: Cunningham, 1989]. Moreover, at this phase, called "*irreversible attachment stage*", the process of attachment is becoming irreversible and can be still supported by the influence of surface free energy or hydrophobicity [McCoy, 1987]. The overall result will help to form a fully developed biofilm.

At the fourth and final phase, following further biofilm growth, a certain number of colonies will detach from the formed biofilm, for example due to the influence of sheer stress in flowing systems. Detachment is most likely in the form of clumps. This stage is entitled as a "*detachment stage*".

The formation of a fully developed biofilm will immediately change the electrochemical conditions at the metal surface-solution interface even though the biofilm structure contains more than 95 % of water. From the moment that the biofilm is fully established on a ferrous alloy surface, it behaves as a dynamic system.

Being a member of a biofilm community has plenty of advantages for a microbial cell compared to a solitude life. Biofilm can offer a physical shelter for the cells and protect them from mechanical forces such as sheer stress. Moreover, in biofilms, cells can take advantage of the close physical contact between microbial cells. This provides the possibility for exchange of genetic material such as extracellular DNA (plasmid) via conjugation. Conjugation occurs at a greater rate between cells in biofilms than between planktonic cells [Ehlers and Bouwer, 1999; Hausner and Wuertz, 1999]. Plasmids may encode for resistance to multiple antimicrobial agents, so consequently biofilms could confer resistance to many antimicrobials (biocides). In addition, biofilm allows cells to "communicate" through cell-to-cell chemical signaling otherwise known as "*quorum sensing*". Quorum sensing mediates vast numbers of processes within biofilms. To sum up, biofilms provide an environment that is stimulating and beneficial for the proliferation of cells.

Bacteria and its attributed building structures e.g. biofilms, affect unprotected ferrous alloys in several basic ways [Stott *et al*., 2010]:

1. Direct effect of metabolic products such as organic acids capable of altering pH locally or hydrogen sulfide production leading towards souring corrosion (the corrosion associated with H_2S).
2. Formation of corrosion cells by deposition of cathodic and conductive corrosion products such as ferrous sulfides formed in the presence of sulfidogenic species.
3. Formation of concentration cells, for example: due to local oxygen depletion or due to biofilm attachment.
4. Cathodic depolarization.
5. Etc.

The effect of biofilms on material electrochemical deterioration comes through their influence on the structure of the metal surface-solution interface [Videla and Herrera, 2005]. This modification of the interface and the impact of the metabolic products of its inhabitants are the most common cause of accelerated deterioration of metals due to the presence of microorganisms. As mentioned previously, elevated corrosion rates are correlated with an increase of potential difference between the electrode potential and associated metallic component redox potential. Microorganisms can influence this driving force of the corrosion process in many different ways, such as the previously mentioned cathodic depolarization or the creation of concentration cells by the formation of biofilm on an electrode surface.

For a WIS built out of ferrous alloys such as carbon steels, sulfidogenic species-mediated sulfide corrosion presents a significant threat to system integrity and therefore a great maintenance challenge. The most recognized group of sulfidogenic microorganisms are Sulfate-Reducing Prokaryotes (SRP). Moreover, sulfidogenic and Acid-Producing Bacteria (APB) of the class *Clostridia* are commonly found in marine environments such as SWIS [Alain *et al*., 2002]. Sulfidogenic species are regarded as the main culprits of anaerobic corrosion in seawater systems as the SWIS. The sulfidogenic species-mediated sulfide corrosion of ferrous alloys encompasses both the production of volatile hydrogen sulfide and the formation of different iron sulfide minerals [Costello, 1975] (Fig. II.4).

Iron dissolution occurs through anodic oxidation reaction and releases iron cations into the surrounding environment (II.2):

$$Fe° - 2e^- \rightarrow Fe^{2+} \qquad \text{(II.2)}$$

The global microbial process involves initial production of sulfide, through reduction of compounds such as sulfate. Organic compounds such as acetate and lactate can serve as the reducing agent in these reactions (II.3):

$$CH_3COO^- + SO_4^{2-} \rightarrow S^{2-} + CO_2 + H_2O + HCO_3^- \qquad \text{(II.3).}$$

Some species use molecular hydrogen as a reducing agent under the intermediation of hydrogenase enzyme, as in the case of hydrogen consuming Sulfate-Reducing Bacteria (SRB), which proliferate in oligotrophic conditions (II.4):

$$SO_4^{2-} + 4H_2 \rightarrow S^{2-} + 4H_2O \qquad \text{(II.4).}$$

Moreover, some sulfidogenic species, such as the class of *Clostridia*, can produce sulfide by reducing, sulfur, L-cysteine or as in the example below from thiosulfate via sulfate (II.5):

$$S_2O_3^{2-} + 4H_2O \rightarrow SO_4^{2-} + HS^- + H^+ \qquad \text{(II.5).}$$

Furthermore, sulfide production is followed by the formation of a thin layer of iron sulfide in the presence of low sulfide concentrations, occurring on the ferrous alloy surface where iron is oxidizing (II.6):

$$Fe^{2+} + S^{2-} \rightarrow FeS \qquad \text{(II.6).}$$

If formed layer is homogeneous, it is protective for metal. Formation of iron sulfide protective layers leads to reduced corrosion rates and protection of the ferrous alloy. On the other hand, the balance between ionic species that leads to protective properties of the formed layer is very fragile. Subsequently, any distortions of the system will lead to a local disruption of the layer exposing the ferrous alloy to an aggressive environment. When the iron sulfide layer is cracked, the surrounding iron sulfide is conductive and cathodic towards the exposed ferrous alloy. Therefore, formation of

corrosion cell (galvanic couple) is inevitable and localized dissolution of metal driven by a much larger cathode takes place. Anodic reaction continues to be based on iron dissolution (II.2). However, the cathodic reactions are as follows (II.7, II.8):

$H_2S + e^- \rightarrow HS^- + 1/2H_2$ (II.7);

$HS^- + e^- \rightarrow S^{2-} + 1/2H_2$ (II.8).

Both these reactions are preferable to the reduction of hydrogen protons. Therefore, this type of corrosion mechanism is pH independent.

In addition, released hydrogen from cathodic reaction (II. 7 and II.8) can serve like electron donor for SRBs. When used as reducing power, coupled with sulfate reduction may generate more sulfides. This process is mediated by hydrogenase enzyme. Consequence of this process is continuous self-sustainable cycle of co-dependent chemical reactions: as more hydrogen is released in cathodic reaction, more sulfide will be generated according to above explained hydrogenase catalyzed reaction, then accumulation of more sulfide will lead to higher corrosion producing more hydrogen in cathodic reaction and so on…In the case of WISs where reduction agents are often available in the required quantities (can be organic), the overall result is constantly increasing corrosion.

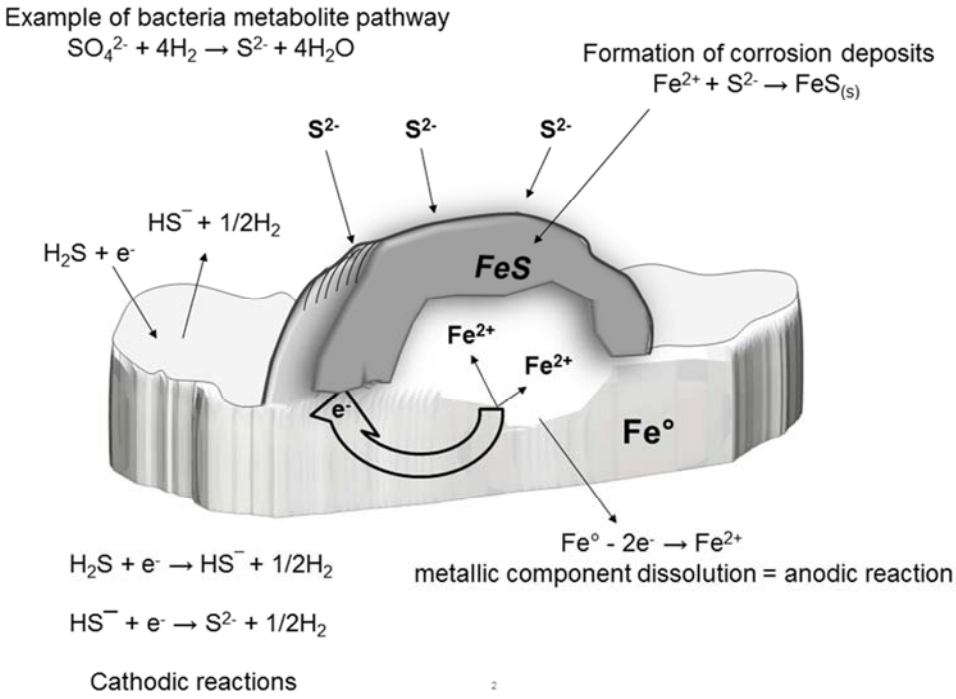

Fig. I.4. Corrosion model of ferrous alloys in presence of sulfidogenic microorganisms [Costello, 1975].

Earlier work involved a cathodic depolarization model of ferrous metals based on the removal from the surface of atomic hydrogen by SRBs and/or hydrogen consumption by intermediation of a hydrogenase enzyme [von Wolzogen Kuhr and van der Vlugt, 1934]. This hypothesis was investigated and can be approved only if the reaction step for forming atomic (and then molecular) hydrogen is not rate-limiting as in the case in presence of weak acid especially when phosphate protonated species are involved [Boopathy and Daniels, 1991; Da Silva et al., 2004; De Silva-Munoz *et al*., 2007]. It was also proved that bacterial hydrogen uptake merely stimulates corrosion in certain anaerobic environments [Cord-Rustwich, 2000]. Furthermore, some researchers [King and Miller, 1971; King *et al*., 1973] revised the theory of SRBs limited role. They were orientated towards the theory suggesting that the depolarizing agent of the hydrogen evolution reaction is likely to be removal of hydrogen atoms linked to ferrous sulfide. Later on, attempts to fully explain the corrosion mechanism in sulfidogenic microorganism corrosion was mainly attributed to the production of corrosive hydrogen sulfide, cathodic depolarization by biological consumption of hydrogen at the cathode and production of EPS [Hamilton, 1985; Yu *et al*., 2002]. However, most reasonable explanations encompasses complete environments incorporating marine biofilms consist of sulfidogenic microorganisms favoring redox reactions that may lead to localized destructive surface events [Castaneda and Benetton, 2008].

The situation gets more complicated when we try to establish a model that would explain corrosion in presence of several different microorganisms, such as in the case of environmental biofilms. Within biofilms retrieved from O&G systems, it is often found that sulfidogenic microorganisms and methanogenic microorganisms coexist in a symbiotic relationship. Sulfidogenic microorganisms are producing hydrogen, carbon dioxide and acetate by fermentation, and methanogens are consuming these compounds, which is a necessary step for fermentation to proceed. In such a relationship, sets of complex interconnected respirational reactions are taking place [Larsen *et al.*, 2010]:

$4Fe^{\circ} + 3H_2S + SO_4^{2-} + 2H^+ \rightarrow 4FeS + 4H_2O$ (II.9);

$4Fe^{\circ} + 4H_2S + CO_2 \rightarrow 4FeS + 2H_2O + CH_4$ (II.10).

These reactions result in the formation of conductive and cathodic iron sulfide and methane, finally leading to metal loss.

Furthermore, aftereffect of biomineralization processes occurring on steel surfaces, the formation of a layer of protective corrosion products can result in the inhibition or suspension of the corrosion processes [Videla *et al.*, 2005].

I.5. Assessment of main factors determining occurrence and scale of MIC in the offshore water injection systems

Generally in corrosion management and specifically in MIC management, there are three features of the SWIS that determine the integrity and the operational capability of it. They can be regarded as an overlapping triangle in formation that defines the contributing effect of each towards the condition of the SWIS and its operational status. These three features are: (a) the environment or the injection medium e.g. seawater, aquifer or produced water and their mixtures, (b) the material, e.g. low carbon steel and (c) the microbiological load (Fig. I.5).

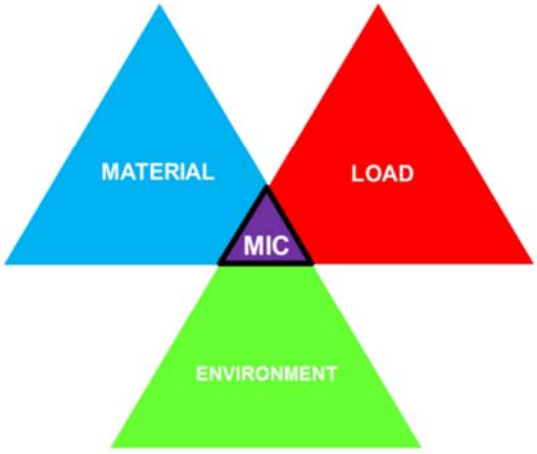

Fig. I.5. Conditions for MIC initiation.

This is in agreement with the definition that indicated the conditions that lead to MIC initiation [Féron *et al.*, 2002] and further development as the concomitance of (a) an aggressive aqueous environment, (b) a construction material selected according to structural demands and (c) microorganisms whose presence is often not taken into consideration.

I.5.1. Microbiological load

The types of microorganisms attributable to MIC include prokaryotes (eubacteria and archaea; organisms without membrane bound structure) and eukaryotes (organisms whose cells contain complex structures enclosed within membranes) [Pace 2006].

Eukaryotes have been associated with MIC, specifically with biofilms found in sewage systems [Cayford *et al.*, 2010]. Up until recently, eukaryotes have not been in the focus of MIC associated with O&G industry. Well-known members of the eukaryotes are algae and fungi. The algae can be found in

SWIS due to their capability to sustain themselves in environments with high salt concentrations and to proliferate in darkness. Thus, algae can flourish in conditions common to the operational conditions typical for SWIS. However, they are not typically found in SWISs and therefore they do not represent a major risk for SWIS. Fungi present a similar level of threat as algae for SWIS, i.e. almost negligible. Fungi generally do not prefer liquid environments but some species can proliferate in water environments. These are mycelium structures, which are an outgrowth of a single cell or spore. Mycelia are immobile and can grow to reach macroscopic dimensions. Their metabolic pathways consist of organic matter uptake and production of organic acids.

Conversely, the main culprits of MIC in all WIS, either SWIS or any other type of WIS are prokaryotes. Typically they are a few micrometers in length. Their shape (examples given in Fig. I.6), their tolerance to oxygen, their metabolic pathways, the temperature range in which they proliferate, their sensitivity to light as well as other features further classifies prokaryotes.

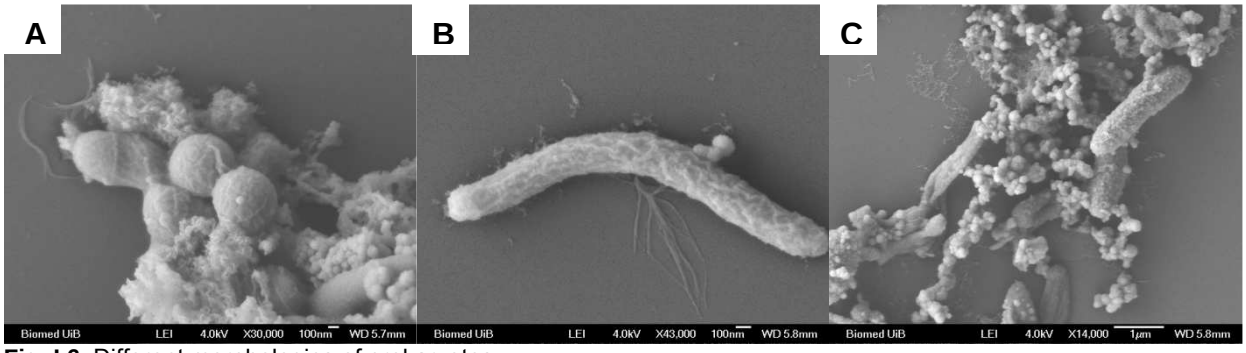

Fig. I.6. Different morphologies of prokaryotes.

WIS's mostly operate with little or no oxygen concentrations that makes them a perfect habitat for anaerobic prokaryotes or prokaryotes that can handle low amounts of oxygen. Moreover, in some systems it is possible to have facultative anaerobic bacteria such as *Marinobacter* sp. strain MB [Sigalevich *et al*., 2000] that can consume low amounts of oxygen present in the system and create preconditions for development of obligative anaerobic bacteria, such as *Desulfovibrio alaskensis* AL1 [Feio *et al*., 1984] in so called "anaerobic niches".

The temperature range in WIS can vary from approximately 20 ℃, found in some SWIS and up to 60-80 ℃, found in some Produced Water Injection Systems (PWIS). This temperature range limits bacteria population present in WI systems to mesophiles (midrange temperature optima) and thermophiles (high temperature optima). However, some bacteria are classified as thermophiles even though their metabolism can be functional at lower temperatures, in a range characteristic for mesophiles.

Bacterial metabolic pathways and products of their metabolism are the most interesting and important for MIC of WIS in O&G industry. According to their reactivity, bacteria can be, on a simplified way, separated into the following:

1. ***Sulfidogenic*** – producing sulfide.

Sulfate-Reducing Archaea (SRA) and Sulfate-Reducing Bacteria (SRB) are well known representatives of phylogenetically diverse Sulfide-Producing Prokaryotes (SPP). Lately, SRA and their roles in MIC occupy more and more attention [Larsen *et al*., 2010]. They are performing dissimilatory reduction of sulfur compounds such as sulfate, sulfite, thiosulfate, polythionate, sulfur or L-cysteine to sulfide, which, by oxidizing molecular hydrogen, forms volatile hydrogen sulfide affecting ferrous metals [Javaherdashti, 2008; Videla, 1998; Szklarska-Smialowska, 1986].

2. ***Methanogenic*** – producing methane.

Methanogenic *Archaea* or Methanogens are the most interesting sub-group of *Archaea*. Methanogenic archaea have repeatedly been associated with MIC of offshore O&G systems [Sulfita *et al*., 2009; Larsen *et al*., 2010]. Methanogens can use the molecular hydrogen as an electron donor accompanied with carbon dioxide as an energy source where the products of reaction will be methane and energy [Boopathy and Daniels, 1991]. By consuming H_2, methanogens perform cathodic depolarization resulting in corrosion, obviously with the restriction described previously: true only if the reaction H^+ +

$e^- \rightarrow H_{ads}$ is not rate-limiting. Moreover, elements in a metal, and in case of ferrous alloys most probably Fe, can be used as an electron donor instead of molecular hydrogen, leading to metal dissolution and material loss.

3. ***Acid Producers*** – producing acids.

Various anaerobic bacteria such as *Clostridium* are capable to produce organic acids [Little *et al*. 1992]. Produced organic acids are a result of reductive microbial fermentation and can cause the pH drop of the local environment into the acidic range, forming pH gradients. Therefore, Acid-Producing Bacteria (APB) are suspected to create preconditions for development of localized corrosion. Moreover, some bacteria are capable of producing inorganic acids too. It is interesting to note that the products of APB metabolism, such as acetate, can be used by SRBs as a source of carbon (Soracco *et al*., 1988).

Other types of microorganisms such as Metal-Reducing Bacteria (MRB) or Metal-Oxidizing Bacteria (MOB) are known to promote corrosion of the ferrous alloys in the environments that can sustain their metabolism. MRBs likewise Iron Reducing Bacteria (IRB) affect metals by reduction of the generally insoluble Fe^{3+} compounds to the soluble Fe^{2+}, exposing the metal beneath the corrosion-resistant oxide film to the corrosive environment [Graff, 1981; Obuekwe *et al.*, 1981]. On the opposite, strains of IRBs *Shewanella* species were able to retard corrosion of mild steel reducing the rate of both the oxygen reduction and anodic reactions [Dubiel *et al*., 2002].

Microorganisms exhibiting completely opposite metabolic pathways compared to IRB are MOB such as Iron Oxidizing Bacteria (IOB) that derives energy from the oxidation of ferrous iron to ferric iron in proximity of neutral pH [Ray *et al*., 2010]. Most IOBs are microaerophilic, requiring oxygen for growth, often not found in WIS and removing them from focus in WIS' MIC failure investigations, even though they have been associated with marine corrosion failures. In addition, it is important to underline the role of microorganisms such as manganese reducers and oxidizers [Dickinson *et al*., 1996] as well as sulfur/sulfide oxidizers and many others in MIC processes.

It is now acknowledged that microbial metabolic activity, which depends on the availability of nutrients and suitable electron donors and acceptors, can influence electrochemical processes on steel surfaces, and therefore play an important role in the processes governing MIC [Caffrey *et al*., 2008]. Indeed, it has been reported that differences in metabolic activities within biofilms established under identical conditions can result in dissimilar corrosion rates [Beech and Sunner, 2004].

I.5.2. Material

The material surface properties, such as surface topography, chemical composition, morphology, free energy, polarization, tension or wettability have a consequential impact on microbial cell surface architecture that is often correlated with MIC. It is well known that the rate of bacterial adsorption on a substratum increases with higher surface free energy [Muller *et al*., 1992]. Moreover, as previously mentioned, irreversible cell attachment is affected by the hydrophobic forces [McCoy, 1987]. The hydrophobicity of the material surface is important because hydrophobic interactions are stronger when one or both surfaces involved (steel and microbial cell) have a nonpolar nature and thereby cell attachment is directly dependent on the surface wettability. It was demonstrated that the greatest cell attachments occur on hydrophobic surfaces [Fletcher and Loeb, 1979]. In brief, the cell boundaries that participate in cell attachment have a hydrophobic nature due to components such as S-layer proteins, amphipathic polymers and lipids [Skvaria, 1993]. Additionally, surface polarization can affect the attachment process and biofilm formation. It was reported that polarizing the metal cathodically enhanced attachment of certain investigated bacteria to metal surfaces, whereas attachment was reduced when the metal was anodically polarized [Gordon *et al*., 1981]. Furthermore, the maximum attachment on carbon steel for *Flavobacterium breve* and *Pseudomonas fluorescens* was observed in the potential range of ±0.5 V/SCE. Applying more positive or negative potentials caused a decrease in the bacterial attachment [Armon *et al.*, 2001].

In the following text, the influence of the surface topography (roughness) and the surface morphology (microstructure) on biofilms formation and development, and therefore MIC, is described in more detail.

Surface topography, e.g. ***roughness***, is one of the parameters that have a major influence on microbial attachment. In the literature overview, it is possible to find different and quite contradictory

reports about the impact of surface roughness on the microbial attachment and the formation of biofilm. According to Flint and Bremer [Flint and Bremer, 1997], these different and sometimes contradictory observations of cell attachment on metal surfaces are not just the result of surface roughness. Other parameters (e.g. strain of bacteria, physico-chemical parameters of the surface, bulk solution properties, adhesion method used to detect bacteria), influencing microbial attachment, can hide the actual effect of surface roughness. As stated in a literature review conducted by Little and Lee [Little and Lee, 2007], different grades of surface roughness have a different effect on the bacteria attachment. The grade of surface roughness influences the reachability and the available surface for microorganism's attachment. Therefore, higher grades of roughness offer a larger surface area available for microorganisms to attach as demonstrated on different materials that are used for dental implants [Teughels *et al*., 2006]. Moreover, some experiments showed that the rate of bacterial adsorption on a substratum increased with increasing surface roughness [Muller *et al*., 1992]. It is shown that irregularities in the surface topography can promote bacterial adhesion and biofilm formation while an ultra-smooth surface with a mirror finish would do the opposite [Yuehuei and Friedman, 2000]. Besides the influence on initial attachment of microorganisms, surface roughness is also affecting cell retention on surfaces [Verran and Boyd, 2011]. The surface roughness of a material is a very important objective of any investigation if the material is used for industrial applications because these materials commonly have a high grade of surface roughness. It is unusual to encounter smooth, fine polished surfaces in industry and in the case of water injection system never.

Each material possesses its own morphological pattern or "manuscript" that is unique for each manufactured material. The ***morphology*** of a material is attributed to the material chemical composition and to the manufacturing processes. The microstructural heterogeneity of ferrous alloys, whether created intentionally or as an artifact of the manufacturing process, affects the material properties. The level of heterogeneity is significant because of the small scale of microbes and it is therefore an important factor in MIC initiation. Moreover, it was experimentally proven that the initial attachment of bacteria takes place on the grain boundaries [Sreekumari *et al*., 2001]. One of possible explanations for these phenomena is the elevated surface energy inside the grain boundary compared to the energy inside the matrix. As the grain boundaries become increasingly overpacked with cells, further attachment will become more spread across the steel surface matrix [Sreekumari *et al*., 2001].

Different processes, such as welding, are significantly perturbing surfaces and changing the microstructure through a combination of physical and compositional alterations. It was hypothesized that a surface alteration caused by welding would lead to an accumulation of organic matter onto the surface, followed by bacterial colonization [Videla and Characklis, 1992]. This was experimentally confirmed [Walsh, 1999, Eashwar and Dexter, 1999]: generally, the base metal exhibited the lowest area of attachment whilst the weld metal showed the highest.

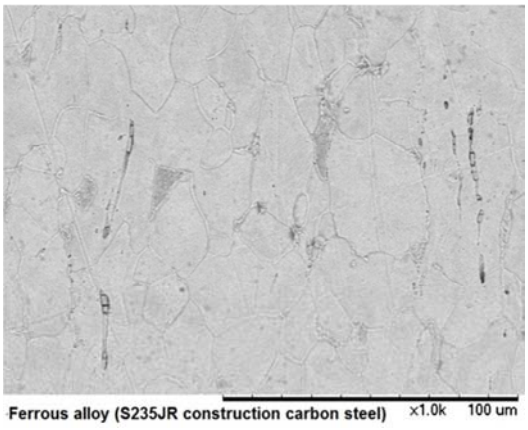

Fig. I.7. Microstructure of typical low carbon construction steel.

The material microstructure by itself influences corrosion. A homogenous distribution of geometrically small grains and short grain boundaries results with a tendency of the surface towards equally allocated degradation and visa-versa. In ferrous alloys, e.g. carbon steels, a ferrite/pearlite microstructure is most often encountered (ferrous phase – light grey, pearlite (or ferrous-carbide) phase – dark grey in Fig. II.7), with manganese-sulfide (MnS) inclusions (long black structures in Fig. II.7) randomly distributed over the general microstructure. It has been postulated that MnS inclusions,

characteristic for ferrous alloys such as carbon steels, can serve as initiation points for pitting corrosion [Wrangler, 1971; Wrangler, 1974]. Recently, different studies showed a correlation between pit initiation and propagation associated with sulfide inclusions and their relation to MIC [Avci *et al*., 2012].

I.5.3. Environment

In the system, the medium has a great importance regarding the development of microorganisms and biofilms and therefore MIC. It has multiple functions: as an electrolyte it takes part into ion transfer, as a provider of nutrients, it plays role in metabolic process of microorganisms and as a mean of transport for microorganisms. Moreover, it can be a factor controlling bacterial diversity in particular system that will determine which species will be the most abundant. There is a wide list of parameters that define the medium and just some of them are described as follows: chemical composition, temperature and rheological properties.

The ***chemical composition*** of a medium will determine its properties, for example pH, and therefore its corrosivity. On the other hand, the influence of the medium chemical composition on the microorganisms is affecting the occurrence of MIC. The effects of medium on microorganisms can be separated in two significant features. These two features are defined by the level of influence that it can have on microorganisms and biofilm in an observed system.

The first feature is the presence or absence of oxygen in the observed system. This strictly defines what group of microorganisms will be abundant in the system. Because of this, the definition of studied systems is divided into two major groups, *aerobic* (presence of oxygen) and *anaerobic* (absence of oxygen) systems. For example, the oxygen concentration dictates the development of SRB in the studied environment. SRB will only proliferate in environments in absence of oxygen [Stott *et al*., 2010]. At the same time, it is necessary to keep in mind that conditions in the bulk medium can be very different from conditions in the biofilm (e.g. anaerobic niches under upper layers of biofilm in aerobic system). As mentioned previously, aerobic and anaerobic organisms have often been found to co-exist in the same location. This is because aerobic species deplete the immediate surroundings of oxygen creating an ideal environment for anaerobes.

The second feature relates to the availability of nutrients for microbial metabolic cycles. As previously mentioned, the availability of carbon is one of the limiting factors that determine microorganisms and biofilm growth kinetics [Flemming *et al*., 2000]. In the same literature, it is stated that an increase of Total Organic Carbon (TOC) will increase the carbon available to the microbial community within the biofilm. This can be taken as a general rule. However, exceptions are always possible. Furthermore, the carbon source can affect the topography of biofilms; if present in large amounts, the observed biofilm structure could be characterized as dense and confluent. In the absence of a carbon source, biofilm appears as scattered piles of cells dispersed over a large area. This could promote establishment of local physico-chemical conditions affecting corrosion pattern e.g. surface degradation topography. Random allocations of EPS piles across surface can lead to formation of galvanic couples due to EPS selective metal binding capacity [Beech and Cheung, 1995; Ford *et al*. 1988]. Moreover EPS can react as physical barrier to transfer of electroactive species from bulk electrolyte to surface and therefore when allocated randomly across steel surface can promote formation of galvanic cells. Additionally, due to its chemical properties it may lead to unequal pH conditions across steel surface forming different pH cells. All this can result in elevated local metal loss.

Other chemical species have certain, usually specific, influences on the metabolic cycles and pathways of the bacteria present in the bulk medium, as well as in the biofilm. The group of elements (sodium, zinc, copper, molybdenum, manganese, and cobalt ions), known as “trace” elements can be a limiting factor for microbial growth and development. Trace elements are required in very minute amounts and they usually function as cofactors in enzymatic reactions being electron donors or electron acceptors. Absence of these elements can even lead towards disruption of the bacteria life cycle and death. Phosphorus, nitrogen and sulfate can be limiting factor in certain systems too. It is shown that SRB growth is much less likely if the aqueous sulfate concentration or the organic carbon content is below ~10mg L^{-1} or the ammoniacal nitrogen is below ~1 mg L^{-1} [Stott *et al*., 2010].

Temperature is a parameter that influences corrosion directly and in addition influences MIC by selecting the population that will be active in the system. The lowest temperature at which a particular species will grow is the minimum growth temperature, while the maximum growth temperature is the

highest temperature at which they will grow. The temperature at which their growth is optimal is called the optimum growth temperature. These three temperatures are known as the "cardinal temperatures" and they are characteristic for any given microorganism. Bacteria species as well as members of whole microbial community can be classified in four groups according to their growth temperature maxima: psychrophiles (low temperature optima), mesophiles (midrange temperature optima), thermophiles (high temperature optima) and hyperthermophiles (very high temperature optima) [Madigan *et al.*, 2010]. From this it can be concluded that the temperature of a medium will define which microbial species will be the most abundant in a given system. The mesophiles are moderate-temperature-loving bacteria, with an optimum growth temperature between 25℃ and 37℃ [Javaherdashti, 2008]. At lower temperatures, these bacteria can remain dormant which means that they can stay alive but not multiply, but at temperatures well above 40℃, they will die. Different temperature gradients can be present at different locations in systems as a byproduct of hydrodynamic fluctuations in the system and chemical reactions (i.e. exothermic, endothermic). Following this and as stated in the literature [Little and Lee, 2007] bulk water temperatures affect the rate of chemical and biochemical reactions as well as transport processes within the biofilm.

MIC has been frequently detected in the flowing systems such as WIS, in which the properties of the fluid dynamic movements have to be taken into consideration. Although the ***fluid flow*** is another parameter that impacts material deterioration directly, through erosion corrosion, it also directly impacts mass transfer and therefore biofilm formation. For the immersed surfaces, the hydrodynamic conditions will determine the rate of transport of cells and nutrients to the surface, as well as the magnitude of the shear forces acting on the developing biofilm. It is proven that a mild agitation rate better facilitated planktonic cell growth compared to growth in a static liquid medium [Wen *et al.*, 2006]. Hence, increased flow velocity up to a certain value increases the biofilm production rate. An exponential relationship was shown between biofilm production rate and flow velocity within the range from 0 to 15 cm s^{-1} [Pedersen, 1982]. This phenomenon is a consequence of increased mass transfer and hence increased access to nutrients for microorganisms. This is also affecting temporal behavior of biofilms [Stoodley *et al.*, 1999].

Flow may also produce a high shear stress that inhibits cell attachment and causes even the detachment of an established biofilm [Stoodley *et al.*, 1999]. Furthermore, importance of hydrodynamic drag on initial cell attachment and biofilm development increases as flow conditions are becoming harsher. A sufficiently high linear flow velocity can prevent biofilm establishment or even dislodge an established biofilm [Wen *et al.*, 2007]. The transition zone is considered to be between 2 and 3 m s^{-1} [Stott *et al.*, 2010]. Moreover, it is reported that at a flow rate of 3.5 m s^{-1}, SRB cells could not adhere on the coupon surface to form an SRB biofilm [Wen *et al.*, 2007].

What's more, it is stated that in a flowing system, flow rates affect the oxygen concentration gradient. By changing the oxygen content, it will select the types of microorganisms proliferating in particular regions, for example: in oxygen depleted regions facultative anaerobes will be domination microorganisms while in oxygen saturated regions facultative aerobes will be dominant microorganisms. This is one of the ways in which flow affects biofilm formation. Moreover, different oxygen concentration gradients over the material surface will affect material by itself creating anodic and cathodic areas on the metal. Areas with lower-oxygen concentrations become anodic and this will induce corrosion.

I.6. MIC assessment, monitoring and mitigation

MIC management for WIS incorporate MIC diagnosing and assessment of the present conditions, monitoring of the microbiological content and of corrosion evolution in the system and optimization/ application of suitable countermeasures.

The MIC diagnosing and assessment of the current conditions starts with collection and analysis of all available data about the system history: Piping and Instrumentation Diagrams (P&ID) analysis, detection of critical locations, corrosion rates, on-site observations, water chemistry, applied treatments, flow regimes, bacterial population… In the next step, it is needed to collect biological samples, e.g. biofilms and minerals (i.e. corrosion products). Samples have to be processed by state-of-the-art techniques to obtain relevant and reliable information. Collection of biological and mineral samples can be conducted through pigging operation, bio-probes or weight loss coupons.

The morphology and chemical composition of collected corrosion and mineralization/biomineralization products are usually assessed by various analytical and microscopical techniques. The most frequently used techniques are Scanning Electron Microscopy (SEM) interfaced with Energy Dispersive X-ray spectroscopy (EDX), X-ray Photoelectron Spectroscopy (XPS), X-ray Diffraction (XRD), electron microprobe complemented with electron microscopy observations and Atomic Force Microscopy (AFM) etc. [Videla *et al*., 2005; Beech and Sunner, 2004]. Information, obtained by these techniques, enables relationships to be identified between corrosion products and/or mineralization/biomineralization products to the corrosion reactions and mineralization process. To fully understand the origin of these products, it is required to get an insight into the particular environment chemistry, encompassing the chemical composition of the medium (with or without chemical treatments) and microbial reactivity, e.g. metabolic paths, taking place in the system [Eckert and Skovhus, 2011]. The same methods can be applied in laboratory studies in order to reveal the corrosion mechanism taking place in particular environments, on specific metallic surfaces.

Assessment of the microbial diversity is crucial because it provides insight into metabolic paths characteristic of specific microorganisms, therefore revealing the relationship between microbial activities with corrosion reactions in a precise environment. Microbial diversity of biofilms can be assessed by means of traditional microbiological techniques (enrichments) [Sørensen *et al*., 2010]. A second and more reliable option is the use of one or a few of the multiple available environmental ecology techniques as Denaturing Gradient Gel Electrophoresis (DGGE) – sequencing of isolated bands [Jan-Roblero *et al*., 2004; Keasler *et al*., 2009], Polymerase Chain Reaction (PCR) cloning–sequencing [Bermont-Bouis *et al*., 2006; Rajasekar *et al*., 2010], Reverse Sample Genome Probing (RSGP) [Nemati and Voordouw, 2000], etc. Recently, novel techniques such as pyrosequencing [Sztyler, 2013] are becoming more frequently used as their costs are decreasing.

Chemical composition of the water used in WIS is determined and monitored by means of Inductively Coupled Plasma–Atomic Emission Spectroscopy (ICP-AES) for inorganic ions, TOC measurements, etc.

Corrosion of each WIS should be monitored from the day of its start-up, and should not be specifically correlated to particular MIC related problems. Corrosion of WI systems is most often monitored by weight loss measurements or by utilization of multiple-electrochemical probes. The most commonly applied electrochemical techniques for monitoring MIC in general and on O&G offshore installations are Electrical Resistance (ER), Linear Polarization Resistance (LPR) and Electrochemical Noise (EN) [Videla, 1996]. Capacity of EN to differ between localized corrosion, e.g. pitting, and general corrosion proved to be a valuable tool for real-time on-line monitoring of corrosion in seawater systems populated with microorganisms [Kane and Campbell, 2004]. Even though they are not absolute methods and have some limitations, electrochemical methods and monitoring electrochemical probes [Cormon USA; Alabama Specialty Products, Inc. USA; CorrOcean ASA Norway; Honeywell USA] enable user to monitor deviations in corrosion behavior of a particular system. Moreover, they are valuable tools for optimization and confirmation of the effectiveness of applied countermeasures [Eden and Moody, 2002]. On the other hand, laboratory electrochemical testing provides information about corrosivity of a particular microbial load and reveals information about possible ferrous metal-microbial interactions [Lee and Little, 2007].

Corrosion monitoring should be fulfilled with microbial reactivity and diversity monitoring. Microbial density can be monitored with the previously described methods of traditional microbiology or environmental ecology. Furthermore, bacterial reactivity is estimated by associating detected microorganisms with three grades of viability: active, inactive, or dead. For this purpose, are suitable techniques such as Most Probable Number (MPN) from traditional microbiological techniques, use of dye 6-diamidino-2-phenylindole (DAPI) and Fluorescence In-Situ Hybridization (FISH) representing microscopic examination techniques or qPCR representing molecular methods [Eckert and Skovhus, 2011].

Please note that in *Chapter II*, Material & Methods, specific techniques and methods are described in more detail as well as their possible application for studying MIC.

In order to mitigate the deleterious effect of microorganisms on ferrous alloys and on the integrity of WIS, it is required to conduct reliable and frequent monitoring that can result in identifying when necessary action is required. Reproducibility and consistent analysis of MIC for pipeline steels is vital

to understand the effect of various operating conditions on corrosion, to evaluate the outcomes of treatment chemicals and to develop more reliable monitoring tools for MIC.

Prior to the application of countermeasures such as antimicrobial chemical treatment a system must be cleaned. Cleaning of a system in O&G operations is most often conducted mechanically by pigging operations where the physical removal of deposits formed on the surface takes place and is applied to remove sludge, scale and encrustations as well as the biomass associated with these deposits [Videla, 2002]. In addition, chemical cleaning with mineral and/or organic acids or specific chelating agents can be applied after mechanical cleaning to increase the effectiveness of cleaning [Videla, 2002]. Currently in industry several antimicrobial chemical treatments are applied, ranging from the application of different biocides to the well-established nitrate treatments that, however, can have unwanted side effects.

Biocides vary from oxidizing ones such as chlorine, chlorine-dioxide or bromine to compounds such as quaternary phosphonium salts, aldehydes or different amine-type compounds, etc. [Carrera and Gabetta, 1995]. The main benefit of aldehydes, particularly glutaraldehyde most often used, is its legal acceptability. Moreover, it is active over a broad range of temperatures and pH values making it multifunctional. The primary functional groups and reactive species of aldehydes are amines and sulfhydryl groups and they react with nucleic acids and basic constituents of proteins (e.g. groups such as –OH, $–NH_2$, –COOH, and, –SH) present in cell membranes, cell walls and in cytoplasm [Videla, 2002]. They interfere with the enzymatic activity, synthesis and function of nucleic acids and by that control other biochemical and physiological process of cells [Ascenzi, 1996]. Moreover, interaction with basic constituents of proteins causes inter- and intramolecular crosslinking of proteins leading to quick cell death.

Conversely, nitrate treatment does not reduce the scale of MIC by killing all present microorganisms. It is a selective technique that can prevent from and remediate souring, the result of SPP metabolism, specifically of SRBs. Nitrate stimulates Nitrate-Reducing, Sulfide-Oxidizing Bacteria (NR-SOB) and heterotrophic Nitrate-Reducing Bacteria (hNRB) that compete with SRB for degradable oil organics serving as electron donors [Hubert and Voordouw, 2007]. The main challenge is the switching metabolisms of specific SRBs, which possess genes responsible for both, sulfate and nitrate reduction [Dunsmore *et al*., 2004]. This mechanism can possibly lead to unwanted effects. Nevertheless, the lack of negative environmental impacts associated with applying inorganic nitrate salts is the benefit of nitrate treatment.

There are different methodologies for evaluating the corrosivity of microorganisms and the effect of biocides. There are two main concepts involving field and laboratory tests and investigations. They encompass different environmental, ecological, electrochemical, chemical and mathematical techniques. The methods and tools are given in more detail in the *Chapter II* entitled “Materials and methods”.

I.7. The “From the Filed to the Laboratory and back to the Filed” applied experimental approach

All along, the focus of this research project was centered on providing useful feedback to operators of offshore installations. In order to achieve representative and useful results that could lead to discussions producing reliable recommendations, it was required to simulate, as close as possible, the real environments and present problematic.

Therefore, during the first stage of the project, presented in C*hapter III*, initial samples were obtained directly from O&G installations currently operating in North Sea. Obtained offshore biological samples as well as samples of injection medium (North Sea seawater) were analyzed by state-of-art environmental ecology techniques providing us with microbial diversity of offshore consortium and injection medium. Moreover, the offshore medium/electrolyte chemical composition was determined by elemental analysis of the injection medium. This indicated what possible chemical/biochemical processes occurring in system and contributing to overall corrosion and scaling process. Type of the test material was selected according to analysis of P&ID diagrams. Sample metabolic nature, analysis of injection medium and analysis of field information resulted in the definition of, and the execution plan for designing and constructing specific flow-loop experimental set-up entitled as “*Bioreactor Flow Loop”*. Constructed experimental set-up enabled studying effect of the bacterial community recovered from North Sea offshore SWIS on corrosion of carbon steel. Isolated consortium was used as an

inoculum in the experimental set-up designed for exposing carbon steel to flowing anoxic seawater conditions, in order to create an approximate simulation of the real O&G SWIS. Results, discussion and conclusions produced during the first stage of project are presented in *Chapter III* in a form of a scientific article entitled "**The effect of bacterial community recovered from North Sea offshore seawater injection system on corrosion of S235JR steel: laboratory investigations**" (Bioelectrochemistry, Special Issue: BIOCORROSION 2012, 2nd revision).

During the next step of the project presented in *Chapter IV*, model organisms with well-known metabolic paths and capable of delivering identical or similar effects on carbon steel were selected in an attempt to explain corrosion processes in sulfidogenic environments during long and short-term exposure periods. The investigation on the corrosion behavior of carbon steel in environments loaded with sulfate-reducing bacteria consisted of:

i) Carbon steel corrosion in presence of sulfate-reducing bacteria in natural seawater environment and antimicrobial treatment

Behavior of carbon steel in seawater environment inculated with SRB *Desulfovibrio* species was studied in specially designed "*continuously feed with fresh media flow loop"* enabling constant income of fresh nutrients. Antimicrobial treatment was applied to disturb healthy bacterial population and acquired electrochemical/chemical response characteristic for alteration of bacterial viability and activity. Focus was on:

a) Influence of microbial activity for corrosion products architecture;
b) Influence of material microstructure to degradation topography in presence of bacteria activity;
c) Capacity of antimicrobial treatment to retard corrosion and microbial activity;
d) Capacity of electrochemical techniques to detect impact of bacterial activity on surface electrochemical events.

Produced results are presented in a form of a scientific article entitled **"Corrosion behavior of carbon steel in presence of sulfate-reducing bacteria in seawater environment"** (Electrochimica Acta, 2nd revision).

ii) Electrochemical interactions between carbon steel and sulfidogenic bacteria

Electrochemical behavior of carbon steel in presence of *Desulfovibrio* species was investigated by means of Electrochemical Impedance Spectroscopy (EIS). An influence of biofilm and formed corrosion/biomineralization products on transfer of electroactive species from the bulk electrolyte to the steel surface was the focus of this work. Work produced is presented under the form of a scientific article entitled **"Surface behavior of carbon steel in presence of sulfate-reducing bacteria: proliferation and mitigation with biocide treatment"** (in preparation).

In real life most of the WI systems are subjected to a certain amount of mechanical stress. In addition, hypothesis that bacterial cells are attracted to locations on the metal surface with higher energy, which can be produced by mechanical stress, indicated possibly to correlate microbial activity and stress corrosion failure mechanisms. *Chapter V* deals with behavior of mechanically stressed carbon steel in the presence of sulfidogenic pure cultures and sulfidogenic offshore consortium, as well as some other bacterial species e.g. iron reducing bacteria. This work is presented under the form of a scientific article entitled **"Electrochemical and Fractographic Analysis of Microbiologically Assisted Stress Corrosion Cracking of Carbon Steel**" (Corrosion Science, 2nd revision).

Finally, a conclusion obtained during this project is presented in *Chapter VI* and can lead to a list of recommendations submitted to the O&G offshore installation's operators.

Chapter II

Materials and Methods

II.1. Introduction

This chapter encompasses description of materials, techniques and methodologies used during this research project. The project has been divided into three different stages. Each stage required specifically designed experimental set-ups as well as use of particular investigation tools. The first stage presented in *Chapter III* was focused on:

a) Microbial diversity investigation of biofilm consortium isolated from the Sea-Water Injection System (SWIS). The SWIS is located on an offshore installation in North Sea
b) Carbon steel corrosivity assessment in the experimental set-up simulating specific SWIS operation parameters and threats
c) Corrosion products architecture mediated by the isolated sulfidogenic offshore consortium

Microbial diversity was investigated by means of microbial ecology techniques. The separation of DNA isolated from obtained offshore samples was performed with Denaturing Gradient Gel Electrophoresis (DGGE) and cloning in the microbiological laboratory at the University of Portsmouth (UoP) (UK). At the next step, prepared DNA samples were sent to GATC Biotech (Germany) in order to acquire RNA sequences. Finally, the microbial diversity was identified based on the obtained RNA sequences. All delivered RNA sequences were checked up with Classifier Programme and on-line blasting provided identification of run RNA sequences.

The influence of the studied microbial consortium on corrosion of carbon steel was assessed mainly by using electrochemical techniques such as corrosion potential (E_{corr}) also called Open Circuit Potential (OCP), Linear Polarization Resistance (LPR) and Electrochemical Noise (EN). In order to complete investigation, surface analysis and analytical chemistry techniques were also employed. Electrochemical investigation was conducted in the facilities of Det Norske Veritas (DNV) (Norway). Surface analysis by Scanning Electron Microscopy (SEM), Energy Dispersive X-ray Spectroscopy (EDX) and optical microscopy was performed the DNV and Molecular Imaging Center (MIC) (Norway) facilities. Chemical analysis was carried on at Laboratoire de Genie Chimique (LGC) of the INP-ENSIACET (France) and Commissariat à l'énergie atomique (CEA) (France).

Second stage of the project, presented in *Chapter IV*, centered on corrosion behavior of carbon steel in environments loaded with Sulfate-Reducing Bactria (SRB). The second approach aims to understand the influence of sulfidogenic bacteria, with well know metabolic pathways, on the corrosion of carbon steel. Moreover, the response of bacteria on mitigation techniques, such as antimicrobial treatments and the influence of stressed bacterial populations on corrosion processes were explored. This was performed in order to fulfill the investigations conducted during first stage of this research project and to provide operator with deeper insight of his actions (mitigation treatments response and consequences).

Two different methodologies were applied to achieve the targeted objective:

a) Investigation of the carbon steel corrosion in the flowing natural seawater environment inoculated with pure SRB cultures and subjected to antimicrobial treatment
b) Electrochemical interactions carbon steel - sulfidogenic bacteria - antimicrobial in stagnant conditions.

This approach centers mostly on the same electrochemical and surface analysis techniques used during the first stage of the project. In addition, Electrochemical Impedance Spectroscopy (EIS) is used to illuminate steel surface response. The electrochemical investigations, with exception of EIS, were carried out at the DNV. The EIS measurements and acquired response signal studies were performed at LGC of the INP-ENSIACET. Surface SEM/EDX analysis was performed at MI-SWACO, a Schlumberger company (Norway), MIC (Norway) and LGC of the INP-ENSIACET (Toulouse). Chemical analyses were conducted at Departamento de Química Faculdade de Ciências e Tecnologia Universidade Nova de Lisboa (FCT-UNL) (Portugal) and CEA.

The third stage, presented in *Chapter V*, centers on behavior of mechanically stressed carbon steel in the presence of pure sulfidogenic cultures and sulfidogenic offshore consortiums. The goal of this particular study was to assess the probability of Stress Corrosion Cracking (SCC) failure mechanism for carbon steel when subject to elevated mechanical load in the presence of specific bacteria and consortiums. This investigation required use of mechanical and metallurgical investigation tools,

specifically tensile and hardness machines. Moreover, to obtain better insight on the behavior of carbon steel along the immersion periods electrochemical techniques; Electrochemical Frequency Modulation (EFM) and OCP, were employed on tensile specimens during immersion periods.

In the following text it is possible to find more detail information about the investigated carbons steel, electrolytes used and microorganisms as well as more detailed information about experimental set-ups and applied analytical techniques.

II.2. Investigated materials

One type of construction carbon steel; e.g. S235JR, was focused upon during the project. According to the EN 10025 - 2: 2004 standard, grade S235JR and number 1.0038 is classified as a non-alloy structural steel applicable for structural purposes. Equivalent grades of grade S235JR (1.0038) are shown in Tab. II.1.

Tab. II.1. Equivalent grades of grade S235JR (1.0038).

Europe new EN 10025 - 2 : 2004	USA	Germ. DIN, WNr	Japan JIS	France AFNOR	Eng. BS	Canada HG	Europe old EN	Belgium NBN
S235JR (1.0038)	1015	RSt37-2	SM400A SS400	E24-2	40B	230G	Fe360BFN S235JRG2	AE235B
Spain UNE	**China GB**	**Swe. SS**	**Austria ONORM**	**Norway NS**	**Russ. GOST**	**International ISO**	**Portugal NP**	**India IS**
AE235B-FN	Q235A Q235B Q235D	1311 1312	Rst360B	NS12123	St2ps St2sp St3ps St3sp	E235B Fe360B	Fe360-B	IS226

The S235JR used in the experimental work was supplied from Descoure and Cabaud (France). The composition of the steel is summarized in Tab. II.2. The mechanical properties of the used steel were investigated in order to detect possible deviations form reported values. Certified yield strength, measured yield and tensile strength are presented in Tab. II.2.

Tab. II.2. Chemical composition of the steels used (wt%), yield and tensile strengths (MPa).

Alloy	C	Mn	Cu	S	P	N	Certified Yield	Real Yield	Tensile
S235JR	0.17	1.40	0.55	0.03	0.03	0.01	235	406	360/510

The steel was delivered in several shapes: a rod shape with a length of 6000 mm (Rod A) and 20 mm (Rod B), both with a diameter of 10 mm, a sheet with a length of 2000 mm, a width of 1000 mm and a thickness of 2 mm and finally a pipe with a length of 6000 mm, an outer diameter of 60 mm and an inner diameter of 50 mm.

A crystallography was performed on the clean steel specimens and a typical microstructure is shown in Fig. II.1. As can be seen, relatively small sized grains and short grains boundaries, indicating a

compact structure, characterize the microstructure. Please note that ferrite is the pure iron phase and perlite is the iron carbide phase.

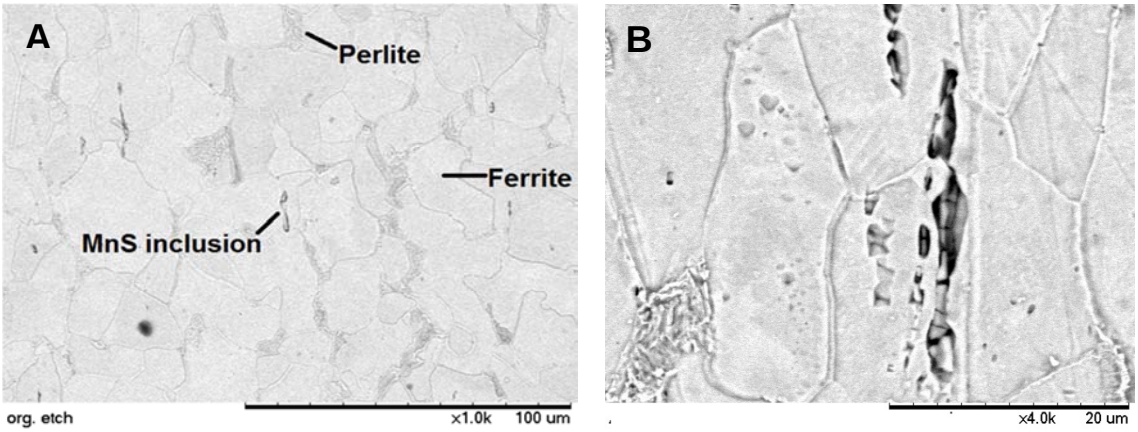

Fig. II.1. Microstructure of a cleaned S235JR carbon steel specimen obtained with SEM: A) 1000x magnification, B) 4000x magnification.

All Working Electrodes (WE), weight loss coupons, coupons for monitoring biofilm formation as well as tensile specimens were machined out of the delivered S235JR construction carbon steel.

For studying the corrosion behavior of acquired steel, WEs with a circular, exposed area of 78.5 mm^2 and/or 314 mm^2 were machined out of the delivered rods. First, rods were cut into cylindrical specimens with a length of either 10 mm or 20 mm. Second, on the upper surface it was drilled 3 mm deep threaded whole that accommodated a/the titanium GR2 electrode holder. Further, the prepared working electrodes were dressed in a polyolefin sleeve (Raychem, USA) leaving only the flat bottom of the cylinder exposed as show in Fig. II.2.

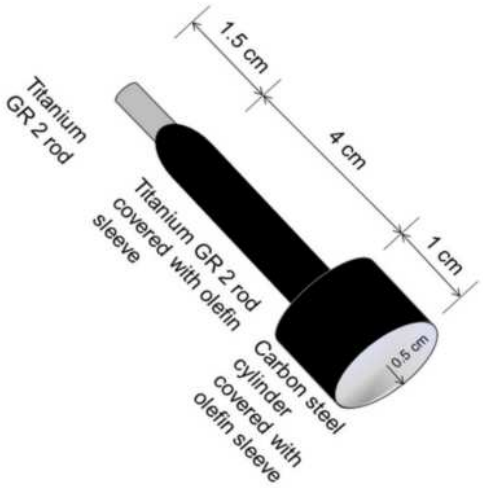

Fig. II.2. Example of a working electrode scheme.

Weight loss specimens were featured with a length of 10 mm, a width of 10 mm and a thickness of 2 mm. Weight loss coupons were manufactured out of the provided steel with a length of 2000 mm, a width of 1000 mm and a thickness of 2 mm. Moreover, for biofilm studies at the 6 o'clock position, half-pipe coupons with a length of 50 mm, an outer diameter of 60 mm and an inner diameter of 50 mm were also constructed/ manufactured.

Tensile specimens that could also serve as a working electrode were required in order to study the steel's corrosion behavior under mechanical stress. The tensile specimens/working electrodes were manufactured out of rod B, as shown in Fig. II.3.

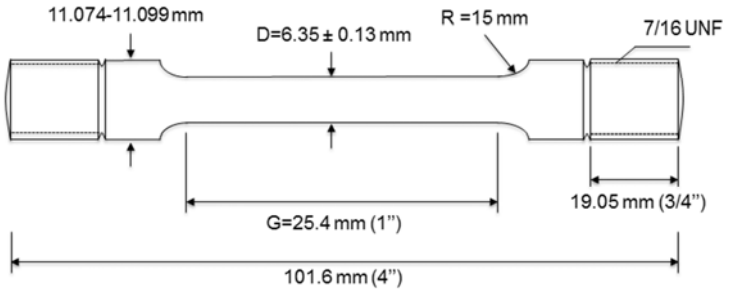

Fig. II.3. Tensile specimen scheme and dimensions.

Surfaces of all exposed steel specimens were prepared by manual grinding using increasing series of fine SiC paper, ending with 600-grit. Grinding debris were rinsed of the surface with sterile deionized water. Specimens were exposed on each side for 12 or 24 hours under UV light (wave length 256 nm: XX-15, sterilization UV lamp, UVP, USA) at 25℃. Se cond applied sterilization protocol consisted of steel specimens immersion in a 70 (v/v) % ethanol solution during 3-5 minutes.

II.3. Counter electrodes

Three types of counter electrodes; inconel, platinum and graphite, were used. Inconel counter electrodes were prepared in-house using Inconel® alloy C276 cylindrical specimens with a length of a 10 mm and a diameter of 10 mm supplied by Salmon's metalen B.V. (Netherlands). Cylindrical specimens were cut out of a cold drawn, wire round, pickled, and solution annealed Inconel® alloy C276 rods with a length of 3000 mm and of a diameter of 10 mm. The Inconel® C276 alloy used was composed of the elements shown in Tab. II.3.

Tab. II.3. Chemical composition of the used Inconel® C276 alloy (wt%).

Alloy	C	Mn	Si	S	P	Co	Cr	Fe	Mo	Ni
C276	0.006	0.43	0.027	<0.001	0.007	0.07	15.58	6.12	15.29	Balance

Preparation of the counter electrodes followed same protocol as for the working electrodes, with a difference of size of the exposed surface, in this case 396 mm^2. In some experiments two inconel counter electrodes were connected in series, doubling the counter electrode surface. Exposed surfaces of all counter electrodes were prepared by manual grinding using increasing series of fine SiC paper, ending with 80-grit. Grinding debris was rinsed of the surface with sterile deionized water.

Commercial graphite counter electrode, in a shape of graphite rod with a length of 300 mm and a diameter of 10 mm, was supplied by Pine Research Instrumentation (USA).

Prior to experiments, both the inconel and graphite counter electrodes were used as start counter electrodes and were exposed for UV-light (wave length 256 nm: XX-15, sterilization UV lamp, UVP, USA) on each side for 12 hours at 25℃.

Platinum counter electrodes were made out of a platinum wire with a diameter of 1 mm or less and connected in one end to a platinum mesh (Goodfellow, USA) with dimensions of a 4 cm × 4 cm. Prior to experiments, these were first exposed to flame and then immersed in 70 (v/v) % ethanol solution during 3-5 minutes.

II.4. Reference electrodes

Two types of reference electrodes; Saturated Calomel Electrode (SCE) and Inconel Pseudo-Reference Electrodes (IPRE), were used. The reference electrode selection process was governed by

the duration of experiments, toxicity and conductivity of electrolyte to name a few. Prior to experiments, reference electrodes were immersed in ethanol 70 (v/v) % during 3-5 minutes.

SCE were supplied by Gamry Instruments (USA). Noise level produced by typical SCE is 2×10^{-8} V^2/Hz at 0.1 Hz sampling frequency. Inconel pseudo-reference electrodes were constructed out of same Inconel® alloy 276C that was used for construction of counter electrodes using same design as for working electrodes. Reliable application of different pseudo-reference electrodes was demonstrated by other researchers [Tait and Maier, 1986; Lin *et al.*, 2003] and producers of electrochemical apparatuses and accessories [Princeton Applied Research, USA].

II.5. Electrolytes

II.5.1. North Sea Seawater

North Sea seawater from the west coast of Norway, directly pumped from 60 m depth, was used as an electrolyte. In-house monitoring of pH, temperature and salinity of seawater was conducted in the period between October 2006 and June 2010. Data analysis showed that the temperature fluctuate between 7-15 ℃, salinity between 32-36 ppt (inform ation from DNV Bergen laboratory data base), and pH between 7.8 and 8.3. Measured salinity levels are directly dependent to temperature; higher temperature was correlated with higher seawater salinity. The chemical composition of seawater was determined by means of Inductively Coupled Plasma–Atomic Emission Spectroscopy (ICP-AES), and is shown in Tab. II.4.

Tab. II. 4. Chemical composition of used Bergen bay North Sea seawater (ppm) in 2011.

Element	Ca	Fe	K	Mg	Na
Concentration	52.6	0.02	228.2	19.6	272.4

II.5.2. Modified VMNI media

Modified VMNI sulfate culture media [Zinkevich and Beech, 2000] was composed of (g L^{-1} distilled water): KH_2PO_4, 0.5; NH_4Cl, 1.0; $CaCl_2 \times 2H_2O$, 0.04; sodium lactate, 6.0; sodium citrate, 0.3; casamino acids, 2.0; tryptone, 2.0; modified Wolfe's mineral elixir (0.1% v/v) and vitamin solution (0.2% v/v), Na_2SO_4, 4.5; $MgSO_4 \times 7H_2O$, 0.06; $FeSO_4 \times 7H_2O$, 0.004. The vitamin solution was composed of (gL^{-1} distilled water): riboflavin, 0.1; nicotinic acid, 0.25; thiamine, 0.3; pentatonic acid, 0.3; pyridoxine, 0.3; cyanocobalamin, 0.025; ascorbic acid, 1; biotin, 0.005. The composition of the modified Wolfes Elixir was (g L^1 distilled water): nitrilotriacetic acid, 1,5; $MgSO_4 \times 7H_2O$, 0.06; $MnSO_4 \times H_2O$, 0.5; NaCl, 1; $FeSO_4 \times 7H_2O$, 0.1; $CoSO_4 \times 7H_2O$, 0.1; $NiCl_2 \times 6H_2O$, 0.1; $CuCl_2 \times 2H_2O$, 0.1; $ZnSO_4 \times 7H_2O$, 0.1; $CuSO_4 \times 5H_2O$, 0.01; $AlK(SO_4)_2 \times 12H_2O$, 0.01; H_3BO_3, 0.01; $Na_2MoO_4 \times 2H_2O$, 0.01; $Na_2SeO_3 \times 5H_2O$, 0.001. For experiments performed with *Desulfovibrio alaskensis* AL1 and *Desulfovibrio desulfuricans* ATCC 27774 media was supplemented with 2 gL^{-1} and 3.5 gL^{-1} of NaCl.

II.5.3. Modified DSMZ 826 Geobacter media

Modified Deutsche Sammlung von Mikroorganismen und Zellkulturen (DSMZ) 826 GEOBACTER media was composed of (in 980 mL of distilled water): NH_4Cl, 1.5; Na_2HPO_4, 0.6 g; KCl, 0.1 g; Na-acetate 0.82 g; trace element solution (medium 141), 10.0 ml; vitamin solution (medium 141), 10.0 ml; selenite-tungsten solution (medium 385), 1.0 ml; Resazurin, 0.5 mg; Na_2-fumarate, 8.00 g; $NaHCO_3$, 2.5 g.

II.5.4. Modified Artificial Sea-Water (ASW)

Modified Artificial Sea-Water (ASW) (g L^{-1}): $NaHCO_3$, 2.5; KCl, 0.1; NH_4Cl, 1.5; NaH_2PO_4 H_20 0.6, 10 mM acetate; 20 mM iron citrate; 10 mL ATCC vitamins; 10 mL ATCC minerals; 10 mM acetate; 25 mM fumarate and API broth (g L^{-1}): yeast extract, 1.0; ascorbic acid, 0.1; $MgSO_4$ $7H_2O$, 0.2; K_2HPO_4, 0.01; NaCl, 10; $Fe(NH4)_2(SO4)_2$ $6H_20$, 0.1 plus 4 mL sodium lactate.

II.6. Bacteria cultures and enrichments

II.6.1. Biofilms retrieved from bioprobes

Microbial consortia, which served as a source of inoculum for the laboratory bioreactor loop, was obtained from the SWIS system located on the offshore installation, code name ***S***, in the Norwegian sector of the North Sea. Two bio-probes (0.3 cm^2 surface area, d=0.8 mm, l=12 mm) manufactured from St-52 carbon steel were removed from an SWIS side-stream rig after one and three months of exposure, following the offshore procedure API-RP 39 for handling biological samples. Upon removal, the bio-probes were immersed in 50 mL of sterile SRB/2 growth-medium (Commercial Microbiology, UK) and subjected to 20 seconds of sonification (UltraMet® 2005 Sonic Cleaner, Buehler, US). Following sonification, 1 mL volumes of biofilm suspensions were inoculated aseptically into six glass vials, each containing 9 mL of deoxygenated sterile SRB/2 medium. The vials/cultures were incubated on site at 20℃ for 28 days. The 28-day-old SRB/2 e nrichments were subsequently used for inoculating a range of anaerobic liquid media, as specified below.

a) Seawater + iron dust (3g/ 50 mL)
b) Seawater + SL-10 trace elements solution
c) Seawater + acetate (10 mM) + SL-10
d) Seawater + acetate (10 mM) + Iron dust (3 g/ 50 mL) + SL-10
e) SRB/2 medium

SL-10 trace element solution is used in the preparation of Widdel medium [Widdel *et al*., 1983]. The resulting re-enrichments were incubated for 21 days as described above.

II.6.2. Pigging debris

The pigging debris samples were collected from a water injection pipeline located at the installation, code name “A”, located in the North Sea between November 2010 and June 2011. The 10-15 km pipeline is made of construction carbon steel with an average operating temperature of 35℃.
The pigging samples were received in modified Schott™ flasks that were flashed with inert gas directly after the sample collection performed by the industrial partner. Bacterial consortia living in the pigging samples were cultured. Used media was modified artificial seawater (ASW).

II.6.3. *Geobacter sulfurreducens*

Geobacter sulfurreducens ATCC 51573 strain was obtained from DSMZ as an actively growing culture suspended in liquid medium. The bacterial suspension received was re-suspended in the medium suggested by DSMZ and incubated during 5 days at 30 ℃.

II.6.4. Sulfate-Reducing Bacteria (SRB)

In order to investigate the behavior of sulfidogenic bacteria on the carbon steel corrosion, two SRB strains were used, *Desulfovibrio alaskensis* strain $AL1^T$ and *Desulfovibrio desulfuricans* subsp. desulfuricans strain ATCC 27774.

One of the well-known corrosive SRB species is *Desulfovibrio alaskensis* strain $AL1^T$ (NCIMB 13491T= DSM 16109T) [Beech and Cheung, 1995], initially recovered in 1991 from a soured oil reservoir in Purdu Bay, Alaska. The *D. alaskensis* strain $AL1^T$ is cable of carbon steel degradation by direct cell impact on the material’s surface or through its metabolic process. This strain is categorized as a medium corrosive strain. Basic information about *D. alaskensis* $AL1^T$ is given in Tab. II.5.

Tab. II.5. Basic features of *Desufovibrio alaskensis* AL1^T [Feio *et al.,* 2004].

Features	Gram-staining	Spore forming	Shape	Length/µm	Width/µm	pH range
	Negative	No	Rod	1-5	0.5-1.2	6.5-8.5
Features	**Temp./ ℃**	**NaCl (w/v)%**	**Oxygen tolerance**	**Electron acceptor**	**Electron donors**	**Major cellular fatty acids**
	10-45	0-10	Strictly anaerobic	Sulfate, Sulfite, Sulfide	Lactate, Pyruvate, Succinate	C(18:0), Iso C(15:0), Iso C(17:1)ω7c

The second strain used was *Desulfovibrio desulfuricans* subsp. desulfuricans strain ATCC 27774. The selection of this particular strain was influenced by metabolic capabilities. *Desulfovibrio desulfuricans* ATCC 27774 characteristic feature is its adoptability to electron-acceptor availability, its capability of utilizing nitrate as well as sulfate during the anaerobic fermentation of lactate in the energy metabolism. This feature is of special interest to O&G industry due to commonly applied nitrate treatment as counter-corrosion measure in WIS. Other SRBs, with similar metabolism capabilities as strain ATCC 27774, for example: *Desulfovibrio gracilis* strain OP102, have been recovered form WIS operating in the North Sea [Dunsmore *et al*., 2004]. The strain ATCC 27774 is characterized as mildly corrosive strain/specie. Basic information about *D. desulfuricans* ATCC 27774 is given in Tab. II.6.

Tab. II.6. Basic features of *Desulfovibrio desulfuricans* ATCC 27774 [Postgate and Campbell, 1966; Vainshtein *et al*., 1992].

Features	Gram-staining	Spore forming	Shape	Length/µm	Width/µm	pH range
	Negative	No	Rod	3-5	0.5-1.0	7.2
Features	**Temp./ ℃**	**NaCl (w/v)%**	**Oxygen tolerance**	**Electron acceptor**	**Electron donors**	**Major cellular fatty acids**
	28-44	0-10	Strictly anaerobic	Sulfate, Sulfite, Sulfide, Nitrite	Lactate, Malate, Pyruvate, Choline	Iso C (15:0), Iso-branched C (17:1) FA

Both SRB strains were grown in modified VMNI medium [Zinkevich and Beech, 2000].

II.7. Experimental set-ups

During this research project multiple experimental set-ups were used, that were prepared in-house. Each of them unique, designed and constructed to simulate specific conditions and provide answers to particular questions. Most attention is given to the design and construction of two large-scale experimental set-ups:

i) Bioreactor loop;
ii) Continuously fed with fresh media test loop.

The design process was complex due to nature of the research. The topic of research was anaerobic Microbiologically Influenced Corrosion (MIC), thus, all construction blocks had to be made out of non-corrosive materials featured with low oxygen permeability. Test systems were constructed from polymers to minimize contamination with exogenous metal ions. All construction materials had to be polymers. Used materials were acryl, polypropylene (PP), perfluoroalkoxy (PFA), polyvinyl chloride (PVC), silicon and Marprene®. When applied with adequate thickness all material had acceptable low oxygen permeability [Everitt *et al.*, 2007; Extrand *et al., 2009*; Watson-Marlow Pump Group; Goodfellow]. Accordingly, PFA with 2 mm thickness, PP 2 cm thickness and acryl 0.5 - 2 cm thickness was used. The following section will describe the detailed description and operational principle of these two experiments set-ups. In addition to these two experimental-set ups, a few small-scale experimental set-ups were used to answer specific questions and they are described in following text.

II.7.1. Flow test-systems

II.7.1.1. Bioreactor loop

The main components of the bioreactor loop were manufactured in-house and comprise a vessel and two cylindrical flow-through cells. While the inoculated seawater freely enters the experimental flow cell, it passes through a 0.2 µm filter (Sartopore 2 MaxiCaps®, Sartorius AG, France) before reaching the control flow cell. The bioreactor set-up is depicted in Fig. II.4.

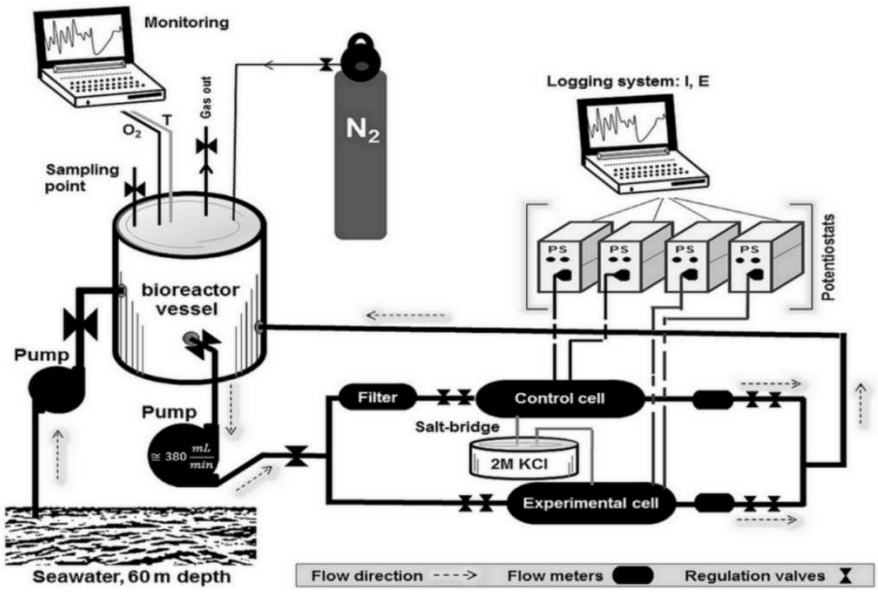

Fig II.4. The bioreactor loop scheme.

The bioreactor vessel consists of a polypropylene body and an acryl lid, fitted with an optical oxygen dipping probe, a temperature sensor interfaced with Fibox 3 fiber optic oxygen transmitter (Presens, Germany), one nitrogen gas inlet (N2, 99.999% purity, Yarapraxiar, Norway), one gas outlet and a pH electrode (pH-meter HI-9125N, Hanna Norden AB, Sweden). The lid also incorporates an in-house fitted sampling point and a fluid injection system. The vessel is also equipped with a heating unit (ISOPAD IP-DASI®, Tyco, USA) and a thermostat (Raychem® AT-TS-14, Tyco Thermal Controls, USA).

A peristaltic pump (W-M 520SN/REL, Watson-Marlow, UK), draws media from the bioreactor vessel, and the output flow is split between the two flow cells, and then returns it back to bioreactor vessel. Perfluoroalkoxy (PFA) tubing (PFA-T8-062-50, Swagelok, UK) was used. Two regulation needle valves (PFA-4RPS8, Swagelok, UK) were installed before and after each flow cell. Each flow cell was also equipped with a flow meter (FTB332 infra-red light beam micro-flow meter, Omega Engineering, UK) located after the exit regulation valve. After passing through the flow cells, the liquid stream rejoins and returns to the bioreactor vessel.

Flow cells were made from acrylic tubes (6 cm inner diameter, 1 cm wall thickness and 48 cm length). Six pairs of feedthroughs (M20 size fittings, produced by OBO Bettermann, Germany) were installed on each flow cell. A schematic drawing of a flow cell showing its cross section and distribution of feedthroughs is presented in Fig. II.5.

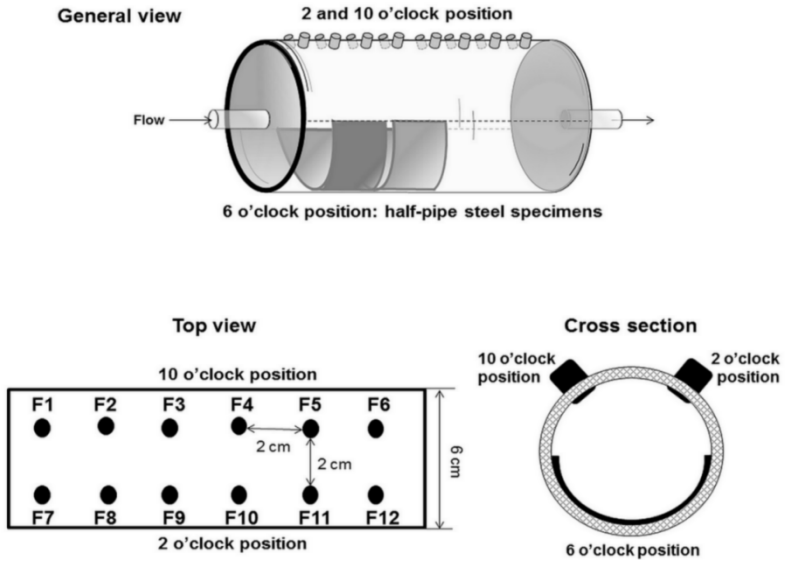

Fig II.5. Scheme, cross-section and fitting distribution of the flow through cell.

Electrodes for the measurements of corrosion rates and open-circuit potentials were installed in the two flow cells, in identical arrangements. The electrode configuration was designed to reproduce that used in offshore electrochemical probes. Six working electrodes (see Section II.1) were installed in the 10 o'clock (F2, F4, and F6) and 2 o'clock positions (F8, F10, and F12), see figure II.5. Each cell was also fitted with four additional electrodes. Two laboratory-made salt-bridges, filled with 2 M KCl solution (VWR, US) were placed between the F1 position in each flow cell and a reference cell, which was also filled with the 2 M KCl solution and fitted with reference electrodes. Electrochemical measurements were performed using Gamry Ref 600 Potentiostat/ Galvanostat/ ZRA unit interacted with PC. An in-house manufactured liquid sampling port with a septum was installed at F7 position in each cell. Further, it was possible to install coupon at 6 o'clock position for monitoring of in line corrosion.

Prior to operation the bioreactor loop was flushed with technical grade alcohol (Kemetyl Norge AS, Norway) and flow cells were exposed for 24 h under UV light (wave length 256 nm: XX-15, sterilization UV lamp, UVP, USA).

II.7.1.2. Continuously fed with fresh media test loop

The main components of the continuously feed with a fresh media test loop (also called "once-through" flow loop) was manufactured in-house and consists of two bioreactor vessels placed one behind the other and two in parallel cylindrical flow-through cells. The "once-through" flow loop set-up is shown in Fig. II.6.

The bioreactor vessels are made of polypropylene. The acryl lid, used for closing the bioreactor vessels, is fitted with an optical oxygen-dipping probe, a temperature sensor interfaced with Fibox 3 fiber optic oxygen transmitter (Presens, Germany), one gas inlet, one gas outlet and a pH electrode (pH-meter HI-9125N, Hanna Norden AB, Sweden). The lid also incorporates an in-house fitted sampling/ fluid injection point. The first bioreactor vessel body was fitted with one fluid injection inlet. Each bioreactor vessel was equipped with one fitting accommodating Teflon tube (Swagelok, UK) via which the two bioreactor vessels were connected. The second bioreactor vessel was also equipped with a heating unit (ISOPAD IP-DASI®, Tyco, USA) and a thermostat (Raychem® AT-TS-14, Tyco Thermal Controls, USA).

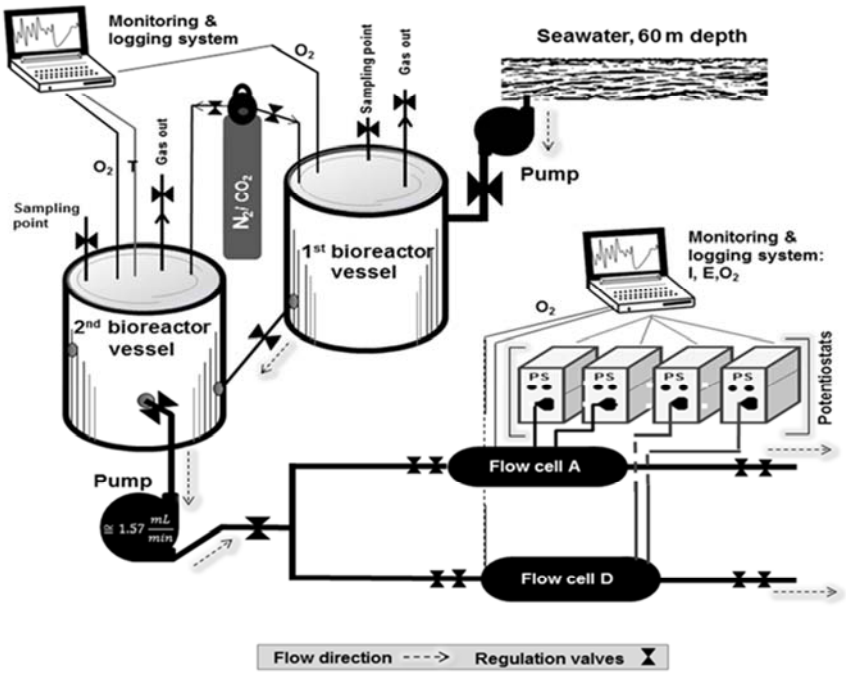

Fig. II.6. Continuously fed with fresh media test loop scheme.

A peristaltic pump (W-M 520SN/REL, Watson-Marlow, UK) drew media from the second bioreactor vessel, and the output flow was split between the two flow cells. Perfluoroalkoxy tubing (PFA-T8-062-50, Swagelok, UK) was used. Two regulation needle valves (PFA-4RPS8, Swagelok, UK) were installed before and after each flow cell. Flow cells were made from acrylic tubes (6 cm inner diameter, 1 cm wall thickness and 34 cm length) and acrylic plates (5 cm × 34 cm × 0.5 cm). Twelve pairs of feedthroughs (M20 size fittings, OBO Bettermann, Germany) were installed on the top of each flow cell. A schematic drawing of a flow cell showing its cross section and distribution of feedthroughs is presented in Fig. II.7. Electrodes (working - WE, counter - CE and reference - Ref) for electrochemical measurements were installed in the two flow cells, in identical arrangements at 12 o'clock positions. Electrochemical measurements were performed using Gamry Ref 600 Potentiostat/ Galvanostat/ ZRA unit interacted with PC. An in-house manufactured liquid sampling port/inlet for dipping oxygen probe (SP) with a rubber septum was installed at F10 position in each flow cell. To monitor biofilm formation, ten carbon steel specimens (rectangular plates with dimensions of a 1 cm × 1 cm × 0.2 cm) were installed at 6 o'clock position in each flow cell.

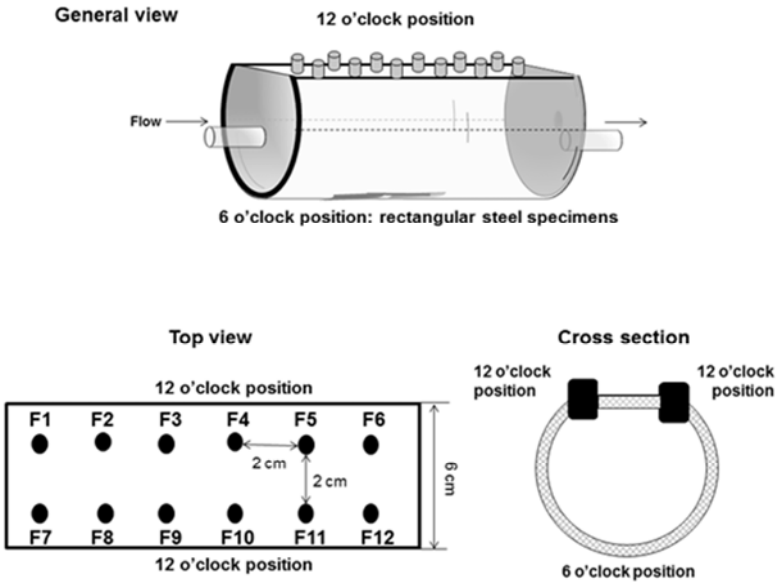

Fig. II.7. Scheme, cross-section and fitting distribution of the flow through cell.

Prior to operation the bioreactor loop was flushed with technical grade alcohol (Kemetyl Norge AS, Norway) and flow cells were exposed for UV light (wave length 256 nm: XX-15, sterilization UV lamp, UVP, USA) for 24 h.

II.7.2. Batch test systems

II.7.2.1. EIS Bioelectrochemical Reactor

The base of the EIS Bioreactor (Figure II.8A) was a modified Schott™ flask of 500 ml. This reactor features a threaded mouth to fit a lid that warranties a controlled atmosphere inside the vessel.

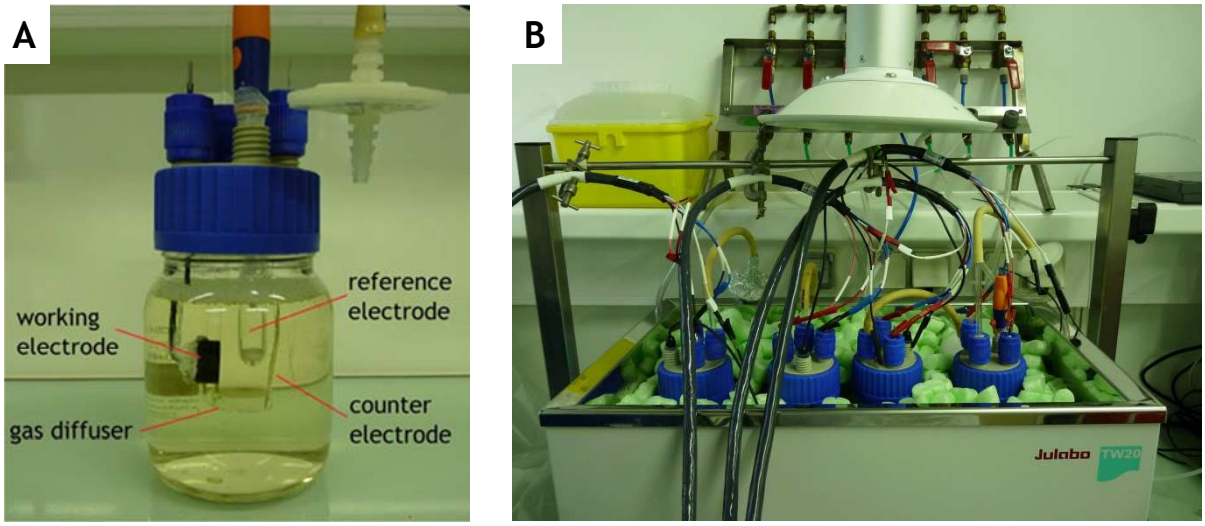

Fig. II.8. Experimentl set-up: A) EIS Biorector; B) multiple-experimens run.

The reactor lid has four openings with caps and fittings used for different purposes; the use of the openings can be described as:

a) Purging system (gas diffuser). A cap and fitting proper to the gas diffuser diameter is used in this opening
b) SCE reference electrode (see Section II.3). No cap is used in this opening
c) Working Electrode Extension. A cap and fittings proper to the working electrode diameter are used (see Section II.1)
d) Counter electrode extension (Platinum). A cap an fittings proper to the counter electrode are used. Beside the cap and fittings, a serum vial cap is used to facilitate the access of needles from this opening (see Section II.2)

Measurements were carried out using a VMP multichannel potentiostat (Bio-Logic, France) connected to a PC interface and monitored with EC-Lab V10.32 software (Bio-Logic, France).

II.7.2.2. Microbially Assisted Stress Corrosion Cracking Experimental set-up

The adjusted Cortest High Temperature Vessels (Cortest, USA) were used as test vessels (Fig. II.9) for assessing the impact of bacterial load on carbon steel while subjected to mechanical stress. These vessels are constructed of a Hastelloy C-276© or Pyrex© bottom and top lids and Hastelloy C-276© or Pyrex© vessel walls. Pyrex© elements of test vessels were used for easy observation of a blackening as a sign of bacterial growth. Fitting on top Hastelloy C-276© or Pyrex© lids were made for installation of in-house manufactured salt-bridges. Vessels, with specimens, were fitted in a tensile test ring (Cortest Proof Rings, Corrtest, USA) used to apply the constant load to the steel specimen as it can be seen in Fig. II.10. All vessels were connected with the reference cell via in-house made salt-bridges.

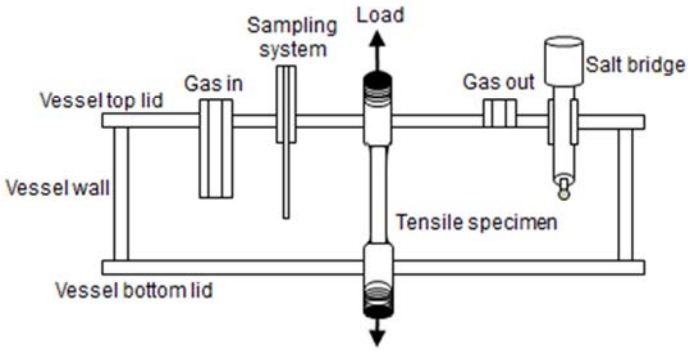

Fig. II.9. Scheme of test vessel with inserted tensile specimen.

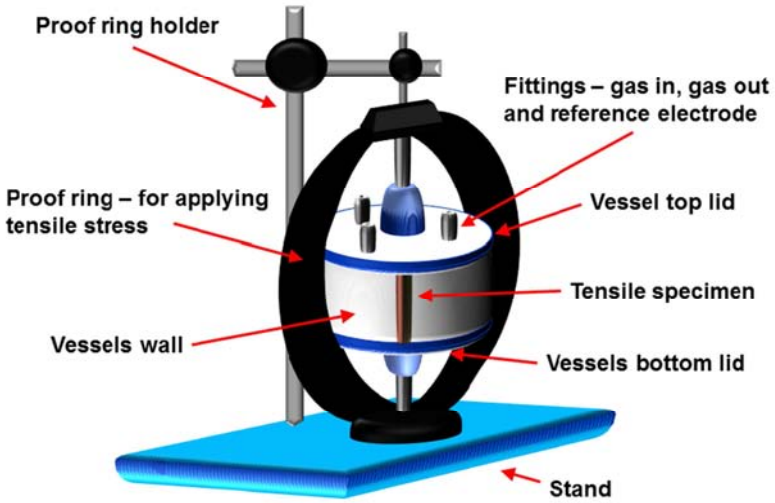

Fig. II.10. Experimental set-up consisting of test vessels installed in tensile test ring.

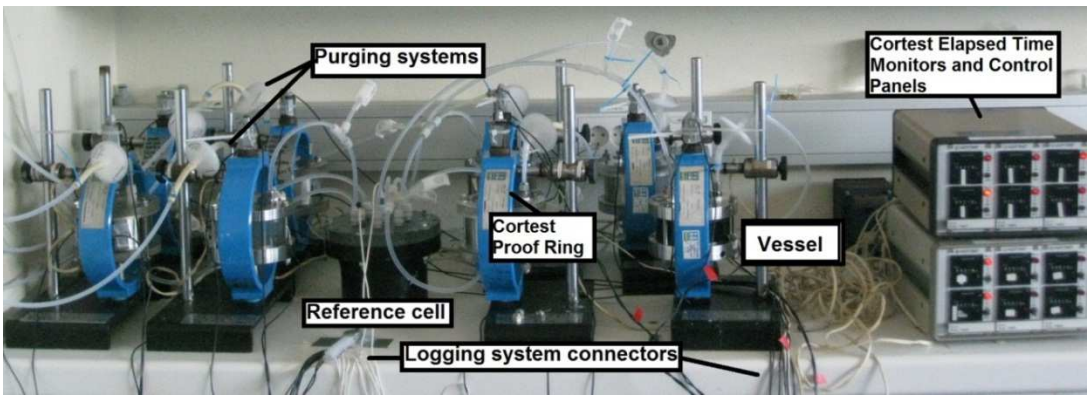

Fig. II.11. Octopus formation of multiple adjusted Cortest High Temperature Vessels interfaced with sensor and logging equipment - multiple test run.

The Cortest Elapsed Time Monitors and Control Panels (Model 52000, Cortest, USA) permitted independent regulation of each Cortest Proof Ring, and together with salt bridge connections provided the possibility to perform multiple tests at once in an octopus formation (Fig. II.11). Electrochemical monitoring was performed using a Gamry Ref600 Potentiostat/Galvanostat/ZRA (Gamry Instruments, USA) unit interacting with a PC or logging system comprising of SCXI-1001 chassis fitted with SCXI modules and controlled by LabVIEW software (National Instruments, USA).

II.8. Corrosion evaluation: methods and techniques

II.8.1. Weight loss

The most used corrosion method for measuring corrosion rates. Design of a particular weight loss determination/test can be different, in dependence to the information we need to obtain must consider the characteristics of the system undergoing corrosion; therefore coupons of different sizes and shapes are used to study different types of corrosion. However, measurements are reliable only a number of assumptions are made: general corrosion, the size and geometry of the coupon…

This chapter is presenting a brief procedure for the weight loss determination for low carbon steel in mild electrolyte. The procedure is separated in five distinct parts:

1. preparation of the coupons;
2. preparation of the test reservoirs;
3. test execution;
4. cleaning the coupons;
5. calculation of the corrosion rate.

In herein reported studies carbon steel specimens were weighted prior- to and post- immersion. All test coupons were ground manually using SiC paper of increasingly fine grain, ending with 600-grit (grinding debris were rinsed off the electrode surface with sterile deionized water) before immersion weighting. All test coupons were cleaned of corrosion product before post immersion weighting. Corrosion products were removed by introducing specimens for 30 s in a 5% (v/w) hexamine (Merck, Germany) in concentrated HCl (VWR, USA). This step was immediately followed by rinsing with deionized water, gentle blotting with a paper towel, and overnight storage in a desiccator. The perfectly dried tensile specimens were weight in an analytical balance. From obtained weight loss corrosion rate was calculated according to:

$$\text{corrosion rate (mmpy)} = \frac{0.465 \times X}{t \times A} \qquad \text{(Eq. I.1)}$$

Where:

0.465 - factor accounting for the dimensional analysis and the density of the steel

X - difference between “initial weight” and “weight after cleaning” in milligrams

t - exposure time in days

A - total area of the coupon in cm^2

II.8.2. Electrochemical methods

II.8.2.1. Open Circuit Potential (OCP)

The Open Circuit Potential (OCP) of ferrous alloys is measured versus a stable reference electrode (assuming no interferences from biofouling or any other scale). For a free-corroding metallic sample, the OCP is equivalent (numerically equal) to the corrosion potential (E_{corr}). Moreover, OCP values can provide worthwhile information about metals behavior, such as tendencies to ennoblement. Briefly, ennoblement of ferrous metals in presence of biofilms most often leads to a breakdown potential which could initiate crevice or pitting corrosion [Little and Lee, 2007]. This event is much faster in biotic environments compared to abiotic conditions. Nonetheless, corrosion-rate evaluation based purely on OCP has certain limitation and cannot provide any insight in corrosion mechanisms.

The OCP measurements were performed with a 34401A $6^{1/2}$ digital multimeter with input impedance of 10 GΩ (Agilent, USA), or they were carried out using multichannel potentiostats; MultEchem™ (Gamry Instruments, USA) that consisted of two Reference 600TM Potentiostat/Galvanostat/ZRA independent units connected to a PC interface and monitored with DC105 (Gamry Instruments, USA) or VMP (Bio-Logic, France) connected to a PC interface and monitored with EC-Lab. OCPs of steel specimens were measured versus SCE.

II. 8.2.2. Direct Current (DC) - electrochemical polarization techniques

In the regions of the large anodic and cathodic overpotentials, correlation between electrode potential and logarithmic value of current density is linear. From polarization scan it is possible to extract values of Tafel slopes angles (β_a, β_c), corrosion current (i_{corr}) and corrosion potential (E_{corr}) also known as an Open Circuit Potential (OCP) (see Section II. 7.2.1) as it is shown on Fig. II.12. Due to fact that Tafel extrapolation is linear, it is possible to use Stern-Geary equation [Stern and Geary, 1957]:

$i_{corr} = \frac{1}{Rp}\frac{\beta a \times \beta c}{\beta a + \beta c} = \frac{B}{Rp}$ (Eq. II.2), where $B = \frac{\beta a \times \beta c}{2.303 \times (\beta a + \beta c)}$ (Eq. II.3) is known as Tafel constant.

Equations II.2 and II.3 are valid if both, cathodic and anodic processes are under activation control. If cathodic process is under diffusion control then equation becomes or is rewritten as:

$$i_{corr} = \frac{\beta a}{2.303 \times Rp} \qquad \text{(Eq. II.4)}$$

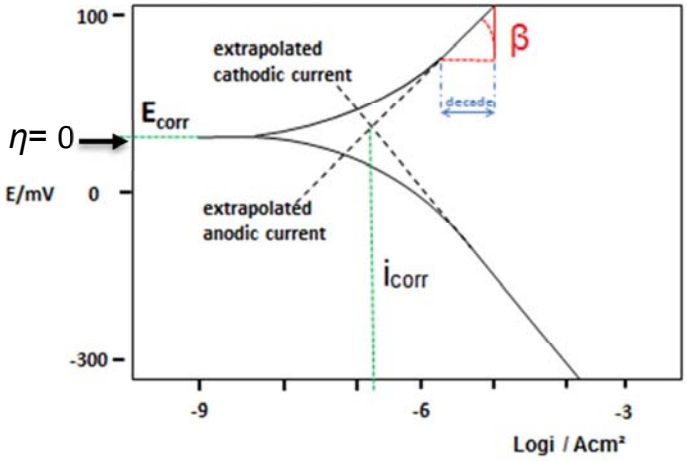

Fig. II.12. Principle of Tafel extrapolation.

In the linear polarization technique (LPR), the Stern-Geary resistance to polarization (R_p) of a metal is measured in the electrolyte of interest in the vicinity of the OCP. Even though this principle was known for many years, Milton Stern [Stern, 1958] in 1958 was first to introduce it for determination of corrosion rate. If applied properly, it is a sensitive electrochemical method for evaluation of materials resistance to corrosion e.g. "instantaneous" corrosion rate [Skold and Larson, 1957]. When all parameters of Stern-Geary equation (Eq. II.2) are know, it can be used as a method to extract "real" corrosion rate.

From mathematical point of view, R_p can be defined as a tangent of polarization slope at corrosion potential (when overpotential is zero). In the area close to equilibrium potential, exponential Butler-Volmer equation (see Appendix I) can be linearized (Taylor's theorem):

$$i = (i_o \frac{zF}{RT})\eta_{equilibrium} \qquad \text{(Eq. II.5)}$$

With assumption that overpotential tends towards zero (no polarization present in system) it is possible to extract tangent on a polarization slope:

$$(\frac{\partial \eta}{\partial i})_{\eta \to 0} = \frac{R \times T}{z \times F \times io} = R_e \qquad \text{(Eq. II.6)}$$

Tangent on a polarization slope is known as a resistance to charge transfer and is a direct measure of electrochemical reaction kinetics e.g. corrosion reaction. R_e can be easily presented as a polarization resistance (R_p) and calculated from Stern-Geary equation (Eq. II.2):

$$R_p = (\frac{\partial E}{\partial i})_{E = Ecorr} \quad \text{(Eq. II.7)} \quad \text{or} \quad R_p = (\frac{\Delta E}{\Delta i})_{\Delta E \to 0} \quad \text{(Eq. II.8)}$$

A great advantage of LPR is that it can be applied under stationary and dynamic conditions by applying voltage signals with low amplitudes (for example: IηI = ±20 mV vs. E_{corr}). Mansfeld [Mansfeld, 1973] attributed this to linearity of current-potential slope in range of ±20 mV vs. E_{corr} (Fig. II.13).

Furthermore, if R_p is known it is possible to use Stern-Geary equation (Eq. II.2) to calculate corrosion current (i_{corr}).

Simplicity of LPR is exhibiting many benefits when used for approximative measurements/calculations of material resistance to corrosion. In this case Tafel constant (B) used in Stern-Geary equation is assumed. This assumption is limiting accuracy of information obtained in LPR scan. On the opposite, when Tafel constant (B) is obtained by some other electrochemical technique, than more reliable information on material corrosion resistance can be acquired.

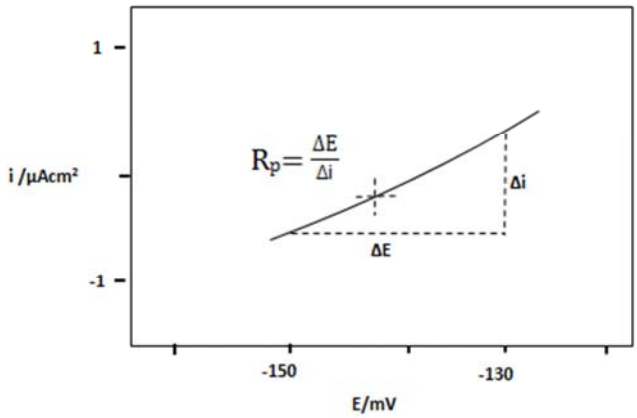

Fig. II.13. Determination of polarization resistance [Mansfeld, 1973].

Furthermore, once when R_p is calculated it can be mathematically converted into Corrosion Rate (CR):

$$CR = (i_{corr} \times K \times EW) / (\rho \times A) \quad \text{(Eq. II.9)}$$

Where:

i_{corr}	Corrosion current in A
K	Constant that defines the units for the corrosion rate
EW	Equivalent weight in grams/equivalent
ρ	Density in grams/cm^3
A	Sample area in cm^2

Thanks to its ability to produce instantaneous corrosion rates and despite being slightly inaccurate, LPR is the most common technique used for determination of corrosion rate in industry. Its wide use in the electrochemical laboratories resides in the capability to leave the systems under scrutiny practically undisturbed [Walter, 1977]. However, it is not recommended for sensitive samples, i.e. biofilms [Lee and Little, 2007].

Moreover, the applicability of LPR and R_p are, to a certain extent, limited due to:

- calculation of corrosion current based on the Stern-Geary R_p are not applicable in a case of localized corrosion, although some attempt were made [Jones and Greene, 1969];

- in presence of high concentrations of aggressive sulfide ions and hydrogen sulfide the accuracy and reliability of technique is questionable [Hilbert *et al*., 2007];

- formation of surface films is affecting the electrochemical response and therefore effecting measurements [ASTM G96-90, 2001].

In the current work, the Linear Polarization Resistance (LPR) were carried out using a multichannel potentiostat MultEchem™ (Gamry Instruments, USA) that consisted of two Reference 600TM Potentiostat/Galvanostat/ZRA independent units connected to a PC interface and monitored with

DC105 or multichannel potentiostat VMP (Bio-Logic, France) connected to a PC interface and monitored with EC-Lab. To determine of R_p, the potential was scanned in the range of OCP ± 10 or 20 mV (with OCP measured using potentiostat) and a sweeping rate of 0.167 mV s^{-1}.

II.8.2.3. Alternative Current (AC) electrochemical techniques

II.8.2.3.1. Electrochemical Frequency Modulation (EFM)

EFM technique allows investigating the material corrosion resistance without perturbing the material under study. This specific technique is usually applied for the determinations of corrosion rate when the Tafel constants are not previously known. Further, according to some authors [Rauf and Bogaerts, 2010] it can indicate occurrence of localized electrochemical process on specimens surface; e.g. pitting, trough analysis of causality factors; e.g. causality factor 2 (CF2) and causality factor 3 (CF3), deviations. These qualities, recommends EFM for laboratory investigations as well as for on-line field monitoring.

While using EFM, a potential perturbation signal composed of two sinusoids waves is applied to any corroding specimen to get the alternating current response. The complex alternating current response is corresponding to different harmonic and intermodulation frequencies. To calculate kinetic corrosion parameters and corrosion rates form obtained current response EFM technique use nonlinearity in the voltage-current response of the electrochemical interface [Frankel, 2008; Kuş and Mansfeld, 2006; Rauf and Bogaerts, 2010; Rauf and Mahedi, 2012]. The principle of EFM is shown in Fig. II.14.

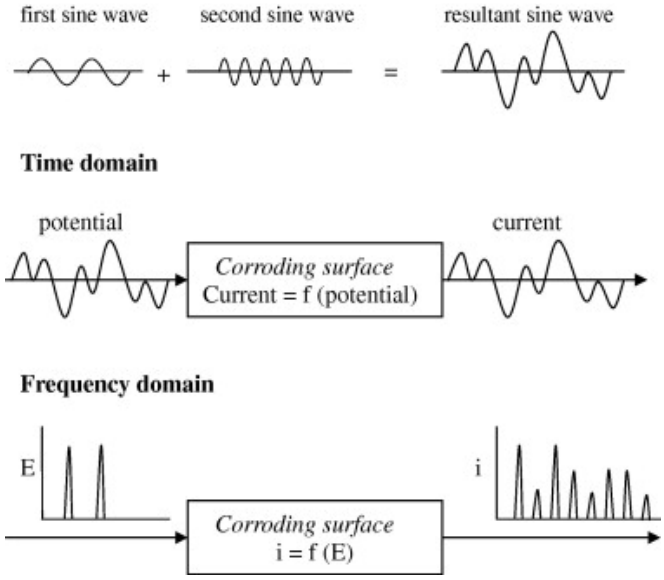

Fig. II.14. Principle of EFM [Rauf and Bogaerts, 2010].

The stepwise analysis of the EFM output signal starts with the inserting input information on reaction mechanism for system under investigation: activation or diffusion control. It can be assumed activation control or diffusion control to be the dominating corrosion process and this assumption is taken in further calculations. Secondly, alternating current signals is transferred via a Fast Fourier Transformations (FFT) in the frequency domain. The resulting alternating current versus frequency curve is known as the "*intermodulation spectrum*". Thirdly, intermodulation spectrum typically displays two distinguished peaks at two applied frequencies of input voltage signals (for example 2Hz and 5Hz). Most often, peaks observed in the region between 1 µA - 20 µA stands for the harmonics of the two excitation frequencies and they are used to calculate the corrosion current and the Tafel constants. Fourthly, the obtained corrosion current and Tafel constants are used for calculation of corrosion rate.

The values of the causality factors CF2 and CF3 can be used for evaluation of acquired data in case of a prevailing general corrosion mechanism or for detection of localized current events as in a case of pitting corrosion. In general, if CF2 and CF3 values are close to values of 2 and 3, it is considered that measurements are conducted correctly and obtained corrosion rates are valid [Rauf and Bogaerts, 2010]. Nevertheless, this generally accepted rule could be misleading as was showed by Kuş and

Mansfeld [Frankel, 2008; Kuş and Mansfeld, 2006] in a case of mild steel corrosion in NaCl solution. On several occasions it have been demonstrated that EFM may show contradictory results when applied to corrosion rate determination. When applied for measurement of high corrosion rates, it provides valid and reasonable values [Frankel, 2008; Kuş and Mansfeld, 2006]; on the other hand, when applied for measuring of low corrosion rates, it provides high and non-reliable values for CR [Bosch and Bogaerts, 1996].

Furthermore, CF2 and CF3 can be applied as a valuable tool for detection of localized corrosion. One example is the work of Rauf [Rauf and Bogaerts, 2010; Frankel, 2008; Kuş and Mansfeld, 2006] who proposed causality factor evaluation mode in presence of localized corrosion. According to proposed model, when localized corrosion is taking place, CF2 and CF3 deviate from value 2 and 3. So far, values of CF2 and CF3 above values of 2 and 3 have been considered as a week indication of pitting corrosion at room temperature [Rauf and Mahedi, 2012]. The same report shows that when CF2 shows values higher than 2 and CF3 shows lower values that 3 could be indication of crevice corrosion at room temperature.

The electrochemical test describe further in this chapter were achieved as follows: A three-electrode arrangement was used for performing the EFM on carbon steel tensile specimens in different test media. The tensile specimen was used as working electrode, while either the Hastelloy C-276© bottom lid or a vessel wall was used as counter electrode. EFM measurements were carried out using a multichannel potentiostat MultEchem™ (Gamry, USA) consisting of two Reference 600TM Potentiostat/Galvanostat/ZRA independent units connected to PC interface and monitored by EFM140® software (Gamry, USA). Applied perturbation sinusoidal wave was composed of sum of two sinusoidal waves with frequencies of 0.02 Hz and 0.05 Hz. Applied overpotential was 10 mV/ SCE.

II.8.2.3.2. Electrochemical Impedance Spectroscopy (EIS)

The Electrochemical Impedance Spectroscopy (EIS) is a method designed to avoid severe deterioration of the exposed surface and was widely used for studying electron transfer reactions, surface properties and monitoring the corrosion of a working electrode [Bard and Faulkner 2000; Orazem and Tribollet, 2008]. The EIS studies the specimen response in a transfer function to the perturbation by a periodic low amplitude sinusoidal wave signal in steady-state condition (Fig. II.15). The input signal is usually voltage and resulting response is usually current making a transfer function. EIS measurements most often are carried out at different frequencies. Analysis of the specimens' response contains information about the interface, its structure and electrochemical reactions taking place on it.

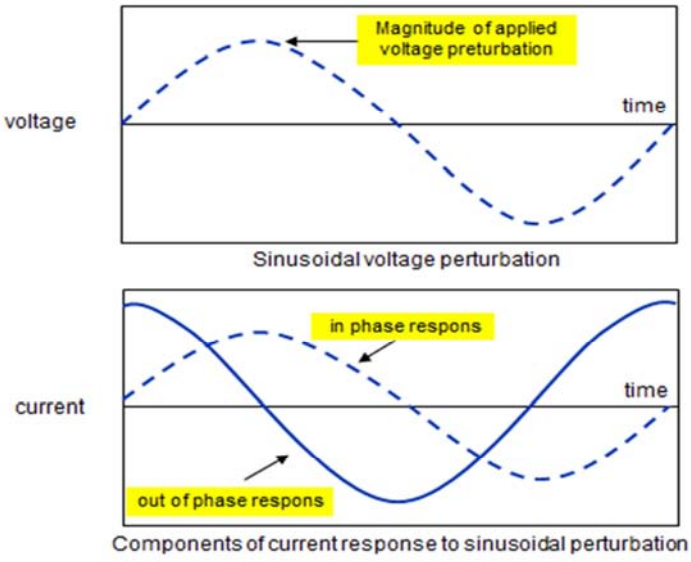

Fig. II.15. Principle of Electrochemical Impedance Spectroscopy (EIS).

Impedance data are acquired as a function of the frequency of perturbation signal at steady state reference point (for example in corrosion studies, reference point is usually corrosion potential where

current is equal to zero) of a polarization curve. Scan frequency range determinate the range of studied surface events and quality of the acquired impedance spectrum. Selected range allows identification of specific events, for example; measurements at high frequencies reveal information about electrolyte resistance while measurements preformed at low frequencies provide information about adsorption/desorption phenomena [Gabrielli, 1998].

As mentioned earlier, EIS provides information on the different components that contribute as structural blocks to overall studied system architecture. For that reason it provides:

- information required for construction of representative electrical model for system under investigation.

- data on the resistance of the solution (R_s), capacitance of double layer or formed deposits layer ($C = C_{dl}$ or C_l), polarization resistance (R_p) or charge transfer resistance (R_{ct}) [Cottis and Turgoose, 1999].

In addition, EIS can offer an insight on the layers formed on studied surfaces, for example: oxide layer, biofilms, iron-sulfide corrosion products or protective coatings, and how they affect charge transfer [Mansfeld, 1990; Manohar *et al*., 2008; Malard *et al*., 2008].

Once the data are obtained, they can be processed on several ways, and usually gateway to further analysis is drawing appropriate diagram. Most common graphical data representation is by:

1. Nyquist Plots, also known as a complex plane plots, gives the dependence of the imaginary part of the impedance (Z'') on the real part of the impedance (Z')
2. Bode Plots, display different impedance parameter (|Z|, Z'', Z' or phase angle) as a function of frequency (f).

According to the shape of the plots and basic assumptions regarding nature and structure of system under investigation, it is possible to model its electrochemical behavior by creating an equivalent Electric Circuit (EC) comprised of different electrical elements resembling specific part and/or interaction of the studied system. Precondition for a proper EIS modeling is that the selected EC model can fit to physically reasonable/possible explanation of studied system and to physico-chemical events taking place in it [Cottis and Turgoose, 1999]. EC models can offer quantitative information about EC constructive blocs, such as R_s, C, R_p, etc, if the equivalent circuit is correct. For corrosion studies the possibility to estimate corrosion rates form acquired EIS data is of great importance. Furthermore, EIS allows the use of charge transfer resistance for corrosion rate estimation separately from polarization resistance corrosion estimation [Cottis and Turgoose, 1999]. Impedance of corrosion or electrochemical systems can reflect a time constant distribution that is usually represented with the Constant Phase Element (CPE) replacing Capacitance (C) in equivalent circuits. CPE explains phenomena occurring on interface as a result of surface porosity and inhomogeneity (corrosion layer), surface roughness (local metal dissolution or effect of polishing)…

Even though graphical representation represents the foundation for further EIS analysis, it is needed to keep in mind that each of the graphical data representation methods has its limitations, and key data and information can be camouflaged by certain graphical representation. For example in the Nyquist representation high frequency limit corresponding to R_s, could be visually hidden.

EIS as a method used for MIC studies has a long history due its non-invasive nature. Previously it was shown that perturbations of the corroding surface subjected to EIS measurements are insignificant for number, viability and activity of microorganisms found with in biofilms [Dowling *et al*., 1988; Franklin *et al*., 1991]. Even thought, EIS is a technique oriented towards general corrosion measurements, some more complex modes were developed for fitting localized corrosion events [Mansfeld *et al*., 1982, 1995] often taking place on specimen's surfaces in presence of microorganisms and biofilms [Little and Lee, 2007]. In recent years, specialized experimental apparatus and nano-electrodes [Suter and Bohni, 2001] for measuring localized impedance were developed, and new technique emerged, Localized Electrochemical Impedance Spectroscopy (LEIS) capable of characterizing localized deterioration processes occurring on metal surfaces [Annergren *et al*., 1997, 1999] and therefore possessing a great potential for studying MIC.

EIS is often employed as a tool for studying corrosion processes in presence of different sulfidogenic microorganisms, e.g. SRBs. Effect of SRBs on corrosion process itself and magnitude of carbon steels

deterioration was investigated by means of EIS [Domfnguez-Benetton and Castaneda, 2005; Miranda *et al*., 2006; Mallard *et al*., 2008; Sahrani *et al*., 2009; AlAbbas *et al*., 2013].

Herein reported experiments were carried out in stagnant conditions (static working electrode and solution). EIS diagrams were plotted at OCP that was measured continuously during the whole test duration, with a frequency domain ranging from 10 kHz to 10 or 1 mHz, 7 points per decade, and amplitude of 10 mV peak-to-peak. Electrochemical measurements were collected by means of an EC-Lab SP-200 system from Bio-Logic.

II. 8.2.4. Electrochemical Noise (EN)

Electrochemical Noise (EN) refers to naturally occurring fluctuations in corrosion potential and corrosion current. The EN data can be obtained as fluctuation of the potential (*E*), as fluctuation of potential (*E*) at an applied current (*I*), or as fluctuations of current (*I*) at an applied potential (*E*) [Little and Lee, 2007]. Signals obtained with the EN measurements can be subdivided into electrochemical potential noise (EPN) measurements and electrochemical current noise (ECN) measurements.

Possibilities for the EN applications in the corrosion investigations and for corrosion monitoring are vast. The most interesting application of EN is in Zero Resistance Ammeter (ZRA) mode. In ZRA mode current fluctuation between two identical electrodes are measured with ZRA and potential fluctuations are measured with a high-impedance voltmeter between coupled electrodes and stable reference electrode. In a case of a general corrosion, the combinations of EPN and ECN obtained by measurements in ZRA mode can be used to estimate corrosion rates; the methodology is related to measuring the well-known polarization resistance (R_p). The electrochemical noise resistance (R_n) is defined as the ratio of the standard deviation of the potential noise to that of the current noise between two identical working electrodes, which are linked by a ZRA [Padilla-Viveros *et al*., 2006]. To verify the accuracy and reliability of method and parameter, R_n has been compared with R_p. It was confirmed to be similar (or equivalent) to R_p when impedance is independent of frequency in the bandwidth of the EN measurement [Nagiub and Mansfeld, 2002].

Furthermore, acquired EN signal can be visually analyzed; shapes of modulated current and potential signals are indicative of general corrosion or pitting corrosion [Padilla-Viveros *et al*., 2006; Jiang and Nešić, 2008] (Fig. II.18). Briefly, the rapid current increase during pit initiation and growth is followed by a slower decay after pit repassivation (Fig. II.16).

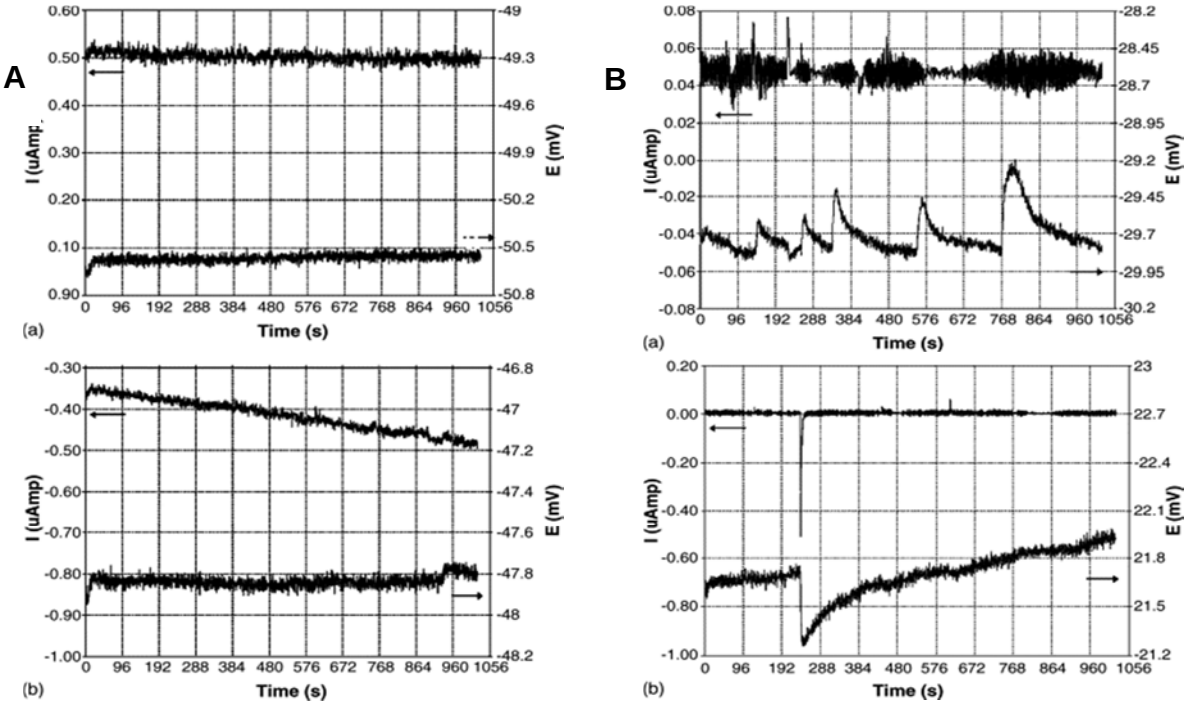

Fig. II.16. Current and potential records for the systems characteristic for: **A)** general corrosion in the presence of *D. alaskensis* strain IMP-7760 in nutritionally rich organic culture conditions; **B)** pitting corrosion in the presence of *D. alaskensis* strain IMP-7760 in oligotrophic conditions [Padilla-Viveros *et al*., 2006].

In addition, a potential drift can reveal information about formation of protective/ partially protective corrosion products; in that case it is particularly pronounced [Cottis and Turgoose, 1999].

Moreover, statistical analysis of ECN and EPN provide the investigator with extensive spectrum of parameters that can be indicative of a prevailing corrosion mechanism as well as of a localized electrochemical surface reactions occurring on studied surface. The Localization Index (LI) is the most frequently used statistical parameter, and it is calculated as a standard deviation of the current noise divided by the root mean square (rms) of current noise [Cottis, 2001]. LI ranges in value from 0 to 1 and it is able to discriminate between the three different corrosion mechanisms (general corrosion i.e. general corrosion zone, mixed corrosion i.e. mixed zone, and localized corrosion i.e. localized corrosion zone) as shown on Fig. II.17 [Men *et al*., 2011; Arteaga *et al*., 2012; Eden, 1998]. Despite the fact that LI capability to indicate occurrence of surface localized events, such as pitting, was repeatedly experimentally supported, one has to take precaution when using LI due to its theoretical limitations [Cottis, 2007; Al-Mazeedi and Cottis, 2004; Mansfeld and Sun, 1999; Sanchez-Amaya *et al*., 2005]. In general conclusion, LI should be considered as a measure of the deviation of a system from the assumed ideal behavior and not as an indicator of corrosion mechanisms [Mansfeld and Sun, 1999].

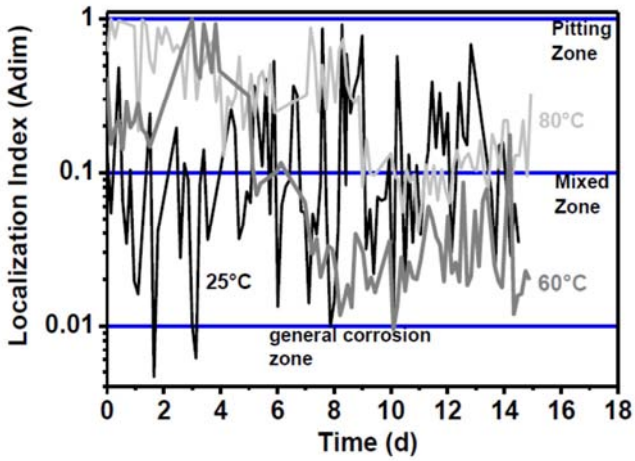

Fig. II.17. Localization Index (LI) of carbon steel at three deferent temperatures in graph indicting three separated corrosion mechanism zones [Arteaga *et al*., 2012].

Other statistical parameters often employed for the identification of changes in the noise signals distribution (i.e. during localized surface events or pitting processes or passive layer breakdown) are Skewness and Kurtosis. Skewness is a third order-statistic, and it is derived as a third moment divided by the cube of the standard deviation [Bury, 1999]. Kurtosis is a fourth-order statistic, derived by dividing the fourth central moment by the fourth power of standard deviation [Bury, 1999].

Skewness and Kurtosis reflect symmetry and peakness in distribution of acquired signals [Bury, 1999; Mansfeld *et al*., 2001]. Hence, their high values point to sudden changes occurring on the metal surfaces and have been used for corrosion mechanism identification [Barr *et al*., 2000, Mansfeld *et al*., 2001]. Numerical values of the skewness and kurtosis indicative to corrosion mechanism are well established [Reid and Eden, 2001].

Although, EN is relatively novel electrochemical technique is has been employed often in laboratory and field MIC studies. Repeatedly it has be used for studying pitting corrosion induced by SRB biofilms and their metabolites [Borsia and Yang, 2003; Huet *et al*., 2002; Padilla-Viveros *et al*., 2006; Galvan-Martinez *et al*., 2010].

Here presented ECN and EPN data were recorded with data sampling rates of 0.1 Hz, 0.2 Hz and 1Hz, a current range of 60 µ to 600 mA, a potential range of +/- 30 mV to 3V, a current resolution of 1 pA and a voltage resolution of 1 µV. Data were sampled at 0.1 Hz, 0.2 Hz and 1 Hz frequency. Acquired EN data were analyzed in the sequence-independent domain within data blocks of 128 sampling data points, and thus the time resolution for each calculated statistical parameter is 21.3 min. Statistical

parameters such as localization index (LI), skewness and kurtosis were calculated. Modulated current and potential signal patterns, as well as transients, characteristic of localized surface events, were visually examined within data blocks of 100 (0.1 Hz sampling frequency), 200 (0.2 Hz sampling frequency) and 1000 or 10000 (1 Hz sampling frequency) points resulting with the time resolution of 1000 seconds.

II.9. Surface analysis

Surface analysis was conducted in order to obtain general information relating to the microstructure of the used carbon steel and later on about degradation topography (optical microscopy). By using a Scanning Electron Microscopy (SEM) it was possible to capture different morphologies of organic nature, e.g. bacteria, as well as corrosion and biomineralization products morphologies.

II.9.1.Optical microscopy

One of the most commonly used tools in metallography is the optical microscope and the most frequently used microscope is the conventional light microscope. Microscopes are required for the examination of the microstructure of the metals. Optical microscopes are used for resolutions down to roughly the wavelength of light (about half a micron). In principle, optical microscopes may be used to look through specimens ("transmission") as well as at them ("in reflection"). However, many materials do not transmit light and the user is therefore restricted to looking at the surface of the specimens with an optical microscope.

The topography of the steel specimens was characterized using optical imaging with a Leica upright DMR microscope (Leica Microsystems GmbH, Germany) and attached ProgRes® C5 camera (JENOPTIK Optical Systems GmbH, Germany). All micrographs were recorded at 50x, 100x, 200x or 500x magnification. Prior to microscopic examination, the steel specimens were cleaned from corrosion products by immersion in a 5 (v/w)% hexamine (MERCK, Germany) solution in concentrated HCl (VWR, USA) or in AP2 solution (gL^{-1} of distilled water: 200, NaOH; 30, KMnO4) for 30 seconds. Rinsing with deionized water, gentle blotting with a paper towel, and overnight storage in a desiccator immediately followed.

II.9.2. Scanning Electron Microscope (SEM)

A Scanning Electron Microscope (SEM) is a type of electron microscope that produces images of a sample by scanning it with a focused beam of electrons. The electrons interact with electrons in the sample, producing various signals that can be detected and that contain information about the sample's surface topography and composition. The electron beam is generally scanned in a raster scan pattern, and the beam's position is combined with the detected signal to produce an image.

The morphology and chemical composition of formed surface deposits as well as steel surface topography were investigated using three different systems:

i) High resolution scanning electron microscope (SEM) JSM-7400F (Joel, Japan);
ii) Low vacuum table SEM TM3000 (Hitachi, Japan) interfaced with energy dispersive X-ray spectroscopy (EDX) system Quantax 70 (Bruker, USA);
iii) SEM Neon 40 EsB (Zeiss, Germany) equipped with a Inca EDX-System (Oxford Instruments, UK);

Different sample preparation protocols:

i) SEM examination of deposits:

a. The specimens were dried under nitrogen stream;
b. The specimens were rinsed with deionized water and dried in desiccator during 24 h;
c. In order to fix the biofilm/ corrosion products layer, the steel specimens were placed in 2.5% w/v glutaraldehyde (Electron Microscopy Science, USA) for 90 minutes at 4℃, and then washed by four 15 min immersions in 0.1M sodium cacodylate buffer (Merck, Germany). Post-fixation was carried out by placing specimens for 1 h in the solution of 1% w/v osmium tetroxide (purity>99.95%, Electron Microscopy Science, USA) in 0.1 M sodium cacodylate buffer (MERCK, Germany). Post-fixed samples were washed in 0.1 M sodium cacodylate

buffer (2×20minutes) and dehydrated performing the following immersions: 15 minutes in 30% v/v, 15 minutes in 50% v/v, 20 minutes in 70% v/v, 2×15 minutes in 96% v/v and 2 x15 minutes in 99.8% v/v aqueous ethanol solutions (Sigma-Aldrich, Norway). De-watered specimens were placed in an oven (Type TS 4057, Thermaks AS, Norway) at 37℃ overnight. Dried samples were mounted on an aluminum stub using adhesive carbon tape, sputter-coated with gold for 3-6 minutes.

ii) Examination of steel surface topography:

a. Deposit removal by immersion in a 5 (v/w) % hexamine (Merck, Germany) solution in concentrated HCl (VWR, USA) for 30 seconds. This was immediately followed by rinsing with deionized water, gentle blotting with a paper towel, and overnight storage in a desiccator;
b. Deposit removal by immersion in AP2 solution (g L^{-1} of distilled water: 200, NaOH; 30, $KMnO_4$) followed by rinsing with deionized water
c. Etching was performed using standard Nital-etching solution (10 (v/v) % HNO_3 in ethanol).

II.9.3. Dye penetrant tests

Dye penetrant tests were used to test for surface cracks in the case when samples were mechanically stressed. Dye penetrant testing is a commonly used Non-Destructive Testing (NDT) method. They are based upon capillary action, where surface tension fluid low penetrates into surface-breaking discontinuities. Several techniques are used for penetrant application to the investigated specimen: dipping, spraying and brushing. After adequate penetration time (depending on penetrant type), the excess penetrant is removed by water or cleaning solution. In a next step a developer is applied. The developer helps to draw penetrant out of the flaw and a previously invisible indication becomes visible to the inspector. Inspection is performed under ultraviolet or white light, depending upon the type of dye used; fluorescent or non-fluorescent.

Bycotest dye penetrant kit was used for the dye penetration testing. This kit consists of Bycotest RP 20 (color contrast penetrant), C10 (penetrant remover) and D 30 A (solvent based developer).

II.10. Elemental analysis

II.10.1. Energy Dispersive X-Ray Spectroscopy (EDX)

Energy Dispersive X-ray Spectroscopy (EDX) was used for studying the chemical composition of corrosion product surface layers and the chemical composition of bare carbon steel surface. EDX is semi-quantitative analysis method. The electrons bombarding are exciting the sample to a higher energy state. When the element (atom) returns to its original energetic state, it emits X-ray energy at different wavelengths that is characteristic for each element, which in turn is collected by a detector. Collected signals (peeks) are processed by the EDX software, which matches the peak locations (on the x-axis) with known wavelengths for each element. The principle of EDX is shown in Fig. II.18.

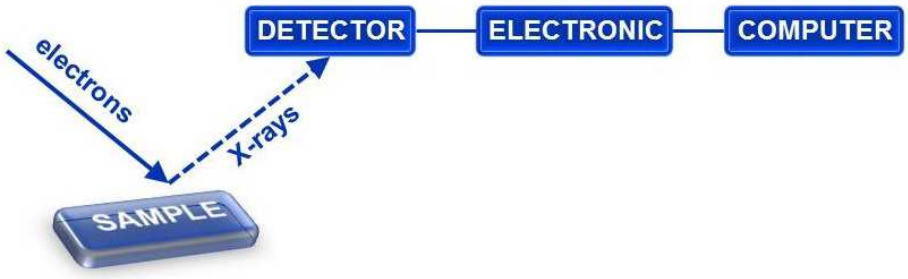

Fig. II.18. Principle of Energy dispersive X-ray spectroscopy (EDX).

EDX analysis is very good at determining what elements are present in samples that are as small as one micrometer, and most elements are detected at concentrations on the order of 0.1%. Results are

plotted with X-ray wavelength on the X-axis and intensity on the Y-axis with each peak labeled with its corresponding element.

Elemental analysis of the specimen's surface prior and post exposure in different experimental environments was conducted with EDX acquisition system (Voyager®, NORAN Instruments Inc., USA) or with EDX system Quantax 70 (Bruker, USA).

II.10.2. Elemental analysis by Inductively Coupled Plasma–Atomic Emission Spectroscopy (ICP-AES)

Inductively Coupled Plasma–Atomic Emission Spectroscopy (ICP-AES) was used for determining the chemical composition of seawater, the total amount of dissolved iron during different experimental stages, as well as identifying the dissolved corrosion product's chemical composition, e.g. inorganic cations and anions. The emission spectrophotometric technique, used for the detection of trace metals detects energy emitted at a specific wavelength by excited electrons as they return to their ground state. Each element emits energy at specific wavelengths specific to its chemical character that is the theoretical base for this technique. In the case of ICP-AES, inductively coupled plasma is used for putting atoms of different elements in an excited state at which they emit energy (electromagnetic radiation) at multiple wavelengths. Atom excitation is followed detection of wavelengths (single or multiple) and radiated energy by emission spectroscopy. The intensity of the energy emitted at the chosen wavelength is proportional to the concentration of particular element in the analyzed sample. Principle of ICP-AES is shown in Fig. II.19.

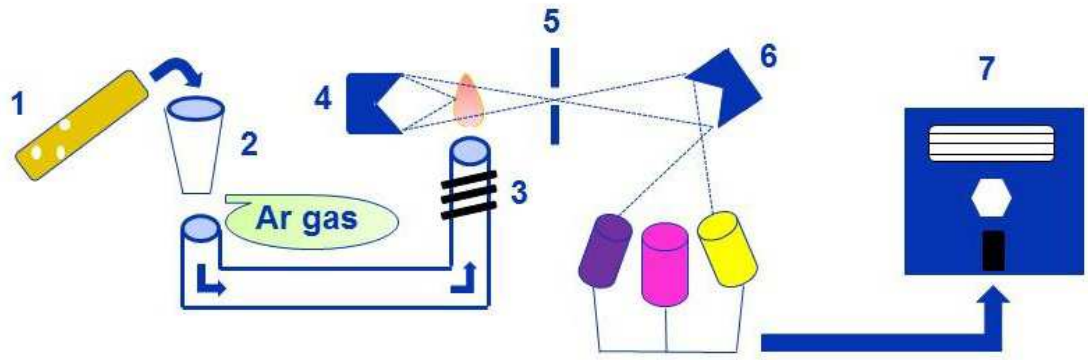

Fig. II.19. ICP-AES principle: In an inductively coupled plasma-atomic emission spectrometer the (1) aqueous sample is pumped and (2) atomized with argon gas into the (3) hot plasma. The sample is excited, emitting light wavelengths characteristic of its elements (4) A mirror reflects the light through the (5) entrance slit of the spectrometer onto a (6) grating that separates the element wavelengths onto (7) photomultiplier detectors.

Therefore, by determining which wavelengths are emitted by an investigated sample and by determining their intensities, it is possible to quantify the elemental composition of the analyzed sample relative to a reference standard/specimen.

Electrolyte samples and corrosion products were analyzed with means of ICP-AES (Ultra-trace 2000 ICP-AES, Jobin Yvon®, Horiba, Japan). In the case of a bulk media analysis, samples were filtered (0.22 μm) and stored at 4 ℃ for further analysis. When analyzing corrosion products, representative parts of it were removed from the surface of the steel specimens and was placed for 1 hour in 20 mL of filtered (0.22 μm) aqueous HCl solution (50 (v/v)%), and stored at 4 ℃ for further analysis. Iron and major seawater cations (Na, Ca, Mg and K) and anions such as sulfur and phosphorus, were analyzed with inductively coupled plasma–atomic emission spectroscopy (Ultra-trace 2000 ICP-AES, Jobin Yvon®, Horiba, Japan).

II.10.3. Photometric methods – sulfate concentration determination

Spectrophotometry is the quantitative measurement of the reflection or transmission properties of a material as a function of wavelength. It works with visible light, near ultraviolet and near infrared. A sulfate concentration was determinated by means of spectrophotometric technique. Spectroquant® sulphate kit (VWR, USA) was used for sulfate quantification.

II.10.4. Volumetric methods – sulfide concentration determination

Titrimetry [Whitney and Smith, 1911] is a common laboratory method of quantitative chemical analysis that is used to determine the unknown concentration of an identified analyte. Because volume measurements play a key role in titration, it is also known as volumetric analysis. Sulfide concentrations were monitored according to Appendix C (Determination of H_2S concentration in test solution by iodometric titration) of the NACE TM0284-2003 standard.

II.11. Microbial diversity and activity monitoring

Assessment and monitoring of the microbial diversity and activity is essential since it provides an understanding into metabolic paths and their kinetics, thereby revealing the relationship between microbial activities with corrosion reactions in a particular environment. Microbial diversity of planktonic consortiums and biofilms can be evaluated and monitored by means of traditional microbiological techniques. However, these methods have some serious drawbacks. The more reliable option is using one or a few of available multiple environmental ecology techniques.

II.11.1. Microbial activity monitoring

Bacteria consortium monitoring was conducted by measuring cell density. Firstly, measurements were performed by Helber Bacteria Cell Thoma counting chamber (Hawksley, UK) with a light. Dilutions were made until it was possible to observe no more than 100 cells in the chamber grid with precondition that only viable cell are counted. Bacteria concentration was calculated in cellsmL^{-1} using the following relation: Concentration (cell mL^{-1}) = Number of cells/ Volume (mL), where the volume was 0.00625 mm^3

Secondly, cell densities of Acid–Producing Bacteria (APB) and Sulfate-Reducing Bacteria (SRB) were conducted with Most Probable Number (MPN) techniques. Two types of media were used for Most Probable Number (MPN) method: the PRD Medium (APB, 25,000 TDS) (Intertek Commercial Microbiology, USA) for APBs and SRB/2 Medium (SRB, 25,000 TDS) (Intertek Commercial Microbiology, USA) for SRBs.

II.11.2. Microbiological diversity assessment

It was required to determine diversity of biological samples acquired. Microbial diversity assessment was conducted in three steps:

1. Extraction of DNA from collected samples and amplification of same
2. Separation of PCR-amplified bacterial 16S rRNA gene by DGGE or Cloning
3. Identification of separated DNA fragments

II.11.2.1. DNA extraction & PCR amplification of bacterial 16S rRNA gene

For each selected sample, total DNA was isolated with the PowerBiofilm™ DNA isolation kit (Mo BIO Laboratories, UK) according to the manufacturer's instructions. The concentration of extracted and purified DNA was determined using a NanoDrop ND-1000 spectrophotometer (Thermo Scientific, USA). All extracted DNA was stored at -20℃ for sub sequent studies. Further, DNA from each sample was subject to polymerase chain reaction (PCR) (peqStar 96 Universal Gradient, PeqLab, UK).

The 16S rRNA gene (550bp) was amplified using universal bacterial primers: 341F+GC (5`- CGC CCG CCG CGC GCG GGC GGG GCG GGG GCA CGG GGG GCC TAC GGG AGG CAG CAG-3`) and 907R (5`- CCG TCA ATT CMT TTG AGT TT-3) [Muyzer *et al.,* 1998] (purchased from Life Technologies, UK).

PCR reactions were performed in 50 µL mixtures, containing 25 µL of 10x GoTaq® Green Master Mix (Promega, UK) and 1 µL of each primer (10 mM). The DNA was initially denatured at 94℃ for 4 min; followed by a touch down PCR: 20 cycles of 94℃ for 1 min, 63-54℃ for 1 min and 72℃ for 1 min followed by 15 cycles of 94℃ for 1 min, 53℃ for 1 min and 72℃ for 1 min with an final 10-min cycle at 72℃. The amplified PCR products were separated on 0.9 % (w/v) agarose gel made by dissolving 0.72 g of agarose powder (Sigma Chemical Ltd, UK) in 80 ml of 1x TAE buffer (20 mM Tris acetate, 10 mM sodium acetate, 0.5 mM Na2-EDTA). In addition, 7 µL of DNA molecular weight markers (1 kb

DNA ladder, Promega, UK) or 3 µL of 1 kb GeneRuler DNA mass ladder (Fermentas Life Sciences) mixed with 3 µL of loading buffer were applied for size determination and quantification of the fragments. The gels were run in a horizontal electrophoresis chamber (Horizontal gel electrophoresis unit, Scie-Plas, UK) or Mini horizontal electrophoresis system (Mini-Sub Cell GT System, Bio-Rad, USA) and covered with 1x TAE buffer. A voltage of 95 V was applied for 15 minutes. The gels was stained with the SYBR Safe DNA gel stain (Invitrogen) (7 µl of reagent mixed with agarose) and were viewed under UV light using Alpha Innotech Gel Documentation System (Alpha Innotech Corporation, USA) and Digital Camera (Olympus C-4000 Zoom) to ensure that the correct size fragment was amplified.

Genomic DNA (16S rRNA), extracted from laboratory type strains (*Escherichia coli* (KB3)), was used as positive controls for all PCR reactions.

II.11.2.2. Denaturing Gradient Gel Electrophoresis (DGGE)

The products of 30-40 µL PCR-amplified bacterial 16S rRNA gene were separated by Denaturing Gradient Gel Electrophoresis (DGGE) using an Ingeny DGGE apparatus (Ingeny International BV, The Netherlands), at the temperature of 60℃ for 20 h. The voltage was set to 90 V, after an initial 10 min at 200 V. The standard gradient was formed of 6% polyacrylamide in 0.5×Tris-acetate-EDTA (TAE) buffer with between 30% and 80% denaturant (7M urea and 40% formamide defined as 100% denaturant). Following electrophoresis, the gel was stained with SYBR® Safe DNA gel stain (Invitrogen Corp., USA), viewed under UV transillumination and a permanent image captured using the Alpha Innotech Gel Documentation System (Alpha Innotech Corporation, USA).

All visible bands were cut from the gel using a sterile scalpel blade. To extract the DNA, the cut-out was transferred into sterile 1.5 mL microcentrifuge tubes containing 30 µL of ultra-pure water and then centrifuged at 13,000 g for 1 minute (Heraeus Fresco 21, Thermo Scientific, UK). Aliquots (5 µL) of supernatants were used for PCR re-amplification as described above. PCR products were purified with the NucleoSpin® Extract II PCR purification kit (Macherey-Nagel, UK) and sequenced by GATC Biotech (UK).

II.11.2.3. Analysis of Microbial Diversity through Cloning and Sequencing

PCR-amplicons of bacterial 16S rRNA gene obtained as described above, were cloned into the pGEM-T Easy Vector (Promega, UK) according to standard methods [Sambrook *et al*., 1989] .*The Escherichia coli* JM 109 (Promega, UK) was used as a host strain for molecular cloning [Messing *et al*., 1981]. *E. coli* JM 109 was grown in Lysogeny broth (LB) medium and Super Optimal Broth with Catabolite repression (SOC) medium (Promega, UK) at 37℃. The solid LB medium was supplemented with 100 µg ampicillin mL^{-1}, 100 µg X-Gal mL^{-1} and 0.5 mM IPTG. Recombinant plasmid DNA was purified using a NucleoSpin® Plasmid QuickPure (Macherey-Nagel, UK) following the manufacturer's instructions.

Recombinant plasmid extraction and purification was carried out from liquid cultures of the positive *E. coli* colonies obtained from the transformation using NucleoSpin® Plasmid QuickPure (Macherey-Nagel, UK) following the manufacturer's protocol (Plasmid DNA Purification User Manual, 07/2010 p.18-19).

Purified plasmids were sent to the GATC Biotech UK DNA sequencing service. Sequencing using T7 vector primers and homology searches in Basic Local Alignment Search Tool (BLAST) identified the DNA fragments.

II.12. Mechanical testing

Mechanical testing was performed to acquire information about possible alterations of the mechanical properties of the used material due to different exposures, especially in the case when they have been under tensile stress.

II.12.1. Tensile test

The yield strength or a yield point of a material is the parameter defined as the critical stress at which a material begins to deform plastically. Prior to the yield point the material will deform elastically and will return to its original shape when the applied stress is removed. Once the yield point is exceeded,

the deformation will be permanent. Typically, steel will preserve its integrity during the expected lifetime given that load is below the yield point and steel is not exposed to an aggressive environment.

The tensile test process involves placing the test specimen in the testing machine, and applying a controlled uniaxial stress to it until the specimen fractures. During the application of uniaxial stress, the elongation of the gauge section is recorded versus the applied force. The tensile test are standardized and normalized by data manipulation, the obtained values are therefore not specific to the geometry of the test sample. The elongation measurement (performed by extensometer) is used to calculate the engineering strain, ε, using the following equation:

$$\varepsilon = \frac{\Delta L}{Lo} = \frac{L\text{-}Lo}{Lo} \quad \text{(Eq. II.10)}$$

In equation II.10, ΔL is the change in gauge length measured with extensometer, L_o is the initial gauge length, and L is the final length. Engineering strain (ε) is the amount that a material deforms per unit length in a tensile test.

The applied load (F), or force, divided by the original cross-sectional area of the material is the engineering stress (σ). The force measurement is used to calculate σ, using the following equation:

$$\sigma = \frac{F}{A} \quad \text{(Eq. II.11)}$$

In equation II.11, F is the force and A is the cross-section area of the gauge section. The tensile machine performs these calculations automatically as the force increases, so that the data points can be graphed into a stress-strain curve. The principle of tensile testing is shown in Fig. II.20.

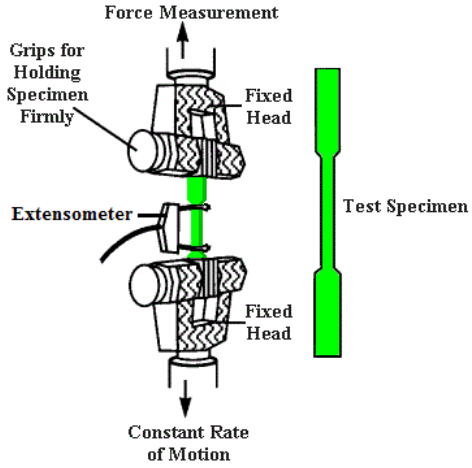

Fig. II.20. Principle of tensile testing with tensile machine.

The aim in this study was to detect changes in the specimens yield strength after long-term immersions in the test solutions. The tensile testing was conducted with Zwick z250 materials testing machine with central ball-lead screw and MTS 810 (MTS, USA) according to ISO 6892-1:2009(E) entitled: Metallic materials - Tensile testing at ambient temperature

II.11.2. Hardness test

The hardness is the resistance of a material to permanent indentation. Moreover, hardness is an empirical test; variations of acquired hardness values depend on the conducted hardness tests method (for example: Brinell or Rockwell). The results of the hardness test are dependent on the used test method and every test result has to have a label identifying the test method used.

Hardness is, however, used extensively to characterize materials and to determine if they are suitable for their intended use. In addition, hardness tests can provide information about material alterations, for example in the case of hydrogen embrittlement. All of the hardness tests involve the use of a specifically shaped indenter, which is significantly harder than the test sample. The indenter is pressed into the surface of the sample using a specific force. The depth or size of the indent is measured to

determine the specific hardness value. The principle of hardness testing is shown in Fig. II.21. The hardness tests were conducted and hardness was evaluated according to the Brinell scale. A tungsten carbide ball with a diameter of 1 mm was used as the indenter and the applied force was 29 kN. The hardness values are represented by Brinell Hardness Number (BHN) and they are calculated according to Eq. II. 12.

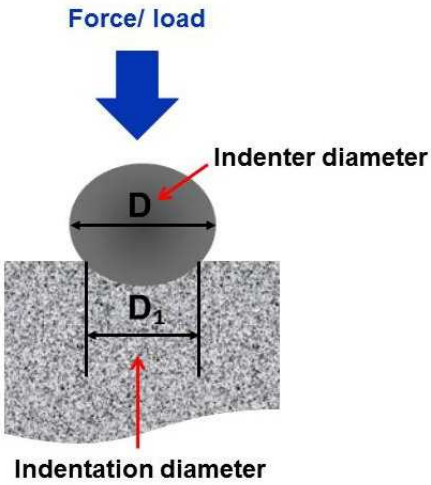

$$BHN = \frac{2 \times F}{\pi \times D \times \left(D - \sqrt{D^2 - D1^2}\right)} \quad \text{(Eq. II.12)}$$

Where: BHN is Brinell Hardness Number
F is applied force;
D is Intender diameter;
D_1 is indentation diameter.

Fig. II.21. Principe of hardness testing.

Chapter III

The effect of sulfidogenic bacterial community, recovered from North Sea offshore seawater injection system, on corrosion of carbon steel

III.1. Introduction

In Oil and Gas (O&G) offshore industry, corrosion is quite a familiar drawback of carbon steel systems integrated in offshore structures. From the 70's on, emphasis was on internal corrosion of injection systems, specifically for Water Injection Systems (WIS). Illustrative example of offshore installation operating by means of WIS, and its associated field is shown in Fig III.1.

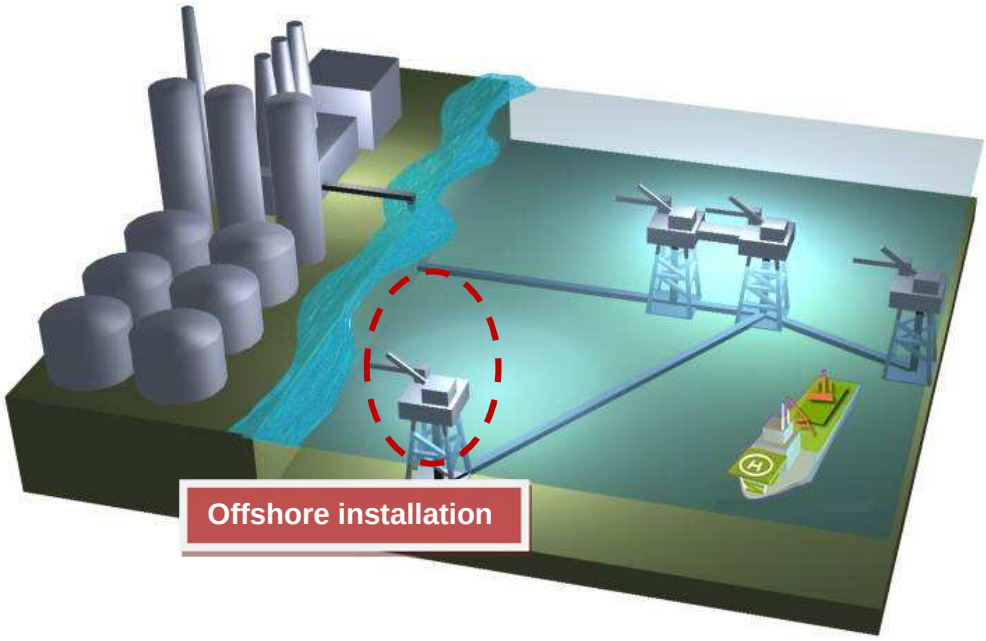

Fig. III.1. Example of offshore installation operating by means of Water Injection System (WIS) (red) and its associated field.

For systems crucial to oil and gas production, failure of the injection system may lead to production losses and therefore to accumulation of economic losses. To avoid, or at least to minimize, the risk of WIS failure, it is required to improve *decision support* through the identification of threats and the systems' most vulnerable components. Each particular system should operate within the range of parameters that can ensure stable oil production, and which is called the *safe operating window*. If microbial life is implicated in a corrosion process occurring in a WIS, the *safe operating window* parameters usually undergo unexpected deviations, often not properly followed-up. Because of common systems' unreadiness to sustain a microbial load and due to neglect of microbial problematic issues, when analysing a system experiencing unexpected deviations in its integrity and corrosion behaviour, the next step should be to assess the bacterial population and bacterial impact on the corrosivity of the environment and material integrity.

A particular offshore installation with the code name "***S***", and production capacity based on the effectiveness of its associated Sea-Water Injection System (SWIS) system has been producing between 63 bpd and 144 bpd since the day production started up. For the ***S*** installation, a representative SWIS layout is shown in Fig. III.2. Seawater is supplied from the seawater distribution system. The need for oxygen removal from the seawater to reduce corrosion potential has to be evaluated. Oxygen can serve as an electron acceptor and thus, when present in high amounts, should be (partially) removed. If oxygen removal is required, the oxygen removal system typically consists of a pre-filter, a feed pump and a deaeration system. Moreover, oxygen concentration can be reduced by using oxygen scavengers as in the case of installation ***S*** where bisulfide compounds are used (Fig. III.3). Fluid pressure is increased by booster pumps and finally by water injection pumps. The booster pump may be integrated into the injection pump. Particle removal is typically installed to protect the pumps and/or sustain reservoir integrity. The low-oxygen water is then distributed to the individual water injection wells in the water injection manifold system.

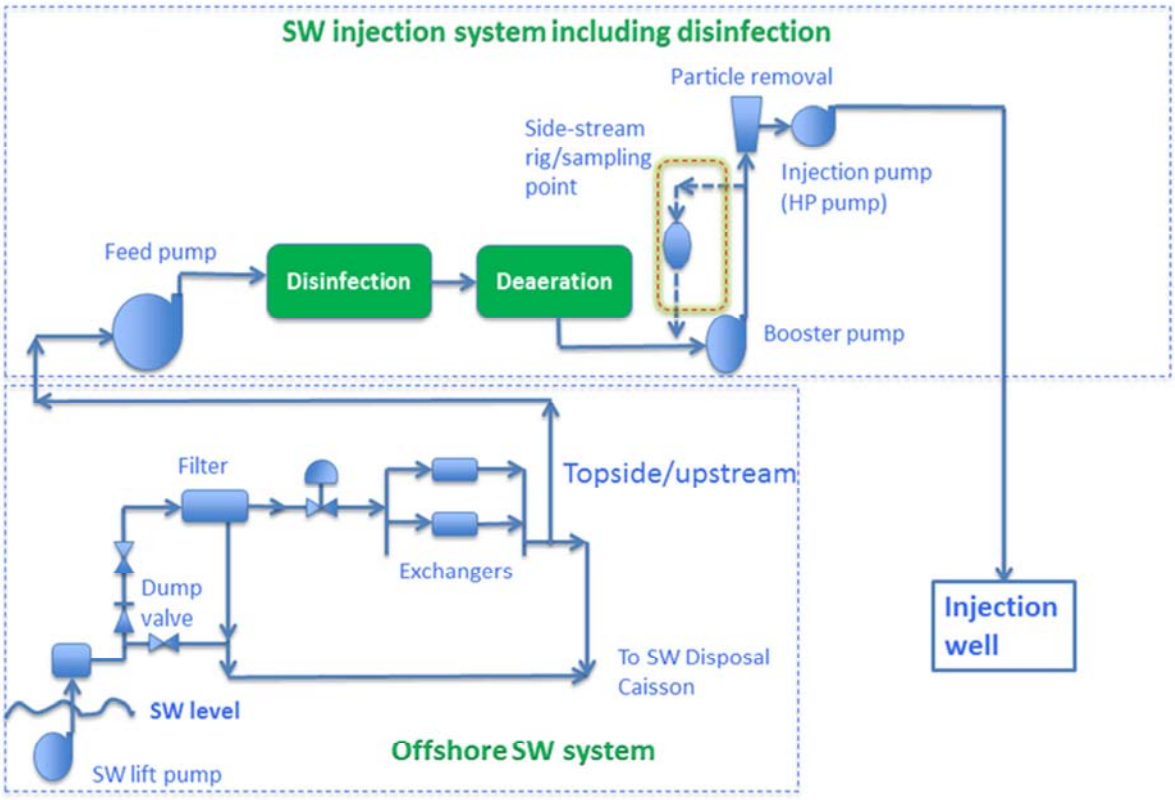

Fig. III.2. Sea-water Injection System (SWIS) layout scheme for installation ***S***.

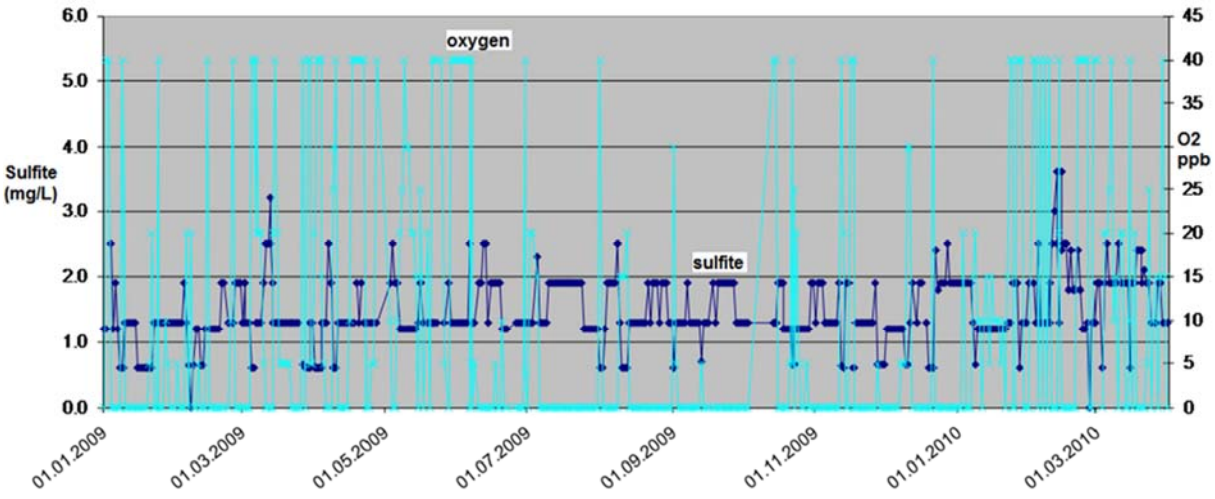

Fig. III.3. Example of oxygen (ppb) and sulfide (mg/L) monitoring in SWIS of offshore installation ***S***.

Production of installation ***S*** has been falling continuously during recent years. The operator has undertaken various production optimization initiatives over the years. In order to increase oil recovery and production, the operator wanted to add some more wells to the field. However, stable and effective functioning of present production systems was imperative. According to established prioritizing system procedures, special attention was paid to SWIS integrity and its corrosion condition. Mitigation steps, such as use of corrosion countermeasures, e.g. corrosion inhibitors and antimicrobial treatments, were based on on-site information; monitoring of corrosion rates (Fig. III.4); water quality monitoring (Fig. III.5); sample processing, culture of biofilms retrieved from bioprobes; controlling and optimizing antimicrobial treatments (Fig. III.5).

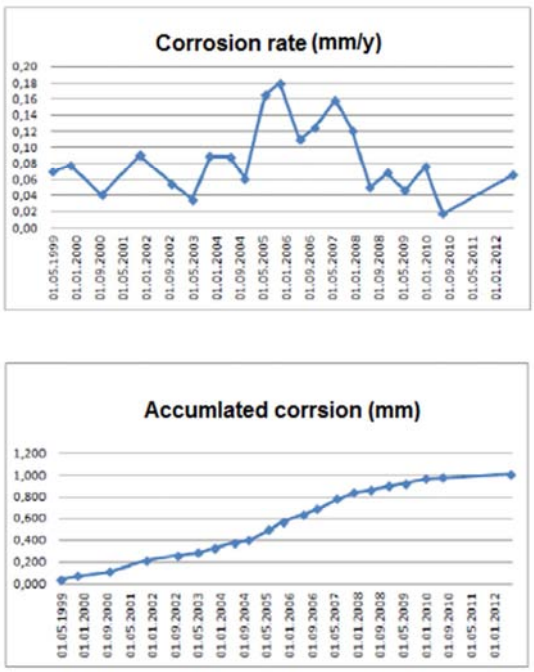

Fig. III.4. Corrosion rate monitoring data in SWIS on offshore installation ***S*** from year 1999 to 2012.

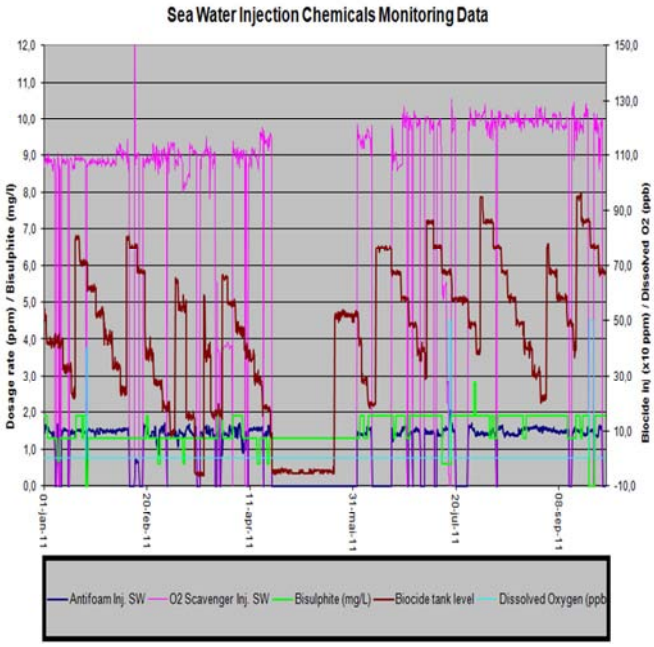

Fig. III.5. Example of injection water quality and antimicrobial treatment dosage monitoring in SWIS on offshore installation ***S***.

Even though the steps applied provided control over the particular SWIS, some questions remained unanswered;

i) What are the main elements responsible for corrosion in system?

ii) How do they contribute to corrosion and the formation of corrosion deposits?

iii) What are the processes occurring in the system?

iv) What are limiting parameters?

To provide answers to the questions raised, it was suggested to assess microbial diversity of the off-shore microbial consortium, to define the nature of the microbial consortium, to pin-point main causes of corrosion in the microbial consortium, to assess the microbial consortium corrosivity, and to evaluate the influence of the microbial consortium on the architecture of corrosion deposits.

Work conducted with in BIOCOR Individual Project 1 (IP1) and presented in this chapter started with acquisition of installation ***S*** documentation. Study of system Pipeline and Instrumentation Diagrams (P&ID) was conducted and it provided some significant information: low line material was construction-grade carbon steel and maximum flow rate in the critical segments of the system was around 800 m^3 h^{-1} (Re= 5.79 - 13.72 × 10^5, v=1.35 - 6.86 m s^{-1} depending on pipe diameter). Following step involved acquisition and analysis of the SWIS operational history, e.g. chemical treatments, corrosion rates, etc., that revealed (i) that the system operated anoxically within the range 0-50 ppb oxygen (Fig. III.2), (ii) that general material loss of piping increased with the time and (iii) that measured instantaneous corrosion rates fluctuated and exhibited erratic behaviour during the system's operational lifetime. It was significant that instantaneous corrosion rates measured during 2011 and 2012 were lower with the reference to corrosion rates measure during previous periods. Furthermore, during the following step, an offshore biological sample (biofilm retrieved from biostuds) was acquired and cultured, and its microbial diversity was assessed. Moreover, in order to assess the origin of the isolated microbial consortium, North Sea seawater was submitted to microbial diversity analysis. To investigate corrosivity of isolated microbial consortium, an in-house bioreactor loop was set-up simulating the following conditions: seawater environment and accommodating construction carbon steel specimens. Moreover, the experimental set-up enabled us to study corrosion deposits/biofilms structure. In the

following text, paper done in cooperation with Florin Turcu, Loic Esnault, Omar Rosas, Régine Basseguy, Magdalena Sztyler and Iwona B Beech and accepted in Bioelectrochemistry (under second revision), experimental work encompassing materials and methods, as well as acquired results and discussion is presented. Finally, observations and results are summarized and conclusions are extracted.

III.2.Article 1

<< The effect of bacterial community recovered from North Sea offshore seawater injection system on corrosion of S235JR steel: laboratory investigations >>

Bioelectrochemistry, Special Issue: BIOCORROSION 2012

Current status: accepted September 2013

Corrosion of carbon steel by bacteria from North Sea offshore seawater injection systems: laboratory investigation

Marko Stipanicev[a,b]*, Florin Turcu[a], Loic Esnault[a], Omar Rosas[b] , Régine Basseguy[b], Magdalena Sztyler[c] and Iwona B Beech[c,d]

[a]*Det Norske Veritas, Johan Berentsens vei 109-111, 5163 Laksevåg, Bergen, Norway*
[b]*Laboratoire de Génie Chimique CNRS-INPT, Université de Toulouse, 4 Allée Emile Monso, 31030, Toulouse, France*
[c]*School of Pharmacy and Biomedical Sciences, University of Portsmouth, Michael's Building, White Swan Road, PortsmouthPO1 2DT*
[d]*Department of Microbiology and Plant Biology, University of Oklahoma, 770 Van Vleet Oval, Norman, OK, USA*

*Corresponding author: Marko Stipanicev, telephone: +47 95936347, e-mail: Marko.Stipanicev@dnv.com

Abstract

Influence of sulfidogenic bacteria, from a North Sea seawater injection system, on the corrosion of S235JR carbon steel was studied in a flow bioreactor; operating anaerobically for 100 days with either inoculated or filtrated seawater. Deposits formed on steel placed in reactors contained magnesium and calcium minerals plus iron sulfide. The dominant biofilm-forming organism was an anaerobic bacterium, genus *Caminicella*, known to produce hydrogen sulfide and carbon dioxide. Open Circuit Potentials (OCP) of steel in the reactors was, for nearly all test duration, in the range -800< E(OCP)/mV (vs. SCE) <-700. Generally, the overall corrosion rate, expressed as $1/(R_p/\Omega)$, was lower in the inoculated seawater though they varied significantly on both reactors. Initial and final corrosion rates were virtually identical, namely initial $1/(R_p/\Omega)= 2\times10^{-6}\pm5\times10^{-7}$ and final $1/(R_p/\Omega)= 1.1\times10^{-5}\pm2.5\times10^{-6}$. Measured data, including electrochemical noise transients and statistical parameters (0.05< Localized Index <1; -5< Skewness < -5; Kurtosis >45), suggested pitting on steel samples within the inoculated environment. However, the actual degree of corrosion could neither be directly correlated with the electrochemical data and nor with the steel corrosion in the filtrated seawater environment. Further laboratory tests are thought to clarify the noticed apparent discrepancies.

Keywords: seawater injection; carbon steel; corrosion; bacterium

1. Introduction

The economic consequences of corrosion of iron and its alloys in various industrial sectors, including oil and gas operations, are well documented [1, 2, 3]. Undisputedly, corrosion causes considerable damage to marine steel infrastructure, such as offshore oil installations and pipeline systems, leading to revenue losses. It has been estimated that nearly 20% of the total corrosion cost is due to Microbially Influenced Corrosion (MIC) [3, 4]. MIC is often seen as pitting attack that is generally associated with the presence of surface-associated microbial communities embedded in a bioinorganic matrix, referred to as biofilm [5]. In both natural habitats and man-made systems, biofilms implicated in corrosion failures, comprise diverse microbial genera and species that often exhibit synergistic and synthropic behavior [6, 7]. Key microorganisms are phylogenetically diverse Sulfide-Producing Prokaryotes (SPP) of which some, but not all, represent Sulfate-Reducing Bacteria (SRB) and Archaea (SRA), i.e. Sulfate-Reducing Prokaryotes (SRP) [8, 9]. In addition to SPP, Sulfur-Oxidizing Bacteria (SOB), Iron-Reducing and -Oxidizing Bacteria (IRB and IOB respectively), Manganese-Oxidizing Bacteria (MOB), carbon dioxide reducing bacteria [3] and methanogenic archaea have been associated with marine corrosion failures [10, 11, 12].

It is now acknowledged that microbial metabolic activity, which depends on the availability of nutrients and of suitable electron donors and acceptors, can influence electrochemical processes on steel surfaces, therefore, play an important role in the processes governing MIC [13, 14]. Indeed, it has been reported that differences in metabolic activities within biofilms established under identical conditions can result in dissimilar corrosion rates [4]. It is also recognized that biofilm formation and associated MIC damage are dependent on the physical and chemical conditions of a given environment [15]. For example, temperature, pH, pressure, light radiation, oxygen content, salinity and redox potential will influence the nature and metabolic activity of a bacterial community [16], thus governing the potential risk of MIC. It is noteworthy that conditions at surfaces may differ significantly

from those in bulk liquid; for example, anaerobic niches may exist within biofilm in a fully oxygenated system or oxygen may be formed in an anoxic environment due to bacterially-mediated disproportionation reactions [17, 18, 19].

Further, fluid flow directly impacts mass transfer and biofilm formation [20, 21]. High shear stress is likely to decrease microbial cell attachment and may even cause detachment of an established biofilm [21, 22, 23].

Importantly, the chemical composition and microstructure of the construction materials determine their susceptibility to both abiotic corrosion and MIC [24, 25]. Carbon steel is a major alloy used in offshore oil extraction and transport systems, including Sea-Water Injection Systems (SWISs). During their operational lifetime, SWISs are exposed to a range of damage-provoking conditions. The presence of microorganisms can lead to complex, and not yet fully understood, deterioration of pipeline material. Carbon steel is particularly vulnerable to sulfide attack; hence biotic sulfide production resulting from SPP activity is of great concern.

In offshore Oil and Gas (O&G) industry, the main target in MIC control and remediation is taxonomically and metabolically diverse SRP. Able to grow within a wide temperature range, SRP are routinely detected in parts of the offshore oil extraction systems where sulfate-rich seawater-containing fluids are being produced or processed and anoxic conditions may prevail [26, 27].

It has to be emphasized that not just SRP, but also other classes of anaerobic dihydrogen sulfide producing organisms, pose equal, if not greater, MIC threat [32]. These include spore forming bacteria belonging to the phylum *Firmicutes* and the class *Clostridia*, which are readily detected in oilfield systems using advanced molecular ecology techniques [28, 29, 30, 31].

The interdisciplinary investigation reported herein aimed to determine whether the selection of S235JR low carbon steel as pipe material for a North Sea offshore seawater injection system would result in an unacceptable MIC risk. The laboratory set-up was constructed as an anaerobic continuous-flow bioreactor, circulating North Sea seawater. Its operating parameters were selected to mimic field conditions. The system was designed as a closed test loop comprising an inoculation vessel and two flow-through cells fitted with steel test specimens. Bioreactor inoculum was obtained from sessile (biofilm) field populations enriched in an anoxic sulfate medium and subsequently re-enriched in sulfate and other anaerobic microbial cultivation media. Special emphasis was placed on the on-line use of electrochemical techniques, in particular Linear Polarization Resistance (LPR) and Electrochemical Noise (EN), to monitor and characterize corrosion events on surfaces of steel specimens. The bioreactor inoculum and the planktonic and biofilm communities in the experimental and control flow cells were characterized employing tools of molecular microbial ecology, namely Polymerase Chain Reaction (PCR), Denaturing Gradient Gel Electrophoresis (DGGE), cloning and sequencing. Scanning Electron Microscopy (SEM) and Energy Dispersive X-ray (EDX) analysis of surfaces of test specimens were performed to image biofilms, visualize topography and to provide elemental composition of corrosion products.

2. Material and Methods

2.1. The bioreactor loop

A high and stable flow rate of seawater, constant temperature, and anoxic conditions were prerequisites of the study. A closed flow-loop bioreactor design was selected as the most suitable system complying with those requirements. The final bioreactor set-up benefitted from the past 20 year experience in MIC research for the selection of construction materials, flow cell design, real-time monitoring techniques and etc. [33, 34, 35, 36]. The main components of the bioreactor were manufactured in-house and comprise a vessel and two cylindrical flow-through cells. While the inoculated seawater freely enters the experimental flow cell, it passes through a 0.2 µm filter (Sartopore 2 MaxiCaps®, Sartorius AG, France) before reaching the control flow cell. The bioreactor set-up is depicted in Scheme 1.

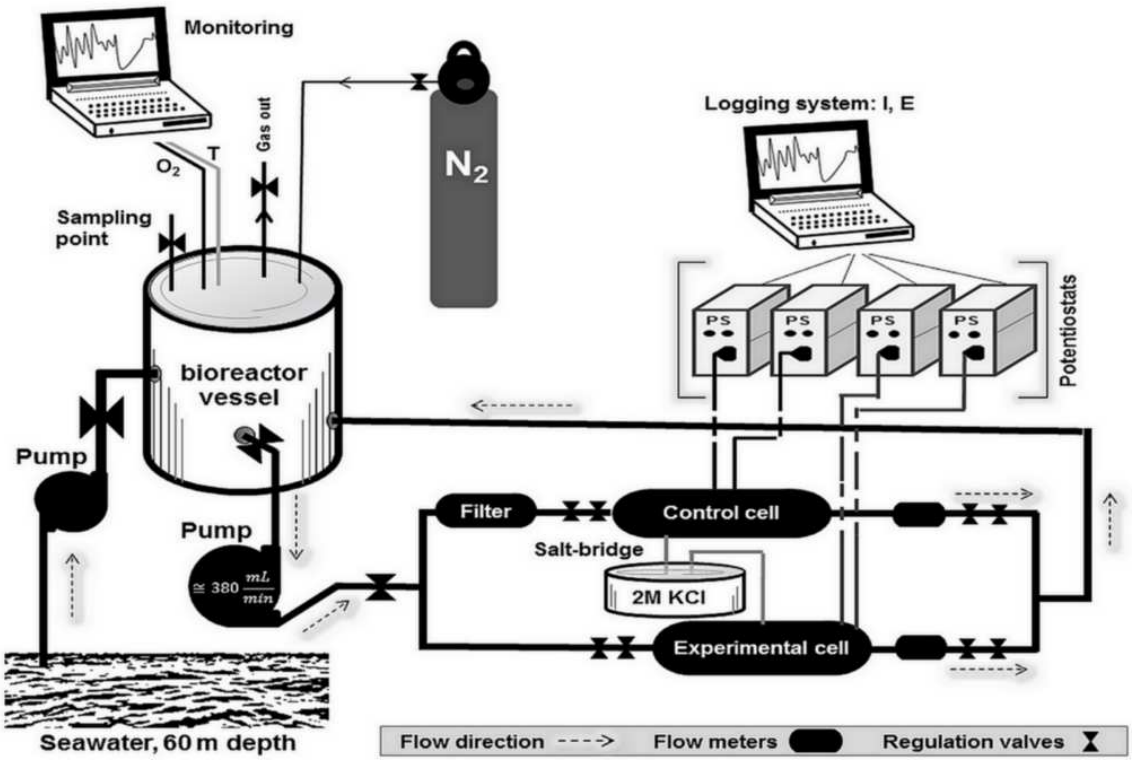

Scheme 1. Schematic representation of the bioreactor loop.

The bioreactor vessel consists of a polypropylene body and an acryl lid, fitted with an optical oxygen dipping probe, a temperature sensor interfaced with Fibox 3 fiber optic oxygen transmitter (Presens, Germany), one nitrogen gas inlet (99.999% purity, Yarapraxiar, Norway), one gas outlet and a pH electrode (pH-meter HI-9125N, Hanna Norden AB, Sweden). The lid also incorporates an in-house fitted sampling point and a fluid injection system. The vessel is also equipped with a heating unit (ISOPAD IP-DASI®, Tyco, USA) and a thermostat (Raychem® AT-TS-14, Tyco Thermal Controls, USA).

A peristaltic pump (W-M 520SN/REL, Watson-Marlow, UK), draws media from the bioreactor vessel, and the output flow is split between the two flow cells. Perfluoroalkoxy (PFA) tubing (PFA-T8-062-50, Swagelok, UK) was used. Two regulation needle valves (PFA-4RPS8, Swagelok, UK) were installed before and after each flow cell. Each flow cell was also equipped with a flow meter (FTB332 infra-red light beam micro-flow meter, Omega Engineering, UK) located after the exit regulation valve. The flow rate through each of the flow cells was controlled at 180 mL/min with the regulation valves. After passing through the flow cells, the liquid stream rejoins and returns to the bioreactor vessel. Liquids were re-circulated in the bioreactor loop for100 days.

The entire bioreactor flow system was constructed from polymers to minimize contamination with exogenous metal ions. Furthermore, materials, including perfluoroalkoxy (2 mm thickness), polyolefin (1 mm thickness), polypropylene (2 cm thickness) and acrylic (1 and 2 cm thickness) polymers with minimal oxygen permeability and minimal deterioration under test conditions were chosen. Prior to operation the bioreactor loop was flushed with technical grade alcohol (art. no.601441, Kemetyl Norge AS, Norway) and flow cells were exposed for 6 h under UV light (XX-15 sterilization UV lamp, UVP, USA).

Flow cells were made from acrylic tubes (6 cm inner diameter, 1 cm wall thickness and 48 cm length). Six pairs of feedthroughs (M20 size fittings, produced by OBO Bettermann, Germany) were installed on each flow cell. A schematic drawing of a flow cell showing its cross section and distribution of feedthroughs is presented in Scheme 2.

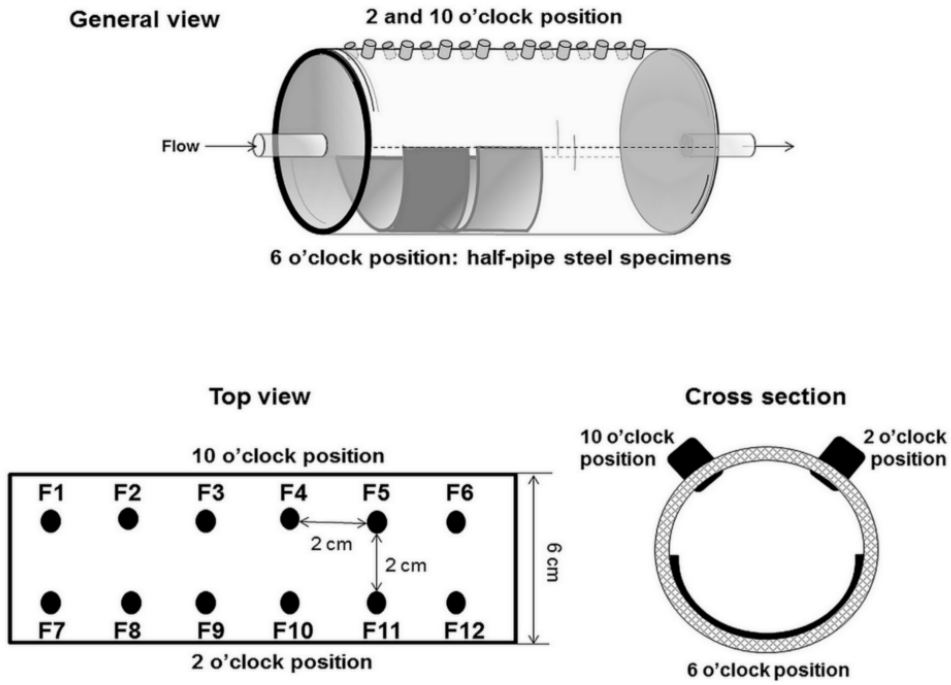

Scheme 2. Schematic representation of cross-section and fitting distribution of the flow through cell.

Electrodes for the measurements of corrosion rates and open-circuit potentials were installed in the two flow cells, in identical arrangements. The electrode configuration was designed to reproduce that used in offshore electrochemical probes. Six carbon steel Working Electrodes (WE) with a circular, exposed area of 0.785 cm^2 (cylindrical specimens, 1 cm long, 1 cm diameter, dressed in polyolefin sleeve and leaving only the flat bottom of cylinder exposed, Scheme 3) were installed in the 10 o'clock (F2, F4, and F6) and 2 o'clock positions (F8, F10, and F12), see Scheme 2. Each cell was also fitted with four additional electrodes. Their design was the same as that of the working electrodes (Scheme 3), except that Inconel® C276 (*E*(Inconel® C276 in anoxic seawater)/ mV (vs. SCE) ≈ 350) was used instead of carbon steel as electrode material and the exposed area was 3.95 cm^2 as the cylinder side was not dressed in polyolefin sleeve). Two of these electrodes, installed in the F5 and F9 positions, were used as Counter Electrode (CE). The other two, installed in the F3 and F11 positions, served As Pseudo-Reference Electrodes (PRE). Two laboratory-made Salt-Bridges (SB) filled with 2 M KCl solution (VWR, US) were placed between the F1 position in each flow cell and a reference cell, which was also filled with the 2 M potassium chloride solution and fitted with two Saturated Calomel Electrodes (SCE). An in-house manufactured liquid Sampling Port (SP) with a septum was installed at F7 position in each cell. To monitor biofilm formation, five carbon steel specimens (half-pipe sections with a 5 cm length, a 5.5 cm outer diameter and a 0.5 cm wall thickness) were installed at 6 o'clock position in each flow cell (Scheme 2).

The test specimens (half-pipe and circular discs) were manufactured from S235JR carbon steel (Descoure and Cabaud, France). The S235JR carbon steel is composed of the following elements and corresponding mass percentage: 0.17% carbon (C), 1.4% manganese (Mn), 0.045% copper (Cu), 0.03% sulfur (S) and 0.03% phosphorus (P). All exposed surfaces were ground manually using silicon carbide (SiC) paper of increasingly fine grain, ending with 600-grit. Grinding debris were rinsed off the electrode surface with sterile deionized water. The specimens were exposed for 3 hours on each side under UV light (wave length 256 nm: XX-15, sterilization UV lamp, UVP, USA) at 25℃.

The bioreactor vessel was filled up with 40 L of seawater, and oxygen was removed by purging with nitrogen for 3 days, i.e. until the optical oxygen probe reached its detection limit of 10 ppb. The flow system was then activated, and the flow rate maintained at 180 mL/min in each of the flow cells for the initial 15 days of the test. 15 days after the start of the test flow was stopped for 2 days, and the bioreactor vessel was seeded with bacterial inoculum. Then flow was re-established. The bioreactor loop was operated continuously for the next83 days. At the end of 100-day period, the reactor was decommissioned. Electrochemical measurements were carried out at regular intervals, as described in Section 2.2.

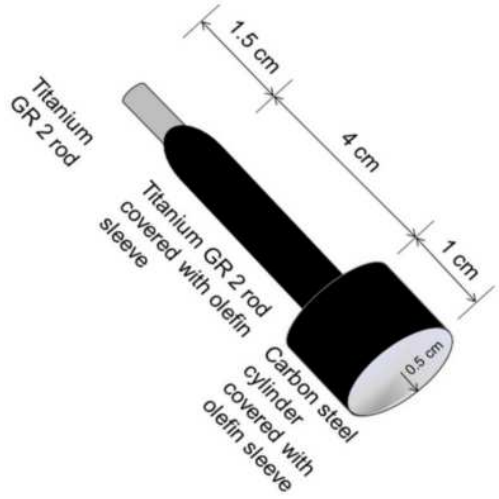

Scheme 3. Working electrode scheme.

Microbial consortia which served as a source of inoculum for the laboratory bioreactor loop were obtained from a SWIS located on an offshore installation, code name S, in the Norwegian sector of the North Sea. Two bio-probes (0.3 cm^2 surface area with 0.08 cm in diameter and a length of 1.2 cm) manufactured from St-52 carbon steel were removed from a SWIS side-stream rig after one and three months of exposure, respectively, following the offshore procedure API-RP 39 for handling biological samples [37]. Upon removal, the bio-probes were immersed in 50 mL of sterile SRB/2 growth-medium (Commercial Microbiology, UK) and subjected to 20 seconds of sonification (UltraMet® 2005 Sonic Cleaner, Buehler, US). Following sonification, 1 mL volumes of biofilm suspensions were inoculated aseptically into six glass vials, each containing 9 mL of deoxygenated sterile SRB/2 medium. The vials/cultures were incubated on site at 20℃ for 28 days, after which period enumeration of viable bacterial cells was carried out using Most Probable Number (MPN) method. Cultivation of biofilms retrieved from one and three month-exposed bio-probes in SRB/2 growth medium resulted with cell densities of 43 $cell^{-1}$ and >1100 cell mL^{-1} respectively. The 28-day-old SRB/2 enrichments were subsequently used for inoculating a range of anaerobic liquid media, as specified below.

1. Seawater + iron dust (3 g/ 50 mL)
2. Seawater + SL-10 trace elements solution
3. Seawater + acetate (10 mM) + SL-10
4. Seawater + acetate (10 mM) + Iron dust (3 g/ 50 mL) + SL-10
5. SRB/2 medium

SL-10 trace element solution is used in the preparation of Widdel medium as described elsewhere [38]. The resulting re-enrichments were incubated for 21 days as described above. Following incubation, all re-enrichments were combined to produce the Bioreactor Vessel Inoculum (BVI) of a total volume of 1.5 L. Prior to bioreactor seeding iron was removed from the inoculum using a strong magnet.

2.2. Analytical methods

2.2.1. Electrochemical methods

The Open Circuit Potential (OCP), e.g. *E*/(OCP)/mV(vs. SCE), measurements were performed with a 34401A $6^{1/2}$ digit multimeter with an input impedance of 10 GΩ in parallel with 100 pF (Agilent, USA). The *E*/(OCP)/mV(vs. SCE) of three working electrodes (circular disc) installed at the F4, F6 and F12 positions of each flow cell were recorded every 3 days.

The Linear Polarization Resistance (LPR) and Electrochemical Noise (EN) measurements were carried out using a multichannel potentiostat MultEchem™ (Gamry Instruments, USA) that consisted of two Reference 600TM Potentiostat/ Galvanostat/ ZRA independent units connected to a PC interface and monitored with DC105 and ESA410 software (Gamry Instruments, USA). The LPR technique was employed to estimate the rate of corrosion of the steel WEs. The polarization resistance (R_p) of the steel/electrolyte interface is measured in the vicinity of the *E*(OCP) and is given in Ω [39, 40]. R_p/Ω is defined as the slope of the polarization curve tangent at the *E*(OCP)/V. The inverse of R_p is proportional to the ''instantaneous'' corrosion rate and given in 1/Ω [15]. To determine of R_p/Ω, the potential was scanned in the range of +20> *E*(OCP)/mV> -20 (with *E*(OCP) measured using 600TM Potentiostat) and a sweeping rate of *v*/(mV/s) = 0.167. Polarization scans were performed every 14 days during the first 91 days and every day during the last 9 days of the test.

Standard three electrode-arrangements included a WE, a CE and of a PRE. Three different electrode configurations were used:
1. WE at F8, 10 o'clock, CE at F9, 2 o'clock, and PRE at F3, 10 o'clock;
2. WE at F4, 10 o'clock, CE at F5, 2 o'clock, and PRE at F11; 2 o'clock
3. WE at F10, 2 o'clock, CE at F9, 2 o'clock, and PRE at F3, 10 o'clock.

Averages ($1/R_p$)-values with associated standard deviations were reported for the three different working electrodes.

Electrochemical Noise (EN) analysis was carried out to determine the type of corrosion attack [41, 42]. Electrochemical Current Noise (ECN) and Electrochemical Potential Noise (EPN) signals were recorded between two equivalent working electrodes (placed at F6 and F12) using a PRE at F11. Here presented ECN and EPN data were recorded with data sampling rates of 0.1 Hz, 0.2 Hz and 1Hz, a current range of 600 mA, a potential range of +/- 3 V, a current resolution of 1 pA and a voltage resolution of 1 µV. Data sampled at 0.1 Hz were collected continuously for the whole testing period of100 days; data sampled at 1 Hz were collected at four different 2-daytime periods; while data sampled at 0.2 Hz were recorded for a 2-dayperiod at the beginning of the test, prior to reactor inoculation.

Due to equipment problems, no EN data were recorded between day 69 and day 72 for either flow cell. Data was also not recorded between test start and day 6 and day 18 and day 24 for the experimental cell.

EN data sampled at 0.1 Hz were analyzed in the sequence-independent domain within data blocks of 128 sampling data points, and thus the time resolution for each calculated statistical parameter is 21.3 minute. Dimensionless statistical parameters such as Localization Index (LI), skewness and kurtosis were calculated [41, 42, 43]. They are all can be presented as indicators of localized corrosion activity [41, 42, 43]. Localization index (LI) was calculated as the ratio between the ECN standard deviation (σ_{ECN}/A) over the root-mean-square current value (I_{rms}/A) [41]. The analysis took into account the different ranges of LI values, which lie between 0 and 1. Skewness was derived as the ECN third central moment ($m_{3,ECN}$/A) divided by the cube of the ECN standard deviation (σ_{ECN}/A). Kurtosis was derived by dividing the ECN fourth central moment ($m_{4,ECN}$/A) by the fourth power of the ECN standard deviation (σ_{ECN}/A).

Modulated current and potential signal patterns, as well as transients, characteristic of localized surface events, were visually examined within data blocks of 100 (0.1 Hz sampling frequency), 200 (0.2 Hz sampling frequency) and 1000 (1 Hz sampling frequency) points resulting with the time resolution of 1000 seconds.

2.2.2. Surface analysis

After reactor decommissioning, the topography of all working electrodes was characterized using optical imaging with a Leica upright DMR microscope (Leica Microsystems GmbH, Germany) and attached ProgRes® C5 camera (JENOPTIK Optical Systems GmbH, Germany). Prior to examination, steel specimens were cleaned from corrosion products by immersion in a 5 (w/v)% hexamine (MERCK, Germany) solution in concentrated hydrochloric acid (VWR, USA) for 30 seconds. This was immediately followed by rinsing with deionized water, gentle blotting with a paper towel, and overnight storage in a desiccator.

Four half-pipe steel specimens, two from each flow cell, were removed from the bioreactor and equally divided into two batches. Specimens were prepared for Scanning Electron Microscopy (SEM) analysis as follows:

a) Batch No1: specimens were dried under nitrogen stream and immediately examined with the high resolution SEM (JSM-5800, Joel, Japan) interfaced with a EDX acquisition system (Voyager®, NORAN Instruments Inc., USA)

b) Batch No2: specimens were placed in 2.5 (w/v)% glutaraldehyde (Electron Microscopy Science, USA) for 90 minutes at 4℃ and then surface deposit s were removed by sterile scalpel blade. Biofilm samples were washed by 4×15 min immersions in 0.1 M sodium cacodylate buffer (MERCK, Germany). Post-fixation was carried out by placing biofilm samples for 1 h in the solution of 1 (w/v)% osmium tetroxide (purity> 99.95%, Electron Microscopy Science, USA) in 0.1 M sodium cacodylate buffer. Post-fixed samples were washed in 0.1 M sodium cacodylate buffer (2×20 min) and dehydrated following serial immersions (15 min in 30 (v/v)%, 15 min in 50 (v/v)%, 20 min in 70 (v/v)%, 2×15 minutes in 96 (v/v)% and 2 x15 minutes in 100 (v/v)% in aqueous ethanol (99.8%, Sigma-Aldrich,

Norway) solutions. De-watered biofilm samples were placed in an oven (Type TS 4057, Thermaks AS, Norway) at 37℃ overnight.

Dried samples were sputter-coated with palladium for 6 minutes and imaged with high resolution SEM (JSM-7400F, Joel, Japan).

All EDX results are given as percentage by number of atoms (At(element)/ %). of each of the elements identified in scanned area.

2.2.3. Elemental analysis

A representative part of corrosion products was removed from the surface of one steel half-pipe specimen from each flow cell. Each specimen was placed for 1 h in 20 mL of filtered (0.22 µm) aqueous hydrochloric acid solution (50 (v/v)%), and stored at 4 ℃ for further analysis. Iron and major seawater cations (sodium (Na), calcium (Ca), magnesium (Mg) and potassium (K)) and anions such as sulfur (S) and phosphorus (P), were analyzed with Inductively Coupled Plasma–Atomic Emission Spectroscopy (ICP-AES) (Ultra-trace 2000 ICP-AES, Jobin Yvon®, Horiba, Japan).

All ICP-AES results are shown as molar concentrations (c(element)/ mM).

2.2.4. Microbiological diversity assessment

The following samples were used for deoxyribonucleic acid (DNA) analysis:

1. As-received North Sea seawater (SW)
2. The biofilm field enrichment in SRB/2 medium (BFE)
3. Bioreactor vessel inoculum consisting of pooled re-enrichments as described in section 2.4.1 (BVI)
4. Biofilms removed from steel specimens exposed in the control flow cell (BCFC)
5. Biofilms removed from steel specimens exposed in the experimental flow cell (BEFC)
6. Water samples from the experimental flow cell (WEFC)

Total DNA was isolated from each sample using the PowerBiofilm™ DNA isolation kit (Mo BIO Laboratories, UK) according to the manufacturer's instructions. The concentration of extracted and purified DNA was determined using a NanoDrop ND-1000 spectrophotometer (Thermo Scientific, USA). All extracted DNA was stored at -20℃.

Isolated DNA was subject to Polymerase Chain Reaction (PCR) (peqStar 96 Universal Gradient, PeqLab, UK). The 16S rRNA gene (550bp) was amplified using universal bacterial primers: 341F+GC (5`- CGC CCG CCG CGC GCG GGC GGG GCG GGG GCA CGG GGG GCC TAC GGG AGG CAG CAG-3`) and 907R (5`- CCG TCA ATT CMT TTG AGT TT-3) [44] ((Life Technologies, UK). PCR reactions were performed in 50 µL mixtures, containing 25 µL of 10x GoTaq® Green Master Mix (Promega, UK) and 1 µL of each primer (10 mM). The DNA was initially denatured at 94℃ for 4 min; followed by a touch down PCR: 20 cycles of 94℃ for 1 minute, 63-54℃ for 1 minute and 72℃ for 1 minute followed by 15 cycles of 94℃ for 1 minute, 53℃ for 1 minute and 72℃ for 1 minute with an final 10-minunte cycle at 72℃. The PCR products were separated on a 1.0% agarose gel stained with SYBR® Safe DNA gel stain (Invitrogen Corp., USA) and viewed under UV transillumination (Alpha Innotech Corporation, USA) and Digital Camera (Olympus C-4000 Zoom) to ensure that the correct size fragment was amplified.

PCR-amplified bacterial 16S rRNA gene products (30-40 µ) were separated by Denaturing Gradient Gel Electrophoresis (DGGE) using an Ingeny DGGE apparatus (Ingeny International BV, The Netherlands), at the temperature of 60℃ for 20 hours. The voltage was set to 90 V, after an initial 10 minutes at 200 V. The standard gradient was formed of 6% polyacrylamide in 0.5×Tris-acetate-EDTA (TAE) buffer with between 30% and 80% denaturant (7M urea and 40% formamide defined as 100% denaturant). Following electrophoresis, the gel was stained with SYBR® Safe DNA gel stain (Invitrogen Corp., USA), viewed under UV transillumination and a permanent image captured using the Alpha Innotech Gel Documentation System (Alpha Innotech Corporation, USA).

All visible bands were cut from the gel using a sterile scalpel blade. To extract the DNA, each cut-out was transferred into sterile 1.5 mL microcentrifuge tubes containing 30 µL of ultra-pure water and then centrifuged at 13,000 g for 1 minute (Heraeus Fresco 21, Thermo Scientific, UK). Aliquots (5 µL) of supernatants were used for PCR re-amplification as described above. PCR products were purified with the NucleoSpin® Extract II PCR purification kit (Macherey-Nagel, UK) and sequenced by GATC Biotech (UK).

PCR-amplicons were cloned into the pGEM-T Easy Vector (Promega, UK) according to standard methods [45] .*The Escherichia coli* JM 109 (Promega, UK) was used as a host strain for molecular cloning [46]. *E. coli* JM 109 was grown in Lysogeny Broth (LB) medium [45] and Super Optimal Broth with Catabolite repression (SOC) medium (Promega, UK) at 37℃. The solid LB medium was supplemented with 100 µg/mL ampicillin, 100 µg/mL X-Gal and 0.5 mM IPTG. Recombinant plasmid DNA was purified using a NucleoSpin® Plasmid QuickPure (Macherey-Nagel, UK) following the manufacturer's instructions.

Recombinant plasmid extraction and purification was carried out from liquid cultures of the positive *E. coli* colonies obtained from the transformation using NucleoSpin® Plasmid QuickPure (Macherey-Nagel, UK) following the manufacturer's protocol (Plasmid DNA Purification User Manual, 07/2010 p.18-19).

Purified plasmids were sent to the GATC Biotech UK DNA sequencing service. Bacterial identification was carried out through sequence homology searches in Basic Local Alignment Search Tool (BLAST).

3. Results

3.1. Evaluation of electrochemical data

Prior to bioreactor seeding, OCPs for working electrodes (circular discs) in both the control and experimental flow cells fluctuated between -950< *E*(OCP)/mV (vs. SCE) < -710 (Fig. 1). Following inoculation OCPs stabilized at -800< *E*(OCP)/mV (vs. SCE) < -700 in both flow cells. Values of 1/(R_p/Ω) for steel coupons in the experimental flow cell are shown in Fig. 2. Preceding inoculation, 1/(R_p/Ω) values were similar to the ones recorded in the control cell.

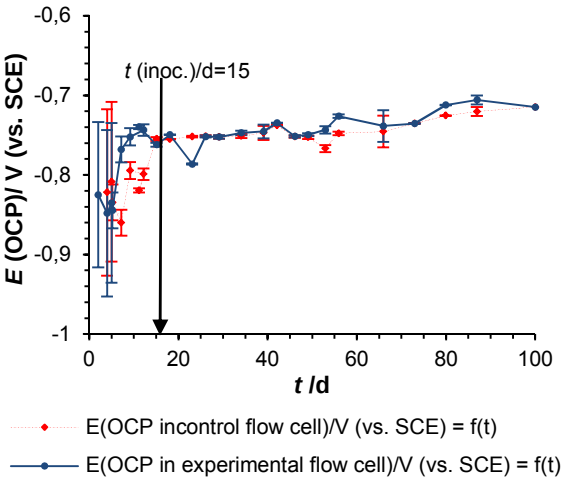

Fig. 1. Open circuit potential of S235JR carbon steel (*E*(OCP)/mV(vs. SCE)) versus time (*t*/d) obtained from steel specimens exposed in control (dashed line) and experimental (full line) cell during the 100 days. Data points are accompanied with standard deviation error bars.

Prior to bioreactor seeding, average 1/(R_p/Ω) values of approximately 2×10^{-6} were recorded for specimens in the control cell (Fig. 2). Between day 24 and day 52, average 1/(R_p/Ω) values increased to approximately 1.1×10^{-5} but with relatively large fluctuations. During the subsequent 27 days of the test, 1/(R_p/Ω) decreased to 4.5×10^{-6} and from day 79 until the test termination 1/(R_p/Ω) gradually increased and reached a final value of 1.1×10^{-5}.

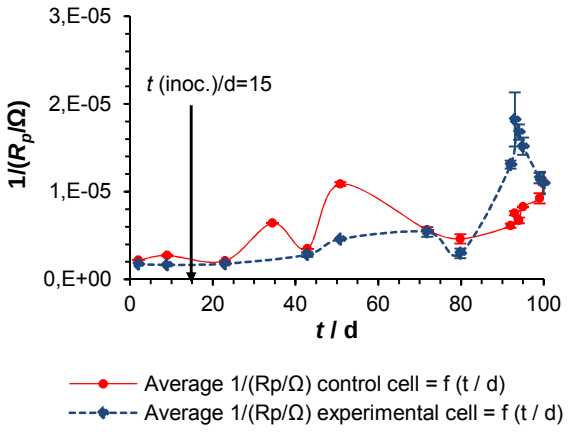

Fig. 2. Average instantaneous corrosion rate (1/(R_p/Ω)) with standard deviation error bars versus time (*t* /d) in the control cell (full line) and experimental cell (dashed line) obtained by LPR technique during the 100 days.

Following inoculation, $1/(R_p/\Omega)$ increased gradually from 2×10^{-6} at day 24 to 5×10^{-6} at day 52 and then remained relatively stable for the next 25 days. After approximately day 77a strong increase in $1/(R_p/\Omega)$ from 5×10^{-6} to approximately 2×10^{-5} Ω^{-1} was measured, and during the last 6 days of exposure, $1/(R_p/\Omega)$ values gradually decreased to 1.2×10^{-5}.

3.1.1. Corrosion monitoring using real-time EN data acquisition and time records analysis

An ECN (and associated EPN) transient, representative of those observed in the control during the initial day 24 of the test, i.e. prior to and just after inoculation, is presented in Fig. 3A. The modulated current and potential signals are indicative of pitting corrosion [47, 48]. Briefly, the rapid current increase during pit initiation and growth is followed by a slower decay after pit repassivation.

Examples of 1000-second ECN and EPN time records, representative of those observed in the control flow cell between day 24 and day 100 are presented in Fig. 4A. Displayed examples were recorded at day 37, day 83 and day 100, with an acquisition frequency of 1 Hz. The ECN and EPN fluctuations are not characteristic of stable localized corrosion. Instead, transients related to metastable pitting and higher localized electrochemical surface activities of carbon steel were observed [48]. The data maintained the same pattern throughout testing period, which would suggest combined uniform and localized attack.

In the control cell, ECN fluctuation with time had a tendency towards high values (higher currents) that corresponds to rise in 1/(Rp/Ω) values, especially in the last period of the test.

An ECN (and associated EPN) transient, representative of those observed in the experimental cell prior to and just after inoculation, during the entire initial 24 days of testing is presented in Fig. 3B. Shape of current and potential signals was very similar to ones observed in control cell.

Moreover, fluctuation pattern i.e. transients observed in experimental flow cell between day 24 and day 100 were almost identical to ones observed in control flow cell as show in Fig. 4B (displayed records were collected at day 37, day 83 and day 100, with an acquisition frequency of 1 Hz).

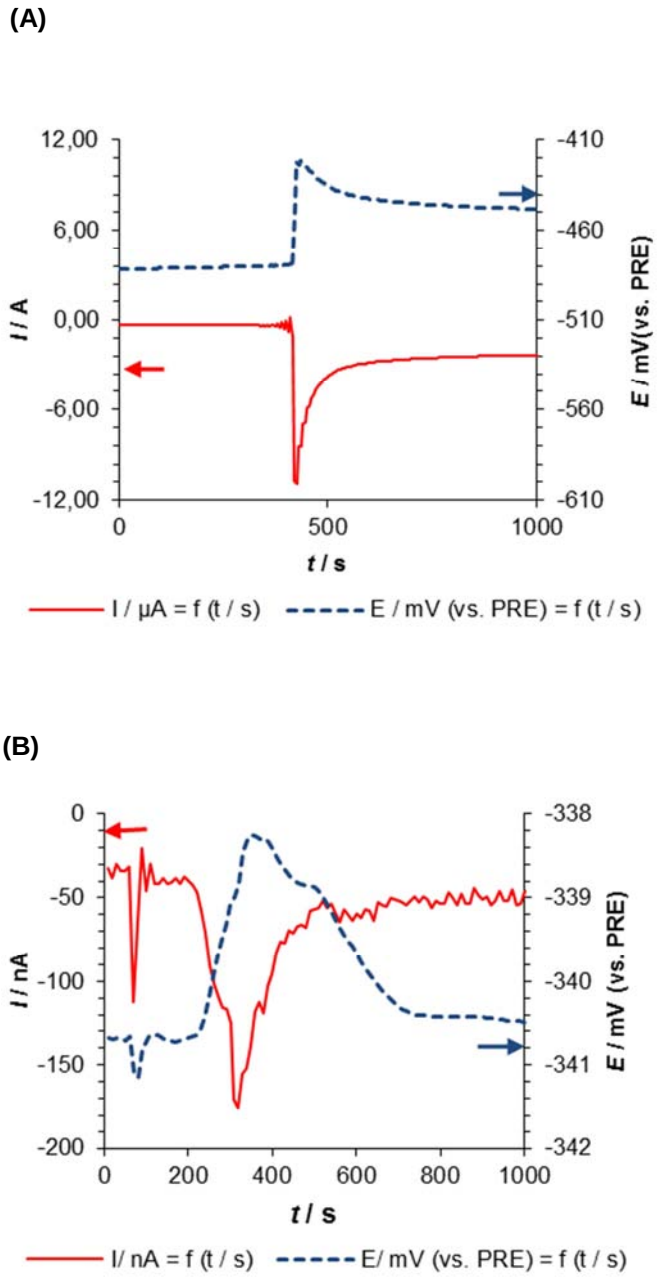

Fig. 3. (A) Typical current time record (*I*/nA= f(*t*/s)) and potential time record (*E*/mV(vs. PRE)= f(*t*/s)), sampled with 0.2 Hz frequency in the control cell during initial 19 days of the test; (B) Typical current time record (*I* /nA= f(*t*/s)) and potential time record (*E* /mV(vs. PRE) = f(*t*/s)), sampled with 0.1 Hz frequency in the experimental cell during initial 19 days of the test.

(A)

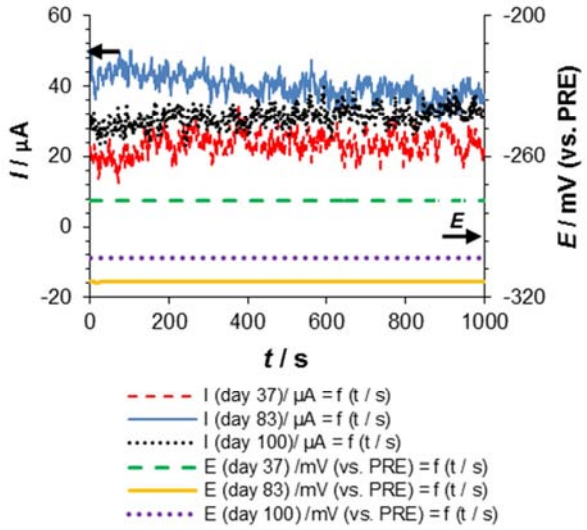

(B)

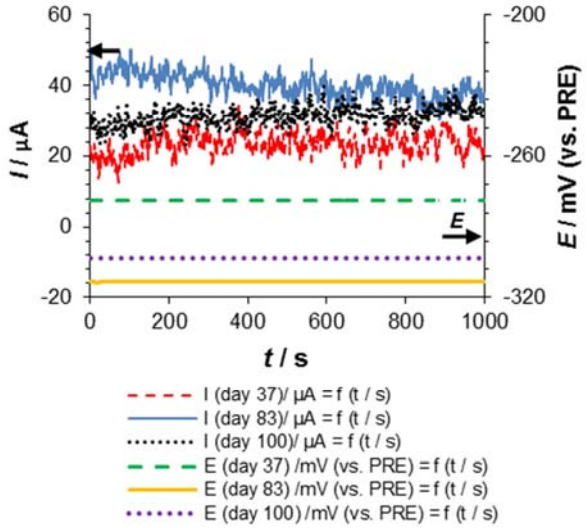

Fig. 4. Typical current time record (/µA= f(*t*/s)) and potential time record (*E*/mV(vs. PRE)= f(*t*/s)), sampled with 1 Hz frequency during the period from day 24 of the test until the test termination: (A) Control cell; (B) Experimental cell.

3.1.2. Corrosion mechanism monitoring by EN sequence independent analysis

Localized Index (LI) values obtained from the sequence-independent analysis of ECN data from the control cell are presented in Fig. 5A. With one LI data point calculated for every 1280 seconds (about 21.3 minutes), fluctuations between 0.005 and 1 were observed during the initial 580 hours. Higher values of LI can be interpreted as increased surface electrochemical activity that could be correlated with the tendency for localized reactions [47], what is in agreement with observed characteristic current and potential trends (Fig. 3A).

The fluctuations of LI correspond to localized corrosion and metastable pitting/uniform corrosion common for low carbon steel in a marine environment [42]. After 30 days, the initial LI decreased to values around 0.1 and it was maintained in that range. Since LI values do not correspond to values characteristic of general corrosion or to any other type of corrosion, they can, therefore, be interpreted as indicative of mixed corrosion [49]. It is likely that the continuous initiation, activation and de-activation of numerous pits resulted in general corrosion.

(A)

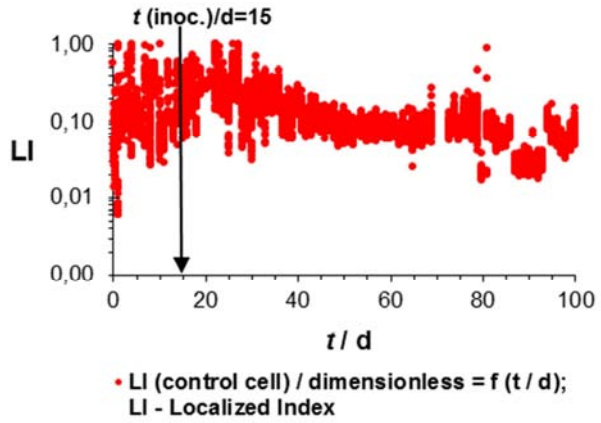

(B)

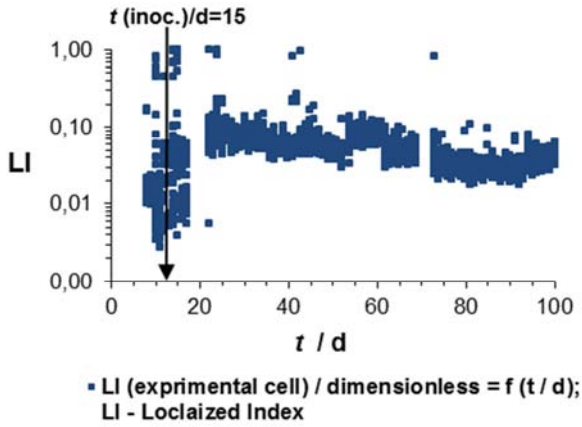

Fig. 5. Localized Index (LI/ dimensionless) values calculated for ECN data acquired in the control cell, versus time (*t*/d), during the 100 days test period for: (A) Control Cell; (B) Experimental Cell. All calculated points plotted (67 point/day).

LI values obtained from the sequence independent analysis of ECN data from working electrodes exposed in the experimental flow cell are presented in Fig. 5B.

Compared to data obtained from the control cell, the LI values are much smaller. During the first19 days, the fluctuations of LI occurred mainly in the range from 0.005 to 0.05 with occasional and random increases to a value of 1. Most likely, the localized corrosion activity was low and uniform corrosion dominated [48]. Furthermore, during the same time period, LI fluctuations up to a value of 1 were noted. This corresponds to transients that were observed during the analysis of current and potential records and which were indicative of pitting (Fig. 3). After 22 days an increase in LI from approximately 0.02 to 0.1 was recorded. It is likely that the prevailing boundary and/or mixed corrosion resulted from the initial metastable pitting attack, which led to uniform corrosion.

Furthermore, acquired ECN data were subjected to additional statistical analysis resulting with calculation of skewness and kurtosis values. Fig. 6A reveals that for WE in the control cell, the skewness fluctuated in the range -0.6< skewness <0.6 and kurtosis in the range of -1.2< kurtosis <1.2 for most of the duration of the test. Larger fluctuations of skewness (up to a value of 5) and of kurtosis (up to a value of 20) were detected mainly during the initial 22 days of testing. For both parameters, values within a range of -1< skewness and kurtosis <1 indicate uniform corrosion [43]. The result thus suggests that this type of corrosion was dominant in the control flow cell. However, randomly occurring higher values of kurtosis signify the presence of sporadic localized surface events.

In the experimental flow cell, skewness and kurtosis values were mostly in the range of -1< skewness and kurtosis <1 (Fig. 6B). Larger fluctuations of skewness, -5< skewness <5 and of kurtosis (up to value of 45) were occasionally observed, in particular during the initial 18 days of the test. The higher value of skewness and kurtosis coincided with higher values of LI. However, even the maximum recorded values fell within the range attributed to uniform corrosion [47]. Although initial fluctuations of skewness and kurtosis were more pronounced in the experimental cell, the general behaviors of these two parameters were rather similar for the two cells during the testing period and indicative of general corrosion.

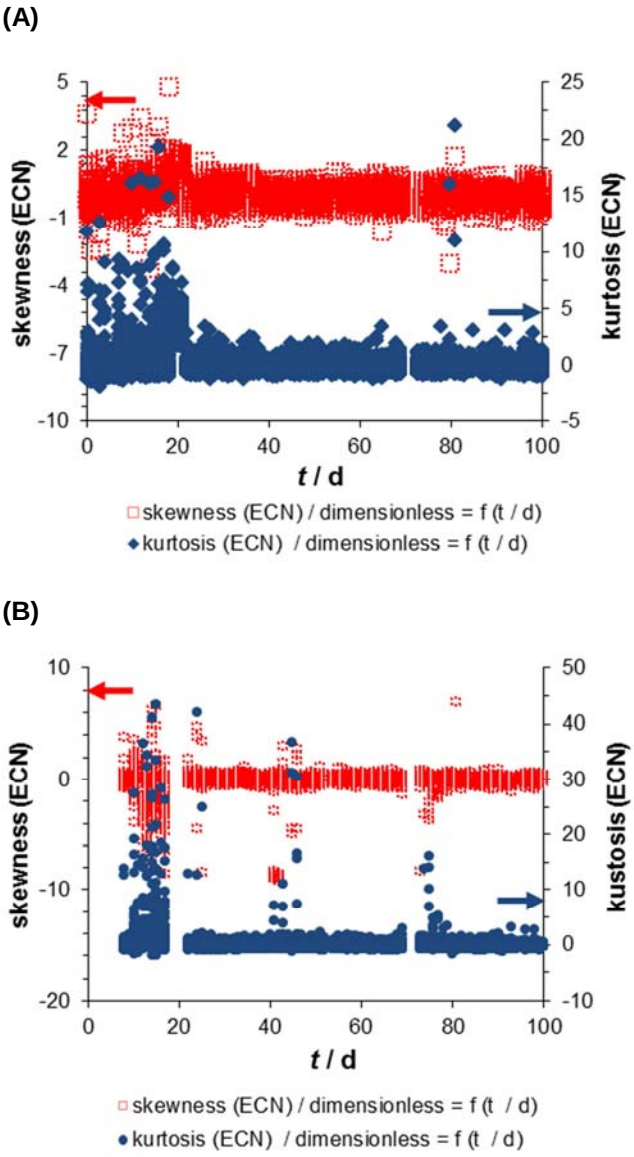

Fig. 6. skewness (ECN)/ dimensionless and kurtosis (ECN)/ dimensionless values calculated for ECN data acquired during the 100 days versus time (*t*/d): A) Control cell; B) Experimental cell. All calculated points plotted (67 point/day).

3.2. Surface analysis

SEM micrographs revealed differences in morphology and abundance of deposits on steel specimens located at 6 o'clock position in the control and experimental cells. In the latter flow cell, abundant black deposits were seen (Fig. 8A), while only scarce greenish deposits were noted in the control cell (Fig. 7A). The presence of biofilms was evident in SEM micrographs depicting surfaces of specimens exposed in the experimental cell (Fig. (B). There was no visible biofilm on surfaces of specimens in the control cell (Fig. 7B).

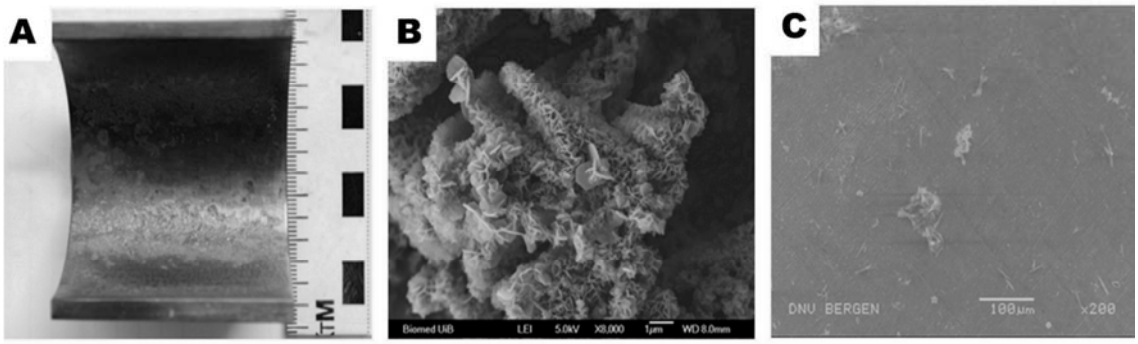

Fig. 7. Macro and micro photographs (6 o'clock position) of specimens after 100 days of a exposure in the control cell: (A) Photography of coupon before preparation for SEM/EDX; (B) SEM image (8000x) of the immobilized corrosion products deposits; (C) SEM image (200x) with of grey/ greenish layer formed in the coupon, total area is scanned by EDX.

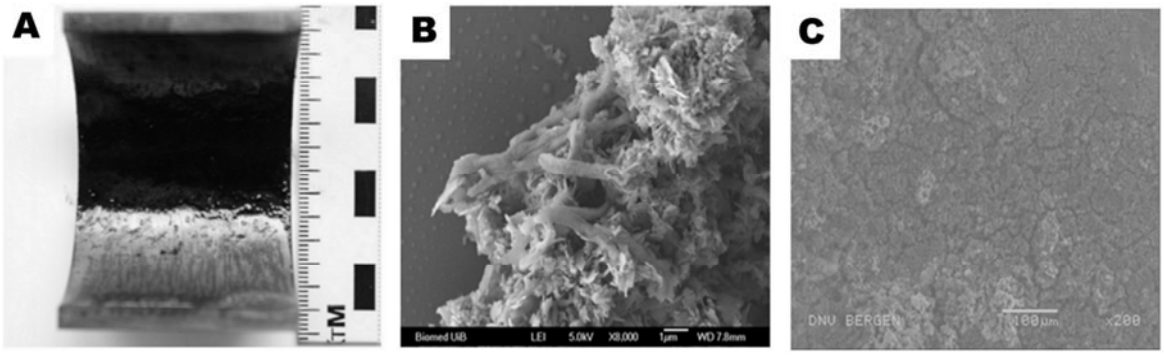

Fig. 8. Macro and micro photographs (6 o'clock position) of specimens after 100 days of a exposure in the experimental cell: (A) Photography of coupon before preparation for SEM/EDX; (B) SEM image (8000x) of the immobilized corrosion products/ biofilm deposits; (C) SEM image (200x) with of black deposit formed in the coupon, total area is scanned by EDX.

EDX analysis (Tab. 1) revealed the presence of iron (Fe), sulfur (S), oxygen (O), magnesium (Mg), calcium (Ca) and chlorine (Cl) in corrosion products on surfaces of steel specimens irrespective of the exposure conditions. However, their atomic fractions for scanned surfaces (At/%), differed between the flow cells. The elemental composition was independently confirmed using ICP-AES analysis of dissolved corrosion products (Tab. 2). The amount of sulfur was statistically significantly higher in corrosion products on surfaces of samples exposed in experimental flow cell. Although EDX cannot provide direct information on the identity of the compound associated with the sulfur peak, the observation of the iron signal in the spectra together with sulfur peek supports that the black deposits, that when exposed to hydrochloric acid produce smell characteristic of sulfide, observed on specimens in the experimental cell (Fig. 8A) were iron sulfides. Bacterial cells imaged on surfaces of these specimens were associated with crystalline structures (Fig. 8B). Spectra of specimens exposed in both the control and experimental cells revealed high levels of calcium and magnesium (Tab.1 and 2). Both chlorine and oxygen peaks were also prominent in these deposits. Although speculative, it is not inconceivable that under ambient temperature conditions biominerals such as e.g. green rusts I and II (Fe(II) Fe(III) hydroxycarbonate, or hydroxysulphate, respectively) or dolomite ($CaMg(CO_3)_2$) were formed [50, 51]. In marine environments, green rust is often identified as a carbon steel corrosion product. The green rust formation could explain visual observations of faint green deposits on surfaces of the specimens from the control cell (Fig. 7A). Although such deposits were not seen on surfaces of specimens from the experimental cell (Fig. 8A), corrosion product analysis (Tab. 2) indicated that these minerals are likely to be present. The absence of biofilms on specimens exposed at 6 o'clock position in the control cell was reflected by different chemical composition of the corrosion products, (low sulfide concentration) and the absence of black deposit (Fig. 7A and 7B). In addition to being present in dolomite, the calcium peak in EDX spectra is probably also associated with calcium

carbonate, most likely aragonite. The long crystal rod seen in SEM micrograph (Fig. 7C) is similar to the reported structure of this mineral [52].

Tab. 1: Results of EDX surface analysis of 6 o'clock coupons after 100 days of exposure in control and experimental cell. Results given in atomic fractions (At(element)/%) for iron (Fe), sulfur (S), oxygen (O), magnesium (Mg), calcium (Ca) and Chlorine (Cl).

	At(Fe)/ % [1]	At(S)/ % [2]	At(O)/ % [3]	At(Mg)/ % [4]	At(Ca)/ % [5]	At(Cl)/ % [6]
Control cell - corrosion product	49.2	1.8	33.8	1.9	0.1	3.3
Control cell - surface after corrosion product removing	80.3	0.3	8.7	NA	0.1	0.1
Experimental Cell - corrosion product	31.5	5.2	48.6	0.7	0.3	9.9
Experimental Cell - surface after corrosion product removing	89.0	0.7	8.4	NA	NA	NA

[1] percentage of iron (Fe) by number of atoms in the scanned area
[2] percentage of sulfur (S) by number of atoms in the scanned area
[3] percentage of oxygen (O) by number of atoms in the scanned area
[4] percentage of magnesium (Mg) by number of atoms in the scanned area
[5] percentage of calcium (Ca) by number of atoms in the scanned area
[6] percentage of chlorine (Cl) by number of atoms in the scanned area

Tab. 2. ICP- AES analysis of corrosion products removed from 6 o'clock positioned steel specimens surface after 100 days of the exposure and dissolved in aqueous HCl solution (50 v/v %). Results given in molar concentrations (c(element)/mM)) for iron (Fe), calcium (Ca), potassium (K), magnesium (Mg), sodium (Na), and sulfur (S).

	c(Fe)/ mM[1]	c(Ca)/ mM[2]	c(K)/ mM[3]	c(Mg)/ mM[4]	c(Na)/ mM[5]	c(S)/ mM[6]
Control Cell	13.9	3.1	0.1	0.3	1.4	0.7
Experimental cell	18.5	1.7	0.1	1.4	1.8	7.3

[1] molar concentration of iron (Fe) in analyzed sample
[2] molar concentration of calcium (Ca) in analyzed sample
[3] molar concentration of potassium (K) in analyzed sample
[4] molar concentration of magnesium (Mg) in analyzed sample
[5] molar concentration of sodium (Na) in analyzed sample
[6] molar concentration of sulfur (S) in analyzed sample

The removal of corrosion products from specimen surfaces exposed general corrosion pattern (Fig 9).

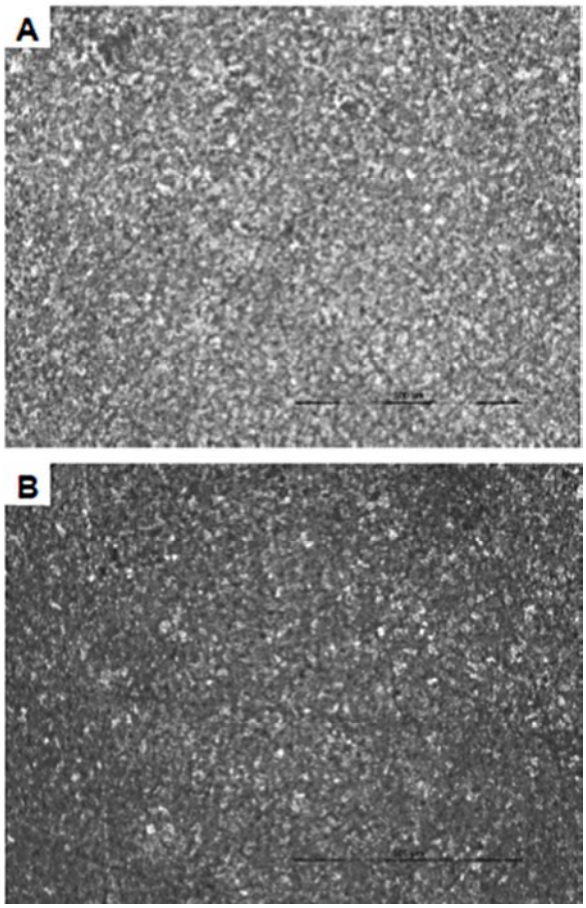

Fig. 9. Working electrode micro photographs (100x) after 100 days of an exposure in the: (A) control cell (after corrosion product removal); (B) experimental cell (after corrosion product removal).

3.2. Characterization of bacterial communities

Five 16S rRNA libraries were generated using DNA isolated from samples listed in section 2.2. The recovery of DNA from biofilms removed from steel surfaces exposed in the control flow cell (BCFC) and from water collected from this cell (WCFC) which would provide meaningful sequences was unsuccessful. The total number of bands in DGGE profiles in samples with recoverable intact DNA (profiles not shown) is summarised in Tab. 3.

DGGE analysis of the seawater sample (SW) revealed 11 unique bands in DNA profile, which indicates the presence of at least 11 different bacterial strains. None of the bands detected in SW could be matched with bands obtained from field enrichments (BFE) or from the bioreactor vessel inoculum (BVI). DNA profile from BVI revealed 7 bands of which 4 were shared with the profile representing biofilms removed from steel specimens exposed in the experimental flow cell (BEFC). This strongly suggests that out of at least 7 strains seeded into the bioreactor vessel only 4 were successful in colonising steel surfaces. At least 2 bands in BEFC profile originated from SW as they were absent from BVI profile. All 4 bands seen in the profile of DNA which represented planktonic population in the experimental cell (WEFC) were common with bands seen in BVI and BEFC profiles. Thus, at the time of sampling, 2 out of 6 bacterial strains detected in BEFC were present solely as sessile populations and were not detectable in the bulk liquid phase. The DNA profile from the biofilm field enrichment in SRB/2 medium (BFE) was the least divers with only 3 visible bands, all of which were represented in BEFC profile.

Three very faint bands were observed in DGGE profiles of DNA from bulk fluid and sessile samples in the control cell. The position of these bands matched the position of the bands in BVI and in BFE profiles. Since DNA can pass freely through a 2 µm filter the bands were representing DNA of dominant bacteria species seeded into the bioreactor vessel. It is important to realize that the presence of the DNA bands alone does not necessarily signify the presence of living bacterial cells. Therefore, it is imperative that molecular data are confirmed with microscopy imaging. The SEM results, reported above, verified the absence of bacterial cells in the control flow cell.

Cloning and sequencing confirmed the presence of 16S rRNA sequences characteristic of sulfate-reducing bacteria of the genus *Desulfovibrio* (99% sequence similarity with *Desulfovibrio profunda* DSM 11384) and sulfidogenic spore forming Firmicutes of the genus *Caminicella* (99% sequence homology with *Caminicella sporogenes* strain AM1114) in biofilm field enrichments used for the seeding of the bioreactor vessel (Tab. 4). However, planktonic and sessile populations in the experimental flow cell revealed H_2S-producing bacteria of phyla Firmicutes and Synergistetes as dominant clones. In the former phylum, the genus *Caminicella* was the most abundant clone in both, biofilms on steel coupons and in the liquid phase. None of the selected clones had 16S rRNA sequences identifiable as belonging to SRB.

Tab. 3: The total number of bands and the number of dominating bends in DGGE profiles in samples with recoverable DNA**.**

Sample	Number of bends	Number of dominating bends
As-received North Sea seawater (SW)	11	5
The biofilm field enrichment in SRB/2 medium (BFE)	3	2
Bioreactor vessel inoculum (BVI)	7	2
Biofilms from the experimental flow cell (BEFC)	6	2
Water samples from the experimental flow cell (WEFC)	4	1

Tab. 4: Identification of bacterial species detected through cloning and sequencing of DNA recovered from field and laboratory samples, including as-received North Sea seawater. Sample description is provided above in the section 2.2.4.

Source of DNA	Bacteria identified through cloning and sequencing
SW	Alphaproteobacteria; Rhodobacterales **[6] *Nautella italica* strain LMG 24365**[6] Gammaproteobacteria; Oceanospirillates **[1] *Alcanivorax dieselolei* strain B-5**[5] **[10] *Alteromonas* spp. (*Alteromonas macleodii*)**[6] Firmicutes; Bacilli **[1] B*acillus smithii* strain NRS-173**[4]
BFS	Deltaproteobacteria **[4] *Desulfovibrio profunda* DSM 11384**[1] Marine bacterium **[2] *Marinifilum fragile* strain JC2469**[4,6]
BI	Firmicutes; Clostridia **[6] *Caminicella sporogenes* strain AM1114**[1,2,3,5]
BEFC	Firmicutes; Clostridia **[4] *Caminicella sporogenes* strain AM1114**[1,2,3,5]
WEFC	Firmicutes; Clostridia **[5] *Caminicella sporogenes* strain AM1114**[1,2,3,5] **[2] *Thermoanerobacter brockii* subsp. Lactiethylicus**[1,5] Synergistetes **[1] *Thermovirga lienii* DSM 17291 strain Cas60314**[1,2,3,5] **[2] *Anaerobaculum thermoterrnum* strain RWcit**[1,5]

[x] Number of clones
Physiology: [1]H_2S production, [2]Acetate production, [3]H_2 production, [4]Nitrate reduction, [5]Thermophilic and [6]Mesophilic

Although DNA from SW contained sequences of alphaproteobacteria and bacteria of the genera *Bacillus*, *Rhodobacterales, Oceanospirillates* and *Alteromonas*, there was no evidence that these organisms persisted as dominant species either in the planktonic phase or in biofilms on steel specimens in the experimental flow cell. Sulfidogenic Synergistetes of genera *Thermovirga* and *Anaerobaculum* were identified only in the bulk fluid of the experimental flow cell and were absent in clones from SW and from the bioreactor inoculum. It is important to note that the selection of clones is a random process. A low abundance of the clone representing certain sequence signifies that DNA representing this sequence is a minor contributor to the overall DNA pool. Therefore, the probability of detecting such sequence is low. The presence of sequences belonging to Synergistetes in the DNA recovered from the liquid phase of the experimental cell and their lack in the bioreactor inoculum and in seawater sample indicates a low frequency of corresponding clones in BVI and in SW DNA samples at the beginning of the experiment. Likewise, the absence of SRB sequences in the experimental flow cell, despite identifying those sequences in the bioreactor inoculum, is likely due to the increase of DNA from Firmicutes of the class *Clostridia*, of which most are thiosulfate and organic sulphur reducers.

DGGE analysis revealed that bacterial diversity in all DNA samples was higher than the cloning results would indicate. However, as already stated, cloning demonstrated that sulfidogenic spore forming bacterium of the phylum *Firmicutes* and the genus *Caminicella* was, most likely, the dominant biofilm and planktonic organism in the experimental flow cell.

4. Discussion

Corrosion measurements carried out by LPR and EN revealed both similarities and differences in the corrosion behavior of carbon steel specimens exposed in the control cell versus the experimental cell.

The observed initial fluctuations of OCP in both cells were likely reflecting chemical changes to the specimen surfaces occurring during short period after specimen immersion. As mentioned previously, OCP stabilized at -800< E(OCP)/mV(vs. SCE) <-700 in both flow cells what corresponds to values reported elsewhere [53].

For most of the testing period, the overall rate of corrosion, e.g. $1/(R_p/\Omega)$, was lower in the experimental flow cell than in the control flow cell. However, at the beginning and towards the end of the experiment, the corrosion behavior was similar in the two cells. In both cells, the corrosion resistance of steel was very high (Fig. 2) during the first 21 days of the test, i.e. before and immediately after inoculation. This indicates that a protective ferrous film remained relatively intact on the metal surface, despite the presence of high concentration of aggressive chloride ions in the seawater. A similarly high corrosion resistance has previously been reported for carbon steel in a sterile artificial growth medium containing high concentrations of aggressive ions [47].

Between day 21 and day 52, there was a marked increase in the $1/(R_p/\Omega)$ values in the control, but not in the experimental flow cell, see Fig. 2. In general, such variations may be due to differences in the mineralization processes [6, 54]. The increase in $1/(R_p/\Omega)$ for the control flow cell is consistent with a breakdown or a gradual weakening of the protective ferrous layer [54] that occurs concurrently with the observed formation of iron oxides and of a thin, sparse and localized ''green rust'' layer on the carbon steel surfaces (Fig. 7 and Tab. 3). Such localized mineral formation has previously been reported to result in increased average $1/(R_p/\Omega)$ values, presumably due to the formation of galvanic concentration cells [15].

The observation that $1/(R_p/\Omega)$ remains at relatively low values in the experimental flow cell, up to about day 83 , can be given different explanations. It may be that the minerals formed in the experimental flow cell do not have as pronounced an effect of weakening the protective ferrous layer as those formed in the control flow cell. In addition, the presence of biofilm and high concentrations of microbial endo- and exo- metabolites will lead to an additional build-up of a biotic layer on the carbon steel surfaces in the experimental flow cell. Finally, higher concentrations of bacterially produced dihydrogen sulfide in the experimental reactor are expected to result in the formation of different iron sulfides layers (Tab. 1). Thus, the biotic layer could be modified by a compact and protective layer of iron(II) sulfide (FeS) and iron(III)-oxide (Fe_2O_3) [53] or green rust in our study. The evidence is that the cumulative effect of these processes is protective relative to the control cell (Fig. 16).

From about day 50 until test termination, the $1/(R_p/\Omega)$ values in the control cell remained relatively stable, with some increase, see Fig. 2A. This may reflect a state of instability of surface deposits with opposing rates of formation and destruction of local defects in the corrosion products layers (54). This is supported by the observations of EN patterns characteristic for metastable pitting (Fig. 3A) and of LI values indicative of a mixed corrosion mechanism (Fig. 5A) [48, 49].

The EN data suggests a mixed corrosion mechanism for both flow cells. The occurrence of localized corrosion events, in particular metastable pitting, is consistent with the observation of large fluctuation (transients) in the acquired EN data from both flow cells. Conditions favorable for pitting may exist even before reactor inoculation. Sulfate ions may/ react with dissolved oxygen (measured at low concentrations during the initial 24 days of the test) to produce aggressive thiosulfate ions [55]. Together with chloride ions, already present at a high concentration in seawater, they create conditions favorable for the onset of localized corrosion events (metastable or stable pitting).

During the course of the experiment, both mineral layers and a microbially-produced protective layer were formed in the experimental flow cell after inoculation, as evidenced by the observation of black deposits comprised of organic matter and mineral corrosion products (Fig. 8B and 8C). Similar types of deposits have been reported in experiments that involved approximately 125 days of anaerobic stagnant exposure of low carbon steel [53]. In the experiments herein, different minerals were deposited on the surfaces in the control flow cell. All such deposits are likely to modify, to a varying extent, the exposure of the steel surfaces to the aggressive anions and, thus, to induce differences both in corrosion resistance and in the extent of pitting between the two environments.

The breakdown of protective layers and subsequent metastable pitting can occur on metal surfaces without significantly changing the corrosion resistance. This has been reported, for example, for SRB harboring marine biofilms [53].

In the experimental flow cell, a substantial increase in corrosion rate was recorded after 92 days of test. This was likely caused by a breakdown of an iron sulfide layer, most probably induced by minor changes to the chemistry of the environment, such as a decrease of pH.

The presence of both calcium and magnesium mineral deposits in flow cells indicate the possible precipitation of carbonates, including an iron-dolomite mineral, e.g. Fe-$CaMg(CO_3)_2$. Dolomite formation is generally observed at high temperatures; however, it has also been described at low temperature [59, 60]. Development of dolomite under anaerobic sulfidogenic conditions has been reported in Lagoa Vermelha and Brejo do Espinho, two supersaturated saline lagoons along the Rio de Janeiro coast of Brazil [56, 58]. Sulfide-producing Firmicutes e.g. *Caminicella* specie, identified as dominant biofilm and planktonic organism in the experimental cell, generates, as reported for many clostridia, high concentrations of carbon dioxide during its growth. The combination of anoxic production of carbon dioxide and sulfide ions would facilitate precipitation of carbonate minerals. It is widely accepted that, if intact, calcareous deposits on steel surfaces act as a protective barrier against chloride and sulfide anions.

Identification of Firmicutes as a dominant phylum in analysed biofilms was not surprising. They are ubiquitous in marine environments and *Clostridia* are typically more versatile in the use of carbon sources and electron donors/acceptors than SRB are. It is most likely that under favourable growth conditions, *Clostridia* outcompete SRB in biofilms on carbon steel. Moreover, presence of sulfidogenic microorganisms other than SRP was expected due to nature of the growth media used for preparing inoculates. The commercial SRB/2 media used for preparing biofilm field enrichments are also selective for dihydrogen sulfide producers other than SRP. A number of reports indicate that the spore forming sulfidogenic and carbon dioxide producing populations representing *Clostridia* are very abundant in oil field systems, frequently outnumbering SRP [10, 30, 59]. It is, thus, conceivable that this group of bacteria poses higher corrosion and souring threat to oilfield installations than SRB alone would.

Moreover, general corrosion deterioration pattern revealed after corrosion products removal in both cells confirms leads that EN analysis provided regarding type of corrosion mechanism that took place on exposed surfaces (mixed mechanism; pitting/general corrosion). It is noteworthy that the uniform corrosion can result from the merging of continuously formed stable and metastable pits [60].

The observed final corrosion rate of carbon steel was relatively moderate, irrespective whether the steel was exposed to seawater or to a combination of seawater and sulfidogenic bacterial community. Corrosion rates of carbon steel observed at the end of 100 days test period in bioreactor flow loop were in agreement with integrity evaluations (corrosion rates acquired by electric resistance (ER) and LPR probes) of low carbon steel SWIS located on an offshore installation in the Norwegian sector of the North Sea (personal communication). It is required to keep in mind that even though acquired corrosion rate values are very similar, it is possible that in a more appropriate experimental set-up (continuously fed with fresh media flow loop enabling higher fluid velocities would be more representative of typical SWIS) acquired values could differ more depending on the presence and activity of biofilms. It was reported that amount of nutrients, in this investigation is possibly limited by experimental set-up volume, may be restricting factor for microbial activity [16], as well as factor inhibiting electrochemical activity of established biofilms [61]. Therefore, lack of sufficient amount of nutrients may result with lower corrosion rates in systems were main culprits of corrosion are bacteria. Even though the bioreactor loop accommodated relatively low volume of test media (approximately 40 L), same volume was sufficient for development of electroactive biofilms that led to relatively low corrosion and formation of specific bioinorganic and corrosion products. Longer exposure periods could lead to elevated corrosion rates. However, 100 day test is relevant as it represents typical period between two pigging operations (cleaning operations) and time between replacements of offshore electrochemical probes.

A number of studies address corrosion of carbon steel, and thus the evolution of carbon steel integrity, in laboratory experiments in which the carbon steel was exposed to pure sulfidogenic cultures or to isolated offshore consortia in different growth media [50, 65, 66]. Additional reports have presented results on long-term exposures of structural steel in natural seawater [64]. Mostly, low corrosion rates and the presence of mixed corrosion mechanisms were reported [47, 64]. These results are in good agreement with the outcome of the present investigation.

5. Conclusion

Our current work has shown that under chosen experimental conditions, metabolic activity of sessile sulfide and carbon dioxide producing bacterial populations dominated by *Caminicella* specie generated abundant sulfide layer, as well as carbonaceous mineral precipitates on the carbon steel samples. The overall impact of the bacterial consortium on the corrosion rate of S235JR carbon steel specimens was minor. The sterile / inoculated condition had apparently no significant influence on the corrosion rate of carbon steel during the 100 days of exposure in the flow reactors. Clearly, the release of biogenic sulfide does not necessarily lead to extensive localized pitting attack. It is apparent that metabolic activities of cells are likely to influence the chemistry of bioinorganic corrosion products and should be considered when evaluating MIC risk.
It is worth mentioning that despite offering valuable insights into complex corrosion processes occurring in biotic systems, strictly controlled laboratory tests are not totally representative for offshore water injection systems. Therefore, before implementing with confidence these findings into the corrosion monitoring routines of the oil and gas industry, it is important to evaluate in-depth all differences between the laboratory and field corrosion measuring methodologies. A perfect alignment of the laboratory and field corrosion data would ensure immediately field-applicable corrosion control measure.

Acknowledgments

Funding was received from the European Community's Seventh Framework Programme (FP7/2007-2013). The authors wish to express their gratitude towards Dr. Jan Sunner from University of Oklahoma, Dr. Karine Drønen from University of Bergen, and Ing. Øystein Birketveit from MISWACO for their support in the production of presented work.

References:

[1] S.W. Borenshtein, Microbiologically influenced corrosion handbook, Woodhead Publishing Limited, Cambridge, UK, 1994.

[2] H.A. Videla, Manual of biocorrosion, CRC Press, Boca Raton, FL, USA, 1996.

[3] E. Heitz, H.C. Flemming, W. Sand (Eds.), Microbially Influenced Corrosion of Materials, Eds. Springer-Verlag GmbH & Co KG, Berlin, Germany, 1996.

[4] I.B. Beech, J. Sunner, Biocorrosion: towards understanding interactions between biofilms and metals. Current Opinion in Biotechnology 15 (2004), 181-186.

[5] M. Madigan, J.M. Martinko, P.V. Dunlap, D.P. Clark. 2012. Brock Biology of Microorganisms, 13th ed. Pearson-Benjamin Cummings, San Francisco, CA, USA, 2012.

[6] J. Duana, S. Wua, X. Zhanga, G. Huangb, M. Duc, B. Houa, Corrosion of carbon steel influenced by anaerobic biofilm in natural seawater, Electrochimica Acta 54 (2008), 22–28.

[7] M. Franklin, D.C. White, B.J. Little, R. Ray, R. Pope, The Role of Bacteria in Pit Propagation of Carbon Steel, Biofouling 15 (2000), 13-23.

[8] A. Agrawal, K.Vanbroekhoven, B. Lal, Diversity of culturable sulfidogenic bacteria in two oil–water separation tanks in the north-eastern oil fields of India, Anaerobe 16 (2010), 12–18.

[9] J. Jan-Roblero, J.M. Romero, M. Amaya, S. Le Borgne, Phylogenetic characterisation of a corrosive consortium isolated from a sour gas pipeline. Applied Microbiology and Biotechnology, 64 (2004), 862–867.

[10] H.S. Park, I. Chatterjee, X. Dong, S-H. Wang, C.W. Sensen, S.M. Caffrey, T. R. Jack, J. Boivin, G. Voordouw, Effect of Sodium Bisulfite Injection on the Microbial Community Composition in a Brackish-Water-Transporting Pipeline, Applied Environmental Microbiology 77 (2011), 6908-6917.

[11] J. Larsen, K. Rasmussen, H. Pedersen, K. Sørensen, T. Lundgaard, T.L. Skovhus, Consortia of MIC Bacteria and Archaea causing Pitting Corrosion in Top Side Oil Production Facilities, Corrosion/2010, Paper no. 10252, NACE International, San Antonio, TX, 2010.

[12] T. Zhang, H.H. Fang, B.C. Ko, Methanogen population in a marine biofilm corrosive to mild steel, Applied Microbiology and Biotechnology 63 (2003) 101-6.

[13] S.M. Caffrey, H.S. Park, J. Been, P. Gordon, C.W. Sensen, G. Voordouw, Gene Expression by the Sulfate-Reducing Bacterium Desulfovibrio vulgaris Hildenborough Grown on an Iron Electrode under Cathodic Protection Conditions, Applied and Environmental Microbiology 74 (8) (2008), 2404–2413.

[14] R.E. Melchers, R. Jeffrey, The critical involvement of anaerobic bacterial activity in modeling the corrosion behavior of mild steel in marine environments, Electrochimica Acta 54, Special Issue BIOCORROSION OF MATERIALS (2008), 80-85.

[15] B.J. Little, J.S. Lee, Microbiologically Influenced Corrosion, Hoboken, John Wiley and Sons Inc., New Jersey, USA, 2007R.

[16] K. Pedersen, Factors regulating microbial biofilm Development in a system with slowly flowing seawater, Applied and Environmental Microbiology 44 (5) (1982), 1196-1204.

[17] P. Lens, V. O'Flaherty, A.P. Moran, P. Stoodley and T. Mahony, Biofilms in Medicine Industry and Environmental Biotechnology, IWA Publishing, London, UK, 2003, 121-124.

[18] K.F. Ettwig, D.R. Speth, J. Reimann, M.L. Wu, M.S.M. Jettenand, J.T. Keltjens, Bacterial oxygen production in the dark, Frontiers in Microbiology 3, Evolutionary and Genomic Microbiology August 3 (2012), Article 273.

[19] J.D. Coates, R.T. Anderson, Emerging techniques for anaerobic bioremediation of contaminated environments, Trends in Biotechnology 18 (10) (2000), 408-412.

[20] T. Richardson, R.A. Cottis, R. Lindsay, S. Lyon, D. Scantlebury, H. Stott, M. Graham, Shreir's corrosion 2010: Corrosion in microbial environments, Volume 2, Elsevier, Oxford, UK, 2010.

[21] J. Wen, K. Zhao, T. Gu, S. Nešić, Effects of mass transfer and flow conditions on SRB corrosion of mild steel, Corrosion/2006, Paper No. 06666, NACE International, Houston, TX, 2006.

[22] P. Stoodley, I. Dodds, J.D. Boyle, H.M. Lappin-Scott, Influence of hydrodynamics and nutrients on biofilm structure, Journal of Applied Microbiology Symposium Supplement 85 (28) (1999), 19-28.

[23] J. Wen, T. Gu, S. Nešić, Investigation of the effects of fluid flow on SRB biofilm, Corrosion/2007, Paper no. 07516, NACE International, Nashville, TN, 2007.

[24] W. Teughels, N. Van Assche, I. Sliepen, M. Quirynen, Effect of material characteristics and/or surface topography on biofilm development, Clinical Oral Implants Research 17 (2006), 68–81.

[25] D. Clover, B. Kinsella, B. Pejcic, R. De Marco, The influence of microstructure on the corrosion rate of various carbon steels. Journal of Applied Electrochemistry 35 (2005), 139-149.

[26] R. Cord-Rustwich, W. Kleinitz, F. Widdel, Sulfate-Reducing Bacteria and Their Activities in Oil Production, Journal of Petroleum Technology 39 (1) (1987), 97-106.

[27] J. Larsen, K. Sørenson, K.Højris, T.L. Skovhus, Significance of Troublesome Sulfate-Reducing Prokaryotes (SRP) in Oil field Systems, Corrosion/2007, Paper no. 09389, NACE International, Atlanta, GA, 2009.

[28] J.M. Suflita, D.F. Aktas, A.L. Oldham, B.M. Perez-Ibarra, K.E. Duncan, Molecular tools to track bacteria responsible for fuel deterioration and microbiologically influenced corrosion, Biofouling 28 (9) (2012), 1003-1010.

[29] D. Li, D.J. Midgley, J.P. Ross, Y. Oytam, G.C.J. Abell, H. Volk, W.A.W. Daud, P. Hendry, Microbial biodiversity in a Malaysian oil field and a systematic comparison with oil reservoirs worldwide, Archives of Microbiology 194 (6) (2012), 513-23.

[30] E. Korenblum, É. Valoni, M. Penna, L. Seldin, Bacterial diversity in water injection systems of Brazilian offshore oil platforms, Applied Microbiology and Biotechnology 85 (2010), 791–80.

[31] K. E. Duncan, L.M. Gieg, V.A. Parisi, R. S. Tanner, S.G. Tringe, J. Bristow and J. M. Suflita, Biocorrosive thermophilic microbial communities in Alaskan North Slope oil facilities, Environmental Science and Technology 43 (2009) 7977–7984.

[32] A. Rajasekar, B. Anandkumar, S. Maruthamuthu, Y.-P. Ting, P. K. S. M. Rahman, Characterization of corrosive bacterial consortia isolated from petroleum-product-transporting pipelines, Applied Microbiology and Biotechnology 85 (2010), 1175 – 1188.

[33] R.D. Kane, Control of microbially induced corrosion in seawater, Corrosion/2004, Paper no. 04579, NACE International, Houston, TX, 2004.

[34] G.J. Licina, C.S. Carney, Monitoring biofilm formation and incipient MIC in real time, Paper no. 175, Corrosion/99, NACE International, Houston, TX, 1999.

[35] J. Lin, J.R. Frank, E.J. St. Martin, D.H. Pope, Electrochemical noise measurements of sustained microbially influenced pitting corrosion in a laboratory flow loop system, Paper no. 198, Corrosion/99, NACE International, Houston, TX, 1999.

[36] M. Faimali, E. Chelossi, G. Pavanello, A. Benedetti, I. Vandecandelaere, P. De Vos , P. Vandamme, A. Mollica , Electrochemical activity and bacterial diversity of natural marine biofilm in laboratory closed-systems, Bioelectrochemistry 78 (2010) 30–

[37] American Petroleum Institute, API-RP 348, 1990.

[38] F. Widdel, G. W. Kohring, F. Mayer, Studies on dissimilatory sulfate-reducing bacteria that decompose fatty acids. 111. Characterization of the filamentous gliding Desulfonema limicola, Microbiology 134 (1983), 286–294.

[39] M. Stern, A.L Geary, Electrochemical Polarization. I. A Theoretical Analysis of the Shape of the Polarization Curves, Journal of Electrochemical Society 104 (1957), 56-63.

[40] M. Stern, A Method For Determining Corrosion Rates From Linear Polarization Data, Corrosion 14 (9) (1958), 440-444.

[41] R.A. Cottis, S. Turgoose, Electrochemical Impedance and Noise, Corrosion Testing Made Easy Series (Ed. Barry C. Syrett), NACE International, Houston 1999.

[42] D.A. Eden, Electrochemical Noise — The First Two Octaves, Corrosion/98, Paper no. 386, NACE International, Houston, TX, 1998.

[43] S.A. Reid, D.A. Eden, Assessment of Corrosion, patent no.: US 6.264.824 B1, United States Patent (2001).

[44] G. Muyzer, T. Brinkhoff, U. Nubel, C. Santegoeds, H. Schafer, C. Wawer Denaturing gradient gel electrophoresis (DGGE) in microbial ecology. Molecular Microbial Ecology Manual (1998) 1-27.

[45] J. Sambrook, E.F. Fritsch, T. Maniatis, Analysis and cloning of eykaryotic genomic DNA, Molecular cloning: a laboratory manual (1989) 9.45-46, Cold Spring Harbor Laboratoty Press, Cold Spring Harbor, NY.

[46] J. Messing, R. Crea, P.H. Seeburg, A system for shotgun DNA sequencing. Nucleic Acids Research 9 (1981), 309-314.

[47] A. Padilla-Viveros, E. Garcia-Ochoa, D. Alazard, Comparative electrochemical noise study of the corrosion process of carbon steel by the sulfate-reducing bacterium Desulfovibrio alaskensis under nutritionally rich and oligotrophic culture conditions, Electrochimica Acta 51 (2006) 3841–3847.

[48] X. Jiang, S. Nešić, Electrochemical Investigation of the Role of Cl− on Localized CO2 Corrosion of Mild Steel, 17th International Corrosion Congress, Paper no. 2414, Las Vegas, NV, 2008.

[49] C.C. Arteaga, J.P. Calderón, C. F. Campos Sedano, J. A. Rodríguez, Comparison of Corrosion Resistance of Carbon Steel and Some Stainless Steels Exposed to LiBr-H2O Solution at low Temperatures, International Journal of Electrochemical Science 7 (2012), 445 – 470.

[50] A. Zegeye, L. Huguet, M.Abdelmoula, C. Carterret, M. Mullet, F. Jorandet, Biogenic hydroxysulfate green rust, a potential electron acceptor for SRB activity Geochimica et Cosmochimica Acta 71 (22) (2007), 5450-5462.

[51] Stefan Krause, Volker Liebetrau, Stanislav Gorb, Mónica Sánchez-Román, Judith A. McKenzie, Tina Treude, Microbial nucleation of Mg-rich dolomite in exopolymeric substances under anoxic modern seawater salinity: New insight into an old enigma, Geology 40 (2012), 587-590.

[52] S.B. Mukkamala, C.E. Anson, A.K. Powell. Modelling calcium carbonate biomineralisation processes, Journal of Inorganic Biochemistry 100 (2006) 1128–1138

[53] J.S. Lee, R.I. Ray, E.J. Lemieux, M.N. Tamburri, B.J. Little, An evaluation of carbon steel corrosion under stagnant seawater conditions, Corrosion / 2004, Paper no. 04595, NACE International, Houston, 2004.

[54] H.A. Videla, L.K. Herrera, R.G. Edyvean, An updated overview of SRB influenced corrosion and protection of carbon steel, Corrosion/2005, Paper no. 05488, NACE International, Houston, TX, 2005.

[55] H.A. Videla, C. Swords, R.G.J. Edyven, Marine Corrosion in Tropical Environments, American Society for Testing and Materials, 2000, p 272.

[56] C. Vasconcelos, J.A. McKenzie, S. Bernasconi, D. Grujic , A.J. Tien, Microbial mediation as a possible mechanism for natural dolomite formation at low temperature, Nature 337 (1995), 220–222.

[57] R. Warthmann, Y.van Lith, C.Vasconcelos, J.A. McKenzie, A.M. Karpoff, Bacterially induced dolomite precipitation in anoxic culture experiments, Geology 28 (2000), 1091–1094.

[58] Y. van Lith, C. Vasconcelos, R. Warthmann, J.C.F. Martins, J.A. McKenzie, Bacterial sulfate reduction and salinity: two controls on dolomite precipitation in Lagoa Vermelha and Brejo do Espinho (Brazil). Hydrobiologia, 485 (2002), 35-49.

[59] B.S Stevenson, H.S Drilling, P.A. Lawson, K.E. Duncan , V.A. Parisi,J.M. Suflita, Microbial communities in bulk fluids and biofilms of an oil facility have similar composition but different structure. Environmental Microbiology 13 (2011), 1078-1090.

[60] R. Jeffrey & R.E. Melchers), The changing topography of corroding mild steel surfaces in seawater, Corrosion Science 49(2007), 2270–2288.

[61] M. Faimali, E. Chelossi a, G. Pavanello, A. Benedetti, I. Vandecandelaere, P. De Vos, P. Vandamme, A. Mollica, Electrochemical activity and bacterial diversity of natural marine biofilm in laboratory closed-systems, Bioelectrochemistry 78 (2010), 30-38.

[62] W. Lee, W.G. Characklis, Corrosion of Mild Steel Under Anaerobic Biofilm, Corrosion 49 (3) (1998), 197-199.

[63] M.J. Hernández Gayosso, G. Zavala Olivares, N. Ruiz Ordaz, C. Juárez Ramirez, R. Garcia Esquivel , A. Padilla Viveros, Microbial consortium influence upon steel corrosion rate, using polarization resistance and electrochemical noise techniques, Electrochimica Acta 49 (2004) 4295–4301.

[64] C.R. Southwell, Influence of marine organisms on the life of structural steel in seawater, Naval Research Laboratory Washington, D.C., 1974.

III.3. Supplementary information: Offshore side-stream monitoring rig and sampling

To conduct proper rick assessment for Microbially Influenced Corrosion (MIC) it is required to acquire relevant biomass/ biofilm samples. Available literature lists different offshore monitoring tools as for example Robbins device [Ruseska *et al*., 1982]. However, design of offshore monitoring equipment is usually adjusted according to specifications of a particular installation or system. In herein reported study, environmental biofilms were collected from standard industrial bio-studs (Fig. III. 6) made of St37 low carbon steel. The stud has a surface area of 0.5 cm^2.

Fig. III. 6. Bio-stud installed in modified-robbins device.

The recommended sampling protocol encompasses several distinctive steps ensuring preservation of the sample.

1. Connect tubing to source of system medium
2. Connect tubing to lid of a transfer container (Fig. III. 7)

Fig. III. 7. Tansfer container.

3. Open transfer container
4. Remove bioprobe from system
5. Place bioprobe in transfer container
6. Fix bioprobe inside transfer conations
7. Close transfer container and start flushing with system medium
8. Flush transfer container with system medium for 5-10 min
9. Close valves and remove tubing
10. Send transfer container ASAP from platform to analysis location (transfer should be fast and not take more than 24-48h)

An important factor is location of sampling equipment. In most situations it predermination with system design, however it is sometimes possible to select position depending on alalysis of flow system, assuring collection of best sample.

This thesis has been framed under the European funded project BIOCOR; the collaborative network expands through Europe with partners in academia and industry. As a result of that cooperation a

particular biomass collection device is designed and placed in use (Fig. III. 8). Unique design enables acquisition of large amounts of biofilms formed on carbon steel specimens featured by surface of 800 cm^2.

Fig. III. 8. Biomass collection device in function.

Chapter IV

Carbon steel behaviour in saline environments with Sulfate-Reducing Bacteria: surface events, deposits architecture and mitigation

IV.1. Introduction, approach, questions and conducted work

Sulfidogenic bacteria are the main culprits in microbiologically influenced corrosion (MIC) in water injection systems (WIS), and specifically in the systems using seawater, rich in sulfate (electron acceptors), basic ingredient for the viability of most of sulfidogenic species. In seawater injection systems (SWIS), the mild operational conditions (for example: T= 20-40℃, flow rate =1-3 ms^{-1}), coupled with the presence of reservoir water rich in organics (electron donors) or the reinjection of mixture (seawater + reservoir water) enable the proliferation of mesophilic sulfidogenic microorganisms. Among the microbial diversity found in SWIS, Sulfate-Reducing Prokaryotes (SRP) as well as some thermophilic sulfide generating microorganisms capable of maintaining metabolic activity at lower temperature such as genera *Anaerobaculum* or *Thermovirga* were identified (Fig. IV. 1) [Cote, 2013]. Interestingly, in situation when there is a lack of organic electron donors, molecular hydrogen can take over that role enabling sulfate reduction. Presence and abundance of above mentioned sulfidogenic species in oilfield samples was confirmed by recent state-of-art environmental ecology techniques and methods that enabled studies identifying species of the phylum Firmicutes or Synergistetes able to generate hydrogen sulfate using thiosulfate and organic sulfur-rich compounds under different temperatures [Crolet and Magot, 1996; Magot *et al.*, 1997; Duncan *et al.*, 2009]. Recently, more attention is given to microorganisms of class *Clostridia*, sulfidogenic and carbon dioxide generating, capable of affecting carbon steel corrosion and altering the biomineralization process (Fig IV.2) [Stipanicev *et al.*, 2013, M. Sztyler *et al.*, 2012].

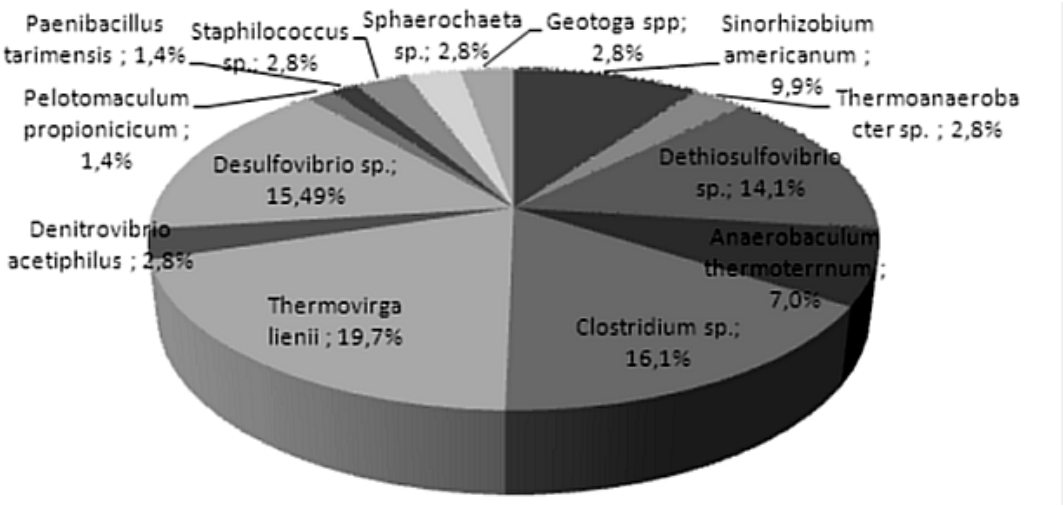

Fig. IV.1. Microbial diversity as found in installation located in the North Sea based on signal intensity of probes for C-cytochrome detection [Cote, 2013].

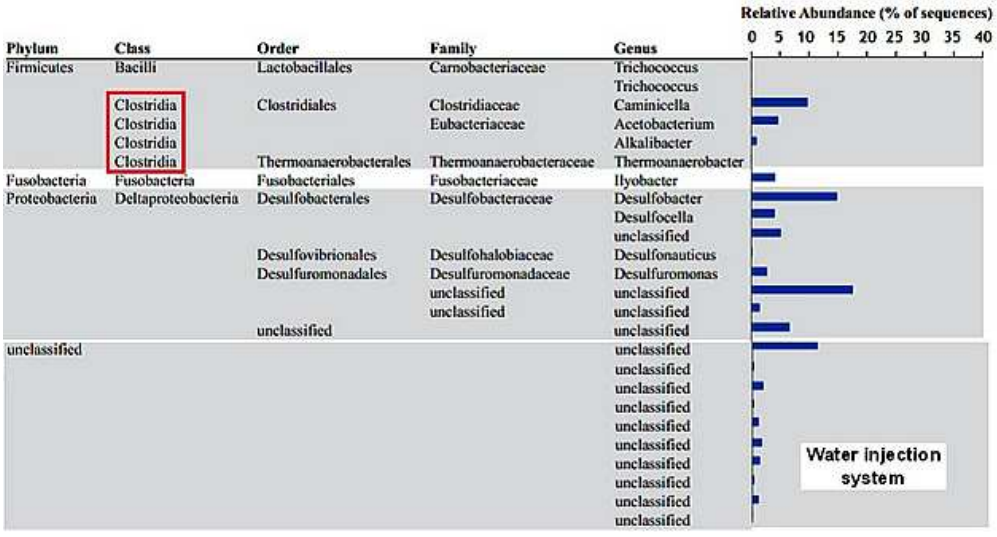

Fig. IV.2. Abundance of Bacteria genus present in pigging samples collected from water injection system located in the North Sea [M. Sztyler *et al.*, 2012].

Undeniably, other microorganisms are present in SWIS; however, the current offshore experience is suggesting that souring corrosion (the corrosion process associated to hydrogen sulfide) is the main problem for all WI systems' life cycle and operational fitness [BP Valhalla, 2009]. When such microorganisms develop biofilms inside the pipelines, there is high probability that the corrosion could rapidly overtake the allowance threshold.

As the previous chapter put in light the domination of sulfidogenic species in analyzed offshore SWIS, a specific pure strain with similar but well-known metabolic capabilities was selected as model organisms for further investigation. For this particular work, SRB strains of *Desulfovibrio alaskensis* and *Desulfovibrio desulfricans* were used. Indeed, both SRB strains routinely perform assimilatory reduction of sulfate to sulfide through anaerobic respiration (Fig. IV.3), characteristic for SRBs.

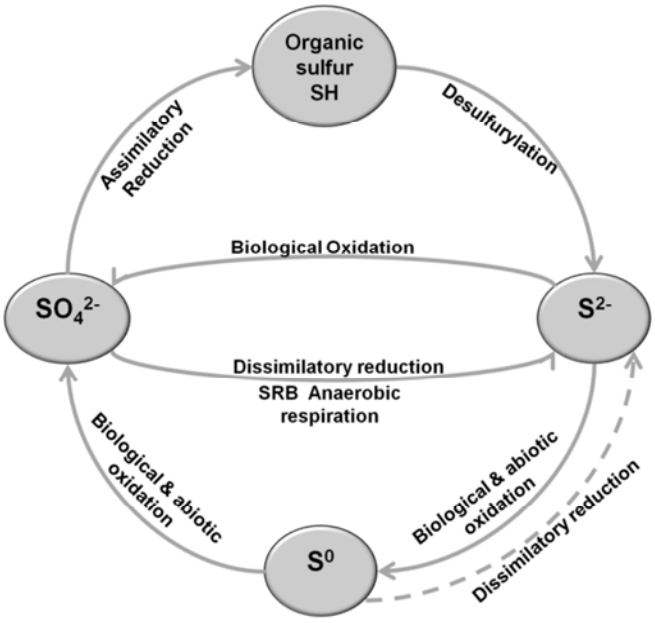

Fig. IV.3. Sulfur cycle in presence of SRB [Dall'Agnol, 2013].

Despite the generally accepted advantages offered by laboratory corrosion simulations with model microorganisms used instead of complex field consortia, laboratory data are rather difficult to extrapolate to offshore installations. Prediction of corrosion rates based on laboratory simulation is challenging since the selected test parameters might not nurture the microorganisms as in a real offshore WIS.

Part of the investigation presented in this chapter focuses on acquiring deeper insight about the modifications of material surface properties (chemical and morphological footprints of the corrosion process) after long-term exposures in sulfidogenic environments. The importance of material features is usually minimized or at least their contribution to failure is attenuated when MIC failure analyses are conducted. Currently, main focus in MIC related failure analysis is the determination of microbial diversity and metabolic activity. Although this aspect shall not be omitted, other parameters should be considered too. Example of this approach is the well-known case of *Valhall* production system failure in 2009 (Fig. IV.4) for which the learning pack document claimed that although all metals are susceptible to MIC, carbon steel has generally been found to be the most susceptible [BP Valhall, 2009]. Nonetheless, according to the available information, further investigation on this matter has not been conducted in this particular case. On the opposite, contribution of material morphology and chemical composition for corrosion and structural integrity in microbial environments, especially after long-term exposures, has been studied by R. Melchers [Melchers, 2012] assessing the impact of inclusions and impurities on material degradation topography. Results indicated significant impact of MnS inclusion on pit initiation. Short-term studies showed initial bacterial attachment and thus corrosion initiation on triple points and grain boundaries, higher energy areas [Castaneda and Benetton, 2008].

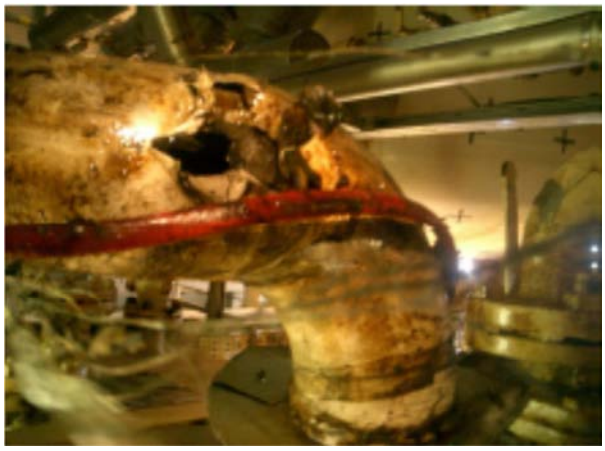

Fig. IV.4. Example of MIC-related failure; Punctured pipe, Valhall 2009.

Dato Avlest	Stud Inn	Stud Ut	SRB Biosid behandlet	SRB ubehandlet	GHB Biosid behandlet	GHB ubehandlet	Biocide	Biocide dosage rate
			MPN/cm2	MPN/cm2	MPN/cm2	MPN/cm2		(ppm)
04.10.2010	29.07.2011	06.09.2011	45	252000	1350	19800	glutaldehyde based	500
02.09.2011	26.06.2011	29.07.2011	54	540000	810	270000	glutaldehyde based	500
25.05.2011	20.03.2011	27.04.2011	<5,4	1710	<5,4	2700	glutaldehyde based	500
05.04.2011	02.02.2011	04.03.2011	1980	No value	<5,4	270	glutaldehyde based	500
	26.11.2011	04.03.2011	270	198000	198000	270000		
02.03.2011	28.12.2010	02.02.2011	135	2520	1980	270	glutaldehyde based	500
	26.10.2011	02.02.2011	1350000	8100000	1980000	1980000		
02.02.2011	26.11.2010	28.12.2010	171	4500	450	270	glutaldehyde based	500
	27.09.2010	28.12.2010	45000	198000	81000	450000		
28.12.2010	26.10.2010	26.11.2010	<5,4	810	5400000	450	glutaldehyde based	500
	29.08.2010	26.11.2010	19800	19800000	8100	8100000		
26.11.2010	27.09.2010	26.10.2010	450	1980	27	450	glutaldehyde based	500
	26.07.2010	26.10.2010	25200	1980000	171	198000		
27.10.2010	29.08.2010	27.09.2010	36	25200	81	27000	glutaldehyde based	500
	28.06.2010	27.09.2010	81	81000	81	1350000		
28.09.2010	26.07.2010	29.08.2010	3600	3600	8100	27000000	glutaldehyde based	595
	30.05.2010	29.08.2010	288	13500	810	19800		
28.08.2010	28.06.2010	26.07.2010	45	810000	810	1350	glutaldehyde based	584
	27.04.2010	26.07.2010	7	2520000	13,0	360000		
01.07.2010	27.04.2010	30.05.2010	<5,4	4500	81	81	glutaldehyde based	581
	04.03.2010	30.05.2010	<5,4	1980000	13,0	25200		
28.05.2010	02.04.2010	27.04.2010	<5,4	ingen prøve	81	ingen prøve	glutaldehyde based	573
	03.02.2010	27.04.2010	6,48	<5,4	16,2	45		
16.05.2010	04.03.2010	02.04.2010	6.5	810000	>25200	>25200	glutaldehyde based	769
	03.01.2010	02.04.2010	13.3	81000	19.8	720000		

Fig. IV.5. Example of glutaraldehyde treatment for offshore SWIS.

Furthermore, the impact of bacterial activity (governing biomineralization process and secreting extra-cellular polymeric substance e.g. EPS) on surface deposits architecture and surface attack topography in bio-sulfidogenic environments was studied in this chapter. Deposits architectures are governed with mineralization and biomineralization process affected by chemical composition of material, electrolyte (media) and bacterial activity. Hence, knowledge on the chemical composition of the different deposit layers may provide information about microbial and chemical system evolution that can enable the identification of the critical corrosion and scaling events. In sulfidogenic environments, Fe-S based compounds would dominate the composition of the corrosion deposits. Additionally, depending on microbial metabolism diversity, other compounds, such as Fe carbonates could contribute to the overall structure. Biological materials are contributing significantly to corrosion process and therefore

to the architecture of the corrosion products. As the volume of the corrosion products is larger compared to the volume of bacterial population, the bacterial metabolic products would disseminate easier over large areas compared to bacterial cells. These far-reaching metabolites will affect the nearby corrosion and scale-formation processes. Moreover, the jelly substance from the biofilm e.g. EPS, due to its structure, is affecting the transfer of electroactive species from the bulk medium to steel surface and hence interfering with the corrosion and mineralization processes.

Finally, injection water is commonly treated with biocides, corrosion and scale inhibitors, and oxygen scavengers (see *Chapter III*). Without application of appropriate treatment, different formations likewise iron sulfide, hydrogen sulfide, iron oxide, biofilms and other impurities may form, precipitate and damage unprotected injection infrastructure and plugged injection wells. Furthermore, a partial attention was given here to the assessment of eco-friendly and legally accepted MIC countermeasures, applied in studied offshore SWI system. Biocide treatment is not always acceptable, depending on the toxicity of the chemicals; glutaraldehyde based biocide applied on offshore system for attacking microbial activity is investigated during this research work. Example of glutaraldehyde treatment on offshore installation is given in Fig. IV.5. This chapter also presents the results of an investigation focused on the impact of glutaraldehyde-based biocide treatment on bacterial activity and corrosion during long-term test as well as its impact on bacterial activity and capacity to affect deposit properties.

To study the implication on electron transfer and therefore corrosion process of deposits formed, either organic or inorganic or their combination, as well as their transformation due to applied antimicrobial treatments, particular electrochemical and surface analysis techniques have been employed. It is required to keep in mind the limitation of the laboratory tests. In many situations, long-term exposures result in different information compared to short-term experiments. Moreover, experimental designs involving constant flow conditions and exchange of electrolyte will generate different results compared to batch experiments.

Results, discussions and conclusion produced during this project stage are presented under the form of two pre-reviewed publications:

1. ***Corrosion behaviour of carbon steel in presence of SRB in seawater environment*** by Marko Stipanicev, Florin Turcu, Loic Esnault, Elmar Werner Schweitzer, Renate Kilian and Régine Basseguy (Electrochimica Acta, Submitted)

2. ***Surface behaviour of carbon steel in presence of sulfate-reducing bacteria: proliferation and mitigation with biocide treatment*** by Marko Stipanicev and Régine Basseguy (in preparation)

IV.2. Article 2

<< Corrosion behavior of carbon steel in presence of sulfate-reducing bacteria in seawater environment >>

Electorchemica Acta

Current status: accepted September 2013

Corrosion behavior of carbon steel in presence of sulfate-reducing bacteria in seawater environment

Marko Stipaničev[a,c,*], Florin Turcu[a], Loic Esnault[a], Elmar Werner Schweitzer[b], Renate Kilian[b] and Régine Basseguy[c]

[a]*Det Norske Veritas, Johan Berentsens vei 109-111, 5163 Laksevåg, Bergen, Norway*

[b]*AREVA GmbH, PTCM-G, Paul-Gossen-Str. 100, 91052 Erlangen, Germany*

[c]*Laboratoire de Génie Chimique CNRS-INPT, 4 Allée Emile Monso, 31432 Toulouse, France*

*Corresponding author: Marko Stipanicev, telephone: +47 95936347, e-mail: Marko.Stipanicev@dnv.com

Abstract

The influence of Sulfate-Reducing Bacteria (SRB) on the corrosion behavior of carbon steel was studied in a laboratory test-loop, continuously fed with nutrient supplemented North Sea seawater. The main parts of the test-loop, represented by two separated flow cells, were fitted with steel specimens. The test-loop was operating anoxically for 2200 h and each flow cell was three times inoculated with *D. alaskensis* or *D. desulfuricans* species. Additionally, each flow cell was two times perturbed with antimicrobial treatments. Steel specimens exposed in flow cells exhibited comparable appearance and systems responding similarly to inoculations and antimicrobial treatments. The effect of the inoculations in both flow cells on the steel coupons electrochemical behavior was materialized as lower resistance to corrosion and higher surface activity or occurrence of localized pitting events. The localized surface attacks recognized in both flow cells after inoculations continued to progress with the time, although bacterial activity was temporarily suppressed by antimicrobial treatment. Post-exposure sample evaluations might suggest that, some particular steel surface areas have been subjected to a dramatic change in the corrosion mechanism from initial localized attack to general corrosion. The long-term exposure of the carbon steel specimens resulted in identifiable formation of biofilms and corrosion products. Corrosion deposits were characterized by a specific structure built of iron sulfides (FeS), sulfated green rust ($GR(SO_4^{2-})$), magnetite (Fe_3O_4), Fe(III) oxyhydroxides (FeOOH), chukanovite ($Fe_2(OH)_2CO_3$), carbonated green rust ($GR(CO_3^{2-})$) and some calcareous deposits. Presented factual evidence reinforced the idea that sulfidogenic species in natural seawater environment may cause localized damage with a specific surface pattern; however, this does not necessarily lead towards significantly elevated corrosion rates.

Keywords: Seawater; Carbon steel, Corrosion; SRB

Introduction

Internal corrosion causes immense damages to the carbon steel offshore infrastructures such as pipelines and water injection systems. A significant part of the carbon steels degradation can be attributed to micro- and macro- environmental conditions alterations by sulfidogenic, e.g. hydrogen sulfide (H_2S) producing, microorganisms [1]. The most recognized group of sulfidogenic microorganisms are Sulfate-Reducing Bacteria (SRB) and they are regarded as the main culprits of anaerobic corrosion in seawater system.

Within the marine biofilm matrix, SRBs thrive, finding favorable conditions inside pre-established anoxic niches. In general, SRB including *Desulfovibrio desulfuricans* ATCC 27774 and *Desulfovibrio alaskensis* AL1, are performing dissimilatory reduction of sulfur compounds such as sulfate (SO_4^{2-}), sulfite (SO_3^{2-}), thiosulfate ($S_2O_3^{2-}$), polythionate ($S_nO_6^{2}$) and sulfur (S) itself to sulfide (S^{2-}), that, combined with oxidized molecular hydrogen, forms volatile H_2S negatively impairing ferrous metals [2,3,4].

Anaerobic corrosion is a well-understood process, exclusively controlled by the oxidizing agent/proton transfer to metal surface. However, in biotic environments different explanations were suggested in order to explain anaerobic corrosion process that resulted in elevated corrosion rates. During past few decades multiple theories explaining corrosion mechanisms were suggested by taking into account SRBs metabolic activities and formation of different sulfide based compounds.

Earlier work evoked a cathodic depolarization model of ferrous metals based on the removal from the surface of atomic hydrogen by SRBs [5] and/or hydrogen consumption thanks to a hydrogenase enzyme [6, 7, 8, 9]. This hypothesis was investigated and can be approved only if the reaction step for forming atomic (and then molecular) hydrogen is not rate-limiting as it is the case in presence of weak acid, especially when phosphate protonated species are involved [10, 11]; it was then proved that bacterial hydrogen uptake merely stimulates corrosion in certain anaerobic environments [12]. Furthermore, by reducing sulfate in sulfide, SRB promotes the conditions for precipitation of iron sulfide (biomineralized Fe_xS_y, particularly FeS), which next catalyzes proton/water reduction into molecular hydrogen and acts as a cathode in a galvanic couple with metallic iron [13, 14, 15]. What's more, direct products of SRB metabolism, e.g. H_2S, can affect metal surface directly by decreasing pH locally and promoting differential cell resulting with localized events on metal surface [16]. Metal ion chelating by Extracellular Polymer Substances (EPS) is also sometimes dealt with [17] as well as galvanic coupling resulting EPS selective metal binding capacity [18]. To sum-up such a complex *marine biofilm/corrosion products/metal* interface, overlapping of proposed mechanisms should be considered rather than one specific mechanism [19]. It is often observed that the microenvironment generated within marine biofilms rich in SRB is favoring electrochemical reactions that may lead to localized destructive surface events [20]. Nevertheless, besides its detrimental impact on steel integrity, the biomineralization process occurring on steel surfaces can be under favorable circumstances beneficial thought the formation of protective corrosion products layers that can suppress the local corrosion processes [21].

Even though SRBs are recognized as the most imminent species taking part in Microbiologically Influenced Corrosion (MIC), microbial consortiums in marine biofilms are usually heterogeneous and therefore deterioration of metal should be affected by interactions of the whole community [22]. Some of the microorganisms commonly found in marine environments, such as Acid Producing Bacteria (APB) of the genera *Clostridia* [23, 24] or *Anaerobaculum* [25], can be characterized by metabolic process capable of generating multiple, aggressive chemical species for ferrous metals, such as H_2S and CO_2. Furthermore, when dealing with MIC, it is required to take into consideration effect of other bacteria than SRB inside marine biofilms and possible quorum sensing effect, which according to authors knowledge, is still neither well investigated nor well defined.

Besides the evaluation of the bacterial load, the relevant characteristics of the metallic substrate, whose corrosion resistance in presence of microorganisms is investigated, must be known or taken into consideration. Carbon steels, often used in Oil and Gas (O&G) industry, are characterized by homogenous distribution of geometrically small grains that have short grain boundaries. This particular microstructure may result in surface susceptibility to equally allocated localized corrosion attack. For carbon steels, most common metallographic structures are ferrite (ferrous phase) and perlite (lamellar structure of ferrite and Fe_3C), with nonmetallic inclusions, e.g. manganese sulfide (MnS) inclusions randomly distributed over the steel surface. These MnS inclusions have been postulated to serve as seeds for pitting corrosion [26, 27]. Recently, different studies showed a correlation between pit initiation and propagation associated with sulfide inclusions and their relation to MIC [28].

In order to get better insight in the complexity of systems such as biofilms, and their interactions with carbon steel surfaces, taking advantages of multiple analytic techniques may be useful. Currently, electrochemical techniques such as Open Circuit Potential (OCP), Linear Polarization Resistance (LPR) and Electrochemical Noise (EN) are widely employed for studying general and localized surface events in the presence of the bacteria and biofilms [29, 30]. More precisely, LPR is often used to monitor corrosion by measuring ''instantaneous'' general corrosion rate [31], taking additional precaution due the limitation of Stern-Geary theory, which is not valid for the diffusion-controlled systems that are often established in presence of biofilms. Localized events (pitting, crevice, stress corrosion…) are studied by Electrochemical Noise (EN). Iverson as a tool originally applied Electrochemical Current Noise (ECN) and Electrochemical Potential Noise (EPN) fluctuations for MIC studying and monitoring [32, 33]. Until now, observations of the modulated current and potential signals patterns as well as the characteristic transients in the time records were successfully used for detection of stable and metastable localized surface events in the presence of bacteria and/or biomineralization products [31, 34, 35].

In the investigation reported herein, corrosion behavior of S235JR carbon steel was studied in the modified North Sea seawater that was multiple times inoculated with one of two different SRB pure cultures, *Desulfovibrio alaskensis* AL1 or *Desulfovibrio desulfuricans* ATCC 27774, and subjected to antimicrobial treatment. LPR and EN techniques were used in order to study general corrosion, and

for identification of localized events on steel surfaces. Scanning Electron Microcopy (SEM) and Energy-Dispersive X-Ray (EDX) spectroscopy were used to investigate biomineralization products and processes governed by presence of bacteria. Surface deterioration and influence of microstructure on degree and location of corrosion attack were investigated by means of optical microscopy.

2. Methodology, materials and methods

2.1. Continuously fed with fresh media test loop

The main components of the continuously fed with fresh media test loop (also called ''once-through'' flow loop) were manufactured in-house and consist of two bioreactor vessels placed one behind the other and two in parallel cylindrical flow-through cells. The ''once-through'' flow loop set-up is depicted in Fig. 1.

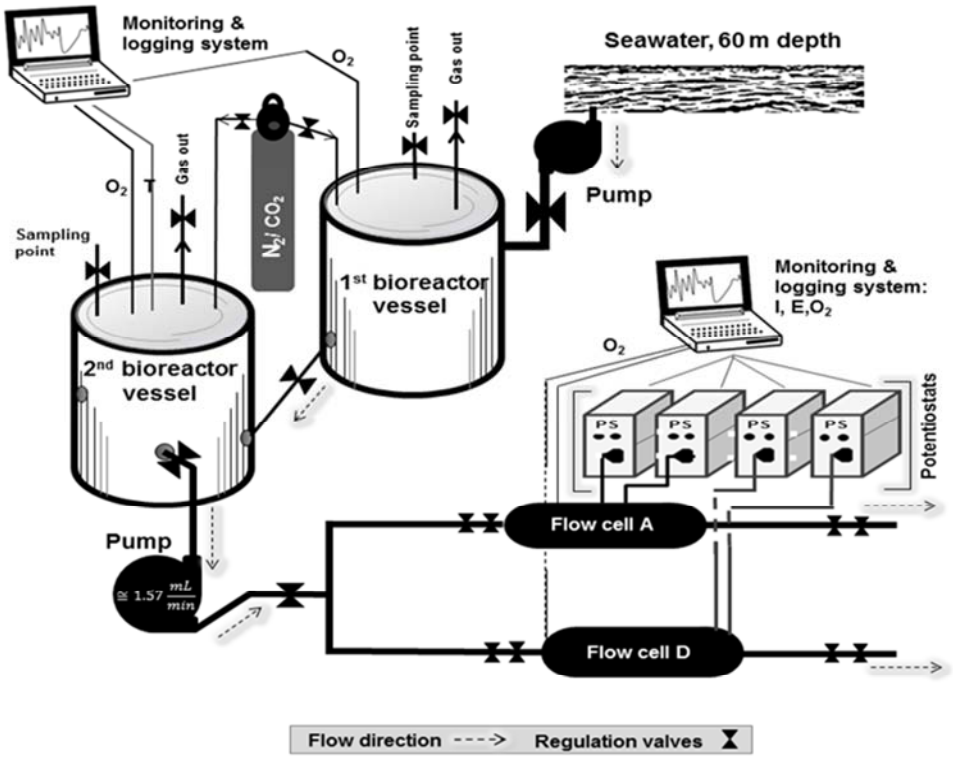

Fig. 1. The continuously fed with fresh media test loop.

The bioreactor vessels are made of polypropylene. The acryl lid, used for closing bioreactor vessels, is fitted with an optical oxygen-dipping probe, a temperature sensor interfaced with Fibox 3 fiber optic oxygen transmitter (Presens, Germany), one gas inlet, one gas outlet and a pH electrode (pH-meter HI-9125N, Hanna Norden AB, Sweden). The lid also incorporates an in-house fitted sampling/ fluid injection point. The first bioreactor vessel body was fitted with one fluid injection inlet. Each bioreactor vessel was equipped with one fitting accommodating Teflon tube (Swagelok, UK) via which the two bioreactor vessels were connected. The second bioreactor vessel was also equipped with a heating unit (ISOPAD IP-DASI®, Tyco, USA) and a thermostat (Raychem® AT-TS-14, Tyco Thermal Controls, USA).

A peristaltic pump (W-M 520SN/REL, Watson-Marlow, UK) drew media from the second bioreactor vessel, and the output flow was split between the two flow cells. Perfluoroalkoxy tubing (PFA-T8-062-50, Swagelok, UK) was used. Two regulation needle valves (PFA-4RPS8, Swagelok, UK) were installed before and after each flow cell. Flow cells were made from acrylic tubes (6 cm inner diameter, 1 cm wall thickness and 34 cm length) and acrylic plates (5 cm× 34 cm× 0.5 cm). Twelve pairs of feedthroughs (M20 size fittings, produced by OBO Bettermann, Germany) were installed on the top of each flow cell. A schematic drawing of a flow cell showing its cross section and distribution of

feedthroughs is presented in Fig. 2. Electrodes (working - WE, counter - CE and reference - Ref) for electrochemical measurements were installed in the two flow cells, in identical arrangements at 12 o'clock positions. An in-house manufactured liquid Sampling Port (SP) that accommodated dipping oxygen probe was installed at F10 position in each flow cell. To monitor biofilm formation, ten carbon steel specimens (rectangular plates with dimensions of a 1 cm× 1 cm× 0.2 cm) were installed at 6 o'clock position in each flow cell.

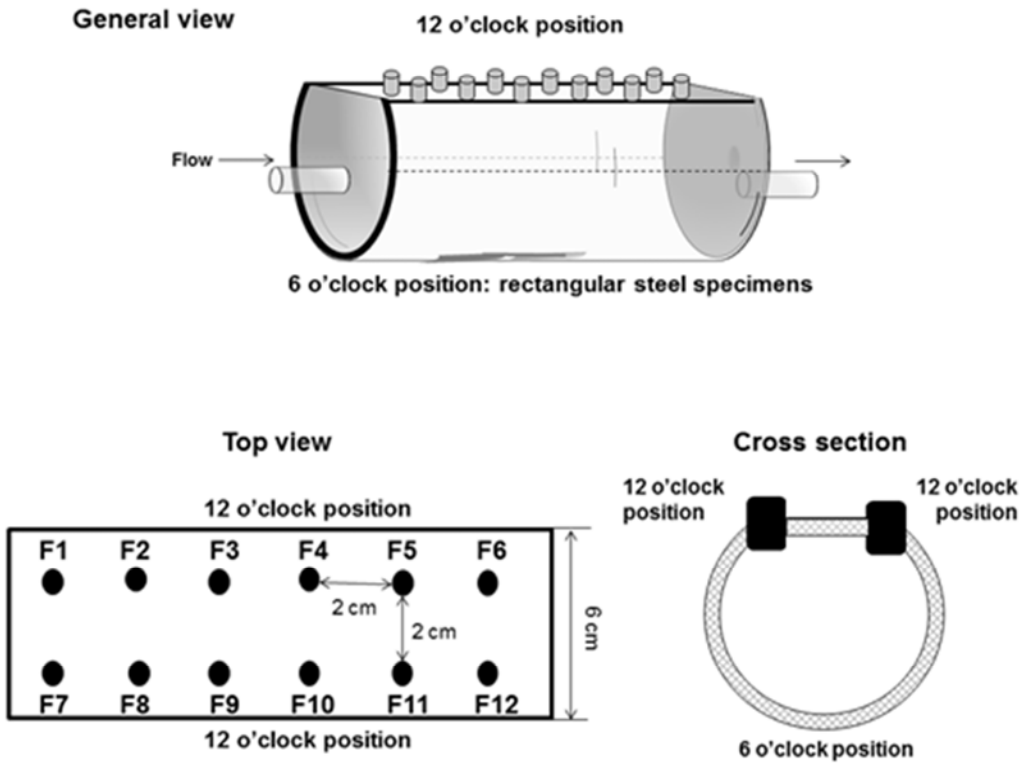

Fig. 2. Scheme, cross-section and fitting distribution of cylindrical flow-through cells, e.g. flow cells

The entire ''once-through'' flow loop was constructed from polymers to minimize contamination with exogenous metal ions. Furthermore, materials, including perfluoroalkoxy (2 mm thickness), polyolefin (1 mm thickness), polypropylene (2 cm thickness) and acrylic (0.5 and 2 cm thickness) polymers with minimal oxygen permeability and minimal deterioration under test conditions were chosen.

Prior to operation the bioreactor loop was flushed with technical grade alcohol (Kemetyl Norge AS, Norway) and flow cells were exposed for 24 h under UV light (wave length 256 nm: XX-15, sterilization UV lamp, UVP, USA). Then, the first bioreactor vessel was filled up with 40 L of seawater, and oxygen was decreased to a level of 30 - 40 ppb by purging with 90/10 (v/v)% N_2/$^oO_2$ gas mixture (Yarapraxiar, Norway) for 24 h. Deareated seawater was then transferred into the degassed second bioreactor vessel where the medium was supplemented with acetate (Merck, Germany) and lactate (Sigma-Aldrich, Germany) up to final concentrations of 10 µmol L^{-1}. Anoxic conditions (10-20 ppb) were established by purging the medium with 90/10 (v/v) % N_2/CO_2 gas mixture for 72 h. Moreover, the temperature was controlled automatically at 28℃ ± 2℃ during whole duration of test. The medium pH inside the second bioreactor vessel was adjusted with phosphate buffer (Sigma-Aldrich, Germany) to values in range of 7.9 to 8.1 before being distributed into the two separated flow cells. The flow system was then activated with a flow rate maintained at 1.57 mL min^{-1}, the lowest possible value for the pump. The continuously fed with fresh media test loop was operated continuously for the next 2200 h. Three time inoculations (with 100 mL at t_e= 792 h, t_e= 936 h and t_e= 1056 h) were performed using pure culture of *Desulfovibrio alaskensis* strain AL1 in flow cell A and *Desulfovibrio desulfuricans* strain ATCC 27774 in flow cell D. Prior to each inoculation, flow cells were isolated from the rest of the loop by closing regulation valves. Flow conditions were reestablished 24 h after each inoculation. Moreover, each flow cell was two times treated with 50 min batch antimicrobial treatment, first after the third inoculation, at t_e= 1075 h and second time at t_e= 2180 h. A 50% glutaraldehyde solution (MB-544C from M-I SWACO a Schlumberger Company, USA) was used as an industry standard antimicrobial.

2.2. Bacteria cultures

The cultures of *Desulfovibrio desulfuricans* ATCC 27774 and *Desulfovibrio alaskensis* AL1 that served as inoculums for the ''once-through'' flow loop were grown in modified VMNI sulfate culture media [36]. VMN was composed of (g L^{-1} distilled water): NaCl, 20.0; NH_4Cl, 1.0; $CaCl_2 \times 2H_2O$, 0.04; Na_2SO_4, 4.5; $MgSO_4 \times 7H_2O$, 0.06; $FeSO_4 \times 7H_2O$, 0.004; sodium lactate, 6.0; KH_2PO_4, 0.5; sodium citrate, 0.3; casamino acids, 2.0; tryptone, 2.0; modified Wolfe's mineral elixir (0.1 (v/v) %) and vitamin solution (0.2 (v/v) %). The vitamin solution was composed of (g L^{-1} distilled water): riboflavin, 0.1; nicotinic acid, 0.25; thiamine, 0.3; pentatonic acid, 0.3; pyridoxine, 0.3; cyanocobalamin, 0.025; ascorbic acid, 1; biotin, 0.005. The composition of the modified Wolfe's elixir was (g L^{-1} distilled water): Nitrilotriacetic acid, 1,5; $MgSO_4 \times 7H_2O$, 0.06; $MnSO_4 \times H_2O$, 0.5; NaCl, 1; $FeSO_4 \times 7H_2O$, 0.1; $CoSO_4 \times 7H_2O$, 0.1; $NiCl_2 \times 6H_2O$, 0.1; $CuCl_2 \times 2H_2O$, 0.1; $ZnSO_4 \times 7H_2O$, 0.1; $CuSO_4 \times 5H_2O$, 0.01; $AlK(SO_4)_2 \times 12H_2O$, 0.01; H_3BO_3, 0.01; $Na_2MoO_4 \times 2H_2O$, 0.01; $Na_2SeO_3 \times 5H_2O$, 0.001.

Cell densities of prepared enrichments were determinated using Thoma counting chamber (Helber Bacteria Cell, Hawksley, UK) with precondition that only viable cells are counted.
Flow cell A was inculated two times with 80 mL and one time with 120 ml of *Desulfovibrio alaskensis* AL1 culture (cell densities≈ 10^7) and flow cell D with *Desulfovibrio desulfuricans* ATCC 27774 (cell densities≈ 10^7).

2.3. Analytical methods

2.3.1. Bacterial activity monitoring

Bacteria consortium monitoring in second bioreactor (indigent population naturally contained in seawater) and both flow cells (indigent population naturally contained in seawater + inculated pure culture that are dominant) was conducted by measuring cell density. Firstly, global measurements were performed using a Thoma counting chamber with precondition that only viable cells are counted. Secondly, determination of cell densities for two groups (APB and SRB) was conducted using the Most Probable Number (MPN) technique. Two types of media were used for these measurements: the full name Acid Producing Bacteria (APB) media containing phenol red dye (APB, 25000 TDS) (Intertek Commercial Microbiology, USA) for APBs and Sulfate Reducing Bacteria (SRB) media 2 Medium (SRB, 25000 TDS) (Intertek Commercial Microbiology, USA) for SRBs. Measurements were performed 24 h after inoculations; samples were collected at the moment when flow conditions were reestablished.

2.3.2. Experimental media chemistry monitoring

Sulfate (SO_4^{2-}) concentrations were determinated spectrophotometrically with Spectroquant® sulfide kit (VWR, USA). Sulfide concentrations were monitored according to NACE TM0284-2003 (Appendix C - Determination of H_2S concentration) by the iodometric titration. Measurements were performed 24 h after inoculations, i.e. samples were collected at the moment when flow conditions were reestablished.

2.3.3. Electrochemical methods

Open Circuit Potential (OCP), Linear Polarization Resistance (LPR) and Electrochemical Noise (EN) measurements were carried out using a multichannel potentiostat MultEchem™ (Gamry Instruments, USA) that consisted of two Reference 600TM Potentiostat/ Galvanostat/ ZRA independent units connected to a PC interface and monitored with DC105 or ESA410 software (Gamry Instruments, USA).

Standard three electrode-arrangements included a Working Electrode (WE), a Counter Electrode (CE) and a Saturated Calomel Electrode (SCE). The WEs, made of S235JR low carbon steel, have a circular exposed area of 0.785 cm^2 (1 cm diameter cylindrical specimens, 2 cm long, dressed in polyolefin sleeve, Fig. 3).

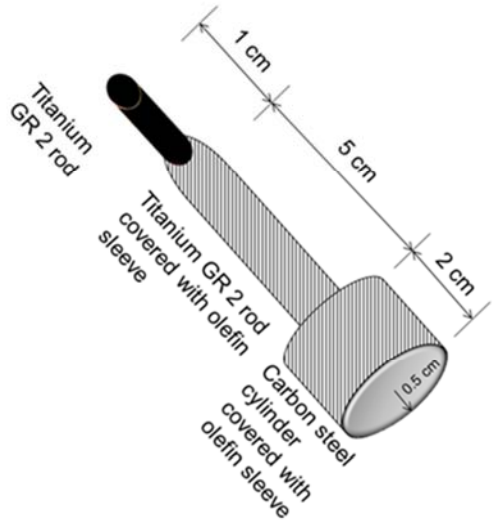

Fig. 3. Working electrode scheme

The carbon steel specimens were manufactured from S235JR carbon (Descoure and Cabaud, France) whose composition is the following (mass ratio): 0.17% C, 1.4% Mn, 0.045% Cu, 0.03% S, and 0.03% P. Surfaces of all exposed steel specimens were prepared by manual grinding using increasing series of fine SiC paper, ending with 600-grit. Grinding debris was rinsed from the surface with sterile deionized water. The specimens were sterilized exposing them on each side for 12 h under UV light (wave length 256 nm: XX-15, sterilization UV lamp, UVP, USA) at 25 ℃.

The CEs are made from Inconel® C276 cylindrical specimens (1 cm long, 1 cm diameter) with an exposed area of 3.95 cm^2 (flat circular face plus the side area).

In each flow cell, the OCP's versus SCE (E(OCP)/V(vs.SCE)) (SCE installed at F4 position) of six working electrodes (circular disc) installed at the F1, F2, F5, F8, F11 and F12 positions were recorded every 24 h in period prior and after flow cells perturbations (inoculations of antimicrobial treatments) or every 168 h during rest of test duration. Average OCP values with standard deviation error bars are reported.

The LPR technique was employed to estimate the corrosion rate of the steel coupons. The polarization resistance (R_p) of the steel/electrolyte interface is measured in the vicinity of the E(OCP)/V(vs.SCE) [37]. R_p is defined as the slope of the polarization curve tangent at the OCP. The inverse of R_p is proportional to the ''instantaneous'' corrosion rate and given in 1/Ω [32]. To determine R_p, the potential was scanned in the range of E(OCP)/mV(vs.SCE) ± 10 mV with a sweeping rate of v= 0.167 mV s^{-1}. Polarization scans were performed every 24 h in period around flow cell perturbations (inoculations or antimicrobial treatments), or every 168 h during rest of test duration. Average 1/(R_p/Ω) values with associated standard deviations were reported for the six different WEs installed at the F1, F2, F5, F8, F11 and F12 positions in each flow cell. Two counter electrodes (position F3 and F9) together connected at the potentiostat were used.

Electrochemical Noise (EN) analysis was carried out to determine the type of corrosion attack [28]. Electrochemical Current Noise (ECN) and Electrochemical Potential Noise (EPN) signals were performed on four different three-electrode set-ups:

1) WE1 at F1, WE2 at F2 and SCE at F4;
2) WE1 at F7, WE2 at F8 and SCE at F4;
3) WE1 at F5, WE2 at F6 and SCE at F4;
4) WE1 at F11, WE2 at F12 and SCE at F4.

EN signals were recorded with frequency of 1 Hz, for 30 and 60 min long intervals, every 168 h during the whole test period. EN signals were recorded with a current range of 60 µA and a resolution of 1 pA and a potential range of +/- 30 mV and a voltage resolution of 1 µV. Only typical ECN signals characteristic for each experimental stage are presented herein. Modulated current signal patterns, as well as transients, characteristic of localized surface events, were visually examined within data blocks of 1000 or 10000 (1 Hz sampling frequency) points resulting with the time resolution of 1000 or 10000 s. The trend was removed from obtained data series by using the linear regression fitting method. The only ECN data are presented herein, while accompanied EPN data are not presented in order to keep clarity of presented data even though EPN data support observed current transients.

2.3.4. Surface analysis

The morphology and chemical composition of formed surface deposits as well as steel surface topography were investigated using four different systems:

i. High resolution Scanning Electron Microscope (SEM) JSM-7400F (Joel, Japan);
ii. Low vacuum table SEM TM3000 (Hitachi, Japan) interfaced with Energy Dispersive X-ray (EDX) spectroscopy system Quantax 70 (Bruker, USA);
iii. SEM Neon 40 EsB (Zeiss, Germany) equipped with a Inca EDX-System (Oxford Instruments, UK);
iv. Leica upright DMR microscope (Leica Microsystems GmbH, Germany) with attached ProgRes® C5 camera (JENOPTIK Optical Systems GmbH, Germany).

Two types of surface preparation were used depending on investigated specimen:

i. In order to fix the biofilm/ corrosion products layer, the steel specimens were placed in 2.5 (w/v) % glutaraldehyde (Electron Microscopy Science, USA) for 90 min at 4℃, and then washed by four 15 min immersions in 0.1 M sodium cacodylate buffer (Merck, Germany). Post-fixation was carried out by placing specimens for 1 h in the solution of 1 (w/v) % osmium tetroxide (purity> 99.95%, Electron Microscopy Science, USA) in 0.1 M sodium cacodylate buffer (MERCK, Germany). Post-fixed samples were washed in 0.1 M sodium cacodylate buffer (2×20 min) and dehydrated performing the following immersions: 15 min in 30 (v/v) %, 15 min in 50 (v/v) %, 20 min in 70 (v/v) %, 2×15 min in 96 (v/v) % and 2×15 min in 99.8 (v/v) % aqueous ethanol solutions (Sigma-Aldrich, Norway). De-watered specimens were placed in an oven (Type TS 4057, Thermaks AS, Norway) at 37℃ ov ernight. Dried samples were mounted on an aluminum stub using adhesive carbon tape, sputter-coated with gold for 3 min;
ii. Steel specimens were rinsed in deionized water to remove loose deposits.

After SEM/ EDX examination, steel specimens were cleaned from surface deposits by following one of two used protocols:

i. Immersion in a 5 (v/w) % hexamine (Merck, Germany) solution in concentrated HCl (VWR, USA) for 30 s. This was immediately followed by rinsing with deionized water, gentle blotting with a paper towel, and overnight storage in a desiccator;
ii. Immersion in AP2 solution (g L^{-1} of distilled water: 200, NaOH; 30, $KMnO_4$). This was immediately followed by rinsing with deionized water, gentle blotting with a paper towel, and overnight storage in a desiccator;

Finally, particular specimens were subjected to cross-section and microstructure examination. Etching was performed using standard Nital-etching solution (10 (v/v) % HNO_3 in ethanol).

Moreover, the presence of sulfide in black corrosion products on steel specimens, either retrieved from flow cells after 1070 h or 2200 h of test, was tested by initiating reaction between concentrated HCl (VWR, USA) and collected corrosion products. Reaction product was H_2S, characterized by distinguish and easily recognizable smell [22].

3. Results and Discussion

3.1. Development of event during test duration

To simplify the presentation and the consequent analyses of the test data, the current laboratory investigation was conveniently divided in three distinctive stages:

i. First test stage refers to the period before the multiple inoculations of flow cells with pure SRBs cultures; from t_e= 0 h to t_e= 792 h
ii. Second test stage covers the period from the first inoculation to first antimicrobial treatment; from t_e= 936 h to t_e= 1075 h
iii. Third test stage comprises the period between the first antimicrobial treatment and test termination; from t_e= 1075 h to t_e= 2200 h

As a general note concerning the bulk test medium, dissolved oxygen (DO) concentration and pH

evolution monitored during the 2200 h of the test are shown in Fig.4. According to the oxygen concentration evolution, the test environments were regarded as anoxic since the DO level was never above 50 ppb (0.049 mg L^{-1}).

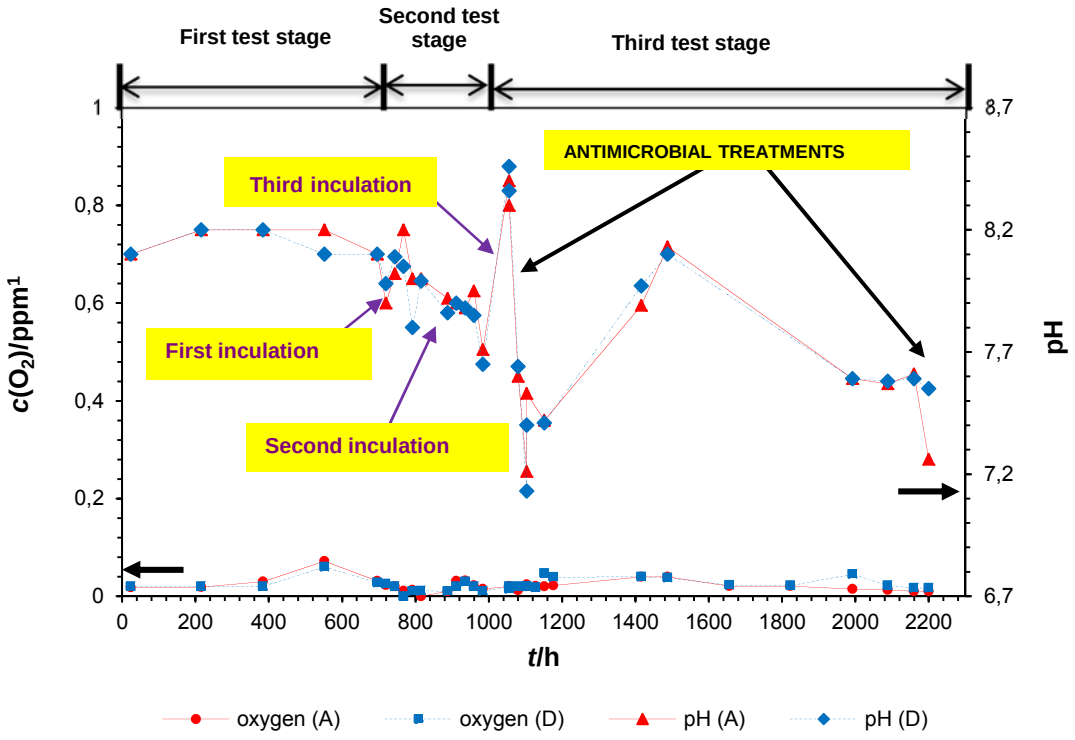

1 - ppm (parts per million) = 0.99 mg L^{-1}

3.1.1. First test stage

During the first test stage, pH around 8.1 (Fig. 4), low cell density (<10^3 cells mL^{-1}), corresponding to indigene population naturally present in seawater, high sulfate (≈ 3.5×10^3 ppm, e.i. 2.7g L^{-1}), and low sulfide (not detectable) concentrations were detected in the bulk medium flowing through the both flow cells (Tab. 1 and 2). It is then possible to conclude that the bulk medium conditions, exhibited in the two different flow cells, are very similar as expected (identical medium was flowing through both flow cells) proving that the further differences found could be attributed to the nature of the inoculations.

Measured instantaneous corrosion rates for WEs exposed in flow cells, obtained during the first test stage, are presented in Fig. 5. In both flow cells, $1/(R_p/\Omega)$ values measured during initial 200 h of tests were low, around 3×10^{-4}. After t_e= 200 h, $1/(R_p/\Omega)$ values decreased to 1×10^{-4}, where they remained (with some fluctuations) until end of the first test stage.

Typical ECN records for WEs exposed in flow cells, obtained during the first test stage, and are presented in Fig. 6. ECN transients are oriented in both directions (up and down), indicating that both WEs are equally subjected to corrosion. This type of signal modulations is characteristic for the carbon steel immersed in chloride solution as seawater [38]. Moreover the magnitude of the ECN first increased with the time, as indicated by comparing the curves obtained for t_e= 20 h and for t_e= 200 h. Since the ECN is produced by independent current sources on steel surfaces [39], higher current reveals greater electrochemical activity and more pronounced anodic reaction being indicative for elevated corrosion rates [39, 21]. Consequently in the test conditions, the initial increase of ECN magnitude can be explained by the breakdown of the initial protective ferrous layer, exposing bare steel surface to high amount of aggressive Cl^- ions present in seawater what may result in metastable pitting attacks. Afterward, since the tendency in corrosion rate showed a lessening ($1/(R_p/\Omega)$ plateau with lowest value in Fig. 5), ECN amplitudes decreased (Fig. 6, curves obtained at t_e= 400 h), indicating lower corrosion and lower surface activity. Theoretically, a protective layer of corrosion products, e.g. sulfated green rust ($GR(SO_4^{2-})$= $Fe^{II}_4Fe^{III}_2(OH)_{12}SO_4\times8H_2O$), produced directly or by oxidation of iron hydroxide ($Fe(OH)_2$), is often found on the carbon steel surface when exposed to environments as described here [40, 41, 42]. Moreover, if any oxygen is present, certain portion of

GR(SO_4^{2-}) will be oxidized into Fe(III)oxyhydroxides such as goethite (α-FeOOH) and lepidocrocite (γ-FeOOH) [40] (please note that some oxygen is present in our system, Fig. 4). Interestingly, GR(SO_4^{2-}) may also serve as a source of sulfate, a terminate electron acceptor in SRBs dissimilatory respiration [40].

Tab. 1. Cell density and chemical monitoring of the bulk medium in flow cell A (inoculation with *Desulfovibrio alaskensis*) during whole test.

Time h	cell density×10^3 cells mL^{-1}	APB×10^3 cells mL^{-1}	SRB×10^3 cells mL^{-1}	c(SO_4^{2-})×10^3 ppm^1	c(S^{2-}) ppm^1	
First test stage						
336	1<	/	/	3.40	/	
672	1<	/	/	3.58	/	
Second test stage						
792	1<	/	/	3.15	/	First inoculation
816	555	/	/	3.00	34	
888	550	/	/	3.00	34	
936	39	/	/	2.95	37	Second inoculation
960	611	>140	>140	2.60	204	
1056	47	/	/	2.45	/	Third inoculation
Third test stage						
1070	678	/	/	2.40	206	First antimicrobial treatment
1094	506	/	/	3.15	136	
1152	468	>140	14	2.80	51	
1416	363	>140	>140	2.95	/	
1992	86	14	14	2.65	12	
2088	226	>140	45	2.45	5	
2180	/	/	/	/	/	Second antimicrobial treatment
2200	/	0.3	0.9	2.30	/	

1 - ppm = parts per million = 0.99 mg/L

Tab. 2. Cell density and chemical monitoring of the bulk medium in flow cell D (inoculation with *Desulfovibrio desulfuricans*) during whole test.

Time h	cell density×10^3 cells mL^{-1}	APB×10^3 cells mL^{-1}	SRB×10^3 cells mL^{-1}	c(SO_4^{2-})×10^3 ppm[1]	c(S^{2-}) ppm[1]	
First test stage						
336	1<	/	/	3.40	/	
672	1<	/	/	3.58	/	
Second test stage						
792	1<	/	/	3.25	/	First inoculation
816	141	/	/	3.20	34	
888	109	/	/	3.20	34	
936	12	/	/	3.18	17	Second inoculation
960	1850	>140	>140	2.15	238	
1056	55	/	/	2.55		Third inoculation
Third test stage						
1070	1600	/	/	2.50	202	First antimicrobial treatment
1094	945	/	/	3.30	34	
1152	429	14	14	2.75	17	
1416	128	25	>140	2.75	/	
1992	70	1	1.4	2.25	20	
2088	166	140	9.5	2.50	20	
2180	/	/	/	/	/	Second antimicrobial treatment
2200	/	0.3	0.2	2.20	/	

1 - ppm = parts per million = 0.99 mg/L

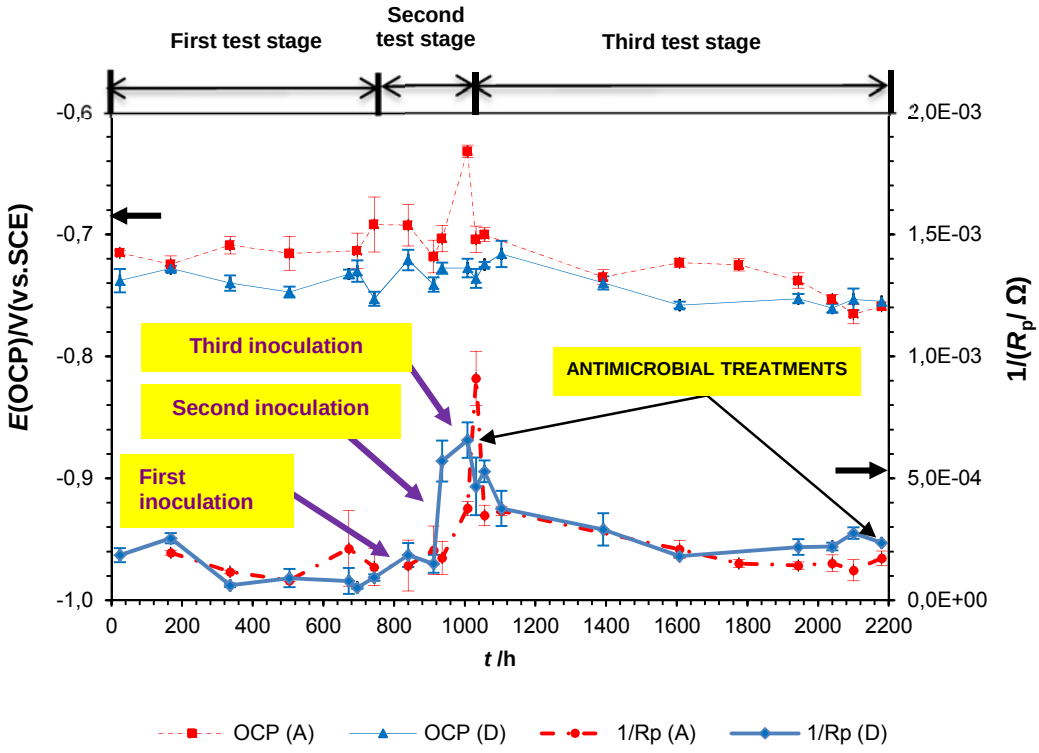

Fig. 5. Average instantaneous corrosion rate (1/(R_p/Ω)) and OCP (E(OCP)/V(vs.SCE)) values with standard deviation error bars for 12 o'clock positioned steel specimens (WE) exposed in flow cell A (inoculation with Desulfovibrio alaskensis) and flow cell D (inoculation with Desulfovibrio desulfuricans) during the 2200 h of test.

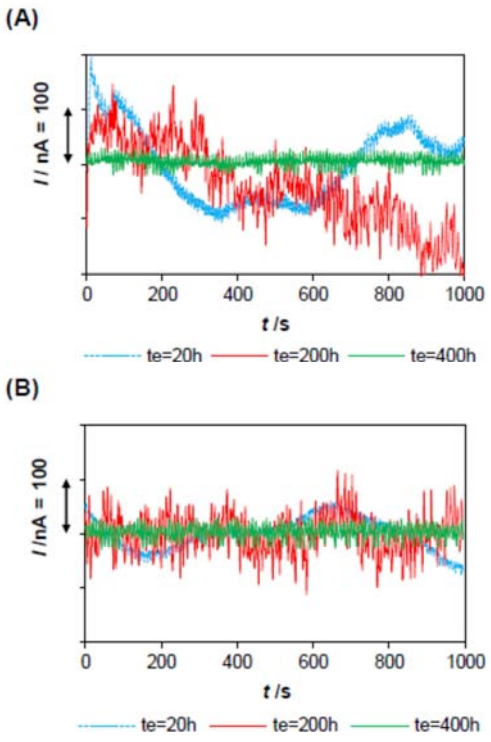

Fig. 6. Variations of typical current noise (I/nA = f(t)) obtained during the first test stage (te=0-792 h, prior to inoculations) at t_e= 20 h, t_e= 200 h and t_e= 400 h: (A) in flow cell D (inoculation with Desulfovibrio desulfuricans); (B) in flow cell A (inoculation with Desulfovibrio alaskensis). Data linearly detrended.

3.1.2. Second test stage

The first inoculation at the beginning of the second test stage (t_e= 792 h) led to an increase of cell density, a decrease in sulfate concentration linked to an increase in sulfide concentration due to the enhanced sulfidogenic metabolic processes (Tab. 1 and 2).

However, no significant modifications were observed in the electrochemical response after this first inoculation: 1/(R_p/Ω) remained stable with low values (Fig. 5). This stable trend in corrosion currents could be attributed to the corrosion product layer that remained stable even with the perturbation of the medium. In addition, sulfidogenic bacteria could enhance protective layer properties by promoting formation of protective iron sulfide (Fe_xS_y) films, a process taking place in a presence of low ferrous ion concentrations [43] as it is the case here. When flow conditions were reestablished, a decrease of the planktonic cell density in the bulk media was also observed in the both flow cells since part of microbial cells was flushed out. On the contrary, there was no change in sulfide and sulfate concentrations. Most likely the microbial activity in the bulk medium was maintained thanks to SRBs attached on steels

surfaces that can detach and colonize the bulk medium.

The second inoculation imposed significant perturbation to the systems and resulted in a noticeable alteration of environment and material corrosion behavior. High cells densities were measured in both flow cells (Tab. 1 and 2) even when the flux conditions were reestablished: Moreover higher densities were found in flow cell A (inoculated by D. alaskensis) than in the D one (inoculated by D. desulfuricans) with respectively 600 and 1850×103 cells mL^{-1}. A pH decrease down to 7.6 was noticed (Fig. 4) that could be product of SRBs metabolic activity (souring due to elevated sulfide production). Side effect of observed microbial flourishing was a significant increase in instantaneous corrosion rate. It can be observed that 24 h after the second inoculation, the stable and low $1/(R_p/\Omega)$ plateau established during the first test stage was disturbed. This was displayed in a significant increase of the average $1/(R_p/\Omega)$ values up to 6×10^{-4} in the flow cell D, and less expressed increase up to 3.5×10^{-4} in the flow cell A, (Fig. 5), that can be correlated with the increase in cell density and metabolic activity (Tab. 1 and 2). Also, ECN exhibited higher magnitude of corrosion current fluctuations and clear transients, characteristic of stable localized corrosion (i.e. pitting) as shown on Fig. 7. The stable localized corrosion was featured by significant current drops (I/nA = 100- 500) followed by a slower increase. Briefly, the rapid current increase during pit initiation and growth is followed by a slower decay leading to pit repassivation [38]. It is possible to assume that second inoculation led to a breach threshold of the protective corrosion product layer. This layer managed to resist to the microbial activity introduced by the first inoculation but after the second inoculation, it suffered local breakdown and could not reestablish instantaneously, exposing localized areas of metal surface to different influences of e.g. aggressive ions as Cl^-, S^{2-} and $S_2O_3^{2-}$, bacteria metabolic products. This often results in formation of large cathodic areas (remained Fe_xS_y, most likely with FeS whereas significantly smaller unprotected regions of steel surfaces are forming anodes, characterized by higher anodic current. Besides, observed increase in corrosion, and therefore most likely increase in dissolved Fe concentration may have inhibited formation of a protective sulfide film on a steel specimens surfaces what could cause higher corrosion rates. This phenomenon has been previously observed by other researchers [44, 45].

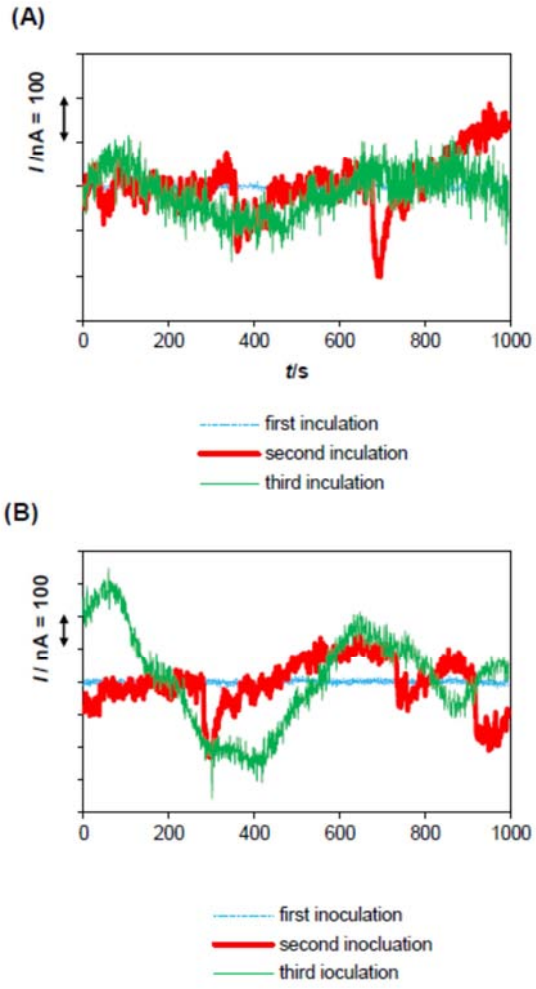

Fig. 7. Variations of typical current noise (I/nA = f(t)) obtained during the second test stage (t_e= 792 - 1070 h) obtained 24 h after each inoculation: (A) in flow cell D(inoculation with Desulfovibrio desulfuricans); (B) in flow cell A (inoculation with Desulfovibrio alaskensis). Data linearly detrended.

Short time after the third inoculation, a sudden pH increase was observed in the both flow cells (up to 8.5, Fig. 4), most probably due to cathodic corrosion reaction of hydrogen evolution and release of hydroxide ions (OH^-) into bulk medium, as a result of substantial increase in corrosion. This was reflected by the increase of the average $1/(R_p/\Omega)$ values (up to 9×10^{-4} for flow cell A and 7×10^{-4} for flow cell D, Fig.5), and of the ECN amplitudes (Fig. 7). However, the ECN did not exhibit the geometry characteristic for pitting. Nonetheless, metastable pitting or conjugation of multiple pits in visually detectable general corrosion pattern would not be revealed by EN signals and surface degradation still would have origin in localized corrosion.

Micrographs presented in Fig. 8A and 8B are typical for steel specimens located at 6 o'clock position and retrieved from each flow cell at the

end of the second test stage.

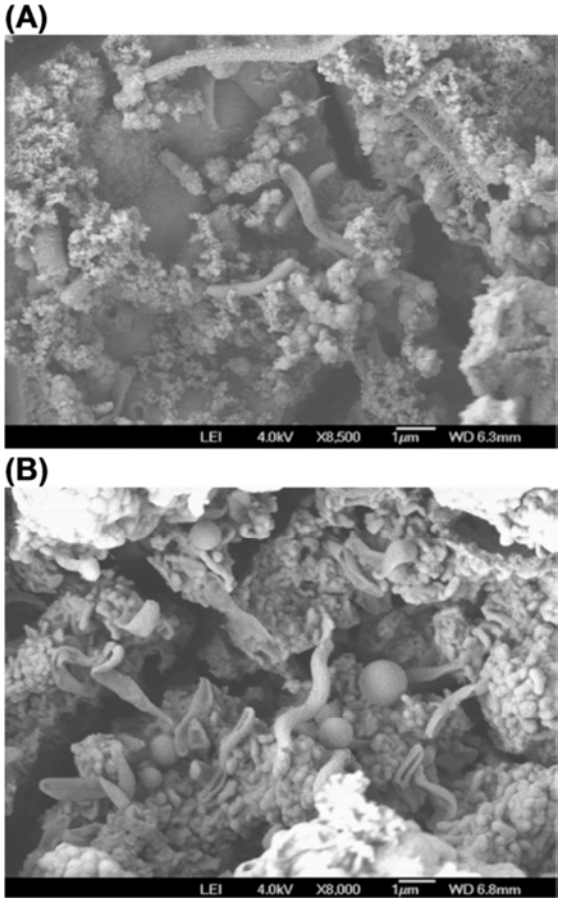

Fig. 8. SEM of steel specimens placed at 6 o'clock position and retrieved from flow cells after 1070 h of exposure: (A) specimen from cell A (inoculation with Desulfovibrio alaskensis) - 8500x; (B) specimen from cell D (inoculation with Desulfovibrio desulfuricans) - 8000x.

The steel specimens were covered with blackish deposits in which Fe_xS_y participated (sulfide presence verified by the chemical test). Deposits were easily removed from steel specimens. This is in agreement with chemical and microbial information obtained during second test stage. Detection of blackish deposits containing sulfide suggests that postulated layer formed during the second test stage is predominantly composed of the Fe_xS_y, a new component formed on steel surface. However, it is required to keep on mind that observed layer may be heterogeneous and may contain other compounds, such as GR(SO_4^{2-}) and/or magnetite (Fe_3O_4), characteristic for steel specimens immersed in seawater with active sulfidogenic microbial population [40, 41, 46]. Furthermore, SEM micrographs revealed a high variety of corrosion/biomineralization products at the metal surface suggesting that more than one mineral is participating in the corrosion deposit architecture. This indicates that members of indigent microbial population naturally contained in seawater (for example *Clostridium* [18]), in addition to the inoculated SRBs, are contributing to biomineralization process occurring on steel surfaces. Proof of this is the APB presence in both flow cells (Tab. 2 and 3).

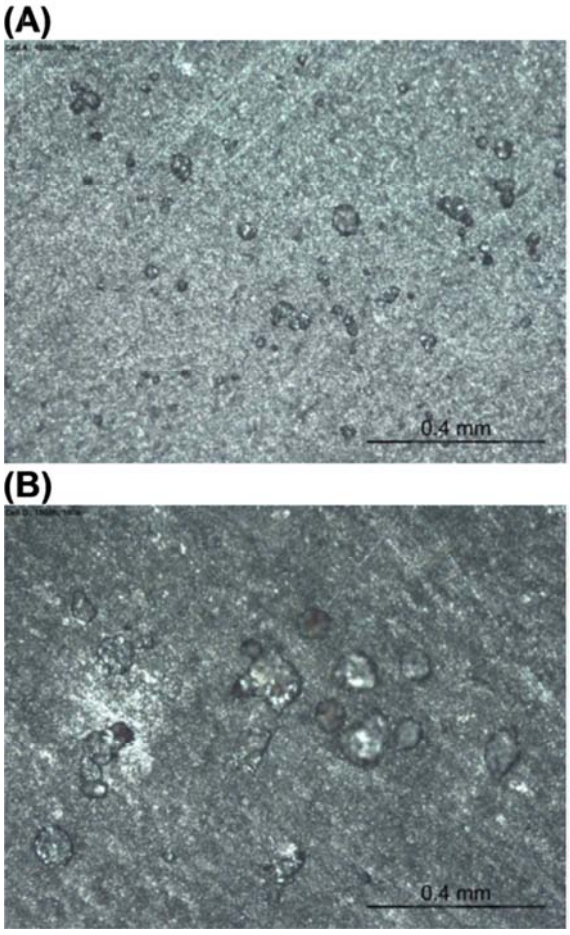

Fig. 9. Micro photographs (100x) of steel specimens retrieved from flow cells after 1070 h of exposure and after corrosion product removal, revealing localized corrosion attacks: (A) specimen from flow cell A (inoculation with Desulfovibrio alaskensis); (B) specimen from flow cell D (inoculation with Desulfovibrio desulfuricans).

Moreover, observed corrosion products seem to be similar in presence of *D. alaskensis* (Fig. 8A) or *D. desulfuricans* (Fig. 8B), featured with particulate aggregates. On both surface observed (from flow cells A - Fig 8A and D - Fig 8B), some bacteria with the characteristic curved rod shape of *vibrio* species [47] were observed incorporated inside the mineral structure instead of formation purely organic biofilms. The *vibrio* shape bacteria occupied a small volume fraction as compared to the formed corrosion products and biomineralized structures. After specimen's chemical cleaning, optical microscopy revealed presence of

numerous pits with a diameter up to 100 µm and an average depth of 5-10 µm as shown on Fig. 9. These pits could be correlated with ECN transients observed 24 h after second inoculation, and indication occurrence of pitting on WEs surfaces.

3.1.3. Third test stage

At the beginning of the third test stage, 19 h after the third inoculation, flow cells were treated with 500 ppm of a glutaraldehyde based antimicrobial chemical for a period of 50 min (flow was stopped). Short time after the applied antimicrobial treatment, the pH decreased due to the intrinsic acidity of the antimicrobial chemical (Fig. 4). A decrease of cell densities was also observed, in a higher range in flow cell D (from 1600 to 945 cells mL^{-1} in few hours) than in the flow cell A (from 678 to 506 cells mL^{-1} in the same period). Consequently to this decrease, an increase of sulfate concentrations as well as a decrease of sulfide concentrations was measured indicating the effectiveness of the antimicrobial treatment. Moreover, $1/(R_p/\Omega)$ in both flow cells decreased to a value of 3.5×10^{-4} and recorded OCPs were E(OCP)/mV(vs.SCE)≈ -720 (Fig. 5).

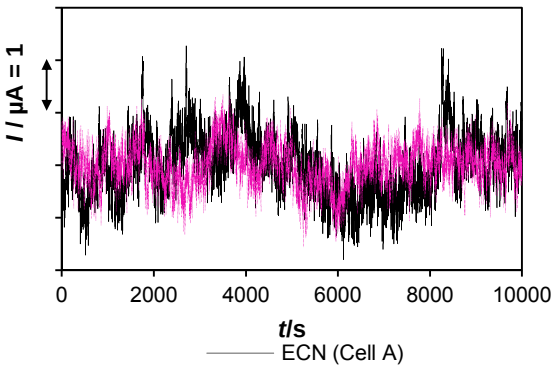

Fig. 10. Variations of typical current noise (I/nA = f(t)) obtained in flow cell A (inoculation with *Desulfovibrio alaskensis*) and flow cell D (inoculation with *Desulfovibrio desulfuricans*) recorded 12 h after first antimicrobial treatment (t_e= 1087).

Current fluctuations were found more expressed (Fig.10) compared to those found before the antimicrobial treatment, maintaining constantly differences between minimum and maximum amplitudes peaks in range of approximately 1 µA (versus 100 nA). Even though graphs are not presented herein, it is significant to mention that in this short period after biocide treatment (2- 10 h), EPN trend rose toward more positive values, from E/mV(vs.SCE)= -720 up to E/mV(vs.SCE)= -680 and then returned back to E/mV(vs.SCE)= -720 in the both flow cells. When antimicrobial was flushed out from flow cells, pH showed increasing trend behavior due to income of fresh media. This process was slow and it resulted in pH 8.1 at t_e= 1450 h (Fig. 4). From that point until the test termination, both flow cells exhibited a decrease in pH with final pH of 7.4 in flow cell A and 7.7 in flow cell D (Fig. 4).

Despite these fluctuations, measured pH was very similar to that of seawater from North Sea (base component of used media). During the same time period cell densities continued to slowly decrease (Tab. 2 and 3). After a temporary increase initiated by the first antimicrobial treatment, sulfate concentration showed a decreasing trend during the whole third test stage (Tab. 1 and 2). Acquired data are suggesting that bacteria continued to consume sulfate present in seawater; however, produced sulfide was found in low concentration in bulk medium (sulfide concentration continued to decrease). In fact, it reacted with iron forming different Fe_xS_y compounds that can be observed on steel specimens' surfaces as well as in bulk medium where black particulates were found. In addition, part of sulfate probably reacted with residual oxygen forming thiosulfate ions, and decreasing amount of available sulfate in bulk medium. Observed reduction in sulfate concentration will reduce the molar ratio $[SO_4^{2-}]$ / $[HCO_3^-]$ and consequently lead to partial transformation of $GR(SO_4^{2-})$ to carbonated green rust ($GR(CO_3^{2-})$= $Fe^{II}_4Fe^{III}_2(OH)_{12}CO_3\times2H_2O$) [42]. Moreover, possible increase of the carbonate concentration could result in the formation of carbonated compounds such as chukanovite ($Fe_2(OH)_2CO_3$) [48, 49].

The $1/(R_p/\Omega)$ decreasing trend observed in both flow cells after antimicrobial treatment was reduced and material corrosion resistance stabilized to the initial level. This was maintained until test termination, and final $1/(R_p/\Omega)$ were around 2×10^{-4} (Fig. 5). OCPs exhibited similar behavior, featured with mildly decreasing OCPs and final value of E(OCP)/mV(vs.SCE)= -770 (Fig. 8). ECN signals acquired 125 h after biocide treatment (Fig. 11, t_e= 1200 h) exhibit lower amplitudes indicting decrease of surface electrochemical activity compared to ECN signals obtained shortly after antimicrobial treatment (Fig. 12.). Later on, the low current fluctuations observed at t_e= 1800 h and t_e= 2000 h in the range of 100 nA (Fig. 11) indicated current intensity decrease, hence lower corrosion too. This is in agreement with observed decrease of $1/(R_p/\Omega)$

and reduced of the planktonic bacterial population. In conclusion, the probable formation of stable corrosion products and the partially suppressed microbial activity can be considered as the origin of the electrochemical behavior of carbon steel after the antimicrobial treatment.

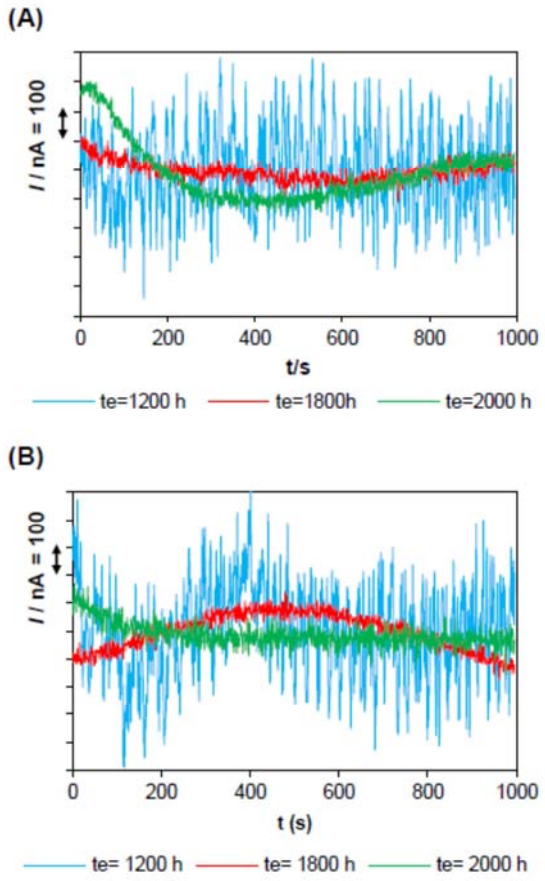

Fig. 11. Variations of typical current noise (I/nA = f(t)) obtained during the third test stage (t_e= 1070 – 2200 h) at t_e= 1020 h, t_e=1800 h and t_e=2180 h: (A) in flow cell D(inoculation with *Desulfovibrio desulfuricans*); (B) in flow cell A (inoculation with *Desulfovibrio alaskensis*). Data linearly detrended.

The second antimicrobial treatment (50 min with 1500 ppm) completely suppressed already decreased planktonic microbial activity. Here again, the pH decreased as a consequence of applied treatment. As previously mentioned, E(OCP)/mV(vs.SCE) and 1/(R_p/Ω) values in both cell remained unchanged. However, as observed immediately after the first biocide treatment, ECN exhibited particular alteration in its behavior (Fig. 12). The ECN in both cells demonstrated more erratic behavior compared to ones observed before antimicrobial treatment application. The observed curve shape and peak magnitude suggest elevated corrosion current and enhanced localized surface activity. These observations could indicate corrosion deposit breakdown, possibly initiated by pH decrease.

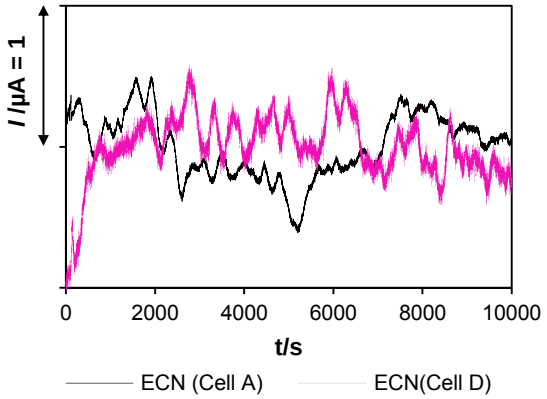

Fig. 12. Variations of typical current noise (I/A = f(t)) obtained in flow cell A (inoculation with *Desulfovibrio alaskensis*) and flow cell D (inoculation with *Desulfovibrio desulfuricans*) recorded 12 h after the second antimicrobial treatment (t_e= 2192 h). Data linearly detrended.

3.2. Post- test surface analysis

After the once-through flow loop was decommissioned, three 6 o'clock positioned steel specimens and one 12 o'clock positioned steel specimen (WE) from each cell were subjected to microscopical (SEM analysis) and chemical (EDX analysis) examination in order to acquire more information about corrosion deposits building blocks and corrosion mechanisms nature.

3.2.1. Corrosion products architecture

The micrographs for 6 o'clock located steel specimens, examined with SEM/EDX system after 2200 h exposure in the flow cell A with a dominant presence of *D. alaskensis* species are presented in Fig. 13. Tab. 3 shows EDX analysis obtained on different points on the observed surface.

The micrographs reveal the deposition of corrosion products characterized with the dominant presence of Fe, Ca, S, C and O, but the proportions and amounts of specific elements are various, suggesting different mineral structures. Indeed, the simultaneous presence of Fe peak with O and C ones (spot Sp1 of Fig. 13A, Tab. 3A; spot Sp2 of Fig. 13B, Tab. 3B; spots Sp1 and Sp2 of Fig 13C, Tab. 3C) is characteristic of the formation of iron minerals, such as $Fe_2(OH)_2CO_3$ and GR(CO_3^{2-})) [48, 49]. These mineral products were found in outer corrosion product structure. Moreover, S peaks were identified with EDX analysis too.

However, S was found in higher proportion at locations where analyses were performed close to the metal surface, as shown in Fig. 13A Sp3 (Tab. 3A), Fig. 13B Sp1 (Tab. 3B) and Fig. 13C Sp1, Sp2 and Sp3 (Tab. 3C).

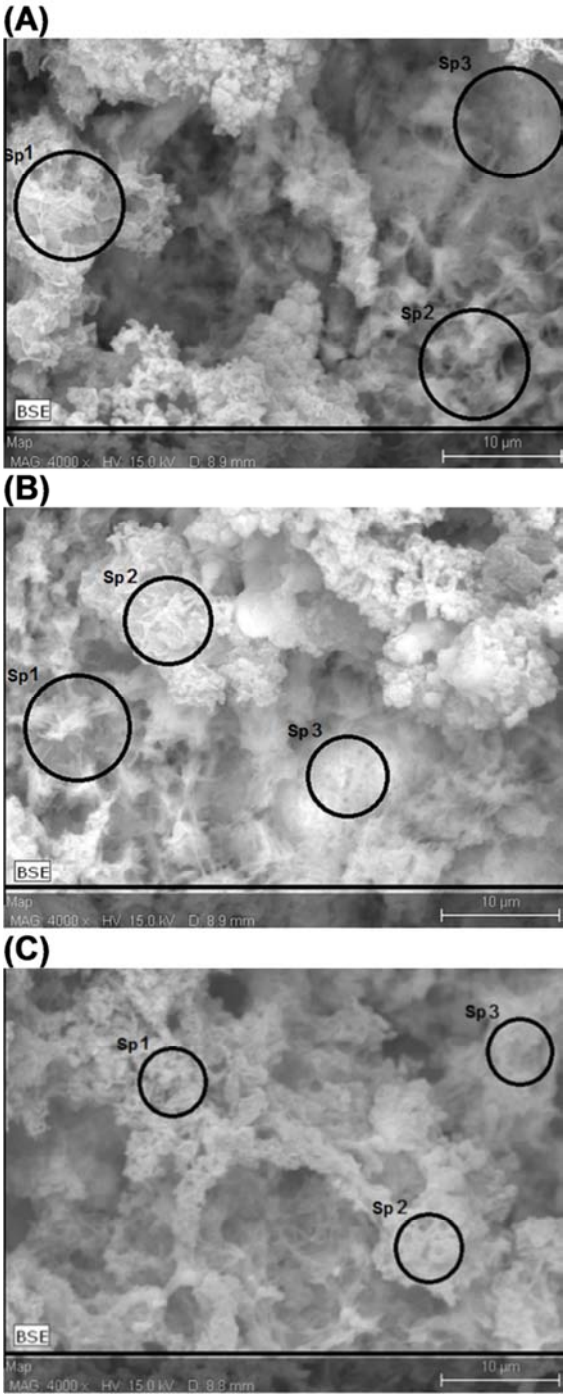

Fig. 13. SEM micrographs (4000x) with emphasized areas submitted to EDX analysis of four 6 o'clock positioned specimens exposed in flow cell A (inoculation with *Desulfovibrio alaskensis*) for 2200 h.

Tab. 3. EDX analysis results of emphasized areas presented on Fig. 13, all results given in weight fractions (wt(element)/%): (A) representative spectrums for Fig. 13A; (B) representative spectrums for Fig. 13B; (C) representative spectrums for Fig. 13C.

Table A

Spec.[1]	C	O	S	Ca	Fe
Sp1	18.2	35.9	5.2	3.0	37.6
Sp2	30.5	11.7	5.0	3.5	49.3
Sp3	2.6	6.9	6.7	13.3	70.5

Table B

Spec.[1]	C	O	S	Ca	Fe
Sp1	3.1	5.3	6.5	13.5	71.4
Sp2	20.0	40.2	3.9	3.2	32.9
Sp3	3.4	6.0	2.5	1.3	86.8

Table C

Spec.[1]	C	O	S	Ca	Fe
Sp1	15.1	19.9	12.6	4.2	48.3
Sp2	25.5	37.1	6.9	1.4	29.1
Sp3	20.1	9.2	13.2	2.6	68.1

1 – Spec.- complete analyzed spectrum for particular surface area

Concerning Ca peaks, analysis is suggesting that Ca was concentrated within localized and visually larger structures established in the outer layers of corrosion products, and often accompanied with the presence of O and C as shown in Fig. 13A Sp3 (Tab. 3A), and Fig. 13B Sp1 (Tab. 3B). The simultaneous presence of Ca, C and O with local alkaline surface conditions (as recorded at the end of second test stage) could indicate the formation of calcite ($CaCO_3$) [50]. To sum-up, taking into consideration relatively low DO in the bulk medium (Fig. 1), mildly alkaline environment (Fig. 4) and OCP in range of *E*(OCP)/mV(vs.SCE)= -750 ± 20 (Fig. 2), it is likely that the corrosion/ biomineralization products belong to several main mineral families: iron sulfides with FeS, iron oxides with Fe_3O_4, iron(III) oxyhydroxides in all likelihood with α-FeOOH and γ-FeOOH, GR(SO_4^{2-}), carbonate minerals most likely with $Fe_2(OH)_2CO_3$ and GR(CO_3^{2-}), as well as calcareous such deposits as $CaCO_3$ on the top of this structure [42, 49].

Otherwise, micrograph presented in Fig. 14 is characteristic for the 12 o'clock positioned

WEs and removed from the flow cell A after 2200 h exposure. They reveal the presence of two dominant regions as corrosion deposits and transfer region defined by spot Sp3. Two dominant regions have similar chemical fingerprints to ones observed in a case of 6 o'clock positioned steel specimens. The first region, defined by spots Sp1, Sp2 and Sp4 on Fig. 14, is dark colored and EDX analysis emphasized the presence of S, as well as high portions of Fe, O and C (Tab. 4), suggesting presence of Fe_xS_y in high amount along with the presence of iron oxides and carbonate minerals. In contrast, the second zone, represented by spots Sp5 and Sp6 on Fig. 14, appears brighter compared to the dark region, is forming outer layer, and reveals high amount of Ca (Tab. 4). Additionally, Fe, O, and C are well represented; suggesting formation of iron oxides, iron carbonates and Ca-based minerals. Interesting to note for this particular region is the complete absence of S peak in investigated spectrums. To sum-up, micrographs suggest an initial formation of Fe_xS_y (inner layer) that is followed by the rise of different Fe minerals and Ca-based minerals on them (outer layer). However, this postulated layered structure may be not so obvious and some detected compounds may participate in construction of the both layers. Additionally, P peak was occasionally recorded (Sp1 and Sp2, Fig. 14) but overall impression differs a lot from observations made in artificial seawater systems inoculated with different SRB strains, *D. gabonensis* and *D. capillatus*, for which P was present in much larger amount accompanied with less S [14]. Moreover, Si, Al and Mg peaks were detected (Fig. 14, Table 4). The Mg, in the form of Mg(II), possibly could substitute Fe(II) in GR compounds but it can also easily substitute Ca in calcite.

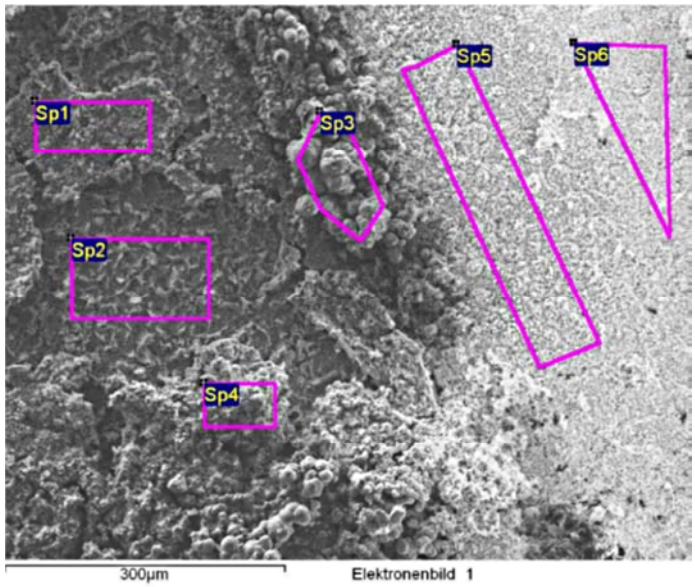

Fig. 14. SEM micrograph (100x) with emphasized areas submitted to EDX analysis of 12 o'clock positioned specimen exposed in flow cell A (inoculation with *Desulfovibrio alaskensis*) for 2200 h.

Tab. 4. EDX analysis results of emphasized areas presented on Fig.14, all results given in weight fractions (wt(element)/%).

Spec.[1]	C	O	Na	Mg	Al	Si	P	S	Cl	Ca	Cr	Mn	Fe	Ni	Cu	Sr
Sp1	8.6	42.7	/	0.4	0.3	/	0.1	16.6	/	0.2	/	0.2	30.8	/	/	/
Sp2	6.5	34.7	/	0.2	0.4	0.2	0.4	7.9	0.6	/	1.1	1.2	42.0	1.1	3.8	/
Sp3	5.1	53.6	/	1.0	0.3	0.3	/	0.1	/	1.0	/	0.4	38.2	/	/	/
Sp4	12.5	36.7	0.8	1.4	0.2	0.2	/	17.8	/	1.4	/	/	28.9	/	/	/
Sp5	5.7	61.9	/	0.6	/	/	/	/	0.2	15.1	/	/	16.5	/	/	/
Sp6	10.6	57.8	0.3	0.1	0.1	/	/	0.1	0.1	27.1	/	/	3.3	/	/	0.5

1 – Spec. - complete analyzed spectrum for particular surface area

Micrographs presented in Fig. 15 show corrosion products formed on steel specimens located at 6 o'clock location after 2200 h immersion in the dominant presence of *D. desulfuricans* species (flow cell D). It is possible to observe corrosion products composed of Ca-based minerals (Fig. 15A SpX, Tab. 5A), carbonate minerals (Fig. 15B Sp4 and Tab. 5B), and also some Fe_xS_y minerals (Fig 12B Sp2, Sp3Sp4 and Tab. 5B). Moreover, a high amount of iron oxide minerals (Fig. 15C SpX, Tab. 5C) is present. It possesses resemblance, in terms of morphology and analysis, with magnetite mineral.

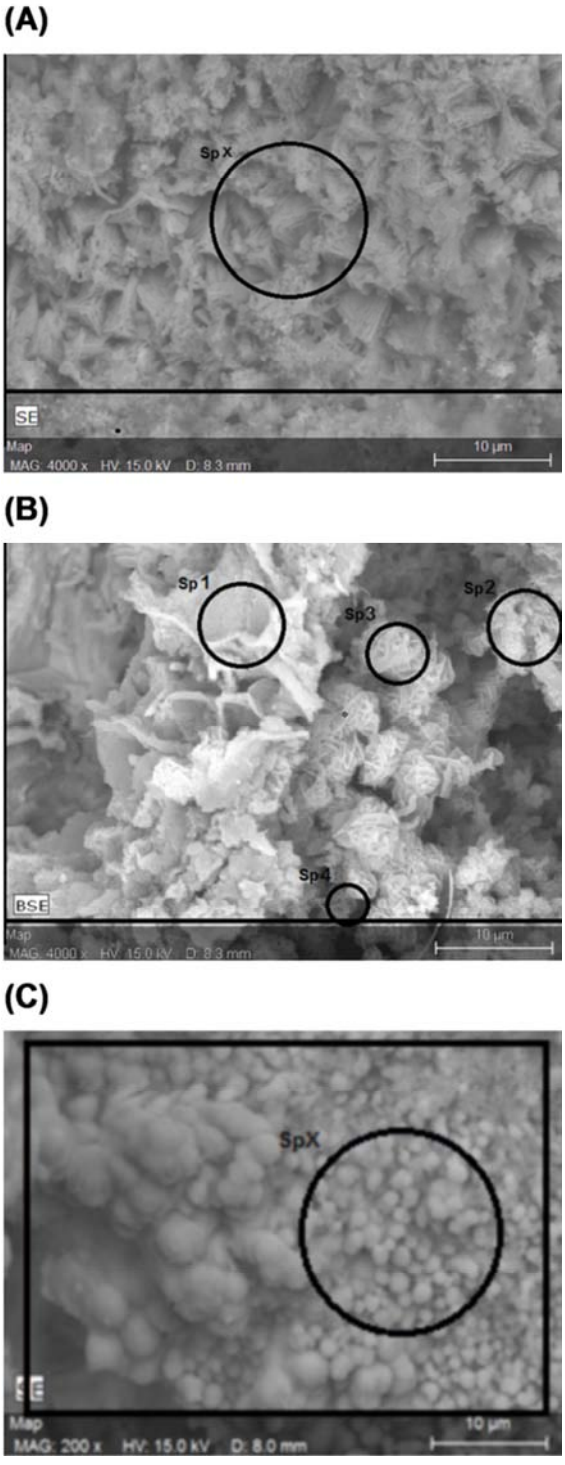

Fig. 15. SEM micrographs (4000x) with emphasized areas submitted to EDX analysis of three 6 o'clock positioned specimens exposed in cell D (inoculation with *Desulfovibrio desulfuricans*) for 2200 h.

Tab. 5. EDX analysis results of emphasized areas presented on Fig. 15, all results given in weight fractions (wt(element)/%): (A) representative spectrums for Fig. 15A; (B) representative spectrums for Fig. 15B; (C) representative spectrums for Fig. 15C.

Table A

Spec.[1]	C	O	S	Ca	Fe	Mg
SpX	15.2	45.0	1.3	26.6	5.2	1.8

Table B

Spec.[1]	C	O	S	Ca	Fe
Sp1	20.1	17.6	4.1	0.9	54.7
Sp2	2.2	7.1	10.7	1.1	78.8
Sp3	/	8.2	11.0	1.8	79.0
Sp4	1.8	6.6	14.2	3.3	74.0

Table C

Spec.[1]	O	Fe
SpX	10.0	90.0

1 – Spec. - complete analyzed spectrum for particular surface area

Micrographs presented in Fig. 16 reveal the presence of relatively homogenous minerals morphologies as corrosion products on the 12 o'clock positioned WE examined with SEM/ EDX system after 2200 h exposure in the flow cell D. The S is very well represented in corrosion deposits (Fig. 16 in Sp2, 3, 4, 5, 7 and 8; Tab. 6). Then again, Ca is well represented only in some part (spot Sp5 in Fig. 16, Tab. 6), regarded as the outer layer, indicating similar corrosion products architecture as previously described for the specimens removed from the flow cell A. This is equally supported by the presence of C and O that are quantitatively dominant compared to other elements discovered in this scan.

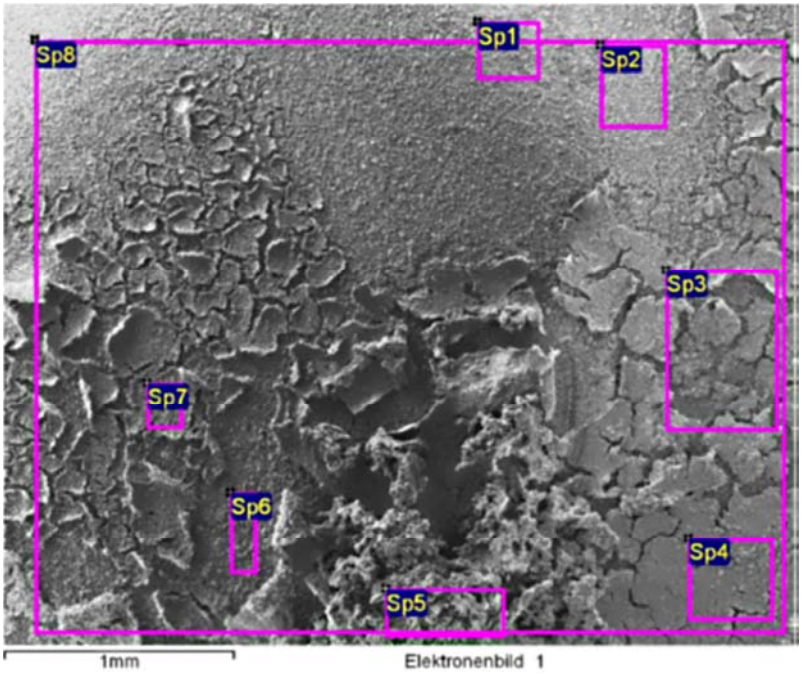

Fig. 16. SEM micrograph (100x) with emphasized areas submitted to EDX analysis of 12 o'clock positioned specimen exposed in flow cell D (inoculation with *Desulfovibrio desulfuricans*) for 2200 h.

Tab. 6. EDX analysis results of emphasized areas presented on Fig. 13, all results given in weight fractions (wt(element)/%).

Spec.[1]	C	O	Na	Mg	Al	Si	P	S	Cl	Ca	Cr	Mn	Fe	Ni	Cu	Zn
Sp1	12.3	47.6	1.2	1.2	0.4	0.2	0.4	4.6	0.4	/	0.4	0.6	28.4	0.8	1.5	/
Sp2	16.0	43.2	0.8	0.9	0.4	0.3	0.5	8.0	0.4	0.2	0.5	0.7	24.9	1.1	1.5	0.6
Sp3	14.2	54.7	0.3	0.9	0.4	/	0.1	11.8	0.5	0.6	0.2	0.2	16.2	/	/	/
Sp4	15.7	52.4	0.3	0.9	0.1	/	0.1	13.6	0.8	1.2	/	0.1	14.7	/	/	/
Sp5	19.6	49.8	0.5	1.1	1.2	/	/	9.9	0.3	7.3	/	/	10.4	/	/	/
Sp6	8.1	66.2	1.8	0.3	0.5	0.1	0.2	2.9	0.6	/	/	0.4	18,4	/	0.2	/
Sp7	23.6	55.1	0.2	1.5	0.2	/	0.2	9.3	0.4	0.7	/	/	8.8	/	/	/
Sp8	17.4	53.1	0.9	1.1	0.5	0.1	0.3	9.4	0.3	0.8	0.2	0.3	15.0	0.3	0.3	/

1 – Spec. - complete analyzed spectrum for particular surface area

Taking all the observations into account, a phenomenological model of the architecture of the corrosion deposits formed in our particular test conditions, is suggested, regardless cells were inoculated with *D. alaskensis* or *D. desulfuricans* species (Fig. 17). As Fe_xS_y minerals seemed placed deeper, in the inner layers of corrosion product structure, it could correspond to the biological sulfate reduction into sulfide ions. Undeniably, *Desulfovibrio* species are anaerobic bacteria capable of reducing sulfur compounds to sulfide, what finally may result with growth of Fe_xS_y.

In our work, where experiments have been conducted under anoxic conditions in North Sea seawater, Fe_xS_y compounds seem to be the construction blocks of the first corrosion product layer which stays stable on the metal surface, even after a long time immersion in presence of elevated metabolic activity of SRBs. This layer may also contain $GR(SO_4^{2-})$ and Fe_3O_4. Then, above this first layer, mixed iron minerals (Fe_3O_4, Fe(III) oxyhydroxides such as α-FeOOH and γ-FeOOH, $GR(SO_4^{2-})$, $Fe_2(OH)_2CO_3$ and $GR(CO_3^{2-})$) with addition of calcareous precipitates ($CaCO_3$) are established. This layer possibly could contain small amounts of Fe_xS_y (most likely FeS) too. This structural environment (corrosion products, bacteria) seems to entail a localized corrosion process with the presence of pits on the steel surface.

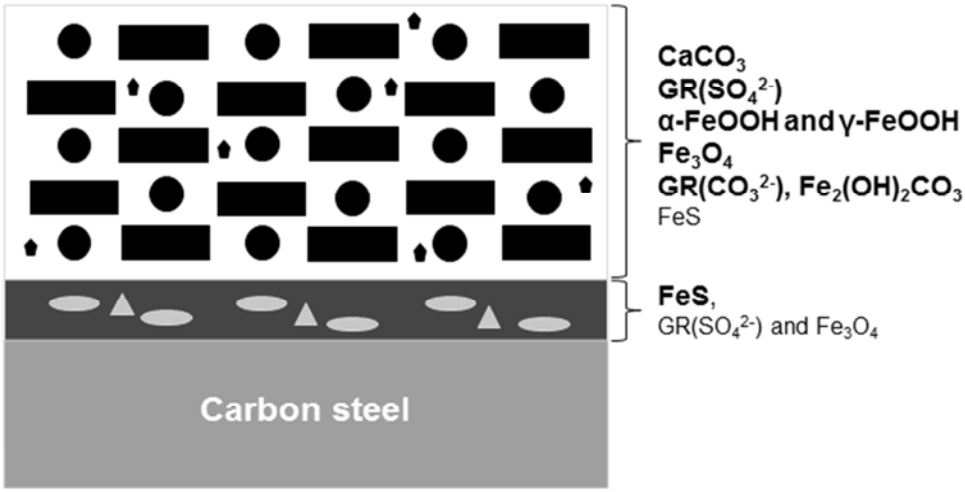

Fig. 17. Phenomenological model for corrosion products formation carbon steel, taking place during and post sulfidogenic bacteria process.

3.2.2. Corrosion attack mechanism and evolution

In order to identify corrosion attack mechanisms and their evolution during the test time, steel specimens were cleaned of corrosion products/ deposits and submitted to microscopical and metallurgical examination.

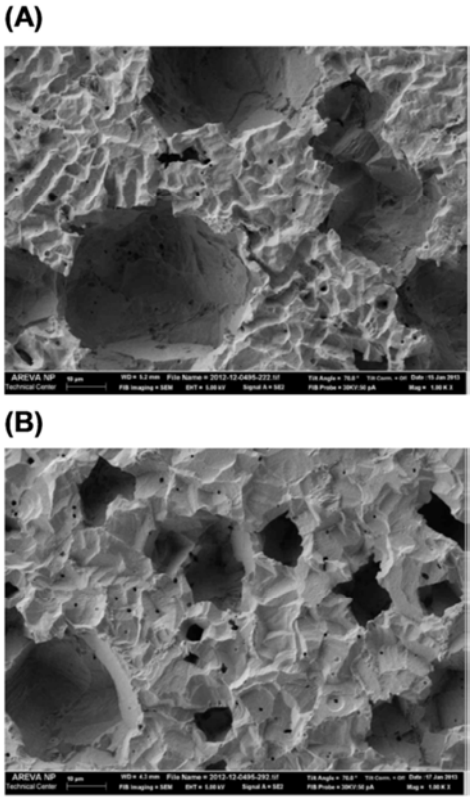

Fig. 18. SEM micrographs (1000x) of 12 o'clock positioned steel specimens retrieved after 2200 of immersion in flow cells and chemically cleaned from corrosion deposits: (A) specimen from flow cell A (inoculation with Desulfovibrio alaskensis); (B) specimen from flow cell D (inoculation with Desulfovibrio desulfuricans).

After corrosion products removal, the surface topography, representative of the 12 o'clock positioned WEs retrieved from both flow cells, appear very rough (Fig. 18) with numerous pits, with a diameter up to 50-60 µm for specimens retrieved from cell A (Fig. 18A) and 20-30 µm for specimens retrieved from cell D (Fig. 18B). Also, metallographic cross sections of same steel specimens were prepared in order to determine the depth and the characteristics of the corrosive attack (Fig. 19 and 20). As previously mentioned (see Section 3.2.1), the corrosion deposits on the surface were subdivided in darker and brighter regions, even after the removal of corrosion products (Fig. 19A & 20B). The darker zones are less spread on the specimens from the flow cell D (inoculated with *D. desulfuricans*). These different visual appearances correspond to different characteristics of attack in the metallographic cross section. The brighter areas are rather smooth, showing only a superficial attack (Fig. 19B) whereas higher roughness and pitting corrosion can be observed in the darker areas (Fig. 19C). While the depth of the corrosion attack varies between approximately 20 to 40 µm on the specimen from the flow cell A (inoculated with *D. alaskensis,* Fig. 19C), the degree of damage is lower regarding depth, in range of approximately 20 µm, on the specimen from the flow cell D (Fig. 20B), indicating lower material deterioration.

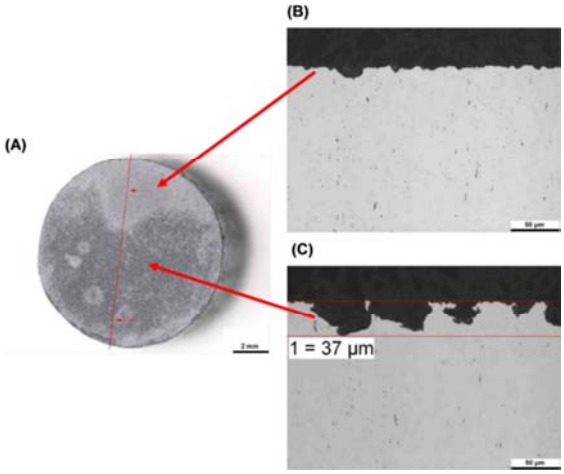

Fig. 19. Macrographs and micrographs of 12 o'clock positioned specimen exposed in cell A (inoculation with Desulfovibrio alaskensis) for 2200 h after corrosion product removal: (A) Macrograph before cross section and cutting line; (B) Micrograph for depth determination of attack in more lighted colored region; (C) Micrograph for depth determination of attack in darker colored region.

This is understandable, having on mind higher results suggesting that *D. alaskensis* has a higher corrosivity than *D. desulfuricans*. Regardless to size and depth of pits, the topographies observed here are coherent with corrosion attack previously recorded in presence of SRBs, supporting hypothesis that biofilms constituted of SRBs lead to pitting corrosion [33].

The bulk microstructure of all steel specimens used in this study consists of ferrite and pearlite with randomly distributed MnS inclusions, which is the typical microstructure of the material S275JR. On the etched cross section of the two specimens, selective attack in the vicinity of inclusion lines can be identified (Fig. 21). However a correlation cannot be clearly shown between a corrosion pit and the presence of an inclusion. The corrosion pits in general show a dependency on the crystallographic orientation, which can be deduced from their square or rectangular appearance in the SEM images and from the rather straight boundaries of the pits in the cross section. This is not surprising knowing that bacterial initial attachment occurs on or in the proximity of the grain boundaries. This phenomenon has origin in differential energy distribution between the grain boundaries and matrix [2, 50], resulting in higher energy allocated in grain boundaries that attract bacteria [50]. Therefore, it is expected that initial localized material deterioration will occur also on grain boundaries as shown in the presented micrograph.

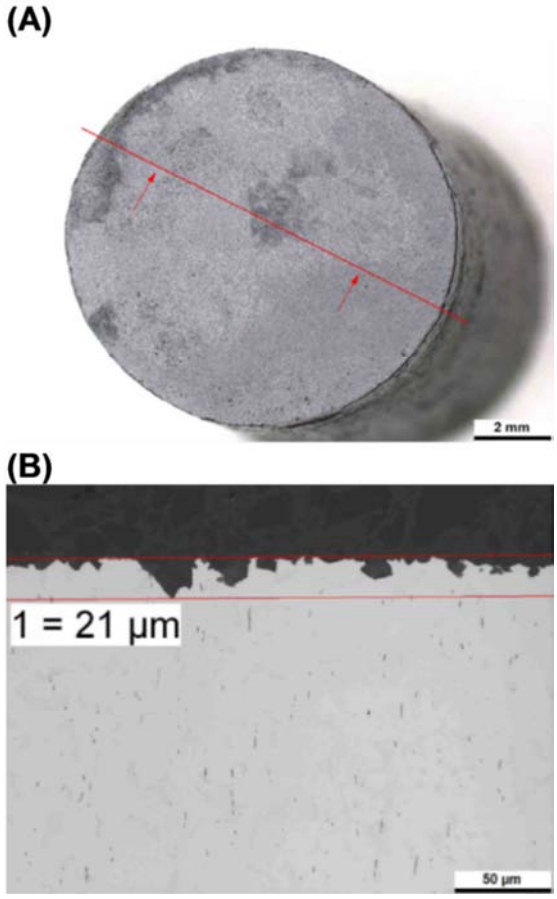

Fig. 21. Etched cross-sections SEM micrographs (250x) of 12 o'clock positioned specimen exposed for 2200 h: (A) from flow cell A (inoculation with *Desulfovibrio alaskensis*); (B) from flow cell D (inoculation with *Desulfovibrio desulfuricans*).

Investigation centered on influence of MnS inclusion on corrosion attack provides inconclusive results. In Fig. 22A and B it is possible to observe beginning of corrosion attack at location of inclusion. In that case the inclusion shows the typical linear appearance of MnS. On the contrary, lack of this mechanism is recorded on Fig. 22B; the inclusion at the onset of corrosion is of circular shape (e.g. oxidic). The remaining corrosion pits are free of nonmetallic inclusions, which might be due to the advanced state of corrosive attack.

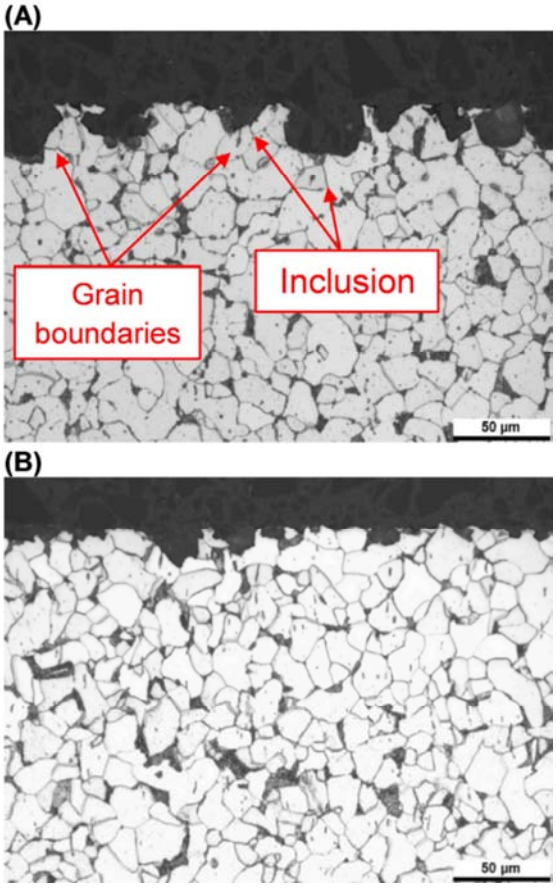

Fig. 22. Cross-sections micrographs of 12 o'clock positioned specimen exposed in cell D (inoculation with Desulfovibrio desulfuricans) for 2200 h after corrosion product removal: (A) Micrograph showing beginning of corrosion attack on location of MnS inclusion; (B) Micrograph showing beginning of corrosion attack in presence and absence of MnS inclusion.

From material structure it is possible to see that corrosion initiation is attracted to grain boundaries and inclusions. Yet, to gain more information it is required to study these processes in a short period after environment inoculation. It may be the case that MnS inclusions play role in the localized corrosion initiation [20, 21]. Nonetheless, their role in further development of corrosion attack with time is attenuate.

4. Conclusion

Herein presented results show that the presence of sulfidogenic species in the seawater environment may result in degradation of the surface of carbon steel, leading to a rougher surface topography as well as localized corrosion damage. However, a long-term exposure in systems where the high bacterial activity was recorded does not have to necessary result in elevated corrosion rates, as has been previously reported. The formation of the observed corrosion attack pattern was investigated for two influencing factors:

a) Influence of the material surface microstructure on the degradation topography:
The influence of the steel surface microstructure in the observed deterioration process and impact on the damage layout is recognized. Grain boundaries and inclusions (e.g. MnS) are playing a significant role during the initial stage of corrosion attack (pit initiation), although this can diminish during latter stages of corrosion and material degradation as shown in the work presented herein.

b) Impact of environment established on the material surface:
Microbial activity is affecting the mineralization process naturally occurring on the carbon steel surface leading to architectures composed of mixed iron (II) and (III) minerals such as iron sulfides, magnetite, iron oxyhydroxides, chukanovite and sulfated and carbonated green rust as well as calcareous deposits. Inner layers of these structures could possibly provide an anaerobic habitat for SRBs, where they can flourish by utilization of sulfate form GR(SO_4^{2-}) as a terminate electron acceptor for their dissimilarity respiration which enables continuous degradation of steel.

Study about mitigation of the microbial hazard in these particular environmental conditions showed that the impact of antimicrobial treatment on a planktonic microbial population is positive even in lower concentrations than typically applied. Consequences of antimicrobial treatment in this case collide with its intended function; to stop biological reaction and the production of aggressive metabolic products (S^{2-}, $S_2O_3^{2-}$, etc…), and therefore decreases general material deterioration. However, the microbial population on the steel surface can be protected by corrosion products and cannot be always reached by antimicrobial product, which implies continuous material deterioration in some regions of material surface. Moreover, with a new available source of energy and electron acceptor, microorganisms, either sessile or planktonic, have the possibility to reinstall their activities which could lead to further material deterioration.

Acknowledgments

Funding was received from the European Community's Seventh Framework Programme (FP7/2007-2013). The authors wish to express their gratitude towards Øystein Birketveit from MISWACO, Anne Karin Nyhaug and Endy Spriet from MIC in Bergen, Leonardo Dall'Agnol and Prof. Jose Moura from FCT-UNL in Lisbon, and to Dr. Marie Libert and Marta Kerber Schutz from CEA in Cadarache for their support in the production of presented work.

References

[1] W. Lee, Z. Lewandowski, P.H. Nielsen, W.A. Hamilton, Biofouling 8 (1995) 165.

[2] R. Javaherdashti, Microbiologically influenced corrosion: an engineering insight, Springer-Verlag, London , 2008.

[3] H.A. Videla, Electrochemical interpretation of the role of microorganisms in corrosion, in: D.R. Houghton, R.N. Smith, H.O.W. Eggins (Eds.), Biodeterioration , Vol. 7, Elsevier Applied Science, London, 1988, p. 359.

[4] Z. Szklarska-Smialowska, Pitting Corrosion of Metals, NACE International, Houston, 1986.

[5] K. Von Wolzogen, C. A. H. and L. S. Van der Vlugt, Water 18 (1934) 147.

[6] R.D. Bryant and E. J. Laishley, Canandian Journal of Microbiology 36 (1990) 259.

[7] I. Pankhania, Biofouling 1 (1988) 27.

[8] R.D. Bryant and E.J. Laishley, Microbiology and Biotechnology 38 (1993) 824.

[9] R.D. Bryant, W. Jansen, J. Boivin, E.J. Laishley, J.W. Costerton, Applied Environmental Microbiology 57 (1991) 2804.

[10] S. Da Silva, R. Basséguy, A. Bergel, Electrochimica Acta 49 (2004) 4553.

[11] L. De Silva Munoz, A. Bergel, R. Basséguy, Corrosion Science 49 (2007) 3988.

[12] R. Cord-Rustwich, Microbially Influenced Corrosion of Steel, in D.R. Lovely (Eds.), Environmental Microbe-Metal Interactions, Ch. 7, ASM Press, Washington D.C., p. 159.

[13] R.A. King, J.D.A. Miller, Nature 233 (1971) 491.

[14] R.A. King, J.D.A. Miller, J. S. Smith, British Corrosion Journal 8 (1973) 137.

[15] B.S. Rajagopal, J. LeGall, Applied Microbiology and Biotechnology 31 (1989) 406.

[16] W.A. Hamilton and W. Lee. Biocorrosion, in: L.L. Barton (Eds.), Sulfate Reducing Bacteria, Plenum Press, New York, 1995, p. 243.

[17] I.B. Beech, C.W.S. Cheung, International Biodeterioration and Biodegradation 35 (1995) 59.

[18] T.E. Ford, J.S. Maki, R. Mitchell (1988). Involvement of bacteria exopolymers in biodeterioration of metal, in: D.R. Houghton, R.N. Smith, H.O.W. Eggins (Eds.), Biodeterioration, Vol. 7, Elsevier, London, 1998, p. 378.

[19] W.A. Hamilton, Biofouling 19 (1) (2003) 65.

[20] H. Castaneda, X.D. Benetton, Corrosion Science 50 (2008) 1169.

[21] H.A. Videla, L.K. Herrera, R.G. Edyvean, An updated overview of SRB influenced corrosion and protection of carbon steel, in: CORROSION 2005, Houston, USA, NACE International, 2005, Paper no. 05488.

[22] I.B. Beech, J. Sunner, Current Opinion in Biotechnology 15 (2004), 181.

[23] K. Alain, P. Pignet, M. Zbinden, M. Quillevere, F. Duchiron, J.P. Donval, F. Lesongeur, G. Raguenes, P. Crassous, J. Querellou and M.A. Cambon-Bonavita, International Journal of Systematic and Evolutionary Microbiology 52 (2002) 1621.

[24] O.A. Ramos Monroy, M.J. Hernández Gayosso, N. Ruiz Ordaz, G. Zavala Olivares, C. Juárez Ramírez, Materials and Corrosion 62 (9) (2011) 878.

[25] C. Cote, Ph.D. thesis: Biocorrosion of Carbon Steel in Water Injection Systems of the Oil and Gas Industry: "New Experimental Models from the Field", Université de Toulouse - MEGEP, Toulouse, 2013.

[26] G. Wranglen, Active sulfides and the pitting corrosion of carbon steels, in: R.W. Staehle (Eds.), International Conference on Localized Corrosion proceedings 1971, Williamsburg, U.S.A. 6-10 December, NACE International, 1971, p. 462.

[27] G. Wranglen, Corrosion Science 4 (1974), 331-349.

[28] R. Avci, B.H. Davis, M.L. Wolfenden, I.B. Beech, K. Lucas, D. Paul, Corr. Sci.,xxx (2013) xxx – xxx, article in press.

[29] B.J. Little, J.S. Lee, Microbiologically Influenced Corrosion, John Wiley and Sons Inc., New Jersey, 2007 .

[30] F. Mansfeld and B.J. Little, Corrosion Science 3 (2) (1991) 247.

[31] J.S. Lee, R.I. Ray, E.J. Lemieux, M.N. Tamburri, B.J. Little, Biofouling 20 (4/5) (2004) 237.

[32] W.P. Iverson, Journal Electrochemical Society 115 (1968) 617.

[33] W.P. Iverson G.J. Olson, L.E. Heverly, The role of phosphorus and hydrogen sulfide in the anaerobic corrosion of the iron and the possible detection of this corrosion by an electrochemical noise technique, in: S.C. Dexter (Eds.), Biologically Induced Corrosion, NACE International, Huston, 1986, p.154.

[34] F. Huet, N. Moros, R.P. Nogueir and B. Tribollet, Electrochemical noise analysis applied to SRB-induced corrosion of carbon steel, in : CORROSION 2002, Denver, USA, NACE International, 2002, paper.no. 02449.

[35] A. Padilla-Viveros, E. Garcia-Ochoa, D. Alazard, Electrochimica Acta 51 (2006),3841.

[36] V.V. Zinkevich, I.B. Beech, FEMS microbiology ecology, 34 (2000)147.

[37] M. Stern, A.L Geary, Journal of Electrochemical Society 104 (1957) 56.

[38] R.A. Cottis, S. Turgoose, Electrochemical Impedance and Noise, in: B. C. Syrett (Eds.), Corrosion Testing Made Easy Series, NACE International, Houston, 1999.

[39] X. Jiang, S. Nešić, Electrochemical Investigation of the Role of Cl^- on Localized CO2 Corrosion of Mild Steel, in: 17th International Corrosion Congress, Las Vegas, USA, NACE International, 2008, paper no. 2414.

[40] S. Pineau, R. Sabot, L. Quillet, M. Jeannin, C. Caplat, I. Dupont-Morral, P. Refait, Corrosion Science, 50 (2008) 1099.

[41] P. Refait, D. D. Nguyen, M. Jeannin, S. Sablé, M. Langumier, R. Sabot, Electrochimica Acta, 56 (2011) 6481.

[42] P. Refait, M. Jeannin, R. Sabot, H. Antony, S. Pineau, Corrosion Science 71 (2013) 32.

[43] C.O. Obuekwe, D.W.S. Westlake, J. A. Plambeck, Applied Microbiology and Biotechnology 26 (1987) 294.

[44] G.H. Booth, A.W. Cooper, P.M. Cooper, Chemistry and Industry 86 (1967) 2084.

[45] G.H. Booth, A.W. Cooper, P.M. Cooper, British Corrosion Journal 2 (1967) 109.

[46] P. Refait, M. Abdelmoula, J.-M.R. Génin, R. Sabot, C. R. Geoscience 338 (2006) 476.

[47] R. Galvan-Martinez, G. Garcia-Caloca, R. Duran-Romero, R. Torres-Sanchez, J. Mendoza-Flores and J. Genesca, Materials and Corrosion 10 (2005) 56.

[48] T. Nishimura, J. Dong, Journal of Power and Energy Systems 3 (2009) 23.

[49] P. Refait, J.A. Bourdoiseau, M. Jeannin, D.D. Nguyen, A. Romaine, R. Sabot, Electrochimica Acta 79 (2012) 210.

[50] H. Möller, E.T. Boshoff, H. Froneman, The Journal of The South African Institute of Mining and Metallurgy 106 (2006) 585

[51] K.R. Sreekumari, K. Nandakumar, Y. Kikuchi, Biofouling (17) (2001) 303.

IV.3. Article 3

<< Surface behavior of carbon steel in presence of sulfate-reducing bacteria: proliferation and mitigation with biocide treatment >>

In preparation

Surface behavior of carbon steel in presence of sulfate-reducing bacteria: proliferation and mitigation with biocide treatment

Marko Stipanicev[a,b] and Régine Basseguy[b]

[a]Det Norske Veritas, Johan Berentsens vei 109-111, 5163 Laksevåg, Bergen, Norway

[b]Laboratoire de Génie Chimique CNRS-INPT, 4 Allée Emile Monso, 31432, Toulouse, France

Abstract

In-situ electrochemical techniques were used to investigate effect of *Desulfovibrio* species and its metabolic products on carbon steel corrosion, as well as to explore capacity of biocide treatment to affect corrosion processes. Open Circuit Potential (OCP) measurements showed a 20-50 mV potential shift toward more positive values appearing just after bacterial inoculations, and on the opposite a stable OCP was observed in abiotic conditions. The OCP shifts could be attributed to a fine balance between biogenic sulfide, produced by bacteria, and ferrous component of steel surface. The analysis of Electrochemical Impedance Spectroscopy (EIS) data suggested different properties of formed surface layers depending on the nature of the environment, abiotic or biotic. Alteration of surface electric properties have been attributed to the complex deposits composed of Extracellular Polymeric Substance (EPS) embedding bacteria and/or biomineralization/corrosion products that synergistically transformed the electrochemical surface interface and increased steels' resistance to corrosion.
The effect of biocide treatment on bacterial activity and surface electrochemical events was studied by performing cell viability and EIS measurements in presence of two different concentrations of biocide. Level of *Desulfovibrio* species activity decreased with increased concentration of applied biocide, what together with raise of environment acidity, led to the transformation of surface layer fitted by a new electric interface model.

Keywords: Carbon Steel, Desulfovibrio, Biocide, Corrosion, EIS

1. Introduction

Presence of microorganisms in the closed environments made of carbon steel, such as Water Injection (WI) systems can cause undesired elevated corrosion. A significant part of the carbon steel deterioration can be attributed to alterations of micro-surface conditions (local pH cells, galvanic couples, concentration cells…) by sulfidogenic, e.g. hydrogen sulfide producing, microorganisms [Lee et al. 1995]. The most eminent group of sulfidogenic microorganisms are Sulfate-Reducing Bacteria (SRB) and they are regarded as the main culprits of anaerobic corrosion in aqueous environments [add some ref on SRB [Enning *et al*., 2012].

On steel surface, cohesive structures, known as biofilms composed of microorganisms and secreted Extracellular Polymeric Substance (EPS) may be established and may promote local modifications of physico-chemical conditions at the interface. Briefly, EPS is a jelly substance produced by bacteria and its function is to embed and cement cells on surface. Further, SRB proliferate using sulfur compounds such as sulfate, sulfite and sulfur itself as an electron acceptor what is resulting in sulfide production. Sulfide can chemically react with hydrogen protons what will result in hydrogen sulfide, capable affecting ferrous metals [Javaherdashti 2008; Szklarska-Smialowska, 1986]. Often, hydrogen sulfide affect metal surface directly and lead to elevated corrosion rates [Richardson *et al*., 2010]; however it may lead to the formation different iron sulfide compounds due to the reaction between dissolved iron and biogenic sulfide. This deposit may form a protective layer whose stability depends on a balance between ionic species [Videla *et al*., 2005]. Some distortions of system may induce the disruption of layer exposing again ferrous alloy to aggressive environment. When iron sulfide layer is cracked, the surrounding iron sulfide, conductive and very effective for hydrogen evolution, constitutes a cathode with a large surface compared to the small one of ferrous alloy exposed inside the crack. Usually, sulfidogenic species-mediated sulfide corrosion of ferrous alloys encompasses both, the production of hydrogen sulfide and deposit (or formation) of different iron sulfides [Costello, 1974].

Biofilms, enclosing bacteria and EPS, can have dual effect on corrosion of carbon steel: inhibit or promote. EPS is highly heterogeneous mixture of chemical compounds exhibiting corrosive properties

[Sand, 2012]. Besides, biofilms cover much larger surface area compared to cells; hence their corrosive nature can affect much larger area compared to a single cell. On the other hand, it is also reported that EPS may limit corrosion in particular saline environments and the inhibitory effect depends on the medium temperature, due to its influence on EPS surface adsorption [Dong *et al*., 2011]. Still, when attached to surface, some components of the EPS may prevent from cell adhesion or induce cell desorption [Neu, 1996] and keep material safe. Moreover, the presence of particular microorganisms inside the biofilm can also offer corrosion protection as in case of *Pseudomonas flava* [Gunasekaran *et al*., 2004].

In complex biofilm/minerals/metal surface interfaces it has to be considered overlapping of different corrosive or inhibitory mechanisms, involving direct influence of bacteria and EPS on steel surface as well as formation of biominerilzed Fe_xS_y and other corrosion products, rather than one specific mechanism [Hamilton, 2003].

Usually negative effects of bacterial activity are fought with different mitigation treatments. Often applied biocides vary from oxidizing ones such as chlorine, chlorine-dioxide or bromine to compounds such as quaternary phosphonium salts, aldehydes or different amine-type compounds [Carrera and Gabetta, 1995]. Broadly used glutaraldehyde-based biocides are active over a broad range of temperatures and pH values making them multifunctional and desirable mitigation tool. The functional group of glutaraldehyde reacts with basic constituents of proteins (e.g. groups such as –OH, $–NH_2$, –COOH, and, –SH) present in cell membranes, cell walls and in cytoplasm [Videla, 2002] and quickly leads to cell death.

To get better insight into the microbially influenced carbon steel corrosion as well as into the complexity of interactions between bacteria, their metabolites and carbon steel surface, a multidisciplinary approach should be considered. Currently, electrochemical techniques such as Open circuit potential (OCP), Linear Polarization Resistance (LPR) and Electrochemical Impedance Spectroscopy (EIS) are widely employed for investigating surface events in the presence of the bacteria and biofilms [Little and Lee, 2007; Little *et al*., 1991]. Scanning Electron Microscopy (SEM) and Energy-dispersive X-ray (EDX) spectroscopy usually were used to investigate biomineralization products and processes governed by bacteria.

The objective of this study is to investigate the impact of sulfidogenic bacteria and their metabolites on the corrosion behavior of construction carbon steel as well as the effect of biocide treatment on surface electrochemical events in environments loaded with these sulfidogenic bacteria. The SRB strains used in this study was *Desulfovibrio alaskensis* (AL1), previously retrieved from oil reservoir and detected in offshore WI system consortium. The investigation reported herein was centered on information acquired by non-destructive electrochemical techniques.

2. Materials and methods

2.1. The electrochemical bioreactor

The electrochemical bioreactor was modified Schott™ flask of 1000 mL (Fig. 1A) whose mouth was threaded to fit a lid that warrants a controlled atmosphere inside the vessel. Moreover, the reactor lid had four openings with caps and fittings used for different purposes: purging system (gas diffuser); introduction of the 3 electrodes (working WE, reference RE and counter CE); a serum vial cap was also used to facilitate the access of needles from this opening. All elements of bioreactor (glassware, lids, fittings, tubing, filters, etc.) were autoclaved at 121ºC for 20 minutes at 20 psi pressure and dried prior to assembling. Using aseptic microbiological techniques, all bioreactors were prepared with 800 mL of autoclaved electrolyte.

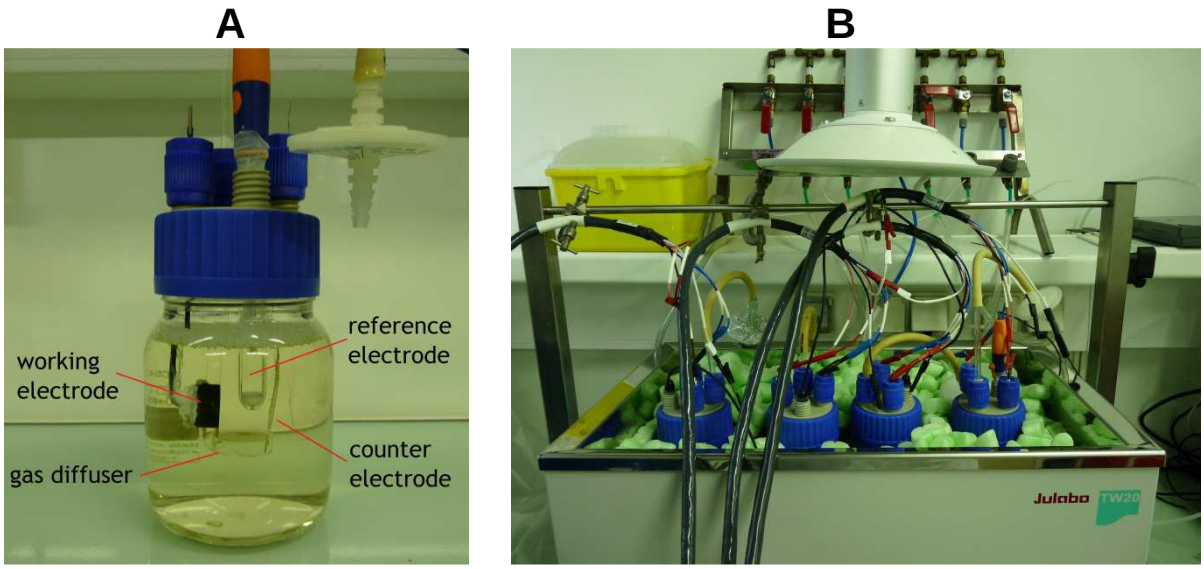

Fig. 1. Experimental set-up: A) Bioreactor; B) Multiple-experiments run.

2.2 Media and bacteria

Modified VMNI sulfate culture medium [Zinkevich and Beech, 2000] served as growth medium for bacteria culturing and as the experimental electrolyte. Modified VMNI was composed of (gL^{-1} distilled water): NaCl, 20.0; NH_4Cl, 1.0; $CaCl_2 \times 2H_2O$, 0.04; Na_2SO_4, 4.5; $MgSO_4 \times 7H_2O$, 0.06; $FeSO_4 \times 7H_2O$, 0.004; sodium lactate, 6.0; KH_2PO_4, 0.5; sodium citrate, 0.3; casamino acids, 2.0; tryptone, 2.0; modified Wolfe's mineral elixir (0.1% v/v) and vitamin solution (0.2% v/v). The vitamin solution was composed of (gL^{-1} distilled water): riboflavin, 0.1; nicotinic acid, 0.25; thiamine, 0.3; pentatonic acid, 0.3; pyridoxine, 0.3; cyanocobalamin, 0.025; ascorbic acid, 1; biotin, 0.005. The composition of the modified Wolfe's Elixir was (g L^{-1} distilled water): Nitrilotriacetic acid, 1,5; $MgSO_4 \times 7H_2O$, 0.06; $MnSO_4 \times H_2O$, 0.5; NaCl, 1; $FeSO_4 \times 7H_2O$, 0.1; $CoSO_4 \times 7H_2O$, 0.1; $NiCl_2 \times 6H_2O$, 0.1; $CuCl_2 \times 2H_2O$, 0.1; $ZnSO_4 \times 7H_2O$, 0.1; $CuSO_4 \times 5H_2O$, 0.01; $AlK(SO_4)_2 \times 12H_2O$, 0.01; H_3BO_3, 0.01; $Na_2MoO_4 \times 2H_2O$, 0.01; $Na_2SeO_3 \times 5H_2O$, 0.001. The pH of the VMNI media was adjusted to ~ 7.4 to give slightly alkaline conditions suitable for bacterial growth.

The bioreactors were degassed for one hour with nitrogen flow to establish an anaerobic environment before WE immersion. Moreover, low flow rate was maintained during whole test duration.

Desulfovibrio alaskensis AL1 (NCIMB 13491T= 16109T) [Beech and Cheung, 1995], used in here in presented work, was initially recovered in 1991 from a soured oil reservoir in Purdu Bay, Alaska. *Desulfovibrio alaskensis* AL1 is grown in VMNI media, and when reached viable cell density of 10^8 cells mL^{-1} was used an inoculum for bioreactors. Each bioreactor was inoculated with 1/10 (v/v) % of *Desulfovibrio alaskensis* AL1 culture. Bacteria consortium monitoring during their preparation for inoculation as well as in bioreactors was conducted by measuring cell density. Measurements were performed by Helber Bacteria Cell Thoma counting chamber (Hawksley, UK) with precondition that only viable cell are counted.

2.3 Electrodes

The WE with shape of circular discs with 2 cm diameter and exposed area of 3.14 cm^2 were used for studying corrosion behavior of steel. The steel specimens were manufactured from S235JR carbon (Descoure and Cabaud, France). The S235JR carbon steel used is composed of the following elements with mass ratio of 0.17% C, 1.4% Mn, 0.045% Cu, 0.03% S, and 0.03% P. Surfaces of all exposed steel specimens were prepared by manual grinding using increasing series of fine SiC papers, ending with 600-grit. Grinding debris was rinsed from the surface with sterile deionized water. The Saturated Calomel Electrode (SCE) (Gamry, USA; Bio-logic, France) served as reference electrode and platinum mesh was used as counter electrode. WE as well as CE and RE were exposed to ethanol (70 % v/v) (VWR, USA) for 10 minutes prior to immersion.

2.4 Electrochemical methods

The Open Circuit Potential (OCP), Linear Polarization Resistance (LPR) and Electrochemical Impedance Spectroscopy (EIS) measurements were carried out using a VMP multichannel potentiostat (Bio-Logic, France) connected to a PC interface and monitored with EC-Lab V10.32 software (Bio-Logic, France). Measurements were carried during 168 h in stagnant conditions (static working electrode and solution). Standard three electrode-arrangements included Working Electrode (WE), Counter Electrode (CE) and Saturated Calomel Electrode (SCE).

The OCP of working electrodes (circular disc) versus SCE were recorded every 600 seconds (0.167 h) during whole duration of the tests.

The LPR technique was employed to estimate the resistance to corrosion of steel coupons. The polarization resistance (R_p) of the steel/ electrolyte interface is measured in the vicinity of the OCP [Stern, 1958]. R_p is defined as the slope of the polarization curve tangent at the OCP and given in ohms (Ω cm^{-2}). To determine of R_p, the potential was scanned in the range of OCP ± 10 mV with a sweep rate of 0.167 mV s^{-1}. Polarization scans were performed every 24 h during whole duration the tests.

EIS diagrams were plotted at OCP that was measured continuously during whole test duration, in a frequency domain ranging from 10 kHz to 1 or 10 mHz with 7 points per decade, and amplitude of 10 mV peak-to-peak. EIS measurements were performed every 24 h during whole duration the tests.

All measurements were duplicated/ triplicated. Still, to keep clarity of data presentation, one representative set of data for each test system is reported.

2.5 Surface analysis

After each bioreactor decommissioning, the topography of steel WE specimens was examined and characterized using a table Scanning Electron Microscope (SEM) TM3000 (Hitachi, Japan) interfaced with Energy Dispersive X-ray spectroscopy (EDX) system (Oxford Instruments, USA).

After removal from bioreactors, steel specimens were placed in desiccator that was flushed with nitrogen for 30 minutes. Dried samples were mounted on an aluminum stub using adhesive carbon tape and analyzed with Table SEM/EDX system.

After SEM/EDX examination, steel specimens were cleaned from corrosion products by immersion in a 5 (v/w) % hexamine (Merck, Germany) plus concentrated HCl (VWR, USA) solution for 30 seconds. Rinsing with deionized water, gentle blotting with a paper towel and overnight storage in a desiccator immediately followed cleaning with hexamine solution. Further, the topography of all cleaned steel specimens was characterized using SEM/EDX system.

3. Results and Discussion

3.1. Impact of bacteria and their metabolites on steel surface

To study the impact of bacteria on the corrosion behavior of carbon steel and to separate the effects due to the cells attached to the surface from those due to their metabolites, two series of biotic experiments were performed using the following conditions:

- Biotic - modified VMNI media inoculated with 10 % (v/v) of *Desufovibrio* culture (10^8 cell mL^{-1});
- Biotic + 6kDa membrane - modified VMNI media inoculated with 10 % (v/v) of *Desufovibrio* culture (10^8 cell mL^{-1}) while keeping WE protected within a 6-8 kDa dialysis membrane (Spectrum Laboratories, Inc., USA) priory filled with sterile modified VMNI media.

The corrosion behaviors in biotic conditions were compared to control Abiotic systems in which modified VMNI media additionally was pretreated with 100 mg L^{-1} of chloramphenicol, an antibiotic in order to maintain sterility in such a rich medium.

Diagrams, shown in Fig.2, present OCP behavior during the 168-hour immersion of two steel specimens exposed to abiotic and biotic conditions. The OCP of steel in abiotic system was stable, around -695 mV/SCE, while the presence of bacteria and their metabolic products initiated OCP shift towards more positive values, entitled as ennoblement; this phenomenon was often associated with SRBs abundance that may lead to localized corrosion attacks [Little and Lee, 2007]. Interestingly, the OCP shift was here a temporary event, even though bacteria were allowed to colonize steel surface what, in other studies, led to a permanent ennoblement [Miranda et al. 2006; Castaneda and Benetton, 2008; AlAbbas et a. 2013]. The concentration of biogenic S^{2-} in the system is certainly a key parameter, the shift of OCP could be associated with the H_2S removal during the constant N_2 bubbling used to purge the system from oxygen; when high purging rate was applied in batch environment loaded with SRBs, the ennoblement was not recorded while lower purging rate was followed by a +100 mV/OCP potential shift [Dall'Agnol, 2013]. The authors suggested that the ennoblement could be attributed to concentration of biogenic sulfide in bulk electrolyte and its interaction with steel surface. In correlation to this, the concentration of sulfide in electrolyte affects the formation of iron sulfide crystals' type at the steel surface, which has significant impact on the corrosion process [Ma *et al.*, 2000]. In our case, cell density is lowered with a reference to other studies [Dall'Agnol, 2103], what suggests lowered sulfide production and coupled with the N_2 flow rate could led to a lack of permanent ennoblement due to insufficient amount of sulfide ions in bulk media to form stable iron sulfide.

In order to go further in the distinction between the influence of bacteria attachment and the influence of the metabolites alone, carbon steel specimens were introduced in a dialysis membrane tube (6-8 kDa cut-off) that protected the surface from bacteria and complex hydrocarbon molecules attachment and exposed the surface solely to SRBs ionic metabolic products. As shown in Fig. 3, system exhibited a permanent ennoblement when there is no bacteria contact supporting idea that other factors besides bacterial surface colonization could be responsible for this phenomenon.

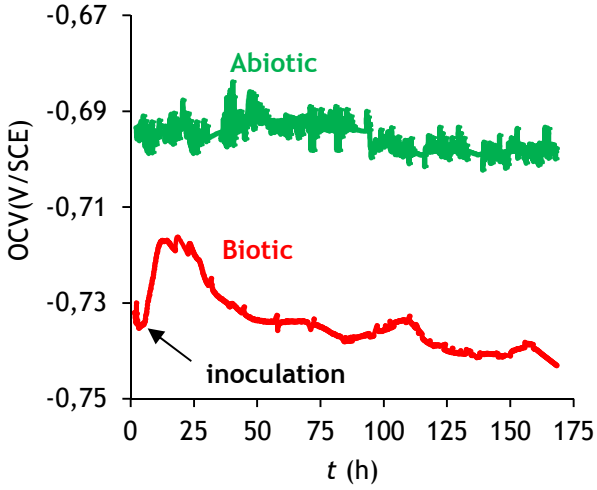

Fig. 2. OCP (V/SCE) during 168 h of tests: Abiotic (green) and Biotic – inoculated at *t*= 4 h (red).

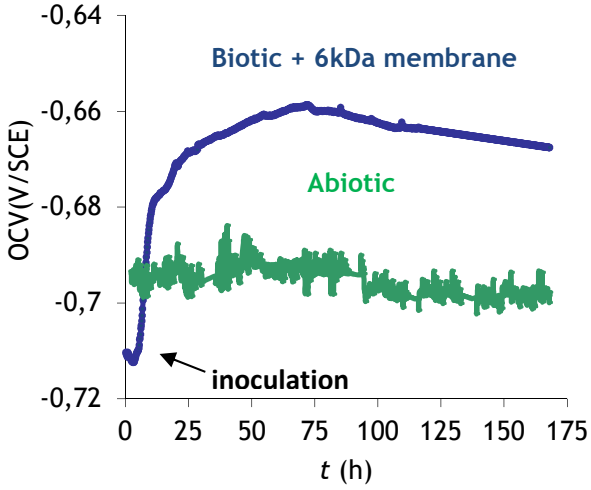

Fig. 3. OCP(V/SCE) during 168 h of tests: Abiotic (green) and Biotic + 6kDa membrane - steel pecimen inside a 6-8 kDa membrane tube – inoculated at *t*= 4 h (blue).

During the immersion test, LPR was performed every 24 h and R_p were calculated (Fig. 4): R_p values were higher when bacteria were able to colonize steel surface compared to abiotic environment. These data suggest that the presence of bacteria inhibits corrosion processes, what can be confirmed by the surface analysis performed at the end of the test (Fig.5 and Tab. 1).

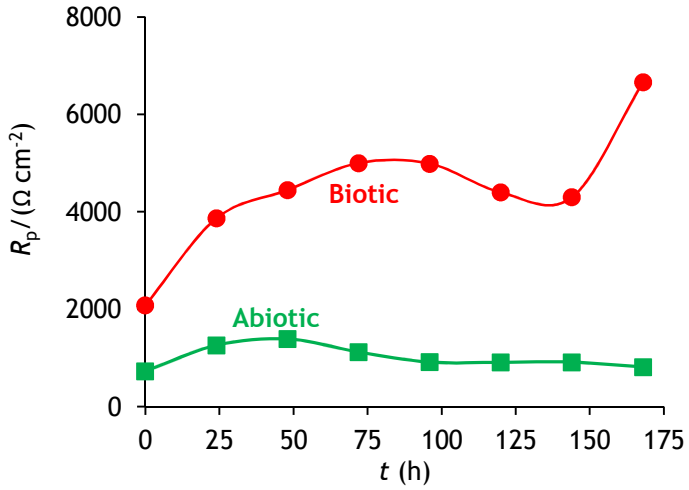

Fig. 4. R_p (Ω cm^{-2}) during 168 of tests: Abiotic (green); Biotic (red).

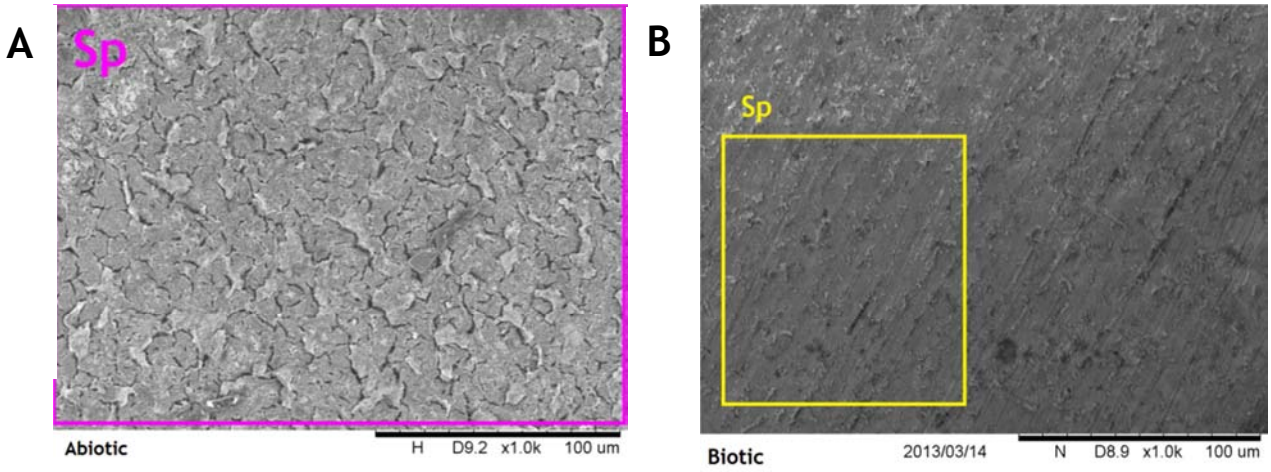

Fig. 5. SEM micrographs of steel surface (1000x) with emphasized areas submitted to EDX analysis: A) after 168 h of immersion in VMNI medium; B) after 168 h of immersion in VMNI medium inculated with Desulfovibrio culture.

Tab. 1. EDX analysis (wt %) displaying main elements (sodium and chlor not presented) found in emphasized area in Fig. 5; A) after 168 h of immersion in VMNI medium; B) after 168 h of immersion in VMNI medium inoculated with Desulfovibrio culture.

Tab. A						
	Ca	P	O	S	K	Fe
Sp	0.9	1.0	28.7	5.6	0.7	30.1

Tab. B						
	O	P	C	O	S	Fe
Sp	42.1	3.4	11.4	42.1	4.1	21.7

Fig. 5A and Tab. 1A show SEM/EDX analysis for steel exposed in abiotic conditions over 168 h immersions. Corrosion deposits morphology resembles homogenous; however, it is possible to observe fracture lines all across surface. Observed surface layer is composed of mineral formation in which iron is the predominant species but also some potassium-base, phosphorus and sulfur-base compounds along with sodium chloride were identified at steel surface. This structure is mostly influenced with chemical composition of electrolyte, rich in sulfate, potassium, phosphate and chloride compounds. Fig. 2B and Tab. 1B display results of SEM/EDX analysis for steel immersed in biotic conditions over 168 h. The surface is less attacked than that found in abiotic system. It seems that the higher accumulation of organic and inorganic deposits occurs in particular areas defined by geometrical straight lines resembling on grinding line. This would be to expect knowing that those

areas are exhibiting higher energies compared to rest of surface (effect similar to grain boundaries or impurities) and due to that are attractive to microorganisms [Sreekumari *et al*. 2001]. However chemical analysis showed the same elementary composition on both surfaces, with exception for carbon, detected only for biotic system. Carbon found in large amount in biotic system suggests formation of iron carbonates as well as possible adsorption of organic matter such as EPS on steel surface. Moreover, in abiotic system, the origin of sulfur is most likely in sulfate component of electrolyte while in biotic system it possesses a biogenic nature, e.g. bacteria produce S^{2-} that react with Fe ions forming Fe_xS_y on steel surface. Observed limited corrosion in biotic environment is previously recorded phenomenon [Nagiub and Mansfeld, 2001; Videla and Herrera, 2009]. Bacteria can protect steel surfaces by forming thin and stable iron-sulfide layer on steel surface when suitable conditions are present, e.g. fine balance between dissolved iron and sulfide [Videla *et al*., 2005]. Moreover, due to its inhibitory capabilities, EPS could also contribute to this result [Dong *et al*., 2011]. Moreover, biofilm can function as a physical barrier for the transfer of aggressive ionic species (for example: chloride ions, thiosulfate ions…) from bulk electrolyte to steel surface and therefore inhibit corrosion. In summary, observed development of events is attributed to the formation of a mixed organic/inorganic layer on the steel surface, which isolates the surface from the environment and shield it physically form aggressive species

Figure 6 gathers the different representations of impedance spectra acquired for abiotic system during the 168-hour immersion test.

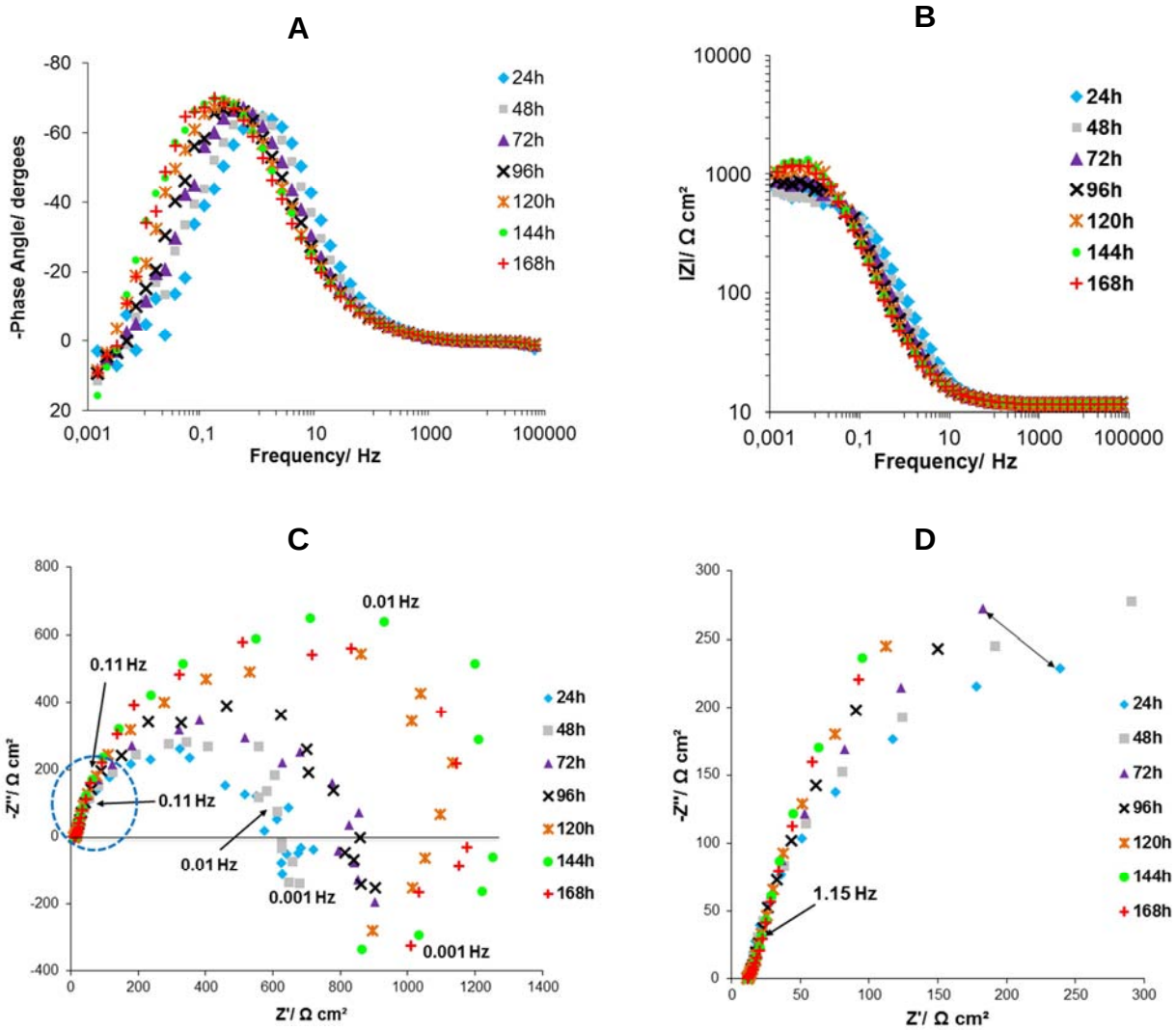

Fig. 6. Impedance spectra of carbon steel S235JR acquired for abiotic system during 168 hours. Data acquired in 1 mHz -100 kHz frequency range. (A) Bode plot - phase angle vs. frequency; (B) Bode plot - impedance modulus as function of Frequency; (C) Nyquist plot; (D) Zoom-up Nyquist diagram of highlighted zone by a dashed blue circle.

All along the immersion, Nyquist representation for impedance data (Fig. 6C) reveal the presence of one depressed semi-circle in High Frequency (HF) domain (zoom-up in Fig. 6D) and a high amount of perturbations in the Low Frequency (LF) domain. Even thought signals are noisy, curves are exibiting negative values in LF domain, suggesting an inductive phenomenon, certainly linked to adorption events [Carvalho *et al.*, 2005]. It is possible to notice slight increase for the diameter of high frequency (HF) depressed semicircles (Fig. 6D). This is in agreement with modulus plots (Fig. 6B) showing increase of the impedance at LF with immersion time. Moreover, in order to evaluate and support visual observation for depressed semi-circle in HF domain, alpha (α) values, defining constant phase elements behavior are calculated and presented in Tab. 2.

Tab. 2. Evolution in time for experimental data of R_s, R, α, Q and C for the abiotic system in presence of a carbon steel working electrode. Data are produced taking into consideration depressed semi-circles only in HF domain.

Time (h)	R_s (Ω cm^2)	R (Ω cm^2)	α	Q (Ω^{-1}cm^{-2}s$^{\alpha}$)	C (μF cm^{-2})
24	12	535	0.86	0.7×10^{-3}	160
48	12	667	0.87	2.2×10^{-3}	603
72	12	853	0.86	4.1×10^{-3}	1120
96	12	1026	0.85	4.8×10^{-3}	1209
120	12	1324	0.84	5.2×10^{-3}	1191
144	12	1487	0.83	5.3×10^{-3}	1091
168	12	1952	0.83	5.7×10^{-3}	1190

It is found that they all were lower than 1 confirming a Constant Phase Element (CPE) behavior, i.e. the system exposed a heterogeneous distribution of time constants. Tab. 2 also gives the values of Q, another parameter of the CPE impedance determinated by fitting. The capacitance values, associated to the parameter Q, were calculated applying the equation derived by Brug *et al.* [Brug *et al.,* 1984] after assuming that the distribution of time constants was all along the surface:

$$C = Q^{1/\alpha} (R_s^{-1} + R^{-1})^{(\alpha-1)/\alpha} \qquad \text{(Eq. I)}$$

Interestingly, calculated C values (Tab.2) are not within range characteristic for double layer capacitance (10 μF cm^{-2} < C_{dl} < 100 μF cm^{-2}) [Orazem and Tribollet, 2008], proving that the phenomenon was not linked to the charge transfer. The resistance R, associated to this CPE behavior, was not a charge transfer resistance but can be attributed to the protective layer formed at the electrode surface. This resistance rises with time meaning experiencing lower corrosion and suggesting the formation of a protective layer. A layer, composed of corrosion products, presumably oxides, along with other compounds precipitated from the nutrient-rich electrolyte, possesses a certain protective character. Hence, based on the acquired electrochemical, microscopical and chemical information, it is possible to propose dominant process affecting architecture of the formed protective layer in abiotic system. This process encompasses anodic dissolution of iron (1), water dissociation (2) and results in formation of protective iron hydroxide (3):

$$Fe^0 \rightarrow Fe^{2+} + 2e^- \qquad (1)$$

$$2H_2O + 2e^- \rightarrow H_2 + 2OH^- \qquad (2)$$

$$Fe^{2+} + 2OH^- \rightarrow Fe(OH)_2 \qquad (3)$$

Fig. 7 shows the impedance response for carbon steel exposed to biotic electrolyte and its evolution with time. In the Nyquist representation, the impedance spectrum reveals different shape of plots compared to the abiotic system. The depressed semi-circle observed at HF was followed by a straight line (angle= 45°) in LF domain that may be associat ed to a diffusion process linked to the bacterial surface colonization as well as the formation of iron sulfides. The presence of these two phenomena with different time constants was clearly shown in the phase angle diagrams which exhibited a mamimum at HF and a minimum at LF.

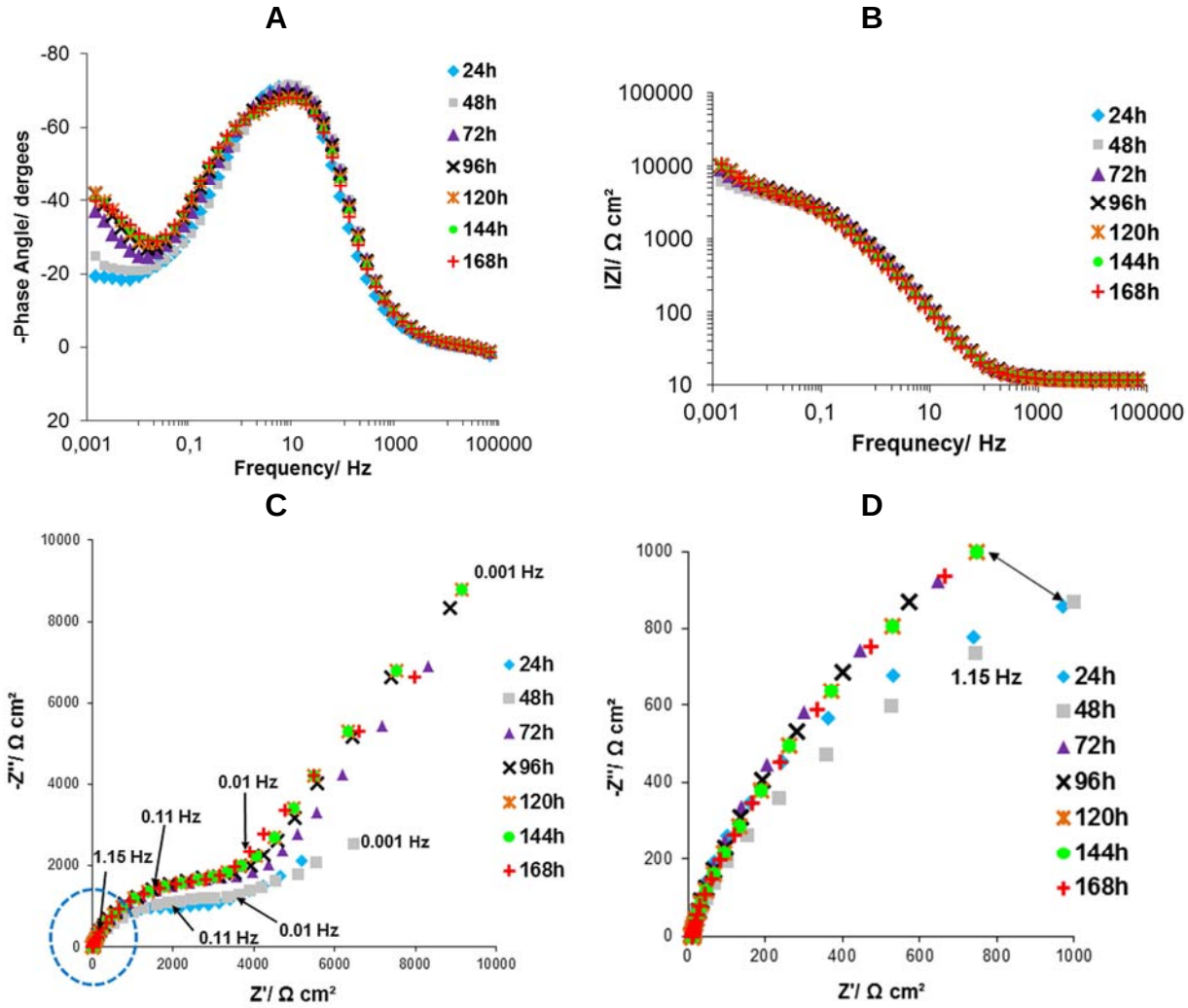

Fig. 7. Impedance spectra of carbon steel S235JR acquired for biotic system during 168 hours. Data acquired in 1 mHz -100 kHz frequency range. (A) Bode plot - phase angle vs. frequency; (B) Bode plot - modulus of the impedance as function of frequency; (C) Nyquist plot; (D) Zoom-up Nyquist diagram of highlighted zone by a dashed blue circle.

Acquired data, EIS and SEM/EDS, were used to design circuit model capable to explain behavior of steel exposed to biotic environment.

In HF domain, the depressed semi-circles can be fitted by a CPE (CPE defined by Q and α) in parallel with a resistance R (diameter of the circle). This behavior is confirmed by obtained α values, all lower than 1 (Tab. 3). Furthermore, according to Brug *et al.* [Brug *et al.,* 1984] calculated C values (Tab. 3) are within the range 10 μFcm^{-2} < C_{dl} < 100 μFcm^{-2}), characteristic for double layer capacitance [Orazem and Tribollet, 2008] suggesting that R was a charge transfer resistance (R_{ct}). As observed for the curves presented in Fig. 7D, biotic system exhibits an increase in diameter for the depressed semi-circle after 48 hours of immersion and then the system remains stable until this end of the experiment. This behaviour indicates an evolution of the system in presence of bacteria, suggesting a necessary time for surface colonization and biofilm development. These visual observations are supported with numerial values being presented in Tab. 3. They show significant increase in resistance ($\Delta R = \Delta R_{ct}$ ~ 600 to 700 Ω cm^2) when the biofilm was grown, indicating a decrease of corrosion rate and confirming the results of LPR.

Tab. 3. Evolution in time of R_s, R, α, Q, C, σ and $|Z_w|$ values for the carbon steel working electrode in the biotic system. Warburg impedance is calculated for f= 0.01 Hz.

Time(h)	R_s (Ω)	R (Ω cm^2)	Q (Ω^{-1}cm^{-2}s$^{\alpha}$)	α	C (μF cm^{-2})	σ (Ω$^{-1/2}$)	$\|Z_W\|$ (Ω cm^2)
24	11	1900	0.23×10^{-3}	0.88	53	258	4487
96	12	2664	0.27×10^{-3}	0.85	41	180	10118
168	12	2420	0.33×10^{-3}	0.85	52	186	10455

At LF, the straight line with a 45° angle can be fitted by a Warburg element that describes diffusion through the formed corrosion product/biofilm structure. Impact of Warburg on electrochemical process is usually described as Warburg impedance (Z_w) defined by Warburg coefficient (σ) and frequency (ω=2πf) and herein calculated according to:

$$|Z_W| = (2^{1/2}\ \sigma)\ \omega^{-1/2} \qquad \text{(Eq. II)}$$

Values of Warburg parameters are given in Tab.3, the Warburg impedance increased ($\Delta|Z_w|$~ 5500 Ω cm^2 at f= 0.01Hz) when compared the data obtained for 24h and 48 h of experiment and those obtained after 48h measurements. This again suggests a stable behavior from 72 h until 168 h of experiment when the biofilm is well established.

Globally the circuit expressed by Eq. III can model the interface in biotic system:

$$R_s + \text{CPE}/(R_{ct} + \text{W}) \qquad \text{(Eq. III)}$$

where R_s is the resistance of the electrolyte;

$CH_3CH(OH)COOH + SO_4^{2-} \rightarrow CH(OH)(HCO_3)_2^- + H_2S$ (1: anaerobic respiration)

$Fe^o \rightarrow Fe^{2+} + 2^{e-}$ (2: anodic dissolution of iron)

$Fe^{2+} + S^{2-} \rightarrow FeS$ (3: formation of biogenic iron sulfide)

Furthermore, biological components themselves are contributing to protective capabilities of this formed layer.

3.2. Impact of biocide treatment on the bacterial population and steel surface

To study the impact of bacteria countermeasure on the corrosion behavior of carbon steel and to assess the effect of biocide treatment dosage on cells viability and carbon steel behavior, two series of biotic experiments were performed using the following conditions:

• Biotic 1 - modified VMNI media inoculated with 10 (v/v) % of *Desufovibrio* culture (10^8 cell m mL^{-1}) at t= 4 hand treated with 500 ppm of glutaraldehyde-based biocide at t= 96 h;

• Biotic 2 - modified VMNI media inoculated with 10 (v/v) % of *Desufovibrio* culture (10^8 cell mL^{-1}) at t= 4 h and treated with 1500 ppm of glutaraldehyde-based biocide at t= 96 h.

The corrosion behaviors in biotic conditions treated with biocide were compared to abiotic systems (Control) in which modified VMNI media was additionally pretreated with 1500 ppm of glutaraldehyde based biocide in order to maintain sterility in such a rich medium. The pH of the control medium was 6.1 due to the acidity of added biocide

Diagrams in Fig. 8 and 9 show OCP behavior and R_p evolution in time of steel electrode in the three systems.

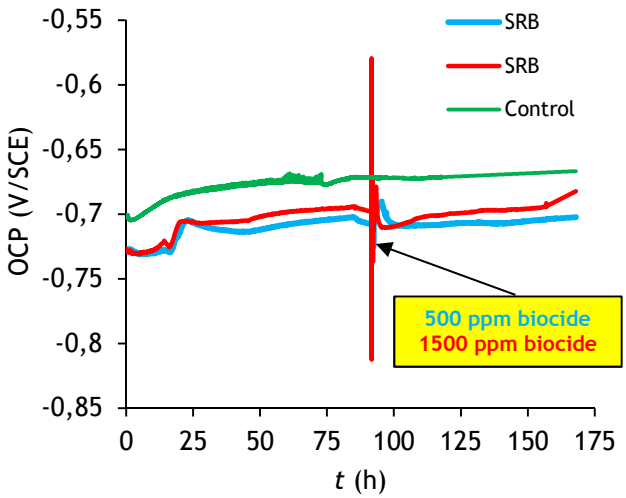

Fig. 8. OCP (V/ SCE) during 168 h of tests: Control abiotic (green); Biotic 1 - biotic treated with biocide (500 ppm) at t= 96h (blue); Biotic 2 – biotic treated with biocide (1500 ppm) at *t*= 96h (red).

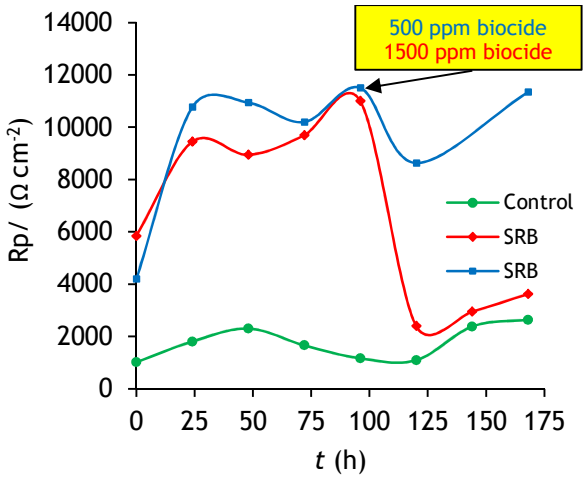

Fig. 9. R_p (Ω cm^{-2}) during 168 h of tests: Control abiotic (green); Biotic 1 - biotic treated with biocide (500 ppm) at t= 96h (blue); Biotic 2 – biotic treated with biocide (1500 ppm) at *t*= 96h (red).

Behavior of steel in abiotic slightly acidic conditions is stable (OCP ~ -690 ± 10 mV/SCE). On the other hand, bacteria inoculations cause low OCP shifts towards more positive values. As previously mentioned, this polarization in positive direction could be the consequence of bacterial metabolic activity and/or bacterial surface colonization. Even though these shifts indicate a permanent ennoblement, they are very low within range of +30 mV/OCP, and most probably not affecting steel integrity. Moreover, both biotic systems experienced significant perturbation when submitted to biocide treatments. Acidity of biocide leads to temporary erratic behavior of OCP signals in both systems (pH change due to biocide treatment: ΔpH_{500} ~ -0.3 and ΔpH_{1500} ~ -1.3). OCP distortion was stronger in the system treated with the higher concentration of biocide (± 100 mV/OCP). However, the biocide influence on OCP had a short life, and soon after OCP in both systems stabilized around -720 ± 10 mV/SCE, where it remained until the tests termination. R_p, data presented in Fig. 9, suggest inhibitory effect of bacteria for corrosion process as previously observed (Fig. 4). Soon after bioreactors inoculations, R_p increased and maintained stable until biocide treatments (~ 11 MΩ cm^{-2}). Stronger biocide treatment (1500 ppm) resulted in significant R_p decrease (ΔR_p~ 9 MΩ cm^{-2}), and then the low value of R_p was found until bioreactor decommissioning. Observation suggests that treatment leads to disintegration of surface layer resulting in breakdown of the protective layer formed on steel surfaces in Desufovibrio presence. It can also be noted that measured post-treatment R_p values (~ 2 MΩ cm^{-2}) are identical to the ones measured in control abiotic system that was treated with 1500 ppm biocide prior to test start. Thus, the acidity of biocide by itself when applied in high concentrations lead to acidification of the electrolytes (ΔpH is -1.5 to 2 units), which may lead to elevated corrosion rates. Moreover the significant decrease of the bacterial population (Tab. 4) may explain the fact that the protective layer cannot be formed again after the breakdown. The 500 ppm biocide treatment perturbed system; however, applied biocide concentration was not sufficient to breach the protective layer and the bacteria amount was still enough to maintain this layer.

Tab. 4. Cell densities (cell mL^{-1}) before biocide treatment and 24 h after biocide treatment.

	Cell density before biocide	Cell density after biocide
500 ppm treatment	2.3×10^7	2.1×10^7
1500 ppm treatment	9.1×10^7	2.5×10^7

Fig. 10A and Tab. 5A show SEM/EDX analysis for the corrosion deposits formation on carbon steel exposed in abiotic conditions after 168 h of immersion. The morphology and chemical footprint of the corrosion deposits is mostly influenced by the chemical composition of VMNI growth medium, rich in sulfate, potassium, phosphate and chloride compounds, as well as by the organic component of biocide (50% glutaraldehyde). Fig. 10B and C and Tab. 5B and C show result of SEM/EDX analysis for the corrosion deposits/organic matter formation on carbon steel when exposed to biotic conditions and then treated with 500 ppm and 1500 ppm of biocide. Formed structures resemble to each other as it is expected for steel surface exposed to similar sulfidogenic environments; corrosion product mostly composed of iron based minerals: carbonates, oxides and sulfides.

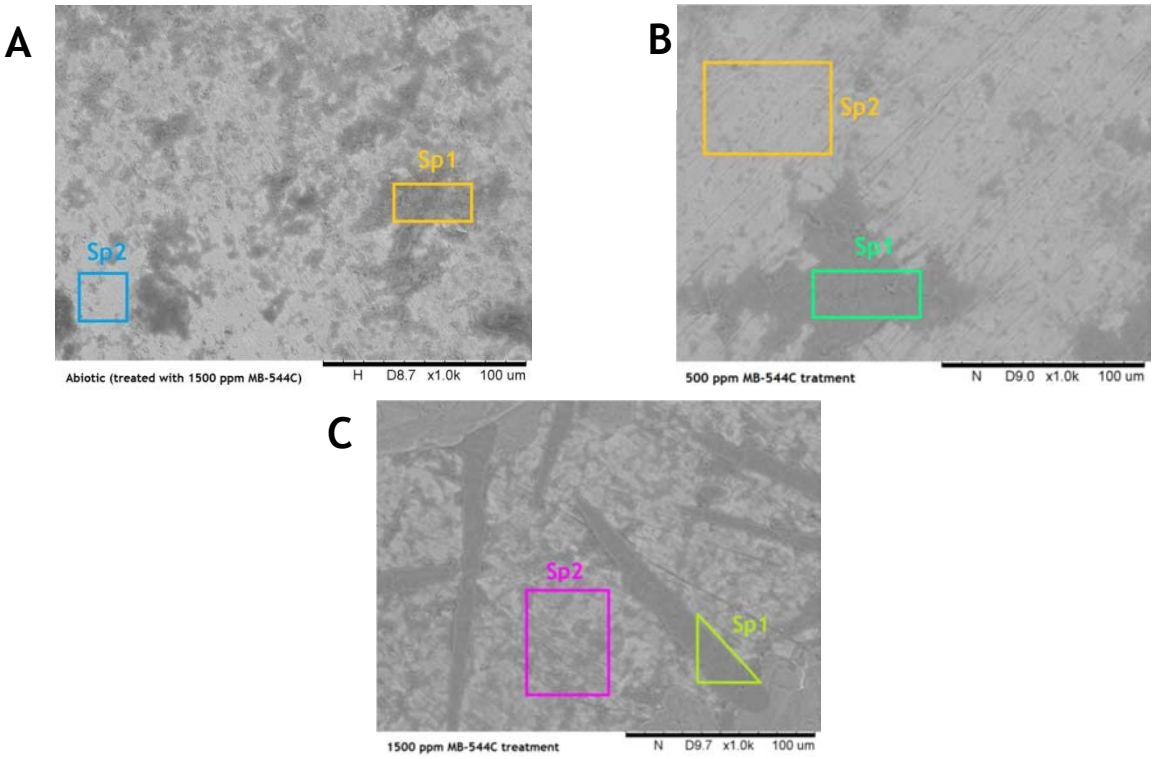

Fig. 10. SEM micrographs of steel surface (1000x) with emphasized regions submitted to EDX analysis: A) Control (abiotic and pretreated with 1500 ppm biocide); B) Biotic 1: biotic system treated with biocide (500 ppm) at *t*= 96h; C) Biotic 2: biotic system treated with biocide (1500 ppm) at *t*= 96.

Tab. 5. EDX analysis (wt %) displaying main elements (sodium and chloride not presented but present) found in emphasized regions demonstrated in Fig. 10; A) Control (abiotic and pretreated with 1500 ppm of biocide); B) Biotic 1: biotic system treated with biocide (500 ppm) at *t*= 96h; C) Biotic 2: biotic system treated with biocide (1500 ppm) at *t*= 96.

Tab. A					
	C	O	S	Ca	Fe
Sp1	27.1	31.4	0.9	1.1	38.5
Sp2	9.8	11.3	1.1	/	77.4

Tab. B				
	C	O	S	Fe
Sp1	/	11.2	/	9.5
Sp2	6.7	14.9	1.6	69.6

Tab. C				
	C	O	S	Fe
Sp1	3.7	40.0	15.4	14.9
Sp2	0.9	22.7	/	66.1

Fig. 11 shows the impedance response for carbon steel exposed to VMNI inoculated with *Desufovibrio* culture and treated treated with 500 ppm of biocide at t= 96h and its evolution with time.

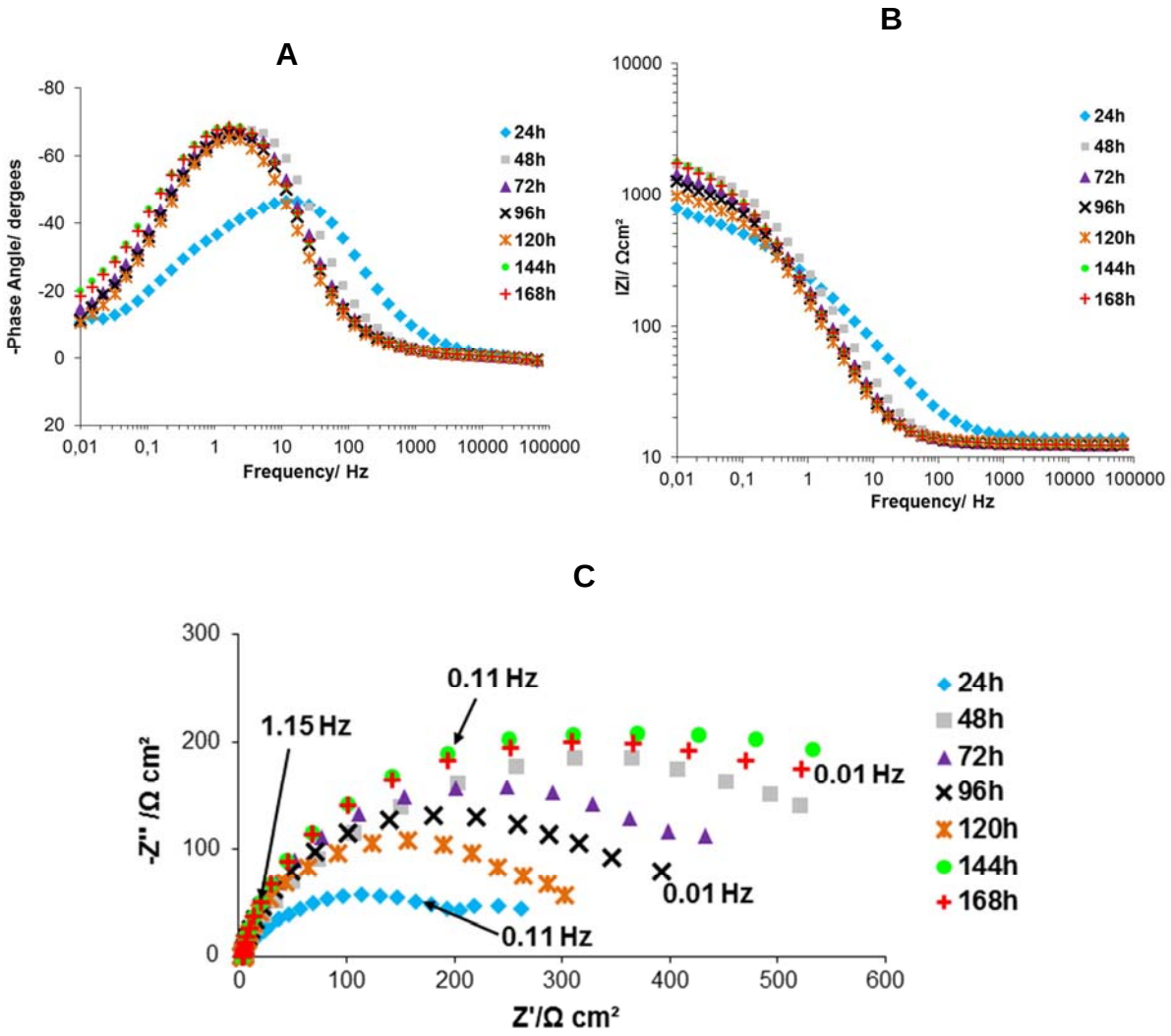

Fig. 11. Impedance spectra of carbon steel S235JR acquired for control (abiotic pretreated with 1500 ppm of biocide) during the 168-hour test. Data acquired in 10 mHz - 100 kHz frequency range. (A) Bode plot - phase angle vs. frequency; (B) Bode plot - impedance modulus as function of frequency; (C) Nyquist plot.

Nyquist representation for impedance data (Fig. 11C) reveals, all along the different times, the presence of one depressed semicircle with fluctuating diameter followed by a second not well-identified signal at LF. Curves in phase angle plots (Fig. 11A) exibit only one visible maximum suggesting one time constant for control system during the whole duration of experiments;however it must be noted that the LF limit was 10 mHz, higher than for the previous experiments (1 mHz), so it was not possible to observe the LF phenomenons but they may exist.Concerning the HF phenomenon, it is possible to notice a first increase in diameter for depressed semi-circles obtained at 24 h and 48 h, then, a decrease for 72 h, 96 h and 120 h and again an increase at the end of the experiment (at *t*= 144h and 168 h). These fluctuations of impedance are also observed in modulus plots (Fig.11B. Morever this is in agrememt with the fluctuations of R_p found with LPR measurement. Again, as in the case of the previous studied systems (abiotic and biotic), the depressed semi-circle can be related to a CPE behaviour: all the obtained α values are below 1 (Tab. 6). Fluctuation of resistance shown in Tab. 2, are obviously following the trend observed for Bode modulus and Nyquist plots. Moreover, *C* values are out of the range for double layer capacitance and thereby we can attribute that resistance to the formed corrosion product layer (R_l).

Tab. 6. Evolution in time of R_s, R, α, Q, C values for the carbon steel working electrode in the the control abiotic system.

Time (h)	R_s (Ω cm^2)	R (Ω cm^2)	α	Q (Ω^{-1}cm^{-2}s$^{\alpha}$)	C (µF cm^{-2})
48	12	1522	0.84	0.82×10^{-3}	132
72	12	1266	0.85	1.11×10^{-3}	216
96	12	1082	0.85	1.23×10^{-3}	244
120	12	873	0.85	1.40×10^{-3}	284
144	12	1665	0.85	1.24×10^{-3}	246
168	12	1601	0.85	1.21×10^{-3}	239

Different representations of impedance spectra for carbon steel S235JR acquired in the Biotic 1 system (biotic environment treated with 500 ppm biocide at t= 96 h) during 168 hours are shown in Fig. 12. On the Nyquist graph, again a depressed semi-circle can be observed at HF followed by the beginning of a straight line at LF. Phase angle plots (Fig. 12A) only demonstrate one visible but we must keep in mind that the LF limit was either than previously. So we can suggest that the beginning part of the straight observed is similar to the straight line clearly previously observed for systems inoculated with *Desulfovibrio* species. The line was better defined in these latter cases because more points were taken in the LF domain. Having on mind this limitation for acquired data, it is logical to model data with the same electrical circuit as in case of biotic system, presuming same behavior of system for frequencies below 10 mHz: the model constructed with R_s, R_{ct}, CPE and W is proposed for this set of data. Selected curves were fitted and numerical values for calculated parameters are shown in Tab. 7.

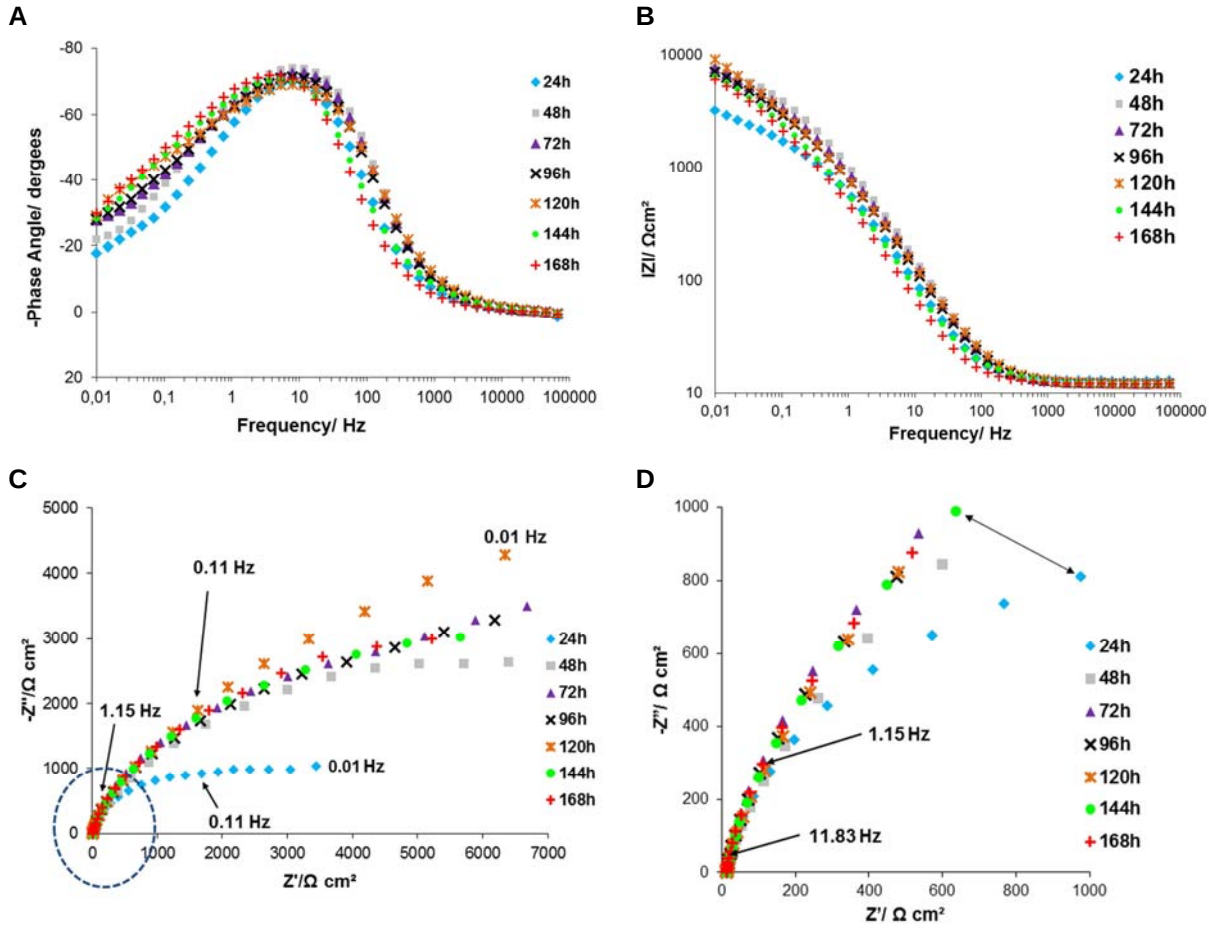

Fig. 12. Impedance spectra of carbon steel S235JR acquired for Biotic 1 system during 168 hours. System is treated with biocide (500) ppm at t= 96h. Data aquired in 10 mHz -100 kHz frequency range. (A) Bode plot - phase angle vs. frequency; (B) Bode plot - impedance modulus as function of frequency; (C) Nyquist plot; (D) Zoom-up Nyquist diagram of highlighted zone by a dashed blue circle.

Tab. 7. Evolution in time of R_s, R, α, Q, C, σ and $|Z_w|$ values for the carbon steel working electrode in Biotic 1 system. Warburg impedance is calculated for f= 0.01 Hz.

Time (h)	R_s (Ω)	R (Ω cm^2)	Q (Ω^{-1}cm^{-2}s$^{\alpha}$)	α	C (μF cm^{-2})	σ (Ω$^{-1/2}$)	$\|Z_W\|$ (Ω cm^2)
48	12	4434	0.19×10^{-3}	0.88	42	102	10183
168	12	3600	0.32×10^{-3}	0.83	37	111	11074

CPE behavior is validated by all α values being below 1. Moreover, for both spectrums, the C values obtained (42 and 37 μF cm^{-2}) correspond to typical values for a double layer capacitance and therefore HF depressed semi-circle observed could be attributed to the charge transfer resistance (R_{ct}) providing an initial estimation on corrosion. Moreover, obtained R_{ct} and $|Z_w|$ are similar confirming visual observations for plotted curves in Nyquist and Bode diagrams.
All the results obtained for Biotic 1 system leads to conclusion that 500 ppm biocide treatment did not affect electrochemical surface events, or surface layer, even though planktonic bacterial activity is decreased a little (Tab. 4).

Fig. 13 shows Bode and Nyquist representations of acquired EIS data for steel exposed to the Biotic 2 system (biotic environment treated with 1500 ppm biocide at t= 96 h). Plotted curves in phase angle diagrams are very similar to the ones drawn for Biotic 1 system, and they are facing the same problem of the too high LF limit. Due to that limitation angle plots shown in Fig. 13A are suggesting one time constant all along experiments.

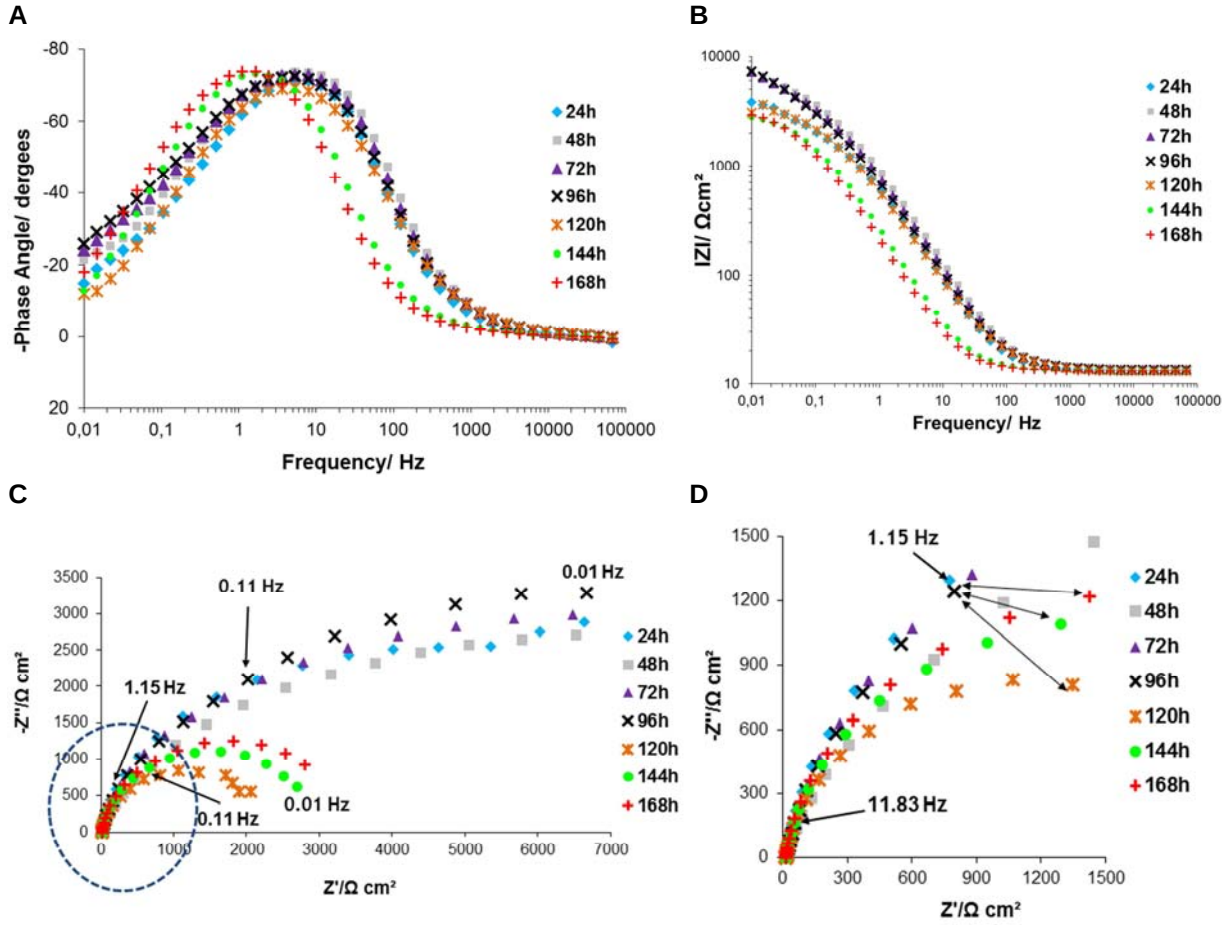

Fig. 13. Impedance spectra of carbon steel S235JR acquired for Biotic 2 systems during 168 hours. System is treated with biocide (1500 ppm) at t= 96h. Data aquired in 10 mHz - 100 kHz frequency range. (A) Bode plot - phase angle vs. frequency; (B) Bode plot - impedance modulus as function of frequency; (C) Nyquist plot; (D) Zoom-up Nyquist diagram of highlighted zone by a dashed blue circle.

Fig. 13C displays a clear separation between plots obtained for measurements conducted prior and post biocide treatment. Interestingly, plotted curves in Nyquist diagram for data obtained at 24 h, 48 h, 72 h and 96 h are very similar to the ones obtained for the Biotic 1 system, facing already mentioned LF limit. This allows us to presume similar behavior (before biocide treatment) to the ones observed for all the biotic system in the frequency domain below the LF limit <10 MHz). On the opposite, impedance spectra obtained after biocide treatment are more similar to the ones obtained for control system, presented a depressed semi-circle whom diameter is increasing along time (120 h towards 168 h). The CPE behavior of all the graphs (before or after biocide treatment) is confirmed by the α values below 1 (Tab. 8). Additionally, for both type of spectrums, the C values obtained (60 and 27 µF cm^{-2}, Tab. 8) correspond to typical values for a double layer capacitance and therefore the resistance linked to the HF depressed semi-circle can be attributed to a resistance to the charge transfer (R_{ct}). Higher R_{ct} is calculated for spectrum before biocide treatment than after. Together with high $|Z_W|$ is making overall resistance to corrosion much higher compared to one after biocide treatment. This is in agreement with observed R_p obtained with LPR measurement.

Tab. 8. Evolution in time of R_s, R, α, Q, C, σ and $|Z_W|$ values for the carbon steel working electrode in Biotic 2 system. Warburg impedance is calculated for f= 0.01 Hz. NC: Not concerned.

Time (h)	R_s (Ω)	R (Ω cm^2)	Q ($\Omega^{-1}cm^{-2}s^{\alpha}$)	α	C (µF cm^{-2})	σ ($\Omega^{-1/2}$)	$\|Z_W\|$ (Ω cm^2)
96	13	3441	0.27×10^{-3}	0.87	60	309	21849
168	13	2742	0.13×10^{-3}	0.88	27	NC	NC

Presented data suggest two types of behavior for system Biotic 2. One attributed to period before biocide treatment while bacteria proliferated in system and most likely colonized steel surface. This period involves diffusion as a factor affecting transfer of electroactive species from the bulk electrolyte to steel surface. Biocide affects surface by altering the interface properties compared to period before biocide treatment. It diminishes diffusion effect and decreases the overall resistance.

4. Conclusion

It is possible to say that bacterial presence affects the interface properties on carbon steel surface and therefore the steel corrosion. Different mechanisms are involved in corrosion processes in biotic systems compared to abiotic ones. Interactions between ferrous component of carbon steel and electrolyte result in formation of inorganic corrosion products layer determining resistance to corrosion. Illustratively, the interface in abiotic/control system is suggested in Fig. 14A. Inorganic layer resistance or charge transfer resistance as a main factor affecting corrosion process kinetics features it.
Bacterial presence in environment modifies the electrochemical behavior of steel due to the contribution of new component capable of affecting surface layer architecture. This newly introduced structural block, e.g. fully developed biofilm, composed of EPS matrix accommodating cells, is affecting mass transport of electroactive species from the bulk electrolyte to surface double layer (Fig. 14B). It represents a new barrier for transfer of electroactive species introducing diffusion (mass transfer) as a limiting step and contributes to overall surface layer resistance making steel more protected.

Experiments demonstrated the importance to apply high concentration of biocide in order to perform an effectiveness treatment. Bacterial activity decreased significantly only when applied biocide dosages were sufficient. Additionally to the fact that the biocide treatment decreased planktonic population, it led to disruption of protective surface layer increasing corrosion. This may be a consequence of dead cells deattachment and therefore decrease of refractory EPS production diminishing effect of protective organic barrier. Nonetheless, contribution of pH decrease on the disruption of the homogenous biomineralized layer should also be taken into consideration.

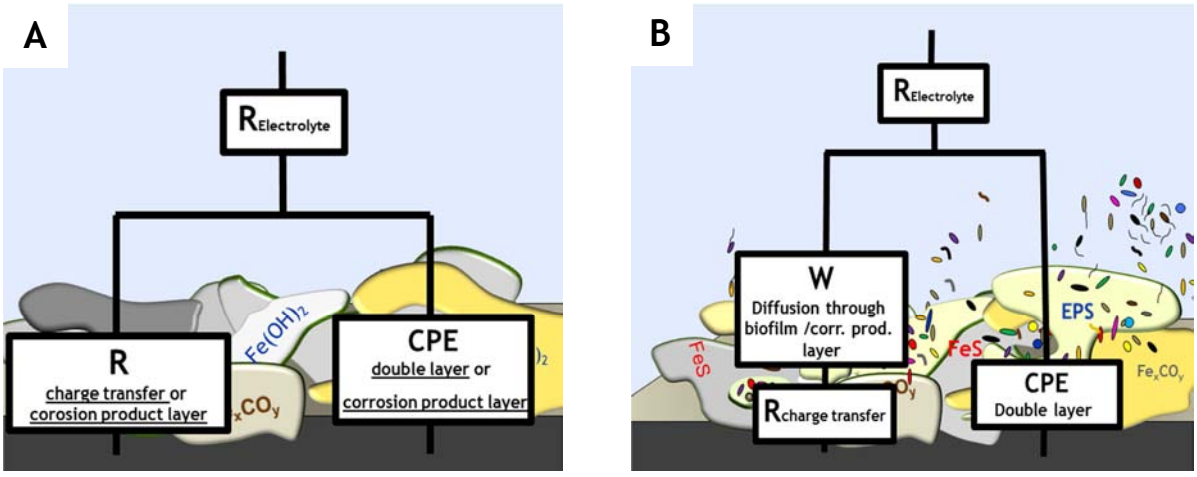

Fig. 14. Illustrative description of electric interface in three specific systems: A) Inorganic corrosion products formed on steel surface or charge transfer determining material corrosion resistance; B) Complex layer composed of different biomineralization/corrosion products and biofilm.

References:

F.M. AlAbbas, R. Bhola, J. R. Spear, D.L. Olson, B. Mishra, **Electrochemical Characterization of Microbiologically Influenced Corrosion on Line-pipe Steel Exposed to Facultative Anaerobic Desulfovibrio sp.**. International Journal of Electrochemical Society 8 (2013), 859 - 871.

I.B. Beech, C.W.S. Cheung, **Interactions of exopolymers produced by sulphate-reducing bacteria with metal ions**. International Biodeterioration and Biodegradation, 35 (1995), 59 - 72.

G.J. Brug, A.L.G. van den Eeden, M. Sluyters-Rehbach, J.H. Sluyters, **The analysis of electrode impedances complicated by the presence of a constant phase element**, Journal of Electroanalytical Chemistry 176 (1984), 275 – 295.

P. Carrera, G. Gabetta, **Biocide options in the offshore industry**. European Federation for Corrosion 19 (1996), 44 - 54.

D.S. Carvalho, C.J.B. Joia, O.R. Mattos, **Corrosion rate of iron and iron–chromium alloys in CO_2 medium**, Corrosion Science 47 (2005), 2974 - 2986

H. Castaneda, X.D. Benetton, **SRB-biofilm influence in active corrosion sites formed at the steel-electrolyte interface when exposed to artificial seawater conditions**. Corrosion Science 50 (2008) 1169 - 1183.

J.A. Costello, **Ph.D. thesis**. University of Cape Town, South Africa, 1975.

L. Dall'Agnol, **Ph.D. thesis**, In Press, Faculdade de Ciências e Tecnologia Universidade Nova de Lisboa, Portugal, 2013.

Z.H. Dong, T. Liu, H.F. Liu, **Influence of EPS isolated from thermophilic sulphate-reducing bacteria on carbon steel corrosion,** Biofouling 5 (27) (2011), 487 - 495.
D. Enning, H. Venzlaff, J. Garrelfs, H.T. Dinh, V. Meyer, K. Mayrhofer, A.W. Hassel, M. Stratmann, F. Widdel, **Marine sulfate-reducing bacteria cause serious corrosion of iron under electroconductive biogenic mineral crust**. Environmental Microbiology 14 (7) (2012), 1772 - 1787.

G. Gunasekaran, S. Chongdar, S.N. Gaonkar, P. Kumar, **Influence of Bacteria on film formation inhibiting corrosion**, Corrosion Science 46 (2004), 1953 - 1967.

H.A. Videla, **Prevention and control of biocorrosion**. International Biodeterioration and Biodegradation 49 (2002), 259 - 270.

W.A. Hamilton, **Microbially influenced corrosion as a model system for the study of metal microbe interactions: a unifying electron transfer hypothesis**, Biofouling 19 (1) (2003), 65 - 76.

R. Javaherdashti, **Microbiologically influenced corrosion: an engineering insight**. 6 McElligott Court, Canning Vale, Western Australia 6155, Australia, Springer-Verlag, London Limited, 2008.

Lee, W., Z. Lewandowski, P.H. Nielsen, W.A. Hamilton, **Role of sulfate-reducing bacteria in corrosion of mild steel: a review**. Biofouling, 8(3)(1995), 165 - 194.

B.J. Little, P. Wagner, F. Mansfeld, **Microbiologically influenced corrosion of metals and alloys**. International Materials Reviews 36 (1991), 253 - 271.

B.J.Little, J. S. Lee, **Microbiologically Influenced Corrosion**. Hoboken, John Wiley and Sons Inc., New Jersey, USA, 2007.

H. Ma, X. Cheng, G.Li, S. Chen, Z. Quan, S. Zhao, L. Niu, **The influence of hydrogen sulfide on corrosion of iron under different conditions**, Corrosion Science, 42 (2000).

E. Miranda, M. Bethencourt, F.J. Botana, M.J. Cano,J.M. Sanchez-Amaya , A. Corzo , J. Garcı´a de Lomas, M.L. Fardeau, B. Ollivier, **Biocorrosion of carbon steel alloys by an hydrogenotrophic sulfate-reducing bacterium Desulfovibrio capillatus isolated from a Mexican oil field separator**. Corrosion Science 48 (2006), 2417 - 2431.

A. Naguib, F. Mansfeld, **Evaluation of microbiologically influenced corrosion inhibition (MICI) with EIS and ENA**. Electorchemica Acta 47 (2002), 2319 - 2333.

T.R. Neu, **Significance of bacterial surface-active compounds in interaction of bacteria with interfaces**. Microbiology and Molecular Biology Reviews 60 (1) (1996), 151 - 166.

M.E. Orazem, B. Tribollet, **Electrochemical impedance spectroscopy**. The electrochemical society series, John Wiley & sons, Inc., publication, USA, 2008.

T. Richardson, R.A. Cottis, R. Lindsay, S. Lyon, D. Scantlebury, H. Stott, M. Graham, **Shreir's corrosion 2010**: **Corrosion in microbial environments**, Volume 2, Elsevier, Oxford, UK, 2010.

W. Sand, **EPS mediate biocorrosion?**. EUROCORR 2012, Paper no. 1736, Istanbul, Turkey (2012).

K.R. Sreekumari, K. Nandakumar, Y. Kikuchi, **Bacterial attachment to stainless steel welds: Significance of substratum microstructure**. Biofouling 17 (2001), 303 - 316.

M. Stern, **A Method For Determining Corrosion Rates From Linear Polarization Data**. Corrosion 14 (9) (1958), 440 - 444.

Z. Szklarska-Smialowska, **Effects of environmental factors in pitting, Composition of the electrolyte in pitting corrosion of metals**. NACE International, Houston, TX, Chap. 9, 201 - 219, 1986

H.A. Videla, L. K. Herrera, **Understanding microbial inhibition of corrosion - A comprehensive overview**, International Biodeterioration and Biodegradation, 63 (2009), 869 - 900.

H.A. Videla, L.K. Herrera, R.G. Edyvean, **An updated overview of SRB influenced corrosion and protection of carbon steel**. Corrosion/ 2005, Paper no. 05488, NACE International, Houston, TX, USA, 2005.

V.V. Zinkevich, I.B. Beech, **Screening of sulfate-reducing bacteria in colonoscopy samples from healthy and colitic human gut mucosa**. FEMS microbiology ecology, 34 (2000), 147 - 155.

Chapter V

Effect of mechanical stress on microbially influenced corrosion of carbon steel

V.1. Introduction

The mechanical stress is an integral byproduct of offshore Oil and Gas (O&G) operational conditions and environments; therefore, it is impossible to avoid it. Mechanical stress can result in a system failure either under the form of fatigue corrosion, or also under the shape of the Stress Corrosion Cracking (SCC) when combined with an aqueous environment. SCC is one of the main failure mechanisms for O&G offshore systems and material susceptibility to SCC is an element to take into account during material selection. SCC is common for numerous alloys and the cracks are generally observed to progress rapidly. The SCC can lead to unexpected failures of ductile metals, such as construction carbon steels subjected to a tensile stress. Moreover, SCC can be defined as a growth of cracks in an aggressive environment. It is a result of combined effect of three factors: a susceptible material, a corrosive environment; and tensile stresses above a threshold. The specific environment is of a crucial importance and only very low concentrations of certain highly active chemicals are needed to produce catastrophic cracking that often leads to devastating and unexpected failure [ASM International 1997]. It is known that microorganisms alter physico-chemical conditions on metal surfaces and lead to formation of local pH cells that create special microenvironments. This alteration of surface conditions can be a trigger for SCC initiation.

Furthermore, the Sulfide Stress Corrosion Cracking (SSCC) is a form of hydrogen embrittlement, which is a cathodic cracking mechanism. Susceptible iron based alloys react with hydrogen sulfide forming iron sulfides and atomic hydrogen as corrosion byproducts. Then, atomic hydrogen either combines to form molecular hydrogen at the alloy surface or diffuses into the alloy matrix. Briefly, since sulfur is a poison for hydrogen recombination, the amount of atomic hydrogen that can recombine to give molecular hydrogen is greatly reduced. Consequently the diffusion rate of atomic hydrogen into the metal matrix increases. Knowing that, bacterial metabolic activity, as is the case with Sulfate-Reducing Bacteria (SRB), can lead to local accumulation of their metabolic products (e.g. sulfide) on steel surfaces in O&G production systems; SSCC initiation and propagation may be supported by bacterial presence and their activity.

A significant role in SCC mechanism is attributed to material composition and microstructures. The critical value of the plane strain stress intensity factor (KISCC), which corresponds to the minimum stress required to produce crack propagation of a given material in a given environment, is influenced by material microstructure [Perez *et al*., 1998]. For example, the presence of large grain boundaries is found to reduce the SSC resistance [Perez *et al.*, 1998]. Interestingly, bacterial initial attachment occurs on or in the proximity of the grain boundaries. This phenomenon has origin in differential energy distribution between the grain boundaries and the matrix [Sreekumari *et al.*, 2001; Javaherdashti, 2008], resulting in higher energy allocated in grain boundaries that can attract and accommodate more bacteria [Cord-Rustwich, 2000]. Therefore, it is expected that the material deterioration in the presence of microorganisms will be initially localized on grain boundaries. It may well be that bacterial attaching and changing of surface microstructure might participate in SCC development.

In addition, each metal has a certain potential energy stored in itself. The growth of a crack creates two new surfaces and hence an increase of the surface energy of the system [Griffith, 1921; Irwin, 1957]. Since surface energy can be correlated to bacterial attachment, relationship between cracking mechanism and bacterial allocation can be drawn. Moreover, the energy released during crack growth [Erdogan, 2000] could attract more bacteria. Even more, surface atomic structures of solids, such as carbon steels, are modified in elastic deformation altering area of grain boundaries and thus affect bacterial attachment and the possibility of MIC.

Knowing the importance of failure mechanisms promoted by mechanical stress, and being aware of microorganisms' capability to participate in those processes, three questions were raised:

i) How can pure sulfidogenic strains and isolated offshore consortiums participate in construction carbon steel deterioration while being under mechanical load?

ii) What could be possible impact of mechanical stress and microorganisms' synergy for carbon steel system integrity?

iii) What is the probability of material failure in saline microbially active environments while being under mechanical stress?

In order to provide a deeper insight into construction problematic, carbon steel was subjected to a tensile mechanical load in the presence of different sulfidogenic strains and isolated offshore consortiums. The effect of bacteria on stressed surface was monitored with acquisition and analysis of electrochemical signals. Surface response to bacterial and mechanical load was investigated with surface analysis techniques.

V.2. Article 4

<< Electrochemical and Fractographic Analysis of Microbiologically Assisted Stress Corrosion Cracking of Carbon Steel >>

Corrosion Science

Current status: under 2nd revision

Electrochemical and Fractographic Analysis of Microbiologically Assisted Stress Corrosion Cracking of Carbon Steel

Marko Stipaničev[a,c,*], Omar Rosas[b,c], Regine Basseguy[c] and Florin Turcu[a]

[a]*Det Norske Veritas, Johan Berentsens vei 109-111, 5163 Laksevåg, Bergen, Norway*

[b]*National Center for Education and Research in Corrosion and Materials Performance, The University of Akron, 264 Wolfledges, Akron OH, 44325, USA*

[c]*Laboratoire de Génie Chimique CNRS-Université de Toulouse (INP, UPS), 4 Allée Emile Monso BP 84234, 31234 Toulouse Cedex 4, France*

*Corresponding author: Marko Stipanicev, telephone: +47 95936347, e-mail: Marko.Stipanicev@dnv.com

Abstract

This study was carried out to evaluate the effect of microorganisms on the corrosion behavior of carbon steel when exposed to mechanical axial stress. Open Circuit Potential (OCP) and Electrochemical Frequency Modulation (EFM) response were measured on the tensile specimens while applying a constant load in various environments inoculated with different sulfidogenic or iron reducing microorganisms. The fractographic analysis revealed a noticeable impact of the enriched environments on the topography of tensile specimens; however, after the tests were carried out, it was not possible to detect any indications of a Stress Corrosion Cracking (SCC) failure mechanism for the tensile specimens.

Keywords: Carbon steel, Microorganism, Corrosion, SCC

1. Introduction

The damage caused by corrosion to marine steel infrastructure, such as offshore oil production installations, is indisputable. Approximately 20% of the total corrosion cost in this industry is due to Microbially Influenced Corrosion (MIC) [1, 2]. MIC is generally found and identified as the localized attack that is associated with the presence of surface-associated biofilms, e.g. microbial communities embedded in a bioinorganic matrix [3].

During oil production, besides the presence of bacteria, mechanical stresses are often seen as an additional component affecting the integrity of the material that leads to failures due to Stress Corrosion Cracking (SCC). SCC is a type of corrosion failure mechanism caused by a complex combination of factors including metallurgical, mechanical and environmental factors. The complexity of SCC has led over the years to numerous hypotheses, models, theories, and controversy on the mechanisms by which SCC occurs. Among them, the dissolution of anodic sites on the metallic surface was sometimes claimed to be the origin for SCC [4]. When carbon steel is exposed to stresses and simultaneously to aggressive environment, the localized electrochemical dissolution of iron can result in mechanically initiated oxide film breakdown that leads to exposure of fresh anodic material to the corrosive medium [5]; in biotic conditions the localized electrochemical dissolution of metals (pitting) may be caused by the tubercle conditions that often lead to pitting corrosion; pitting is the predominant morphology of MIC [6]. The colonization of the metallic surfaces by bacteria and thus development of a biofilm may change the chemical conditions at the interface metal/ environment. Biofilm can create gradients of concentration of species across its thickness (100 - 400 µm) and the pH under the biofilm can decrease inducing severe corrosion conditions underneath the localized biomass.

A few more merging aspects regarding SCC and MIC acting on metal surfaces exist. Besides of their importance for SCC mechanism, microstructure irregularities, such as MnS inclusions, serve as initiation points for pitting in abiotic corrosion [7, 8] and during MIC [9]. Avci *et al*. [9] suggested that, in presence of sulfidogenic bacteria, the initiation of an anodic reaction (dissolution of the metallic iron (Fe) matrix) and the subsequent pitting of steel in the surrounding areas of MnS inclusions is due to the disorder and strain exerted on the Fe matrix by MnS regarded as a contamination of the interface from metallurgical processes. Therefore, it is possible to assume that mechanical stress and bacterial activity may target the same locations on the material surface and synergistically accelerate the deterioration process. Moreover, hydrogen is playing a different but important role in MIC and SCC

deterioration processes jeopardizing both, the material integrity and the mechanical properties [10]. This is often associated with absorption of hydrogen in metal structures, which is known as hydrogen embrittlement [11]. The SCC and MIC environments support corrosion reactions due to capability to produce hydrogen in various circumstances [10], for example, ferrous material being subject to tensile stress in an environment supporting the proliferation of hydrogen consuming Sulfate-Reducing Bacteria (SRB). Tensile stresses coupled with biological activity are an example of the synergic effect between SCC and MIC that may be responsible for producing a local distribution of hydrogen [10].

Despite the wide variety of bacteria found in aqueous environments, Sulfate-Reducing Bacteria (SRB) seem to have received extensive attention from the corrosion community due to their abundance in industrial facilities and in the oil and gas industry; however, the efforts for studying this type of environments have focus on either, the microbiological side or the electrochemical side; a combined study of electrochemical, topographical and mechanical characteristics of materials has not being carried out, especially considering recently developed electrochemical methods. Javaherdashti *et al*. [4, 12] used pure and mixed cultures of SRB in Slow Strain Rate Testing (SSRT) on carbon steel, stainless steel and duplex steel finding that such materials are likely to fail in a shorter time compared to abiotic systems. However, these studies could be improved by estimating corrosion rates through electrochemical characterizations of systems under stress. On the microbiology side, focusing on one type of bacteria seems to limit the effect of bacteria other than SRB, such as iron reducing bacteria (IRB).

IRBs, such as *Geobacter sulfurreducens* ATCC 51573, have been widely studied for their use in microbial fuel-cells due to its electron exchange capabilities with solid substrates [13]. On the other hand, their role in corrosion process is still uncertain. Electrochemical tests have shown that these bacteria can exert two different effects: i) accelerating the cathodic reaction on the material hence, increasing the corrosion risk; and ii) shifting the pitting potential towards positive values, which may be interpreted as a reduction of localized corrosion risk. In the absence of an electron donor these bacteria promote the propagation of pitting whereas in the absence of electron acceptor is able to delay pit occurrence [14]. Since bacteria can assist pitting and therefore lead to SCC it is imperative to understand the role of bacterial activity on the Microbiologically Assisted Stress Corrosion Cracking (MASCC). For these reasons, studying the effect of different microorganisms on the corrosion of materials exposed to mechanical stress is imperative and the tool to complement this study is the use of electrochemical techniques.

Open Circuit Potential (OCP) has been used in corrosion studies for long time, especially for detecting potential ennoblement [15] which, is the tendency of the electrode potential to become more positive. Ennoblement of ferrous metals in presence of biofilms most often leads to reaching the breakdown potential leading to crevice or pitting corrosion initiation. On the other hand, Electrochemical Frequency Modulation (EFM) [16, 17] is a rather new technique used for corrosion monitoring in various environments and conditions [18, 19]; however, there are just few references for EFM used for monitoring MIC [20] and none for carbon steel specimens exposed to biotic environments while being under tensile stress. An advantage of using EFM resides in the small polarizing signals and its ability to provide promptly corrosion currents and causality factors (considered to be a factor determining measurement reliability), all in a single experiment. In addition, preliminary knowledge of kinetic parameters, e.g. Tafel slopes, are not required. Since EFM possess a non-aggressive nature (minor system perturbation), it could be a promising method to monitor corrosion rates in environments supporting biological activity and therefore development of MIC. The current study comprises a combination of mechanical, topographical and electrochemical descriptions for S235JR carbon steel, when subjected to a constant load, in presence and absence of bacteria. Pure cultures of SRB, *Desulfovibrio alaskensis* AL1 and *Desulfovibrio desulfuricans* ATCC 27774, as well as IRB pure culture of *Geobacter sulfurreducens* and consortiums selected from water injection systems of the North Sea Oil and Gas (O&G) industry were used. A constant-load ring was used to apply a uniaxial stress on a tensile specimen while measurements of OCP and EFM were simultaneously carried out.

2. Materials and Methods

2.1. Test Material

Carbon steel S235JR rod (original diameter 2 cm) (Descoure and Cabaud, France) was used to fabricate rounded tensile specimens with the dimensions shown in Fig. 1. The composition and reported mechanical strength of the material are shown in Tab. 1. Specimens were ground manually

using SiC paper of increasingly fine grain, ending with 600-grit and then rinsed with sterile deionized water to eliminate remaining debris from the grinding process. The specimens were exposed for 24 hours to UV light (wave length 256 nm: XX-15, sterilization UV lamp, UVP, USA) at 25℃ before being introduced in the test vessels for sterilization.

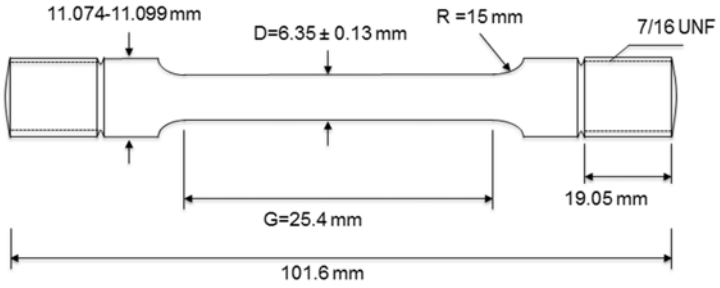

Fig. 1. Characteristics of the tensile specimen fabricated form S235JR carbon steel rod (with a 2 cm diameter)

Tab. 1. Chemical composition (wt %) and mechanical characteristic of S235JR carbon steel

Alloy	C	Mn	Cu	S	P	N	Certified Yield (MPa)	Tensile (MPa)	Real Yield (MPa)
S235JR	0.17	1.40	0.55	0.03	0.03	0.01	235	360/510	406

2.2. Microbial cultures and growth media

Desufovibrio desulfuricans ATCC 27774 and *Desulfovibrio alaskensis* AL1 were provided by Bioin Departamento de Química Faculdade de Ciências e Tecnologia Universidade Nova de Lisboa. *Geobacter sulfurreducens* ATCC 51573 was purchased from DSMZ (Deutsche Sammlung von Mikroorganismen und Zellkulturen). Consortiums used in experiments originated from pigging debris collected in water injection pipeline.

Saline modified-VMNI medium (2% or 3.5% NaCl) [21] served as a growth media for the pure cultures of SRB. The 2% and 3.5% NaCl modified VMNI media contained 0.37 mol L^{-1} and 0.62 mol L^{-1} of chloride ions. VMNI was composed of (g L^{-1} distilled water): NaCl, 20.0; NH_4Cl, 1.0; $CaCl_2 \times 2H_2O$, 0.04; Na_2SO_4, 4.5; $MgSO_4 \times 7H_2O$, 0.06; $FeSO_4 \times 7H_2O$, 0.004; sodium lactate, 6.0; KH_2PO_4, 0.5; sodium citrate, 0.3; casamino acids, 2.0; tryptone, 2.0; modified Wolfe's mineral elixir (0.1 % v/v) and vitamin solution (0.2 % v/v). The vitamin solution was composed of (g L^{-1} distilled water): riboflavin, 0.1; nicotinic acid, 0.25; thiamine, 0.3; pentatonic acid, 0.3; pyridoxine, 0.3; cyanocobalamin, 0.025; ascorbic acid, 1; biotin, 0.005. The composition of the modified Wolfe's elixir was (g L^{-1} distilled water): Nitrilotriacetic acid, 1,5; $MgSO_4 \times 7H_2O$, 0.06; $MnSO_4 \times H_2O$, 0.5; NaCl, 1; $FeSO_4 \times 7H_2O$, 0.1; $CoSO_4 \times 7H_2O$, 0.1; $NiCl_2 \times 6H_2O$, 0.1; $CuCl_2 \times 2H_2O$, 0.1; $ZnSO_4 \times 7H_2O$, 0.1; $CuSO_4 \times 5H_2O$, 0.01; $AlK(SO_4)_2 \times 12H_2O$, 0.01; H_3BO_3, 0.01; $Na_2MoO_4 \times 2H_2O$, 0.01; $Na_2SeO_3 \times 5H_2O$, 0.001.

Geobacter sulfurreducens ATCC 51573 growth media was prepared following the DSMZ protocol for preparation of DSMZ 826 GEOBACTER [22], and containing 0.05 mol L^{-1} of chloride ions. The DSMZ 826 GEOBACTER media was composed of (in 980 mL of distilled water): NH_4Cl, 1.5 g; Na_2HPO_4, 0.6 g; KCl, 0.1 g; sodium acetate 0.82 g; trace element solution (medium 141), 10.0 mL; vitamin solution (medium 141), 10.0 mL; selenite-tungsten solution (medium 385), 1.0 ml; Resazurin, 0.5 mg; Na_2-fumarate, 8.0 g; $NaHCO_3$, 2.5 g. Pigging debris were cultivated in North Sea seawater supplemented with 10 mM sodium acetate (Merck, Germany).

The assessment of viable bacterial cells in enrichments was carried out with a counting chamber (Helber Bacteria Cell Thoma from Hawksley, UK).

2.3. Test Environments

The initial chemical composition of each test environment was identical to the growth media described in Section 2.2.

Inoculum-free filter-sterilized North Sea water or autoclaved modified-VMNI and DSMZ media were used for control tests. The pH of test environments was measured every 72 h (HI-9125N, portable pH meter, HannaNorden AB, Sweden). Each test vessel containing 333 mL of test media was inoculated with 37 mL of a particular culture. The control vessels were only filled with 370 mL of test media. Oxygen exclusion was achieved by bubbling argon gas (Yara Praxair, Norway) at high rate for 72 h before tests start. Moreover, low flow rate of argon was maintained during the tests.

For the sake of clarity, each test system (test vessel + bacteria) was assigned an identification code as indicated below:

CTRL1 system - specimen immersed in 2.0 % NaCl modified-VMNI (autoclaved – no bacteria);

CTRL2 system - specimen immersed in DSMZ 826 GEOBACTER media (autoclaved – no bacteria);

SW system - specimen immersed in North Sea water (filter sterilized – no bacteria);

DAL system - specimen immersed in 2.0 % NaCl modified-VMNI inoculated with *D. alaskensis* AL1 culture;

DDS system - specimen immersed in 3.5 % NaCl modified-VMNI inoculated with *D. desulfuricans* ATCC 27774 culture;

GBS system - specimen immersed in DSMZ 826 GEOBACTER media inoculated with *Geobacter sulfurreducens* ATCC 51573 culture;

PG system - specimen immersed in North Sea seawater inoculated with pigging debris isolate and being under tensile stress.

2.4. Constant load technique

A tensile test-ring (Cortest Proof Rings, Corrtest, USA) was used to apply the constant load to the steel specimen as shown in Fig. 2. Modified Cortest High Temperature Vessels (Cortest Proof Rings, Corrtest, USA) were used as test vessels. The wall and/or lids of these vessels were either made of Hastelloy C-276© or of Pyrex©. Transparent Pyrex© construction elements allowed for easier observation of the vessel's interior which permitted visual monitoring of the blackening resulting from the metabolic activity of sulfidogenic species (Fig. 3).

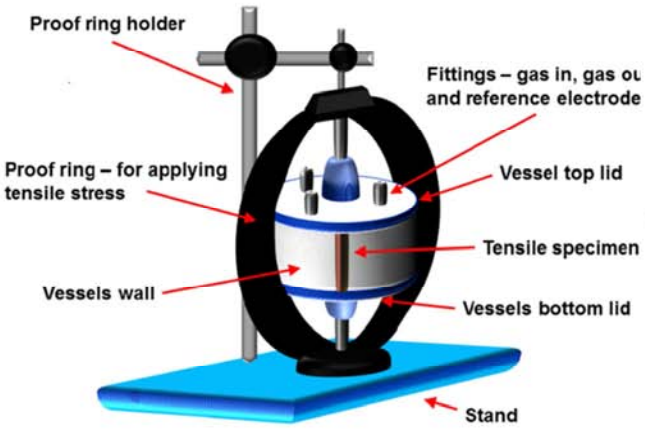

Fig. 2. Experimental set-up

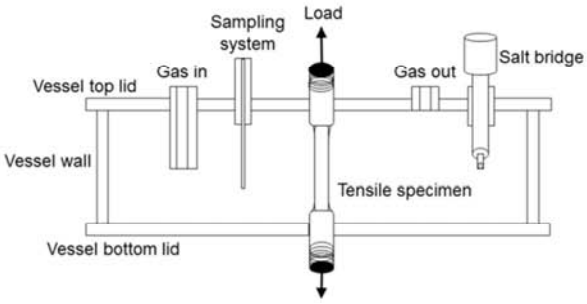

Fig 3. Cross-section of test vessel

The design of the original test vessels was altered in way to permit the installation of salt-bridges for accommodation of reference electrodes, and deaeration system.

All test elements (i.e. tensile specimens, vessels) were exposed for 24 h to UV light to eliminate any microorganism since they could have a collateral effect on the results.

The applied constant load was the same for all the experimental conditions; this load was chosen to not be greater than the yield strength to avoid any permanent deformation of the specimen. Initial applied load was 90% of material real material yield strength (Tab. 1). The Cortest Elapsed Time Monitors and Control Panels (Model 52000, Corrtest, USA) permit us independent regulation of each Cortest Proof Ring and provide possibility to perform multiple tests

2.5. Tensile tests

The yield strength or a yield point of a material is the parameter defined as the critical stress at which a material begins to deform plastically. Prior to the yield point the material will deform elastically and will return to its original shape when the applied stress is removed. Once the yield point is exceeded, the deformation will be permanent. Typically, steel will preserve its integrity during the expected lifetime given that load is below the yield point and steel is not exposed to an aggressive environment. One aim of the current work was to assess the combined effect of biotic environment and mechanical load on the operational lifetime of the steel.

The assessment relied on a post-test analysis of tensile steel test specimens. Tensile tests were applied with aim to detect alterations in specimens yield strength after exposure. Tensile testing was conducted with Zwick z250 materials testing machine with central ball-lead screw and MTS 810 (MTS, USA) according to ISO 6892-1:2009(E) entitled: Metallic materials-Tensile testing at ambient temperature.

2.6. Electrochemical Techniques

A three electrode arrangement was used for performing the Electrochemical Frequency Modulation (EFM) and Open Circuit Potential (OCP) measurement on carbon steel tensile specimens in the different test media. The tensile specimen was used as working electrode, while either the Hastelloy C-276© bottom lid or a vessel wall was used as counter electrode. Electrochemical potentials were measured versus a commercial Saturated Calomel Electrode (SCE) (Gamry, USA) (Fig. 2) that was interconnected with test systems via salt bridges. Electrochemical tests were carried out using a multichannel potentiostat MultEchem™ (Gamry, USA) consisting of two Reference 600TM Potentiostat/Galvanostat/ZRA independent units connected to PC interface and monitored by EFM140® software (Gamry, USA). Logging system comprised of SCXI (National Instruments, USA) modules and LabVIEW software (National Instruments, USA) was used for the continuous recording of OCPs. Data were not recorded for the SW system.

OCP measurements were performed during the entire duration of the experiments. OCP of tensile specimens were sampled every 5 minutes. EFM measurements were performed every 72 h. A complex excitation signal consisting of two overlapping sine waves with frequencies of 0.02 Hz and 0.05 Hz and 10 mV amplitude vs. OCP was imposed to carbon steel specimen.

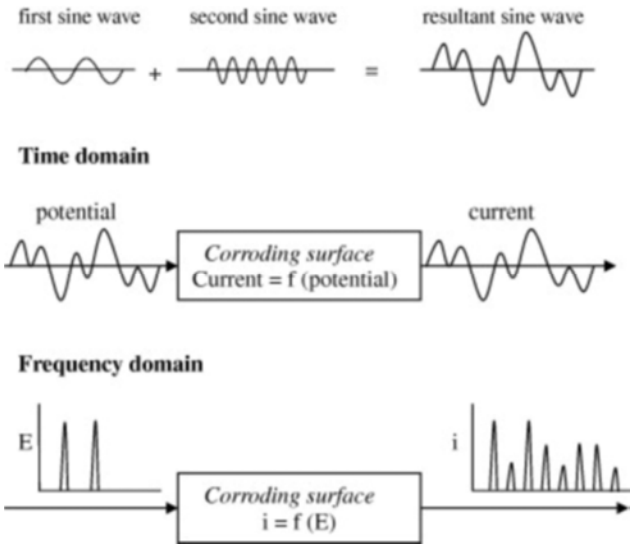

Fig 4. Principle of electrochemical frequency modulation (EFM)

While using EFM, a potential perturbation signal composed of sum of two sine waves is applied to the corroding specimen to obtain the current response corresponding to different harmonic and intermodulation frequencies [22, 23, 24, 25]. The fundamental principle of EFM is schematically presented in Fig. 4.

The stepwise analysis of the EFM output signal was performed by means of the Echem Analyst software (Gamry, USA). Firstly, activation controlled was assumed to be the dominating corrosion process and this assumption was taken in further calculations [16, 17]. Secondly, Alternating Current (AC) signals were transferred via a Fast Fourier Transformations (FFT) in the frequency domain. The resulting AC versus frequency curve is known as the ''intermodulation spectrum''. Thirdly, the intermodulation spectrum typically displays two distinguished peaks at 0.02 Hz and 0.05 Hz. Peaks observed in the region between 1 µA - 20 µA stands for the harmonics of the two excitation frequencies and they are used to calculate the corrosion current and the Tafel constants. Finally, the obtained corrosion current and Tafel constants are used for calculation of corrosion rate.

Further, Echem Analyst (Gamry, USA) software was used for calculating values of causality factor 2 and causality factor 3.

2.7. Gravimetric measurements

Weight loss measurements were conducted on tensile specimens. The tensile specimens were weighted prior and post to immersion (immersion period was 620 h). Tensile specimens were cleaned from corrosion products before post immersion weighting. For this tensile specimens were introduced in a 5% (v/w) hexamine (Merck, Germany) in concentrated HCl (VWR, USA) during 30 s, rinsed with deionized water and dried in the excess in a paper towel. Furthermore, tensile specimens were rinsed in acetone (Sigma-Aldrich, Norway) and left to dry in desiccators for 24 h. The perfectly dried tensile specimens were weight in an analytical balance. Corrosion rate (CR) is given in mm y^{-1}, and calculated according to equation (Eq. I):

$$\textbf{CR}\ (\text{mm y}^{-1}) = \frac{\mathbf{11.16} \times \boldsymbol{X}}{\boldsymbol{t} \times \boldsymbol{A}} \qquad \text{(Eq. I)}$$

Where:

11.16 is the factor accounting for the dimensional analysis and the density of the steel (7.85 g cm^{-3}),

X is the difference between “initial weight” and “weight after cleaning” in milligrams,

t is the exposure time in hours,

A is the total area of the tensile specimen in cm^2.

2.8. Surface analysis of samples

All test specimens that were exposed to the test environments were analyzed with different surface analysis tools and methods. Photographs of all exposed specimens were taken immediately after removal of specimens from test environments. Moreover, the presence of sulfide in formed black corrosion products was tested by initiating reaction between concentrated HCl (VWR, USA) and collected corrosion products [15].

Texture and morphology of each steel specimen after corrosion products removal were studied and documented with an upright DMR microscope (Leica, Germany) interfaced with ProgRes® C5 camera (JENOPTIK Optical Systems GmbH, Germany). All micrographs were recorded at 1x, 4x and 10x magnifications. Surface analysis was supported by micrographs obtained by means of table Scanning Electron Microscope (SEM) TM3000 (Hitachi, Japan) interfaced with Energy Dispersive X-ray (EDX) spectroscopy system Quantax 70 (Bruker, USA).

Dye penetrant testing was applied for detection of possible cracks. The acceptance criterion was in accordance with ISO 4987:2010, entitled: Steel castings - Liquid penetrant inspection. Dye penetrant test kit produced by Bycotest (Sweden) was used.

3. Results and Discussion

In order to evaluate the bacterial activity in the biotic test vessels, the number of bacteria at the end of the test period (620 h) was compared to the initial number of bacterial cells present in test vessels 1 hour after the inoculation. According to Tab. 2, the cell density in each test vessel was on average an order of magnitude higher at the end of the test. Considering that the control systems were sterile during 620 h of test, cell counts were not performed on CTRL1 system, CTRL2 system and SW system respectively.

Tab. 2. Cell density (cell mL^{-1}) monitoring for DAL, DDS, GBS and PG test systems

	***Desulfovibrio alaskensis* AL1** (Code: DAL)	***Desulfovibrio desulfuricans* ATTC 27774** (Code: DDS)	***Geobacter sulfurreducens* ATCC 51573** (Code: GBS)	**Pigging isolate** (Code: PG)
t_e= 1 h cell mL^{-1}	1.2×10^7	1.2×10^7	3.0×10^6	2.0×10^6
t_e= 620 h cell mL^{-1}	9.0×10^7	8.0×10^7	2.2×10^7	2.0×10^7

Tab. 3 presents the pH evolution in all test systems for the entire duration of the test. It can be noticed three trends of pH, each one characteristic for a subgroup of test systems. The first subgroup, consisting of bacteria containing DAL system and sterile CTRL1 systems, is featured with pH oscillating around 7.5. This stability observed in a case of CTRL1 system is attributed to the absence of bacterial communities which otherwise could alter the environmental conditions. The second subgroup, comprising bacteria containing DDS system and sterile SW system, shows a decreasing pH trend, from 7.5 to 6.7 and from 7.9 to 7.3, respectively. The third group: encompassing CTRL2 system and GBS system, demonstrates increase of pH toward alkaline values, for the GBS system this is caused by the presence of bicarbonate ions in the medium; in the case of PG system, a similar behavior was observed for most of the test period.

Tab. 3. pH values for CTRL1, CTRL2, SW, DAL, DDS, GBS and PG systems during 620 h of tests

t (h)	**CTRL1**	**DAL**	**DDS**	**SW**	**CTRL2**	**GBS**	**PG**
	Subgroup I.		**Subgroup II.**		**Subgroup III.**		
0	7.5	7.5	7.5	7.8	7.5	7.5	7.5
50	7.3	7.4	6.8	7.6	7.8	7.9	7.9
200	7.5	7.9	7.0	7.9	8.5	8.2	8.3
350	7.4	7.4	7.0	7.2	8.4	8.4	8.3
500	7.5	7.5	6.6	7.3	8.5	8.4	8.1
620	7.5	7.7	6.7	7.3	8.5	8.3	/

Tab. 4. Corrosion rates (CR) given in mm y^{-1} and obtained by weight loss (mg) measurements of S235JR carbon steel tensile specimens after 620 h exposures in CTRL1, CTRL2, DAL, DDS, GBS and PG systems

System	**CTRL1**	**DAL**	**DDS**	**CTRL2**	**GBS**	**SW**	**PG**
Weight Loss (mg)	23.7	217.4	2472.2	154.3	11.5	72.1	264.8
CR (mm y^{-1})	0.02	0.16	1.85	0.12	0.01	0.05	0.20

Values of corrosion rates obtained by weight loss for test systems are shown in Tab. 4 and photographs of all exposed specimens, taken immediately after removal of specimens from test environments are shown in Fig. 5.

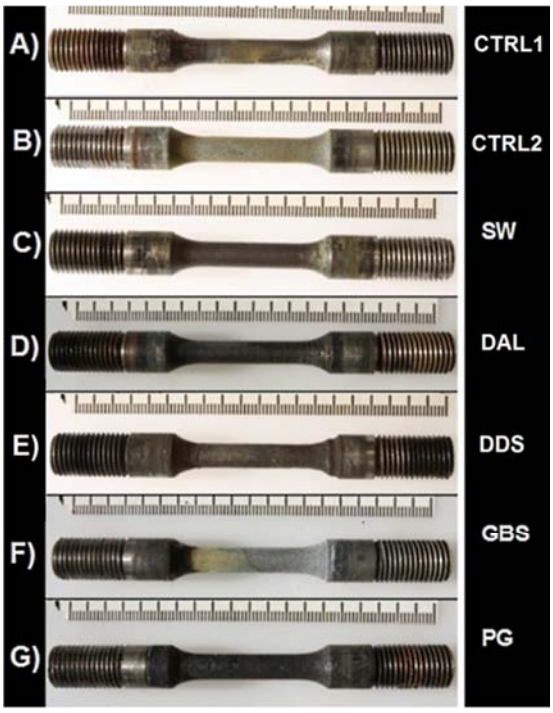

Fig. 5. Photographs of tensile specimens (before cleaning) after 620 h of immersion in CTRL1, CTRL2, DAL, DDS, GBS and PG systems

The Fig. 6A presents OCP of all systems that used VMNI as a test media, e.g. CTRL1, DAL and DDS systems.

In the case of systems CTRL1 the OCP remained stable (-710 ± 15 mV/SCE) during the whole duration of the tests which is not surprising for a control system, e.g. anoxic saline media. Similar OCP values for carbon steel in seawater were previously obtained by other researches [26]. The stability of the recorded electrochemical signals (system CTRL1) noticeable within the first 50 hours of the test could be attributed to a steady protective layer formed at the metal- electrolyte interface. The steady layer might be explained by the low corrosion rate and consequently low iron concentration in bulk medium. In a neutral or slightly alkaline environment as in the case of CTRL1, the cathodic reduction of hydrogen ions would lead to hydrated hydroxide ions. Once the solubility product of iron hydroxide is reached in the vicinity of the metal surface it is imminent that a layer of ferrous hydroxide would loosely attach to the carbon steel thus conferring on it certain level of protection. Values of instantaneous corrosion rate obtained by EFM were ranging between 0.003 and 0.044 mm y^{-1} (Fig. 6B) in the control systems. Furthermore, the figures obtained by weight loss measurements preformed on tensile specimens indicated 50% lower corrosion rates, of 0.02 mm y^{-1} (Tab. 4). This is not unexpected, knowing different natures of instantaneous corrosion rate measurements (EFM) and absolute corrosion rate measurements (weight loss). Corrosion tests, mostly weight loss measurements, performed in similar environments with identical S235JR steel material (coupons, 2 cm^2) exhibited one order of magnitude lower corrosion rates than the ones presented here; however, specimens (coupons, 2 cm^2) were not subjected to any mechanical stresses [27, 28]. In addition, different dimensions of specimens used in two investigations could affect the result. There is a possibility that mechanical stress contributed additionally to the level of the metal loss by increasing the total corrosion of the specimen.

On the other hand, the OCP of DAL system largely varied on the first 48 hours subsequent to test start. Moreover, OCP values of DAL system revealed a slow decline from -670 mV/SCE to -750 mV/SCE). The large transients affecting the electrochemical potential trend of the DAL system tensile specimen at the beginning of the tests could be associated with the attack of the chloride ions on the metallic surface; the dynamic formation and dissolution of oxides could have produced the rapid changes in the electrochemical potential. As soon as the charge transfer between the metal and the electrolyte stabilizes the transient phenomena are less prominent. In the case of the DAL system, the low sulfide concentration emerging form SRB's metabolic processes, could have promoted the formation of a stable and protective layer of pyrite or a different stoichiometry of iron sulfide. A presence of iron sulfides was confirmed by quick test with concentrated HCl and visually was observed black layer, Fig. 5D. This is reflected in the steady OCP of DAL system. From a corrosion point of view, DAL system showed a higher instantaneous corrosion rate compared to CTRL1 system during the whole test. This rate increased the first 360 h, and remained constant at 0.18 ± 0.05 mm y^{-1}. On the other hand, corrosion rates estimated from weight loss measurements were 0.16 mm y^{-1} (Tab. 4), a

value similar to the ones obtained by EFM technique.

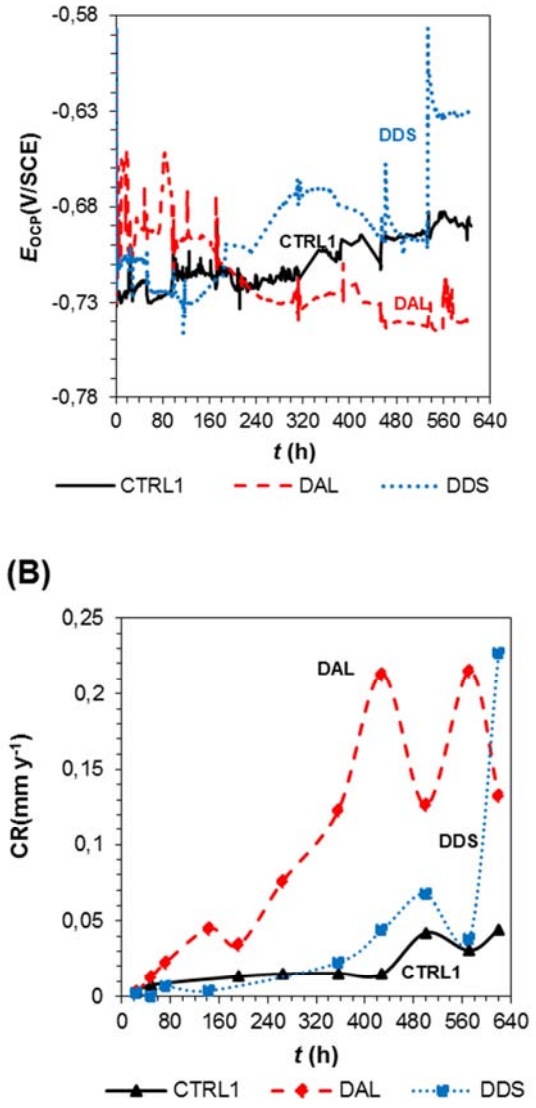

Fig. 6. (A) Open circuit potential (EOCP(V/SCE)) for CTRL1, DAL and DDS systems during 620 h of tests; (B) Average corrosion rates (mm y-1) obtained with electrochemical frequency modulation (EFM) for CTRL1, DAL and DDS systems during the 620 h of tests

For DDS system, OCP increased from approximately -710 mV/SCE to -680 ± 15 mV/SCE (Fig. 6A). Unlike the other test systems, the DDS exhibited a porous and loosely bound black deposit observed immediately after the tensile specimen extraction from the test environment (Fig. 5E). The difference between this deposit and the one formed on the DAL system, originates in the particular chemical reaction pathway determined by the actual ratio between iron and sulfide ions [29]. Accidental detachment of this layer might produce sudden large changes in the OCP. Corrosion rates reported by the EFM for DDS system were mostly low with the exception of very last measurement which indicated a higher corrosion rate (0.23 mm y^{-1}) (Fig. 6B). Nevertheless, the absolute corrosion rate obtained by the weight loss was significantly higher (1.85 mm y^{-1}) (Tab. 4).

Although differences in biomineralization processes occurred on surfaces of the tensile specimens in DAL and DDS systems, the amount of aggressive chloride ions present in each system is possibly playing the major role in degradation process. Pineau et al. [30] observed a corrosion rate of 1.93 mm y^{-1} for carbon steel exposed to seawater conditions while in an estuarine site, which implies that the salinity is often much lower than the average salinity of seawater, observed corrosion rates were around 0.35 mm y^{-1}. There is an obvious analogy between differences observed between DAL (CR= 0.16 mm y^{-1}, 2% NaCl) and DDS (CR= 1.85 mm y^{-1}, 3.5% NaCl) systems and differences between estuarine and seawater conditions

A comparison of OCP values measured in the system GBS and the corresponding control system CTRL2 (Fig. 7A) shows that the OCP of CTRL2 drifts towards more positive values while in the case of GBS the drift is less pronounced. It is known that Geobacter sulfurreducens promotes the formation of layer of iron phosphate in this medium that is able to reduce corrosion on the steel surface (Fig. 5F) [4, 19]; such layer is probably stabilizing the OCP of the tensile specimen in period between t_e= 0 h and t_e= 240 h. Fluctuations observed after te= 240 h may be attributed to the close relationship established between the bacterial life cycles and general chemistry of test environment; hence, the global redox potential of the electrolyte changing upon the variations in the bacterial growth and/or activity could be reflected in the OCP vs. time. However, it is important to notice that the OCP alone cannot completely describe the electrochemical behavior of an interface especially when bacteria are in close proximity. The absolute and instantaneous corrosion rates obtained at the end of test period are relatively low (Tab. 4 and Fig. 7B), but are lower in presence of Geobacter sulfurreducens: for GBS system, 0.015 mm y^{-1} obtained by EFM and 0.01 mm y^{-1} obtained by weight loss and for CTRL2 system, 0.06 mm y^{-1} obtained by EFM and 0.12 mm y^{-1} obtained by weight loss. It seems that the corrosion rates found here agreed with what is mentioned about a protection mechanism in

presence of this bacteria as well as good correlation between the very last instantaneous corrosion rates and the absolute corrosion rate. The observed protective effect was found previously [14, 27] and it was attributed to the reduction of ferric ions by the iron reducing bacteria to ferrous ions, promoting the thermodynamic stability of iron phosphate compound, such as vivianite.

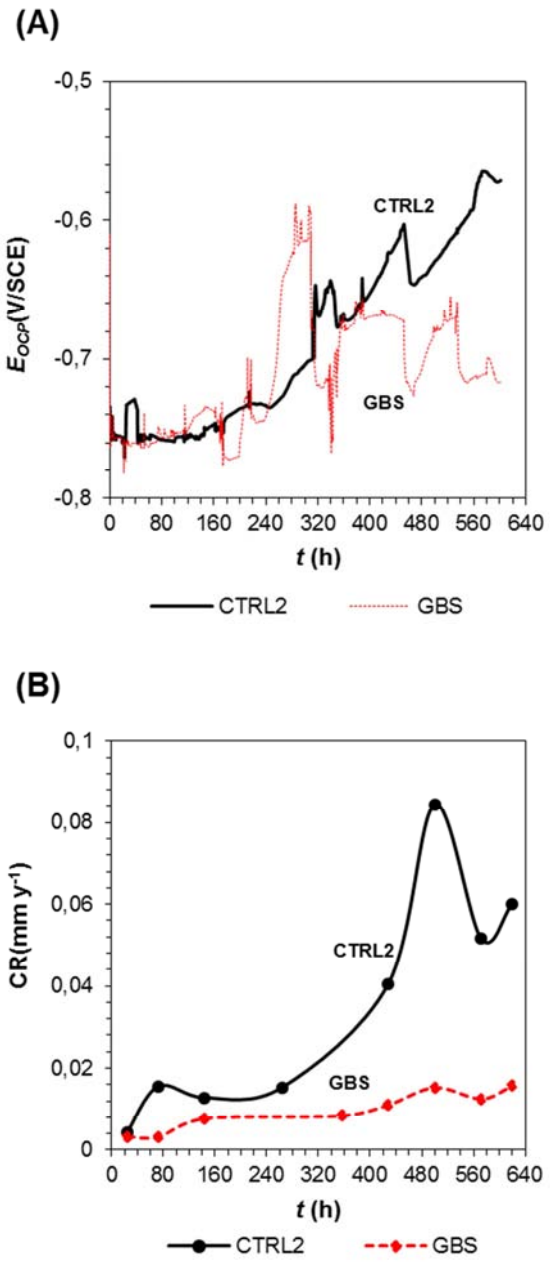

Fig. 7. (A) Open circuit potential (EOCP(V/SCE)) for CTRL2 and GBS systems during 620 h of tests; (B) Average corrosion rates (mm y^{-1}) obtained with electrochemical frequency modulation (EFM) for CTRL2 and GBS systems during the 620 h of tests

Fig. 8A compares the OCP values for PG system and its control (SW system).

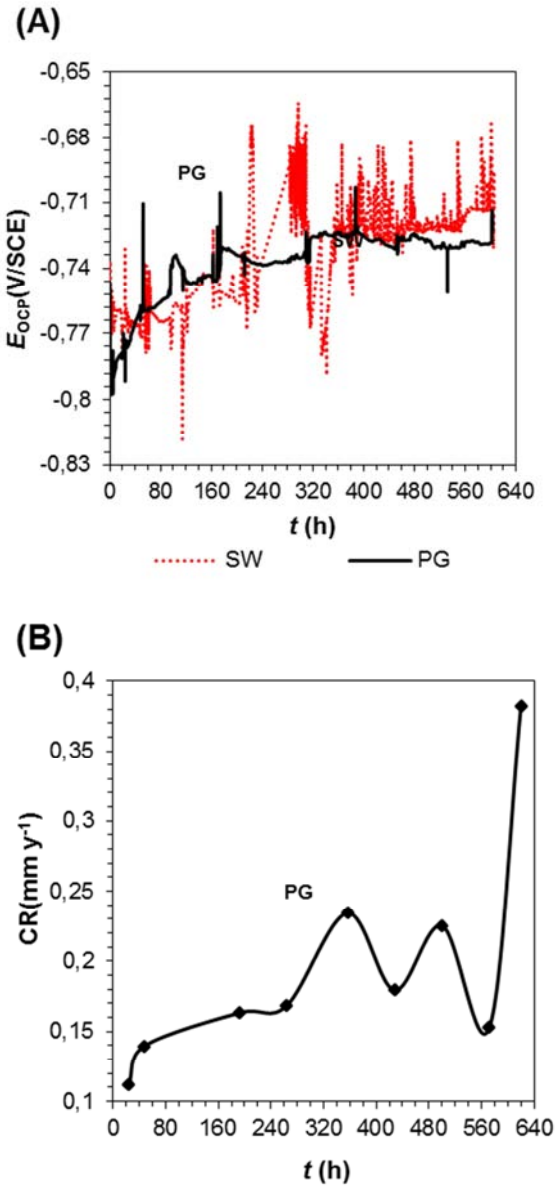

Fig. 8. (A) Open circuit potential (EOCP(V/SCE)) for SW and PG systems during 620 h of tests; (B) Average corrosion rates (mm y^{-1}) obtained with electrochemical frequency modulation (EFM) for the PG system during the 620 h of tests

The OCP values remained stable for both systems during the whole duration of the test. Unlike the SW system on which no deposits were found (Fig. 5C), the tensile specimen of the PG system was covered by black precipitates of iron sulfide nature (Fig. 5G). For the PG system, EFM corrosion rate (very last value of 0.38 mm y-1, Fig. 8B) and weight loss corrosion rate (0.20 mm y^{-1}, Tab. 4) were considerably higher than for the control system (weight loss corrosion rate 0.05 mm y^{-1}). This higher corrosion rate is attributed to the effect of the SRBs found in the “pigging” debris used to cultivate this inoculum [27]. In this case, black deposits were observed (that released

the smell characteristic for H_2S in reaction with diluted hydrochloric acid) indicating the presence of iron sulfides. Even though they are different microbial population, it is possible to observe similar behavior and corrosion rates between the two sulfidogenic systems, PG and DAL .According to the available literature, EFM may show contradictory results when applied to corrosion rate determination as it was shown in particular examples presented above. Obviously, there is an apparent discrepancy between the corrosion rates obtained by weight loss and EFM technique, however, deviations varies from system to system. Some discrepancies are enormous, for example in the case of the DDS system, while in other cases most of the deviations are acceptable. The reasoning why these differences are considered as acceptable is the very nature of the corrosion techniques that were used; EFM provides instantaneous corrosion rate while weight loss provide absolute corrosion rate. From other point of view, reliability of EFM corrosion rates can be questionable depending on the situation and may be the cause of the observed discrepancies. When EFM is applied for measurement of high corrosion rates, the technique provides valid and reasonable values, for example for mild steel in a 0.05 M H_2SO_4 solution where it can reach value of 2.1 mm y^{-1} [19]; on the other hand, when applied for measuring low corrosion rates, it provides non-reliable values [19]. In order to validate EFM measurements, causality factors were used. Causality Factor 2 (CF2) and Causality Factor 3 (CF3) are in general used to validate the data obtained by EFM in case of uniform corrosion. Usually, if the CF2 values are close to 2 and the CF3 values are close to 3, it is considered that measurements are conducted correctly and obtained corrosion rates are valid [24]. These assumptions are valid only when uniform corrosion mechanism is present and care must be taken when localized attack is dominant; in this latter case, a deeper analysis regarding corrosion rate and the values for CF must be carried out. For example, CF2 and CF3 can be applied as a valuable tool for detection of localized corrosion as it is shown by Rauf [24] who proposed a causality factor evaluation model for localized corrosion. The values for CF2 and CF3 were analyzed following the main observations and conclusions extracted from the literature but having on mind the possible impact of tensile stress on the acquired data.

In Fig. 9A, it is possible to observe that most of the CF2 values are in range between 0.5 and 2; there are few exceptions above the upper limit of this range and they are deviating for the general corrosion expected value of 2. Fig. 9B reveals that most of the CF3 values are in the range between 0.5 and 2; although only some exceptions fall outside the mentioned upper and lower limits, most of the values are still deviating from the expected value of 3.

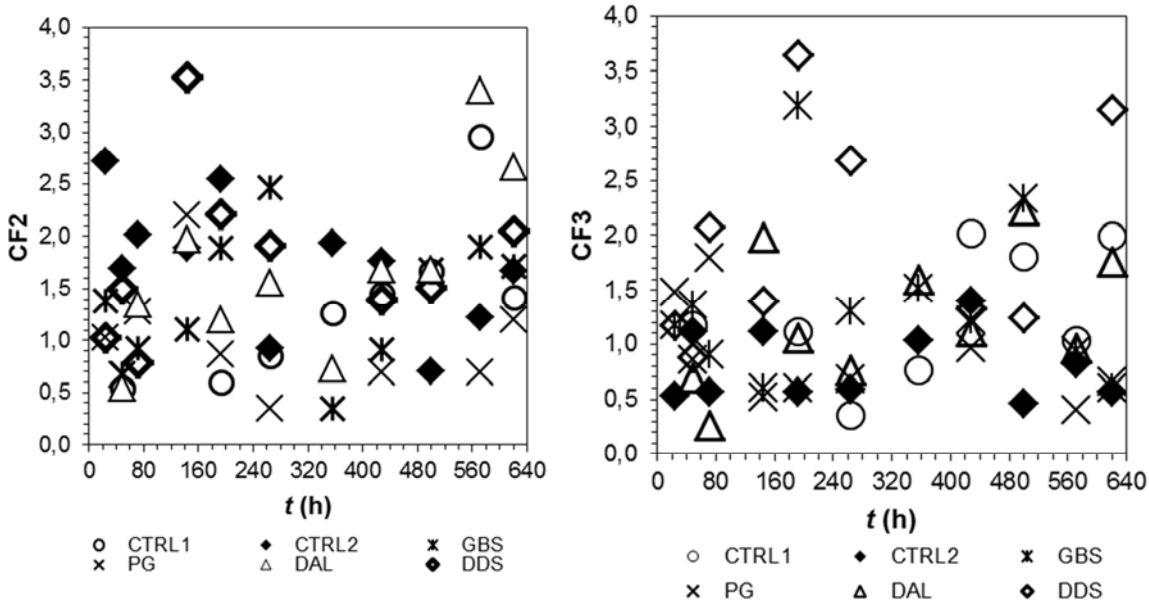

Fig. 9. Causality factors values obtained by electrochemical frequency modulation (EFM) for CTRL1, CTRL2, DAL, DDS, GBS and PG systems during the 620 h of tests; (A) Causality factor 2 (CF2); (B) Causality factor 3 (CF3)

The PG system showed EFM corrosion rate values (with exception of very last one) not too far from the ones obtained by weight loss, which is in agreement with CF2 values; however, CF3 deviates from the expected value of 3. Similar good correlation between corrosion rates obtained by EFM in seawater environment as in a case of PG system was presented by Han and Song [18], however, causality factors values were not reported in that particular case. The values for CF2 and CF3 for the DDS system on the time interval t_e= 140 h to t_e= 180 h, were above 2 and below 3 respectively. These CF values were previously used as an indication of localized and crevice corrosion [24], and it the case of DDS system an elevated localized surface attack by sulfidogenic bacteria was observed; it is believe that this amount of localized attack influences the calculation of corrosion rate and it is the cause for the discrepancies found between the EFM method and weight loss method for corrosion rate. The DAL system, that had sulfidogenic nature, was showing high CF3 but low CF2 values which possibly could be regarded as an indication of localized pitting events occurring on the specimen surface [24]; however this is not always applicable as it was shown for this particular case.

To validate the electrochemical findings and to provide an insight into the surface degradation mechanism, visual and microscopical examinations of the exposed specimens were conducted. Black corrosion products were observed along the body of the tensile specimens immersed in the DAL, DDS and PG media as it was expected due the sulfidogenic nature of the systems (Fig. 5).

The morphology of the black deposits built on these specimens varied significantly among the three test systems. Tensile specimens from DAL system were covered by a thin, homogenous and strongly adhering black layer, which is consistent with the low corrosion rates and stable OCP. On the other hand, the specimens immersed in PG and DDS environments showed a high volume and loosely bond black products. As previously mentioned, the DDS system experienced a massive deterioration noticed as high EFM and weight loss corrosion rates (Fig. 10).

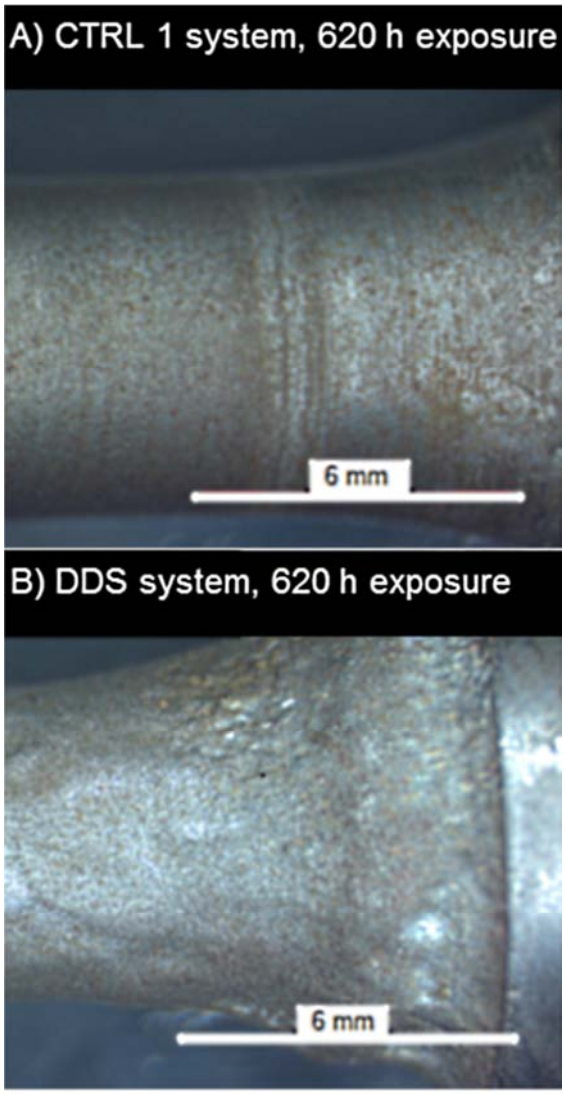

Fig. 10. Macrographs (1x) of tensile specimens after 620 h of immersion in DDS and CTRL1 (belonging control system) systems

The chemically cleaned tensile specimens previously exposed in DDS system were characterized by severe localized corrosion as it is shown on Fig. 11E, where large pits are observed (diameter of a 1 - 2 mm and depth between 10 and 30 µm). The severity of the localized corrosion damage in terms of affected area was much lower for the PG system compared to the DDS specimens (Figures, 11G, respectively). The observed pit morphology on specimens immersed in DDS, BS and PG systems is not the typical featured in standard SSC tests.

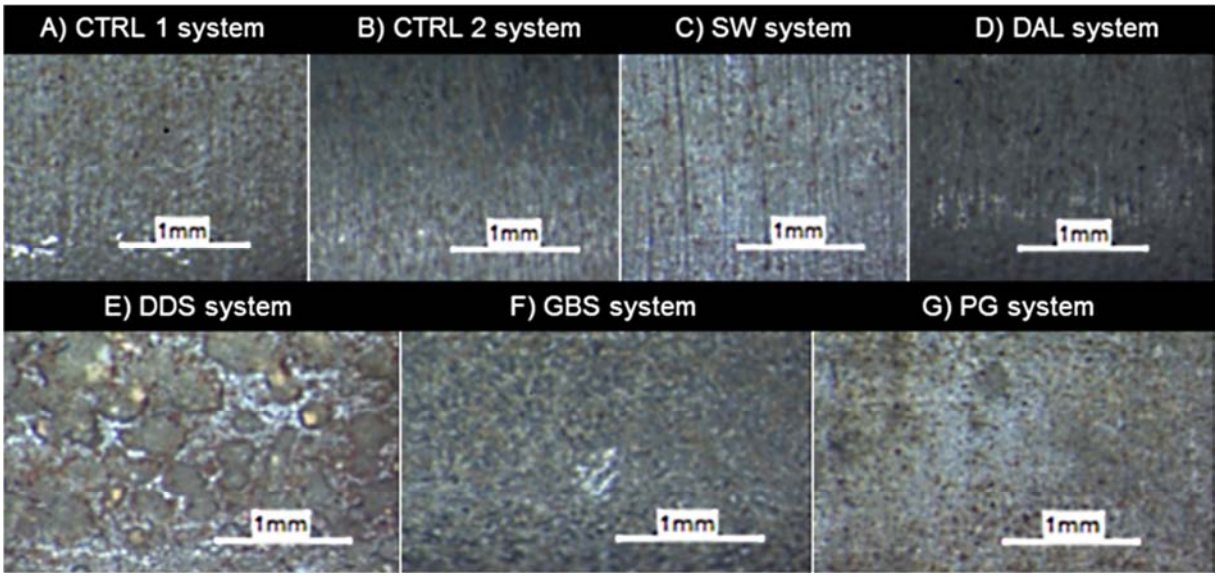

Fig. 11. Macrographs (4x) of cleaned tensile specimens after 620 h of immersion in CTRL1, CTRL2, DAL, DDS, GBS and PG systems

The tensile specimens from DAL system (Fig. 11D) are characterized, after a chemical cleaning, by a smooth surface and the absence of localized damage which could be attributed to a stable and thin black protective surface layer of iron sulfides. A similar condition was previously observed by other workers in low sulfide environments [28, 31].

Evidence of pitting was found in tensile specimen in GBS test; however, these pits were smaller in size compared to DDS system and homogeneously distributed all along the surface of the metallic specimen (Fig. 11F). Observations are in correlation with previously observed *Geobacter* nature. *Geobacter* was earlier tested due to the ability of this microorganism to exchange electrons with solid substrates, it is believed that during the constant mechanical load, cathodic and anodic micro-zones are created on the surface of the specimen which attracts the bacteria and facilitates their settlement.

In order to achieve a definitive result on the extent of the pitting, all specimens, regardless the presence of visible pits, were subjected to a dye-penetrant test and to careful microscopic examination. Nevertheless, none of the tensile specimens produced any evidence of crack initiation. Common post-exposure mechanical tests, such as hardness and tensile, performed on all tensile specimens exhibited a pronounced plastic deformation (necking) before suffering ductile fractures. An as example, the tensile specimen exposed to DAL system is shown on Fig. 12.

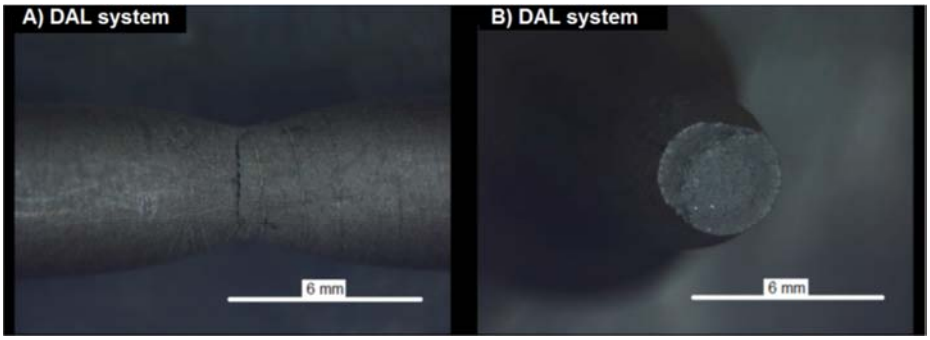

Fig. 12. Macrographs (1x) of tensile specimens that was submitted to tensile test after 620 h of immersion in the AL test system under load of 90% of its actual yield strength; A) Elongated sample (necking) B) Ductile brake

Tensile tests revealed differences and similarities in properties of the exposed specimens (Tab. 5). A dummy specimen (not exposed in any media and machined according to standard requirement for tensile testing) was subject to tensile test in order to provide reference values. This sample exhibited a yield curve characterized with upper and lower yield point, and displayed tensile strength (R_m) of capped carbon steel [32]. Tensile specimens form CTRL1, SW, DDS and PG systems exhibit identical

shape of yield curve as the dummy specimen, and they demonstrated tensile strength similar to dummy specimen.

A contrasting behavior is discovered in the case of the tensile specimens who were immersed in CTRL2, DAL, and GBS systems. Those systems have shown a yield curve with offset yield point and a slightly higher tensile strength (from 468 MPa to 588 MPa) compared to dummy specimen. At the same time, for these tensile specimens, the percentage of elongating (A) was reduced compared to dummy specimen. This gives an indication of an increased embrittlement of the tensile specimens, most probably due to hydrogen (present as a product of the cathodic reaction) diffusion in metal structure. Embrittlement was expected in the case of hydrogen sulfide environments, like in the DAL system, hence, a lower mechanical resistance was also expected in the samples exposed in this test system.

The irregularities in the tensile tests results could be caused by variations in post-exposure tensile specimens dimensions (heterogeneous distribution of deformations due to weight loss). Tensile test are based on a standardized geometry and surface finish of samples which means that irregularities can lead to deviation in results.

Even though tensile test are performed on unstandardized specimens it is possible to detect certain common patterns in their mechanical behavior. For example, percentage reduction of area (Z) of all specimens was in range of 60 - 70 %, as well as modulus of elasticity (E) in range of 195 - 230 MPa, indicating similar behavior of all tested specimens.

Tab. 5. Results of post-exposure tensile tests performed on steel specimens immersed in CTRL1, CTRL2, SW, DAL, DDS, GBS and PG systems during 620 h of tests. Presented parameters: A= fracture percentage elongation, $Rp_{0.2}$ and Rp_1= proof strength (plastic extension), R_{eL}= lower yield strength, R_{eH}= upper yield strength, R_m= tensile strength, Z= percentage reduction of area, E= modulus of elasticity

System	A	$R_{p0.2}$	R_{p1}	R_{eL}	R_{eH}	R_m	R_{eH}/R_m	Z	E
	%	MPa	MPa	MPa	MPa	MPa	%	%	GPa
Dummy*,[1]	35.7	338	333	327	391	455	89.40	69	224.0
CTRL1	32.3	322	335	322	373	461	80.91	68	198.3
SW	38.5	330	320	320	382	462	82.68	63	196.2
DDS	47.4	321	319	309	352	447	78.75	70	204.0
PG	37.2	332	332	324	416	460	90.44	70	230.0
CTRL2	29.4	406	405	/	/	515	/	65	211.8
DAL	20.2	515	528	/	/	588	/	62	209.1
GBS	34.2	324	342	/	/	468	/	68	225.5

A= fracture percentage elongation, $Rp_{0.2}$ and Rp_1= proof strength (plastic extension), R_{eL}= lower yield strength, R_{eH}= upper yield strength, R_m= tensile strength, Z= percentage reduction of area, E= modulus of elasticity, *average of three, [1]Dummy- is the specimen not exposed in any media and machined according to standard requirement for tensile testing

Hardness for all tensile specimens, including dummy specimen, was in the same range, around value of 180 according to Rockwell scale (it decreases in close proximity of break point) indicating same mechanical properties of tested specimens, either they were exposed to environment inoculated with bacteria or not, or even not being exposed to any aqueous environment (dummy specimen). Further investigation revealed homogenous ferrite/perlite microstructure characterized by small grains and relatively short grain boundaries (20 - 40 μm). In addition, long and narrow MnS inclusions were present in carbon steel structure (Fig. 13). In this particular investigation it was not possible to detect pit initiation on week points in carbon steel microstructure (MnS inclusion) [9] that could lead to crack initiation. This result shows that there was not change in microstructure properties of tested specimens.

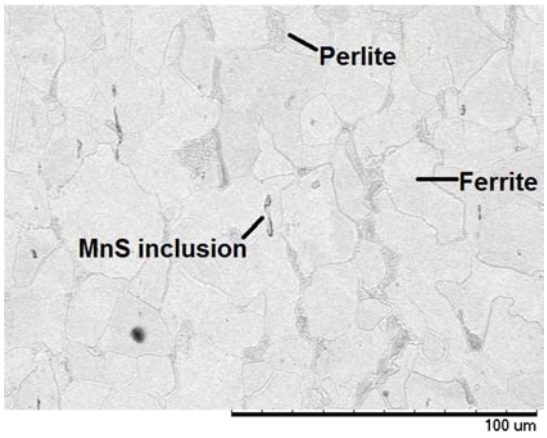

Fig. 13. SEM micrograph (1000x) of ferrite/ perlite microstructure typical for all tested S235JR carbon steel tensile specimens

4. Conclusion

The current study comprised a combination of mechanical, topographical and electrochemical descriptions for S235JR carbon steel subject to a constant axial load in presence and absence of different types of bacteria from the water injection systems of the North Sea Oil and Gas (O&G) industry.

The presence of microorganisms produced accelerated corrosion rates in some test systems but the pits formed as a result of this corrosion do not present a threat that would lead to initiation of cracks. There was no evidence of SCC initiators, such as intergranular or transgranular corrosion failure mechanisms.

According to results, it is clear that the presence of bacteria may change the metallic surfaces by inducing the formation of pits. In the case of the DDS system, the pits are produced under a layer of corrosion products like iron sulfides; in the case of GBS, the presence of bacteria produces a non-uniform layering of iron phosphate, it is believed that the pits are produced by a non-uniform bacterial attachment when the stress produces cathodic and anodic micro-zones. It was not possible to correlate the formation of pits with the presence of MnS inclusions or possible synergetic effect of mechanical stress and microbial activity on weak spots in carbon steel microstructure. To investigate this feature it is most likely required to study this phenomenon at earlier stages, when pit initiation is expected, and at higher tensile stress.

The type of surface degradation e.g. pit morphology for tensile specimens exposed in sulfidogenic systems (shallow and wide pits), such as in the case of tensile specimen retrieved from DDS system, do not correlate with pit morphology observed in standard SCC tests conducted in inorganic hydrogen sulfide environments. This is indicating that surface degradation is more likely to be the result of bacteria activity within biofilms formed on tensile specimens surfaces, than to be a product of global test environment. In addition, is it likely that formation of porous and unstable iron sulfide corrosion products lead to localized corrosion attacks [29]. Iron sulfide corrosion product alone, or coupled with formed organic biofilm structures, could lead to the establishment of suitable conditions for formation of galvanic couples what could explain higher weight loss for studied DDS system. In the case of DAL system, a layer of stable protective iron sulfides was formed [29], protecting the specimen from corrosion but not from hydrogen penetration.

The environment was affected by the presence of micro-organisms and their metabolic activity; this may lead to larger alterations in the material corrosion resistance rather than in the mechanical behavior of the exposed tensile specimens. Signs of embrittlement were observed from the mechanical tests, but it is not possible differentiate the origin of this behavior, or to attribute it solely to microbial activity or to effect of mechanical stress or maybe to joined action of these two parameters.

The discussed observations on causality factors and obtained corrosion rates suggest that EFM measurements conducted on mechanically stressed specimens in microbial environments may give

correct corrosion rates even though causality factors indicate failed measurements. Nonetheless, deeper investigating on this particular issue is required.

Acknowledgments

Funding was received from the European Community's Seventh Framework Programme (FP7/2007-2013) under grant agreement number 238579. The authors wish to express their gratitude towards Inge Buanes Roth from Det Norske Veritas in Bergen and to Dr. Leonardo Dall'Agnol and Prof. Jose Moura from Faculdade de Ciências e Tecnologia Universidade Nova de Lisboa for their support in the production of the present work.

References

[1] E. Heitz, H.C. Flemming, W. Sand, Microbially Influenced Corrosion of Materials, first ed., W. Sand (Eds.) Springer-Verlag GmbH & Co KG, Berlin, 1996.

[2] I.B. Beech, J. Sunner, Biocorrosion: towards understanding interactions between biofilms and metals, Curr. Opini. in Biotechnol. 15 (2004) 181-186.

[3] M. Madigan, J.M. Martinko, P.V. Dunlap, D.P. Clark, Brock Biology of Microorganisms, twelfth ed., L.Berriman and G. Carlson (Eds.), Pearson-Benjamin Cummings, San Francisco, 2012.

[4] R. Javaherdashti, R.K. Singh Raman, C. Panter, E.V. Pereloma, Microbiologically assisted stress corrosion cracking of carbon steel in mixed and pure cultures of sulfate reducing bacteria, I. Biodeteriorat. & Biodegradat. 58 (2006) 27-35.

[5] H.H. Uhlig and R.W. Revie, Corrosion and Corrosion Control, An Introduction to Corrosion Science Engineering, H.H. Uhlig and R.W. Revie (Eds.), fourth ed., John Wiley and Sons, New York, 2008,

[6] R. Javaherdashti, Microbiologically Influenced Corrosion, An Engineering Insight, Springer, first ed., R. Javaherdashti (Eds.), London, 2008

[7] G. Wranglen, Active sulfides and the pitting corrosion of carbon steels, International Conference on Localized Corrosion, Williamsburg, VA, USA (1971) 462-476.

[8] G. Wranglen, Pitting and sulphide inclusions in steel, Corros. Sci. 4 (1974) 331-349.

[9] R. Avci, B.H. Davis, M.L. Wolfenden, I.B. Beech, K. Lucas, D. Paul, Mechanism of MnS-mediated pit initiation and propagation in carbon steel in an anaerobic sulfidogenic media, Corros. Sci. xxx (2013) xxx – xxx, article in press.

[10] M. V. Biezma, The role of hydrogen in microbiologically influenced corrosion and stress corrosion cracking, Int. J. Hydrogen Energ. 26 (2001) 515-520.

[11] V. Novokshchenov, Brittle Fractures of Prestressed Bridge Steel Exposed to Chloride-Bearing Environments Caused by Corrosion-Generated Hydrogen, Corrosion 6 (50)(1994) 477-485.

[12] R. Javaherdashti, R. K. Singh Raman, C. Panter, and E. V. Pereloma, Role of Microbiological environment in chloride stress corrosion cracking of steels, Mater. Sci. Tech. 21 (9) (2005) 1094-1098.

[13] D. Bond, D. R. Lovley, Electricity production by *Geobacter sulfurreducens* attached to electrodes, Appl. Environ. Microbiol. 69 (2003) 1548-1555.

[14] M. Mehanna, R. Basseguy, M-L. Delia, A. Bergel, *Geobacter sulfurreducens* can protect 304L stainless steel against pitting in conditions of low electron acceptor concentrations, Electrochem. Commun. 12 (2010) 724-728.

[15] B.J. Little, J.S. Lee, Microbiologically Influenced Corrosion, first ed., Hoboken, John Wiley and Sons Inc., New Jersey, USA, 2007.

[16] R.W. Bosch, W.F. Bogaerts, Instantaneous corrosion rate measurement with small-amplitude potential intermodulation techniques, Corrosion 52 (1996) 204-212.

[17] R.W. Bosch, J. Hubrecht, W.F. Bogaerts, B.C. Syrett, Electrochemical frequency modulation: a new electrochemical technique for online corrosion monitoring, Corrosion 57 (2001) 60-70.

[18] L. Han, S. Song, A measurement system based on electrochemical frequency modulation technique for monitoring the early corrosion of mild steel in seawater, Corros. Sci. 50 (2008) 1551-1557

[19] E. Kuş, F. Mansfeld, An evaluation of the electrochemical frequency modulation (EFM) technique, Corros. Sci. 48 (2006) 965-979.

[20] P.I Beese, H. Venzlaff, J. Srinivasan, J. Garrelfs, M. Stratmann, K. J. J. Mayrhofera, Monitoring of anaerobic microbially influenced corrosion via electrochemical frequency modulation, Electrochim. Acta 105 (2013) 239-247.

[21] V.V. Zinkevich, I.B. Beech, Screening of sulfate-reducing bacteria in colonoscopy samples from healthy and colitic human gut mucosa, FEMS Microbiol. Ecology 34 (2000) 147-155.

[22] Deutsche Sammlung von Mokrooganismen und Zellkulturen DSMZ GmbH, Microorganisms, 826. Geobacter medium, 2007.

[23] G. S. Frankel, Electrochemical Techniques in Corrosion: Status, Limitations, and Needs, J. ASTM In. 5 (2) (2008) 1921-1929.

[24] A. Rauf and W.F. Bogaerts, Employing electrochemical frequency modulation for pitting corrosion, Corros. Sci. 52 (2010) 2773-2785.

[25] A. Rauf and E. Mahedi, Comparison Between Electrochemical Noise and Electrochemical Frequency Modulation Measurements during pitting corrosion, J. New Mater. Electrochem. Syst. 15 (2012) 107-112.

[26] F. M. AlAbbas, R. Bhola, J. R. Spear, D. L Olson, B. Mishra, Electrochemical Characterization of Microbiologically Influenced Corrosion on Linepipe Steel Exposed to Facultative Anaerobic *Desulfovibrio sp*., Int. J. Electrochem. Sci. 8 (2013) 859 -871.

[27] C. Cote, PhD thesis, University of Toulouse, France, 2013.

[28] L. Dall'Angol, PhD thesis, Faculdade de Ciências e Tecnologia Universidade Nova de Lisboa, Lisbon, 2013.

[29] H.A. Videla, L.K. Herrera, R.G. Edyvean, An updated overview of SRB influenced corrosion and protection of carbon steel, Corrosion 2005, NACE International, Houston, TX, (2005), Paper no. 05488.

[30] S. Pineau, R. Sabot, L. Quillet, M. Jeannin, C. Caplat, I. Dupont-Morral, P. Refait, Formation of the Fe(II–III) hydroxysulphate green rust during marine corrosion of steel associated to molecular detection of dissimilatory sulphite-reductase, Corros. Sci. 50 (2008) 1099–1111.

[31] M. Stipanicev, PhD thesis, University of Toulouse, France, 2013.

[32] By the ASM committee on Carbon and Alloy Steels, Properties and Selection: Irons and Steels, in: B. P. Bardes (Eds.), Metals Handbook Ninth Edition, Vol. 1, ASM, Ohio, 1978, pp. 253-259.

Chapter VI

General conclusions, recommendations & perspectives

Nowadays, the involvement of microorganisms and their metabolic activity in corrosion and scaling processes is receiving ever more attention from both academic and engineering communities. Their impact on the operational capacity and lifetime of various assets and infrastructures in the Oil and Gas (O&G) industry is undeniably becoming a key element on today's O&G agenda.

In order to establish a "*safe operating window*" that would enable continuous oil and/or gas production at a desirable rate with minimal risks, it is necessary to assess the impact of the different factors that contribute to the development of undesirable events. For Sea-Water Injection Systems (SWIS), the biological component may contribute to the corrosion allowance threshold being reached rapidly and may limit the flow integrity, so that flow might no longer be ensured. Additionally, other elements, such as but not limited to mechanical stress, material impurities, manufacture defects and irregularities, or hydrodynamic drag, may contribute in a negative manner. They interaction with the microbial component should be addressed properly for instance by introducing these factors as variables into models to create computerized tools to minimize the probability of failure and establish a safe operating window.

The main objective of this thesis was to assess the impact of different factors lowering the corrosion resistance of construction material (e.g. carbon steel) and its integrity in the environments that are likely to be affected by microorganisms, such as found within SWIS. In order to achieve this, the study has been divided into three parts:

i) Field simulations

The experimental work provided insights into the anaerobic corrosion of carbon steel and the scaling process. The laboratory conditions simulated some of those parameters found in the field: presence of selected SWIS bacterial populations, electrolytes/media, temperature, flow regime, etc. A closed flow-loop bioreactor design incorporating state-of-art monitoring tool was selected as the most suitable system complying with those requirements.

ii) Model microorganisms

The second approach-involved model Sulfate-Reducing Bacteria (SRB), i.e. *Desulfovibrio* sp., representing the sulfidogenic nature of selected SWIS consortia considered as the main threat in SWIS. Its implication in the corrosion of carbon steel and the scaling process was revealed, together with the capacity of antimicrobial treatment to delay the development of corrosion. Based on "lesson learned" experience on limitations of batch bioreactor set-up a fully equipped circulating loop for electrochemical measurements with retrievable coupons has been designed and built in order to improve decision support through better monitoring of biocorrosion before and after treatment under conditions as close as possible to the field.

iii) Impact of material metallurgy and mechanical stress on Microbiologically Influenced Corrosion (MIC)

This part of the study provided information on the impact of the microbial component on carbon steel subjected to mechanical stress. The study revealed clear connections between the material microstructure and surface deterioration topography in environments loaded with sulfidogenic species.

Until recently, SRB have been considered as being principally responsible for the unexpectedly high levels of corrosion in SWIS. Lately, other microbial groups, different from SRB, have also been suspected of being involved in corrosion. For the work presented here, using Cloning/DGGE-Sequencing analysis for the most abundant 16S rRNA gene sequence identified the relevant population from the microbial consortium acquired in SWIS. The identification revealed sequences similar to those of bacteria from the genera *Clostridium* and *Desulfovibrio.* Moreover, long-term (100 days) laboratory experiments using water from the North Sea as the electrolyte/growth medium, and a SWIS selected consortium as the inoculum, resulted in an enrichment of the bulk medium in several species (planktonic population). For example, bacteria with 16S rRNA gene sequences similar to *Thermovirga lieni, Caminicella sporogenes or Thermoanerobacter brockii* were found in solution. Meanwhile, 16S rRNA gene sequences of the sessile population developed on carbon steel were similar only to those of bacteria from the genera *Clostridium*, e.g. *Caminicella sporogenes,* even though DGGE results indicated the presence of six different species. It is interesting to note that, under mild temperature conditions (25-35℃) in an offshore system, or during laboratory simulations, some thermophilic microorganisms were detected, e.g. *Caminicella sporogenes,* possibly because

these microorganisms should be able to maintain metabolic activity even at lower temperatures, at least theoretically.

Interestingly, most members of the consortia analyzed (both from the selected SWIS consortium and those developed under laboratory simulations) had a sulfidogenic nature, which caused them to be a threat to carbon steel integrity. Given that the majority of these bacteria do not belong to the well-known SRB group, it implies that their role has been severely underestimated in SWIS corrosion studies. Conversely, SRB have been considered as being principally involved in corrosion but their role should be re-evaluated, since this may lead to errors in Risk Based Inspection (RBI) and Integrity Management (IM) due to the occurrence of additional metabolic/biochemical events in the system: acid production, carbon dioxide production, utilization of electron acceptors other than sulfate, etc., resulting in different scaling processes. The probability that this could lead to errors in mitigation decisions taken for this particular SWIS, and that these errors would result in system failure, is nevertheless low since the main objective of retarding sulfide and bisulfide production, and indeed any microbial activity, is achieved with antimicrobial treatment that covers all microbes, regardless of their metabolic activity.

Additionally, it can be concluded that these microbial diversity analyses did not allow detection of the complete diversity of the indigent microbial communities of the SWIS studied. This is not surprising since bacterial diversity decreases when the offshore samples are cultured in selective media. Other factors contributing to the uncertainty are the limitations of the analytical techniques employed here. Moreover, sampling protocols and sample transport can significantly influence the results obtained by environmental ecology methods. The development of new monitoring strategies that incorporate the latest environmental ecology techniques and provide reliable information on microbial diversity and activity should be considered as essential input information for integrity management and operational decision support.

Experimental work performed to assess the impact of sulfidogenic bacterial populations (either a selected SWIS consortium or *Desulfovibrio* sp.) on carbon steel corrosion in saline environments provided an insight into the resistance of the material to corrosion, the evolution of corrosion events, and the biomineralization/mineralization processes on steel surfaces in the studied environments.

The main conclusions for the chosen experimental conditions are that average instantaneous corrosion rates ($1/R_p$) were relatively low, far away from typical values indicating corrosion allowance threshold. Nonetheless, for the carbon steel, *Desulfovibrio* species exhibited more aggressive attack than the selected SWIS consortium, caused a rapid increase in corrosion rates. This was particularly facilitated by the high sulfate concentration in natural seawater (≈2.7 g/kg). This potential electron acceptor, when coupled with organic electron donors, can easily set off anaerobic dissimilatory respiration of *Desulfovibrio* species. The sulfide generated increases corrosion rates, and also induces production of cathodic molecular hydrogen, which may be used as an electron donor too. As experienced during the experimental work presented here, this set of conditions immediately leads to increased corrosion. On the other hand, the selected SWIS consortium mostly comprised thermophilic species, such as those of the *Clostridium* genus, whose metabolic kinetics is partially reduced at lower temperatures. In turn, less corrosive species were generated and a more gradual decrease of material corrosion resistance was obtained. This could significantly affect the operational fitness and lifetime of SWIS. Even though similar processes that resulted in sulfide generation were observed, a decreased thermophilic metabolic activity could prolong the time taken for the installation to reach the corrosion allowance and therefore prolong the system lifetime as compared when SRB activity is concerned.

Concerning the electrochemical surface activity and corrosion attack patterns experienced, the metabolic diversity and lowered activity of the selected sulfidogenic SWIS consortium had local effects on the steel surface. However, localized corrosion attacks were of low intensity, resulting in a final surface deterioration topography characteristic for uniform corrosion. In contrast, the presence of *Desulfovibrio* species led to marked pitting. This confirms that the presence of SRB leads to elevated localized corrosion, as reported by many researchers and found in O&G industry investigations into MIC failure. Hence, the probability of failure due to intensive pitting is higher in SRB environments than in systems operating in the presence of selected sulfidogenic SWIS consortium. Microbial diversity significantly affects the operational lifetime of SWIS and increases the probability of localized failure due to severe pitting. Microbial metabolic activity, which generates ionic species that are aggressive for carbon steel, will affect the boundaries determining safe and stable production conditions and should be one of the parameters taken into consideration when establishing a safe operating window.

A range of acceptable microbial activity should be set for consortium found in particular SWIS, and microbial activity should be kept within the established range by various countermeasures. Precautions should be taken when standard offshore electrochemical techniques (linear polarization resistance, electric resistance) are employed. The active metabolism of *Desulfovibrio* strains results in elevated localized deterioration, which may not be detected by standard offshore electrochemical techniques. Therefore techniques capable of detecting prominent localized activity during operations, such as Electrochemical Noise (EN), or during cleaning, such as ultrasound inspection via intelligent ''pigs'', should be considered and used more often.

Furthermore, the general observation during this research study was that corrosion potentials (E_{corr}) were stable, around -730 mV (*vs.* SCE). The ennoblement effect, often found by researchers working with SRBs, was rarely observed. It occurred only in the environment where there was high *D. Alaskensis* activity. It seems that ennoblement is not a process run exclusively by sulfidogenic bacteria in the environment or microbial surface colonization, as has been shown in batch experiments. Instead, the formation and architecture of corrosion deposits governed by interactions of active ionic species (biogenic sulfides, bisulfides and iron) play a major role in this phenomenon.

Concerning the influence of bacterial activity on the architecture of surface deposits, a dual effect of the microbial components under study was observed.

In our work, where experiments have been conducted under anoxic conditions in North Sea seawater, Fe_xS_y compounds seems to form the first construction block of the corrosion products architecture which stays stable on the metal surface, even after a long time immersion in presence of elevated metabolic activity of SRBs. This layer may also contain GR(SO_4^{2-}) and Fe_3O_4. The dominant component of this inner layer (Fe_xS_y) corresponded to the interaction of biogenic sulfides and bisulfide ions with the ferrous component of carbon steel. However, the process involved for its formation depended on the type of microbial component. *Desulfovibrio* species undeniably reduced sulfate, which is highly abundant in seawater, to sulfide, which finally resulted in the growth of iron sulfides. On the other hand, iron sulfide production in an environment dominated by bacteria of the *Clostridia* genus is a consequence of L-cystin and thiosulfate reduction. Thus, reduced amount of electron captors for bacteria of the *Clostridia* genus (compared to sulfate conc. in seawater*)* may reduce the rate of sulfide production. Inner layers of this architecture could provide anaerobic habitat for SRBs, where they can flourish by utilizing SO_4^{2-} form GR(SO_4^{2-}) as a terminate electron acceptor for their dissimilatory respiration what enables continuous degradation of steel. Then, above this first layer, mixed iron minerals (Fe_3O_4, Fe(III) oxyhydroxides such as α-FeOOH and γ-FeOOH, GR(SO_4^{2-}), $Fe_2(OH)_2CO_3$ and GR(CO_3^{2-})) with addition of calcareous precipitates ($CaCO_3$) are established. This layer possibly could contain small amounts of Fe_xS_y (most likely FeS) too. It is important to note that calcium could also replace iron in sulfated or carbonated green rust. This structural environment, (corrosion product/ bacteria) seems entail localized corrosion process with the presence of pits on the steel surface. In the case of the selected SWIS consortium, carbon dioxide generating bacteria of the *Clostridia* genus*,* coupled with the indigenous bacterial population of North Sea seawater, contributed to the construction of the outer layer while, in the experiments inoculated only with *Desulfovibrio* species, this process was mostly governed by the activity of the indigenous seawater population, which was capable of producing acids and carbon dioxide.

In relation to mitigation strategies, it is possible to conclude that glutaraldehyde-based treatment is effective; it reduces bacterial viability and therefore the microbial activity. However, the treatment has some side-effects: (i) in static batch conditions, high concentration will significantly reduce pH and affect the integrity of the deposits formed and (ii) it will affect electrochemical measurements and make them temporarily unreliable. Therefore, it is recommended that testing of this type of MIC countermeasures should be performed in a flowing system characterized by constant inflow of fresh media. Moreover, when electrochemical techniques are used to monitor corrosion rates, it is necessary to know the possible implications of allied treatments on the reliability of the information acquired. Misinterpreted electrochemical information could lead to wrong decisions being made and the safe operating window not being respected. Moreover, glutaraldehyde-based treatment is effective when targeting planktonic microbial population, whereas, when the purpose is to decrease sessile microbial population, it is not so effective. Microbial population on the steel surface can be protected by corrosion products and cannot be always reached by antimicrobial product, which implies continuous material deterioration in some regions of material surface.

Finally, information on the impact of mechanical stress on the integrity of material, and also the influence of metallurgical properties of the material on corrosion development in the environments that sustain microbial activity should be evaluated before system start-up, i.e. during the design stage incorporating material selection procedures. This should be taken as a general recommendation. Of course, mechanical stress would increase the energy capacity of the regions (grain boundaries, triple points of chemical impurities) that already exhibit higher energies than the steel matrix. Thus, even more microorganisms would be attracted and an increase in corrosion could be expected. However, the impact of regions with higher energies (impurities, grain boundaries, etc.) on later stages of microbial corrosion attack can most likely be dismissed. Elevated bacterial activity coupled with mechanical stress may lead to an increase in material deterioration but the mechanisms are not different from those usually observed for unstressed steel. Moreover, sulfidogenic microbial activity does not seem to lead to a failure mechanism related to stress corrosion cracking (SCC). It is interesting to note that pH in test environments didn't go below 6, even though bacterial sulfidogenic activity was substantial. The observations of pH coupled with recorded bacterial activity suggest that sulfidogenic microbial activity will not lead to embrittlement (SCC mechanism) if pH of environment (even locally) does not change enough to support this embrittlement.

Due to the limited amount of time allocated to this project it was not possible to conduct some additional experiments that would have provided further insight into the problems studied here. Several recommendations, which are presented below, could complement the set of results presented here. This list of recommendations for further research work was drawn up with a view to integrating conclusions needed to solve the present problems of SWIS biocorrosion.

i. It is recommended that more extensive analysis of the SWIS sessile population should be performed so as to determine the complete microbial diversity. This should clarify biogenesis of all carbon steel corrosive species. Special emphasis should be placed on sulfide and carbon dioxide generation.

ii. It is suggested that a series of electrochemical experiments should be conducted with bacteria of *Clostridia* genera at elevated temperatures. This might reveal the impact of their metabolic kinetics on material corrosion resistance.

iii. It is suggested that the experiments should be conducted with a mixed population of bacteria of *Clostridia* and *Desulfovibrio* genera (dominant seed in SWIS) in different ratios and at different temperatures. This might provide valuable information on the dominant corrosive and biomineralization processes.

iv. It is recommended that antimicrobial treatments should be evaluated in flowing systems with mixed microbial populations.

v. It is recommended that the influence of material chemical impurities should be investigated at different stages of microbially initiated localized corrosion.

Appendix 1

Corrosion processes fundamentals: Butler-Volmer, Wagner-Traud and Tafel equations

Corrosion processes fundamentals: Butler-Volmer, Wagner-Traud and Tafel equations

A basic electrochemical reaction can be represented by two simple equations:

$\text{Red} \xrightarrow{i_+} \text{Ox} + ze^-$ and $\text{Ox} \xrightarrow{i_-} \text{Red} - ze^-$

where i_+ and i_- are partial anodic and cathodic currents corresponding to the anodic and cathodic reactions that occur on the same electrode.

Equilibrium state for reversible processes at reversible equilibrium potential is defined by equilibrium between partial reactions:

$i_+ = |i_-| = i_o$ (Eq.1)

where i_o is exchange current density.

The rate of an electrochemical reaction is expressed as a current density:

$i = zF\upsilon$ (Eq. 2)

where υ is the rate of the chemical reaction.

According to Eq. 2, rates of partial anodic and partial cathodic reactions are:

$$\upsilon(\text{cathodic}) = -\frac{\mathrm{d}c(\text{ox})}{\mathrm{d}t} = k_- a_{\text{ox}} \exp\left(-\frac{\Delta G(\text{ox})}{RT}\right) \quad \text{(Eq. 3)}$$

$$\upsilon(\text{anodic}) = -\frac{\mathrm{d}c(\text{red})}{\mathrm{d}t} = k_+ a_{\text{red}} \exp\left(-\frac{\Delta G(\text{red})}{RT}\right) \quad \text{(Eq. 4)}$$

where c(ox) and c(red) (a_{ox} and a_{red}) are concentrations (activities) of oxidized and reduced component, respectively, of the anodic and cathodic partial reactions, while $\Delta G(\text{ox})$ and $\Delta G(\text{red})$ are associated Gibbs activation energies for the reversible reaction, when drop of potential through solid part of double layer is zero.

Correlation (dependence) between partial current densities and potential is possible to get by combining Eq. 1, 3 and 4:

$$i_+ = zFk_+ a_{\text{red}} \exp\left[-\frac{\Delta G(\text{red})-(1-\alpha)zF\Delta\varphi}{RT}\right] \quad \text{(Eq. 5)}$$

$$i_- = zFk_- a_{\text{ox}} \exp\left[-\frac{\Delta G(\text{ox})+\alpha zF\Delta\varphi}{RT}\right] \quad \text{(Eq. 6)}$$

where $i_+ \propto a_{\text{red}}$ and $i_- \propto a_{\text{ox}}$, while α is the factor of symmetry or charge transfer coefficient.

$\alpha_{\text{anodic}} + \alpha_{\text{cathodic}} = 1$ and therefore $\alpha_{\text{cathodic}} = 1 - \alpha_{\text{anodic}}$. When $\alpha_{\text{anodic}} = \alpha_{\text{cathodic}} = \alpha = 0.5$, equilibrium conditions are established and the process is reversible. In contrast, for the irreversible processes $\alpha \neq 0.5$ is valid.

At reversible equilibrium potential, partial current densities can be expressed as exchange current density i_o:

$$i_0 = zFk_+ a_{\text{red}} \exp\left[-\frac{\Delta G(\text{red})-(1-\alpha)zF\Delta\varphi(\text{rev.eq})}{RT}\right] \quad \text{(Eq. 7)}$$

$$i_0 = zFk_- a_{\text{ox}} \exp\left[-\frac{\Delta G(\text{ox})+\alpha zF\Delta\varphi(\text{rev.eq})}{RT}\right] \quad \text{(Eq. 8)}$$

Eq. 5,6, 7 and 8 can be re-written to give:

$$i_+ = i_0 \exp\left\{-\frac{\alpha zF[\Delta\varphi-\Delta\varphi(\text{rev.eq})]}{RT}\right\} \quad \text{(Eq. 9)}$$

$$|i_-| = i_0 \exp\left\{-\frac{(1-\alpha)zF[\Delta\varphi-\Delta\varphi(\text{rev.eq})]}{RT}\right\} \qquad \text{(Eq. 10)}$$

Where $\Delta\varphi - \Delta\varphi(\text{rev.eq})$ is electrochemical overpotential (η) Butler-Volmer equation for reversible processes can be formulated from Eq. 9 and 10

$$i = i_+ + |i_-| = i_0 \left\{\exp\left[\frac{\alpha zF\eta}{RT}\right] - \exp\left[-\frac{(1-\alpha)zF\eta}{RT}\right]\right\} \qquad \text{(Eq. 11)}$$

Butler-Volmer equation is elemental equation in electrochemical kinetics. It defines correlation between overall current flow through external electrical circuit and electrochemical (activation) overpotential. In general, it indicates if the current is anodic or cathodic and it describes reaction that occurs on the same electrode.

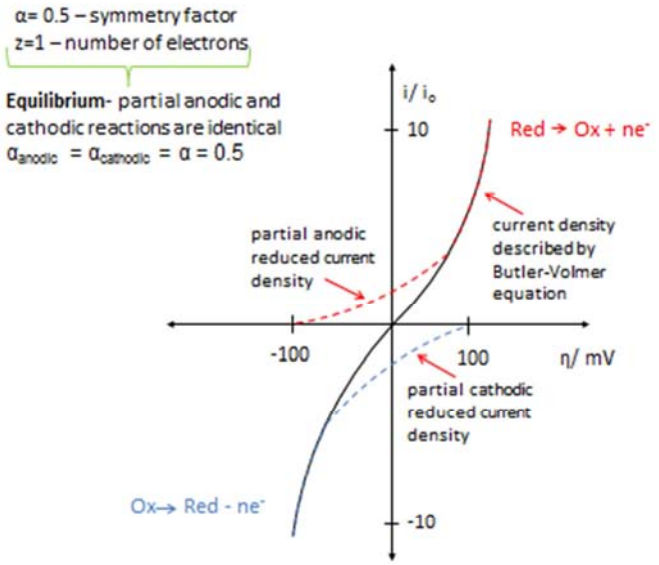

Fig.1. Current vs. potential graph for electrochemical reaction under activation control equilibrium conditions.

When system is out of equilibrium, $\alpha \neq 0.5$ and ΔE is a polarization potential. Eq.11 can be re-written:

$$i = i_+ + |i_-| = i_0 \left\{\exp\left[\frac{\alpha(\text{anodic})zF\Delta E}{RT}\right] - \exp\left[-\frac{\alpha(\text{cathodic})zF\Delta E}{RT}\right]\right\} \qquad \text{(Eq. 12)}$$

Fig. 2 describes polarization of system in negative or positive direction.

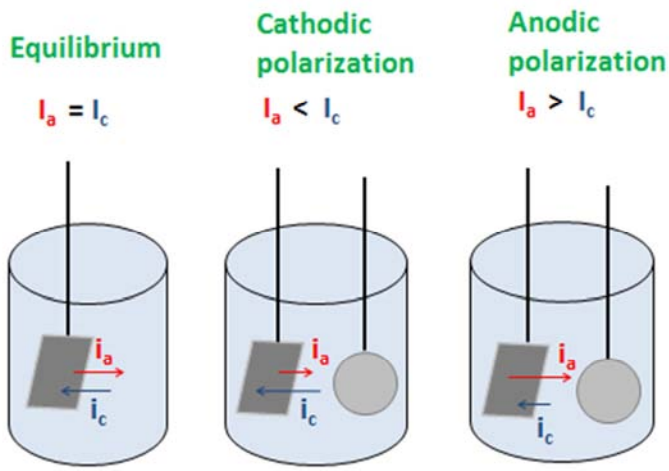

Fig. 2. Electrochemical system in equilibrium and out of equilibrium (polarization).

In equation (12) it is possible to neglect either cathodic or anodic part of equation if anodic or cathodic overpotential is massive, respectively.

In that case Butler-Volmer equation can be written as:

$$i = i_0 \left\{ \exp\left[\frac{\alpha z F (E - E_{\mathrm{eq}})}{RT}\right] - \exp\left[\frac{(1-\alpha) z F (E - E_{\mathrm{eq}})}{RT}\right] \right\} \qquad \text{(Eq. 13)}$$

When corrosion processes are concerned, the interaction between partial reactions is well described with Evans diagrams.

Example: Evans graph below describes corrosion process of a metal in acidic environment.

Process no. 1: the equations concerning the metal

Me ⟶ Me^{+z} + ze^- is the anodic reaction and current is $i_+ = i_{0(Me)} \exp\left[\frac{\alpha(\mathrm{Me}) z F \eta}{RT}\right]$,

Me ⟵ Me^{+z} + ze^- is cathodic reaction and current is

$i_- = i_{0(Me)} \left\{ -\exp\left[-\frac{(1-\alpha(\mathrm{Me})) z F \eta}{RT}\right] \right\}$.

The overall current is: $i_{\mathrm{Me}} = i_+ + |i_-| = i_0 \left\{ \exp\left[\frac{\alpha(\mathrm{Me}) z F \Delta E}{RT}\right] - \exp\left[-\frac{(1-\alpha(\mathrm{Me})) z F \Delta E}{RT}\right] \right\}$

Process no. 2: the equations concerning the acid medium

$H^+ + e^-$ ⟶ $1/2H_2$ is the cathodic reaction and current is:

$i_- = i_{0(H2)} \left\{ -\exp\left[-\frac{(1-\alpha(\mathrm{H_2})) z F \eta}{RT}\right] \right\}$

½ H_2 ⟶ H^+ + e- is the anodic reaction and current is:

$i_+ = i_{0(H2)} \exp\left[\frac{\alpha(\mathrm{H_2}) z F \eta}{RT}\right]$.

The overall resulting current is:

$$i_{\mathrm{H_2}} = i_+ + |i_-| = i_0 \left\{ \exp\left[\frac{\alpha(\mathrm{H_2}) F \Delta E}{RT}\right] - \exp\left[-\frac{(1-\alpha(\mathrm{H_2})) F \Delta E}{RT}\right] \right\}$$

These current are represented in the Evans diagram (Fig. 3). The corrosion process corresponds to the junction of the curves: the anodic part from the metal reaction and the cathodic part from the electrolyte reaction

The overall corrosion process is:

Me + zH^+ ⟶ Me^{+z} = ½ H_2 where

Me ⟶ Me^{+z} + ze^- is partial anodic reaction,

$H^+ + e^-$ ⟶ $1/2H_2$ is partial cathodic reaction.

And the overall resulting corrosion current is:

$i_{\mathrm{corr}} = i_+ + |i_-| = icorr \left\{ \exp\left[\frac{\alpha(\mathrm{Me}) z F \Delta E}{RT}\right] - \exp\left[-\frac{(1-\alpha(\mathrm{H_2})) z F \Delta E}{RT}\right] \right\}$

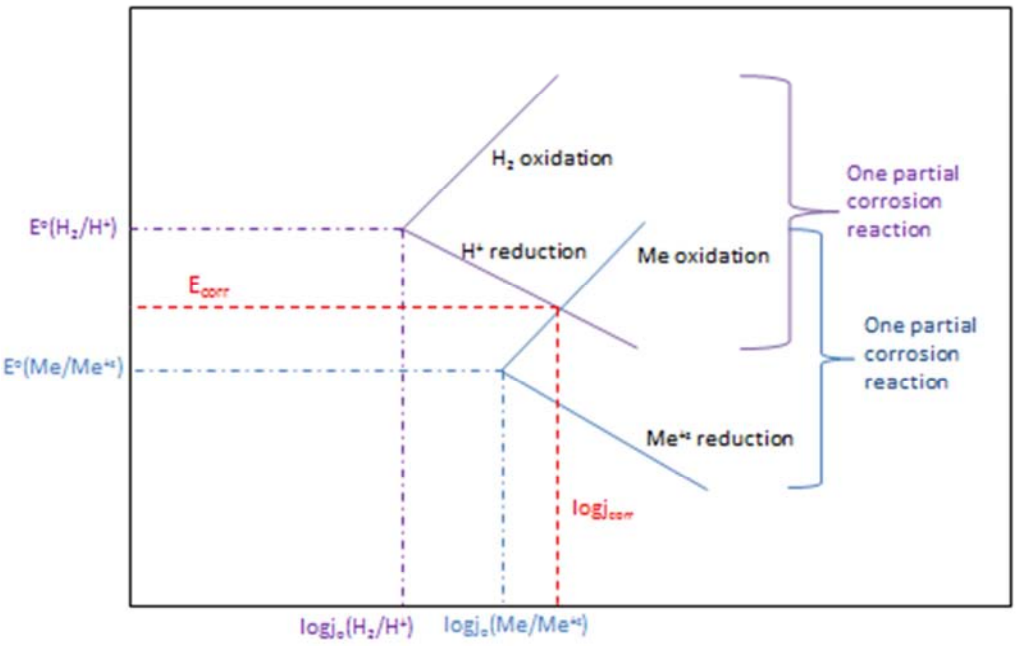

Fig. 3. Evans diagram for corrosion of metal in acid solution.

If anodic and cathodic partial reactions are controlled by charge transfer (activation polarization) than Butler-Volmer reaction can be expressed as:

$$i = i_{\mathrm{corr}} \left\{ \exp\left[\frac{2.3(E-E_{\mathrm{corr}})}{b_{\mathrm{a}}}\right] - \exp\left[-\frac{2.3(E-E_{\mathrm{corr}})}{b_{\mathrm{c}}}\right] \right\} \qquad \text{(Eq. 14)}$$

Eq. 14 is known as a Wagner-Traud equation, where b_a and b_c are known as angles of Tafel slopes, i_{corr} is the corrosion current, E_{corr} is the corrosion potential. Wagner-Traud equation is defined for each particular metal that corrodes in a specific corrosive environment. Furthermore, Wagner-Traud equation expresses dependence of the current density versus the electrode potential at the metal (electrode)/electrolyte interface. It is a non-linear function of corrosion parameters and can serve as a valuable tool for determination of corrosion parameters.

The Wagner-Traud theory of mixed potentials implements the idea that:

1. all corrosion processes can be divided into two or more anodic and cathodic partial reactions
2. during corrosion process there should be no any charge accumulation

According to Wagner and Traud, the sum of all partial anodic and cathodic current densities must be equal to zero at corrosion potential (equilibrium state of corrosion system, reversible processes). This law is called Wagner-Traud principle of additivity of partial processes: $i_{corr} = \Sigma i_a = \Sigma\, |i_c|$, $itotal = \Sigma i_a - \Sigma\, |i_c| = 0$ at $E = E_{corr}$ (Eq. 15)

If the system is not at corrosion potential (electrode is polarized with certain overpotential) then the resulting current is a sum of all anodic and cathodic reactions that take place at metal (electrode)/electrolyte interface:

$j = \Sigma i_a - \Sigma\, |i_c| \neq 0$ at $E = E_{corr} + \Delta E$ (Eq. 16)

In Eq. 16 electrode is polarized for ΔE, whereas E is metal (electrode)/electrolyte interface potential. In general, if $\Delta E > 0$ then anodic polarization is present, while if $\Delta E < 0$ then cathodic polarization takes place in a system.

In Tafel polarization, Wagner-Traud equations are applied for large values of potentials (large polarizations).

For large overpotentials (IηI > 120 mV) the resulting current is equal to partial anodic current or is equal to partial cathodic current ($i = i_+$ or $i = |i_-|$) and irreversible process is taking place. In this situation, the Butler-Volmer equation loses the anodic or cathodic part in dependence of anode and cathode overpotential.

If anode overpotential is huge, then cathodic current can be neglected:

$$i = i_+ = i_0 \exp\left[\frac{\alpha(\text{anodic})zF\eta}{RT}\right] \quad \text{(Eq. 17)} \longrightarrow \ln i_+ = \ln i_0 + \frac{\alpha(\text{anodic})zF\eta}{RT}, \text{ or}$$

$$\log i_+ = \log i_0 + \frac{\alpha(\text{anodic})zF\eta}{2.3RT} \quad \text{(Eq. 18)}$$

If cathode overpotential is massive, then anodic current can be neglected:

$$i = i_- = i_0 \exp\left[-\frac{\alpha(\text{anodic})zF\eta}{RT}\right] \longrightarrow \text{(Eq. 19)} \quad \ln i_- = \ln i_0 - \frac{\alpha(\text{cathodic})zF\eta}{RT}, \text{ or}$$

$$\log i_- = \log i_0 - \frac{\alpha(\text{cathodic})zF\eta}{2.3RT} \quad \text{(Eq. 20)}$$

Eq. 18 and 20 can be reorganized to get logarithmic correlation between partial anodic and partial cathodic current density and overpotential. Those equations are known as Tafel equations.

$$\eta = \frac{2.3RT}{\alpha(\text{anodic})zF} \cdot \log i_0 + \frac{2.3RT}{\alpha(\text{anodic})zF} \cdot \log i_+ \quad \text{(Eq. 21) – Tafel equation for anodic process}$$

$$\eta = \frac{2.3RT}{\alpha(\text{cathodic})zF} \cdot \log i_0 - \frac{2.3RT}{\alpha(\text{cathodic})zF} \cdot \log i_- \quad \text{(Eq. 22) – Tafel equation for cathodic process}$$

Due to the fact that in the case when η >120 mV then $i = i_+$ or $i = |i_-|$, Tafel equation has the shape of a straight line:

$\eta = a_{\text{anodic}} + b_{\text{anodic}} \log i$ (Eq. 23)

$\eta = a_{\text{cathodic}} - b_{\text{cathodic}} \log i$ (Eq. 24)

For Eq. 23 and 24, constants *a* and *b* have a different meaning for anode and cathode reaction.

$a_{\text{anodic}} = \frac{2.3RT}{\alpha(\text{anodic})zF} \cdot \log i_0$ and $\beta_{\text{anodic}} = \frac{2.3RT}{\alpha(\text{anodic})zF}$ for anode reaction.

$a_{\text{cathodic}} = \frac{2.3RT}{\alpha(\text{cathodic})zF} \cdot \log i_0$ and $\beta_{cathodic} = -\frac{2.3RT}{\alpha(\text{cathodic})zF}$ for cathode reaction.

β_{anodic} or β_a and o $\beta_{cathodic}$ r β_c are known as angles of Tafel slopes.

Bibliographic references

A

A. Agrawal, K. Vanbroekhoven, B. Lal, **Diversity of culturable sulfidogenic bacteria in two oil –water separation tanks in the north-eastern oil fields of India**. Anaerobe 16 (2010), 12 - 18.

F.M. AlAbbas, R. Bhola, J. R. Spear, D.L. Olson, B. Mishra, **Electrochemical Characterization of Microbiologically Influenced Corrosion on Linepipe Steel Exposed to Facultative Anaerobic Desulfovibrio sp.**. International Journal of Electrochemical Society 8 (2013), 859 - 871.

K. Alain, P. Pignet, M. Zbinden, M. Quillevere, F. Duchiron, J.-P. Donval, F. Lesongeur, G.Raguenes, P. Crassous, J. Querellou and M.-A. Cambon-Bonavita, **Caminicella sporogenes gen. nov., sp. nov., a novel thermophilic spore-forming bacterium isolated from an East-Pacific Rise hydrothermal vent**. International Journal of Systematic and Evolutionary Microbiology 52 (2002), 1621 - 1628.

H.A.A Al-Mazeedi., R.A. Cottis, **A practical evaluation of electrochemical noise parameters as indicators of corrosion type**. Electrochimica Acta 49 (2004), 2787 - 2794.

I. Annergren, D. Thierry, F. Zou, **Localized electrochemical impedance spectroscopy for studying pitting corrosion on stainless steels**. Journal of Electrochemical Society 144 (1997), 1208 - 1215.

I. Annergren, F. Zou, D. Thierry, **Application of localized electrochemical techniques to study kinetics of initiation and propagation during pit growth**. Electrochimica Acta 44 (1999), 4383 - 4393.

R. Armon, J. Starosvetsky, M. Dancygier, D. Starosvetsky, **Adsorption of Flavobacterium breve and Pseudomonas fluorescens P17 on different metals: electrochemical polarization effect**. Biofouling, 17 (2001), 289 - 301.

C.C. Arteaga, J.P. Calderón, C.F. Campos Sedano, J.A. Rodríguez, **Comparison of Corrosion Resistance of Carbon Steel and Some Stainless Steels Exposed to LiBr-H2O Solution at low Temperatures**. International Journal of Electrochemical Science 7 (2012), 445 - 470.

ASTM G96-90(2001)e1, **Standard Guide for On-Line Monitoring of Corrosion in Plant Equipment** (Electrical and Electrochemical Methods).

R. Avci, B.H. Davis, Z. Suo, K. Lucas, L. Loetterle, I.B. Beech, D. Paul, **Nanopit initiation at MnS nano-inclusions on carbon steel exposed to anaerobic bacterium *D. alkanexedens***. EUROCORR 2012, Paper no. 1630, Istanbul, Turkey (2012).

J.M. Ascenzi**, Handbook of Disinfectants and Antiseptics**. Marcel Dekker, Inc., NY, USA, 1996.

B

R. Baboian, **Corrosion Tests and Standards: Application and Interpretation**, ASTM, Philadelphia, USA, 1995.

A.J. Bard, L. R. Faulkner, **Electrochemical Methods: Fundamentals and Applications**. 2nd edition, John Wiley & Sons, New York, USA, 2000.

E.E. Barr, R. Goodfellow, L.M. Rosenthal, **Noise monitoring at Canada's Simonette Sour Oil Processing Facility**. Corrosion/ 2000, Paper no. 414, NACE International, Huston, TX, USA, 2000.

I.B. Beech, C.C. Gaylarde, **Recent advances in the study of Biocorrosion - An ove**rview. Revista de Microbiologia 30 (1999), 177 - 190.

I.B. Beech, J. Sunner, **Biocorrosion: towards understanding interactions between biofilms and metals**. Current Opinion in Biotechnology 15 (2004), 181 - 186.

I.B. Beech, C.W.S. Cheung, **Interactions of exopolymers produced by sulphate-reducing bacteria with metal ions**. International Biodeterioration and Biodegradation, 35 (1995), 59 - 72.

L.D Bermont-Bouis., M. Janvier, P.A.D. Grimont, I. Dupont, T. Vallaeys, **Both sulfate-reducing bacteria and Enterobacteriaceae take part in marine biocorrosion of carbon steel**. Journal of Applied Microbiology 102 (2007), 161 - 168.

R. Boopathy, L. Daniels, **Effect of pH on Anaerobic Mild Steel Corrosion by Methanogenic Bacteria**. Applied Environmental Microbiology 57 (7) (1991), 2104 - 2108.

S.W. Borenshtein, **Microbiologically influenced corrosion handbook**, Woodhead Publishing Limited, Cambridge, UK, 1994.

C.S. Borsia, L. Yang, **Studies of Microbiologically Influenced Corrosion using Coupled Multielectrode Array Sensor**. Corrosion/ 2003, Paper no. 03575, NACE International, Houston, TX, USA, 2003.

E.J. Bouwer, **Theoretical investigation of particle deposition in biofilm systems**. Water Research 21 (1987), 1489 - 1498.

R.W. Bosch, W.F. Bogaerts, **Instantaneous corrosion rate measurement with small-amplitude potential intermodulation techniques**. Corrosion 52 (3) (1996), 204 - 212.

R.D. Bryant, E.J. Laishley, **The role of hydrogenase in anaerobic biocorrosion**. Canandian Journal of Microbiology 36 (1990), 259 - 264.

K. Bury, **Statistical Distribution in Engineering**, Cambridge University Press, Cambridge, UK, 1999.

C

S.M. Caffrey, H.S. Park, J. Been, P. Gordon, C.W. Sensen, G. Voordouw, **Gene Expression by the Sulfate-Reducing Bacterium Desulfovibrio vulgaris Hildenborough Grown on an Iron Electrode under Cathodic Protection Conditions**. Applied and Environmental Microbiology 74 (8) (2008), 2404 - 2413.

P. Carrera, G. Gabetta, **Biocide options in the offshore industry**. European Federation for Corrosion 19 (1996), 44 - 54.

H. Castaneda, X.D. Benetton, **SRB-biofilm influence in active corrosion sites formed at the steel-electrolyte interface when exposed to artificial seawater conditions**. Corrosion Science 50 (2008) 1169 - 1183.

B.I. Cayford, G.W. Tyson, J. Keller, P.L. Bond, **Microbial community composition of biofilms associated with sewer corrosion**. 6th international conference on Sewer Processes and Networks, 7-10 November 2010, Surfers Paradise, Golden Coast, Australia.

D. Clover, B. Kinsella, B. Pejcic, R. De Marco, **The influence of microstructure on the corrosion rate of various carbon steels**. Journal of Applied Electrochemistry 35 (2005), 139 - 149.

R. Cord-Rustwich, **Microbially Influenced Corrosion of Steel, in Environmental Microbe-Metal Interactions**. Ed.: D.R. Lovely, ASM Press, Washington D.C., USA, 2000.

R. Cord-Rustwich, W. Kleinitz, F. Widdel, **Sulfate-Reducing Bacteria and Their Activities in Oil Production**. Journal of Petroleum Technology 39 (1) (1987), 97 - 106.

J.A. Costello, **Ph.D. thesis**. University of Cape Town, South Africa, 1975.

C. Cote, **Ph.D. thesis**, In Press, Université de Toulouse - MEGEP, France, 2013.

R.A. Cottis, **Interpretation of Electrochemical Noise Data**, Corrosion 3 (57) (2001), 265 - 285.

R.A. Cottis, S. Turgoose, **Electrochemical Impedance and Noise, Corrosion Testing Made Easy Series** Ed.: Barry C. Syrett, NACE International, Houston, USA, 1999.

R.A. Cottis, **Sources of Electrochemical Noise in Corroding Systems**. Russian Journal of Electrochemistry 42 (5) (2007), 497 - 505.

J.-L. Crolet, M.F. Magot, **Non-SRB sulfidogenic bacteria in oilfield production facilities**. Materials and Performance 35 (1996), 60 - 64.

A.B. Cunningham, **Hydrodynamics and solute transport at the fluid-biofilm interface**. In: **Structure and function of Biofilms**, Ed.: W.G. Characklis, P.A. Wilderer, John Wiley, NY, USA, 1989.

D

L. Dall'Agnol, **Ph.D. thesis**, In Press, Faculdade de Ciências e Tecnologia Universidade Nova de Lisboa, Portugal, 2013.

S. Da Silva, R. Basséguy, A. Bergel, **Electrochemical deprotonation of phosphate on stainless steel,** Electrochimica Acta 49 (2004), 4553-4561

L. De Silva Munoz, A. Bergel, R. Basséguy, **Role of the reversible electrochemical deprotonation of phosphate species in anaerobic biocorrosion of steels**. Corrosion Science 49 (2007), 3988-4004.

Deutsche Sammlung von Mokrooganismen und Zellkulturen DSMZ GmbH, Microorganisms, 826. Geobacter medium, 2007.

X. Dominguez-Benetton, H. Castaneda, **SRB-Biofilm Growth and Influence in Corrosion Monitoring by Electrochemical Impedance Spectroscopy**. Corrosion/2005, Paper no. 05486, NACE International, Houston, TX, USA, 2005.

R.M. Donlan, **Biofilms: Microbial Life on Surfaces**. Emerging Infectious Diseases, 8 (9) (2002), 881 - 890.

N.J.E. Dowling, J. Guezennec, M.L. Lemoine, A. Tunlid, D.C. White, **Analysis of carbon steels affected by bacteria using electrochemical impedance and direct current techniques**. Corrosion 44 (12) (1988), 869 - 874.

J. Duana, S. Wua, X. Zhanga, G. Huangb, M. Duc, B. Houa, **Corrosion of carbon steel influenced by anaerobic biofilm in natural seawater**. Electrochimica Acta 54 (2008), 22 - 28.

M. Dubiel, C.H. Hsu, C.C. Chien, F. Mansfeld, D.K. Newman, **Microbial iron respiration can protect steel from corrosion**. Applied and Environmental Microbiology 68 (3) (2002), 1440 - 1445.

K.E. Duncan, L.M. Gieg, V.A. Parisi, R.S. Tanner, S.G. Tringe, J. Bristow and J.M. Suflita, **Biocorrosive thermophilic microbial communities in Alaskan North Slope oil facilities**. Environmental Science and Technology 43 (2009), 7977 - 7984.

B. Dunsmore, T. Whitfield, P.A. Lawson, M.D. Collins, **Corrosion by Sulfate Reducing Bacteria that Utilize Nitrate**. Corrosion/ 2004, Paper no. 04763, NACE International New Orleans, La, USA, 2004.

E

M. Eashwar, S.C. Dexter, **Relation of bacterial settlement patterns to anodic activity on stainless steel weldments**. Corrosion/ 99, Paper no. 00174, NACE International, Houston, TX, USA, 1999.

R. Eckert, T.L. Skovhus, **Using molecular microbiological methods to investigate MIC in oil and gas industry**. Materials Performance 50 (8) (2011), 50 - 54.

D.A. Eden, **Electrochemical Noise - The First Two Octaves**- Corrosion/98, Paper no. 00386, NACE International. Houston, TX, USA, 1998.

D.A. Eden, S.S. Moody, **Control Of Microbially Induced Corrosion in Seawater Injection Systems using Electrochemical Noise Technology**. Corrosion/ 2002, Paper no. 02338, NACE International, Houston, TX, USA, 2002.

L.J. Ehlers, E.J. Bouwer, **RP4 plasmid transfer among species of Pseudomonas in a biofilm reactor**. Water Science Technology 7 (1999), 163 - 171.

E. Erdogan, **Fracture Mechanics**. International Journal of Solids and Structures, 37 (2000), 171 - 183.

G.E. Everitt, E. C. Potter, R.G. Thompson, **Some analytical implications of the interaction between the water and oxygen permeabilities of polymers**. Journal of Chemical Technology and Biotechnology 9 (15) (1965), 398 - 402.

C.W. Extrand, L. Monson, S.I. Moon, **Gas permeation resistance of various grades of perfluoroalkoxy–polytetrafluoroethylene copolymers**. Journal of Applied Polymer Science 1 (111) (2009), 141 - 147.

F

M.J. Feio, V.V. Zinkevich, I.B. Beech, E. Llobet-Brossa , P. Eaton, J. Schmitt, J. Guezennec, **Desulfovibrio alaskensis sp. nov., a sulphate-reducing bacterium from a soured oil reservoir**. International Journal of Systematic and Evolutionary Microbiology 54 (5) (2004), 1747 - 1752.

H.C. Flemming, I.B. Beech, A. Bergel, A. Molica, V. Scotto, W. Sand, **Biofilm Fundamentals**. In: Microbially Influenced Corrosion of Industrial Materials, Brite-Euram III thematic Network N°ERB BRRT-CT98-584, 2000.

M. Fletcher, G.I. Loeb, **Influence of substratum characteristics on the attachment of a marine pseudomonad to solid surfaces**. Applied Environmental Microbiology 37 (1979), 67 - 72.

S.H. Flint, P.J. Bremer, J.D. Brooks**, Biofilms in dairy manufacturing plant description: current concerns and methods of control**. Biofouling 11 (1) (1997), 81 - 97.

T.E. Ford, J.S. Maki, R. Mitchell, **Involvement of bacteria exopolymers in biodeterioration of metal**, In Biodeterioration 7, Ed.: D.R. Houghton, R.N. Smith, H.O.W. Eggins, Elsevier Applied Science, London, UK, 1998, 378-384.

G.S. Frankel, **Electrochemical Techniques in Corrosion: Status, Limitations, and Needs**. Journal of ASTM International 5 (2) (2008), 1 - 27.

M.J. Franklin, D. E.Nivens, J.B. Guckert, D.C. White, **Effect of electrochemical impedance spectroscopy on microbial biofilm cell numbers, viability and activity**. Corrosion 47 (7) (1991), 519 - 522.

G

C. Gabrielli, **Identification of electrochemical processes by frequency response analysis**. Solartron, Technical report number 004/83 (1998).

R. Galvan-Martinez, G. Garcia-Caloca, R. Duran-Romero, R. Torres-Sanchez, J. Mendoza-Flores and J. Genesca, **Comparison of electrochemical techniques during the corrosion of X52 pipeline steel in the presence of sulfate reducing bacteria (SRB)**. Materials and Corrosion 10 (56) (2005), 1 - 8.

A.S. Gordon, S.M. Gerchakov, L.R. Udey, **The effect of polarization on the attachment of marine bacteria to copper and platinum surfaces**. Canadian Journal of Microbiology 27 (1981), 698 - 703.

W.J. Graff, **Introduction to offshore structures**. Ch. 12, Gulf Pub Co., Houston, Texas, USA, 1981.

A.A. Griffith, **The phenomena of ruptures and flow in solids**. Philosophical Transactions of the Royal Society of London, A 221 (1921) 163 - 198.

H

M. Hausner, S. Wuertz., **High rates of conjugation in bacterial biofilms as determined by quantitative in-situ analysis**. Applied Environmental Microbiology 65 (1999), 3710 - 3713.

W.A. Hamilton, Annual Review of Microbiology 39 (1985), 195 - 217.

E. Heitz, H.C. Flemming, W. Sand (Ed.), **Microbially Influenced Corrosion of Materials**, Springer - Verlag GmbH & Co KG, Berlin, Germany, 1996.

M.J. Hernández - Gayosso, G. Zavala Olivares, N. Ruiz Ordaz, C. Juárez Ramirez, R. Garcia Esquivel , A. Padilla Viveros, **Microbial consortium influence upon steel corrosion rate, using polarization resistance and electrochemical noise techniques**. Electrochimica Acta 49 (2004), 4295 - 4301.

L.R. Hilbert, T. Hemmingsen, L.V. Nielsen, S. Richter, **Reliability of Electrochemical Techniques for Determining Corrosion Rates on Carbon Steel in Sulfide Media**. Corrosion 4 (63) (2007), 246 - 358.

C. Huber, Voordouw, **Oil Field Souring Control by Nitrate-Reducing Sulfurospirillum spp. that Outcompete Sulfate-Reducing Bacteria for Organic Electron Donors**. Applied Environmental Microbiology 8 (73) (2007), 2644 - 2652.

F. Huet, N. Monfort Moros, R.P. Nogueir and B. Tribollet, **Electrochemical noise analysis applied to SRB-induced corrosion of carbon steel**. Corrosion/ 2002 Paper no. 02449, NACE International, Houston, TX, USA, 2002.

I

G. Irwin, **Analysis of stresses and strains near the end of a crack traversing a plate**, Journal of Applied Mechanics 24 (1957), 361 - 364.

J

J. Jan-Roblero, J.M. Romero, M. Amaya, S. Le Borgne, **Phylogenetic characterization of a corrosive consortium isolated from a sour gas pipeline**. Applied Microbiology and Biotechnology 64 (2004), 862 – 867.

R. Javaherdashti, **Microbiologically influenced corrosion: an engineering insight**. 6 McElligott Court, Canning Vale, Western Australia 6155, Australia, Springer-Verlag, London Limited, 2008.

X. Jiang, S. Nesic, **Electrochemical Investigation of the Role of Cl^- on Localized CO_2 Corrosion of Mild Steel**. 17th International Corrosion Congress, Paper no. 2414, NACE International, Las Vegas, NV, USA, 2008.

D.A. Jones, N. D. Greene, **Electrochemical Measurement of Low Corrosion Rates**. Corrosion 22 (1969), 367 - 370.

K

R.D. Kane, S. Campbell, **Real-Time Corrosion Monitoring of Steel Influenced by Microbial Activity (SRB) In Simulated Seawater Injection Environments**. Corrosion/ 2004, Paper no. 04579, 2004 NACE International, Houston, TX, USA, 2004.

R.D. Kane, **Control Of Microbially Induced Corrosion In Seawater**. Corrosion/ 2004, Paper no. 04579, NACE International, Houston, TX, USA, 2004.

V.V. Keasler, B. Bennett, R.O. Diaz, P.M. Lindemuth, D. Kasowski,C. Adelizzi, L.Z. Santiago Vazquez, **Identification and Analysis of Biocides Effective Against Sessile Organisms**. SPE International Symposium on Oilfield Chemistry 2009, paper no.121082, SPE, Aberdeen, U.K., 2009.

R.A. King, J. D. A. Miller, **Corrosion by sulphate - reducing bacteria**. Nature 233 (1971), 491 - 492.

R.A. King, J. D. A. Miller, J. S. Smith, **Corrosion of mild steel by iron sulphides**. British Corrosion Journal 8 (1973), 137 - 143.

D.R. Korber, J.R. Lawrence, H.M. Lappin-Scott, J.W. Costerton, **Growth of microorganisms on surfaces, in Microbial biofilms**, Ed.: Lappin-Scott HM, Costerton JW, Cambridge: Cambridge University Press, U.K. 1995.

E. Korenblum, É. Valoni, M. Penna, L. Seldin, **Bacterial diversity in water injection systems of Brazilian offshore oil platforms**. Applied Microbiology and Biotechnology 85 (2010), 791 - 798.

E. Kuş, F. Mansfeld, **An evaluation of the electrochemical frequency modulation (EFM) technique**. Corrosion Science 48 (2006), 965 - 979.

L

J. Larsen, K. Rasmussen, H. Pedersen, K. Sørensen, T. Lundgaard, T. L. Skovhus, **Consortia of MIC Bacteria and Archaea causing Pitting Corrosion in Top Side Oil Production Facilities**. Corrosion/ 2010, Paper no. 10252, NACE International, San Antonio, TX, USA, 2010.

J. Larsen, K. Sørenson, K.Højris, T.L. Skovhus, **Significance of Troublesome Sulfate-Reducing Prokaryotes (SRP) in Oil field Systems**. Corrosion/ 2007, Paper no. 09389, NACE International, Atlanta, GA, USA. 2009.

J.-Y. Leu, C.P. McGovern-Traa, A.J.R. Porter, W.J. Harris, W.A. Hamilton, **Identification and Phylogenetic Analysis of Thermophilic Sulfate-Reducing Bacteria in Oil Field Samples by 16S rDNA Gene Cloning and Sequencing**. Anaerobe 3 (4) (1998), 165 - 174.

D. Li, D.J. Midgley, J.P. Ross, Y. Oytam, G.C.J. Abell, H. Volk, W.A.W. Daud, P. Hendry, **Microbial biodiversity in a Malaysian oil field and a systematic comparison with oil reservoirs worldwide**. Archives of Microbiology 194 (6) (2012), 513 - 23.

G.J. Licina, C.S. Carney, **Monitoring biofilm formation and incipient MIC in real time**. Paper no. 175, Corrosion/ 99, NACE International, Houston, USA, TX, 1999.

J. Lin, J.R. Frank, E.J. St. Martin, D.H. Pope, **Electrochemical noise measurements of sustained microbially influenced pitting corrosion in a laboratory flow loop system**. Paper no. 198, Corrosion/9 9, NACE International, Houston, TX, USA, 1999.

Y.-P.J. Lin. E. J. St. Martin, J.R. Frank, **Monitoring and Mitigation of Sustained Localized Pitting Corrosion**. Submitted to U.S. Department of Energy (DOE), National Petroleum Technology Office, 2003.

B.J. Little, J. S. Lee, **Microbiologically Influenced Corrosion**. Hoboken, John Wiley and Sons Inc., New Jersey, USA, 2007.

B.J. Little, P. Wagner, F. Mansfeld, **An overview of microbiologically influenced corrosion**. Electrochimica Acta, 12 (37) (1992), 2185 - 2194.

M

M. Madigan, J.M. Martinko, P.V. Dunlap, D.P. Clark, **Brock Biology of Microorganisms**, 13th ed. Pearson-Benjamin Cummings, San Francisco, CA, USA, 2012.

M. Magot , G. Ravot , X. Campaignolle , B. Ollivier , B.K. Patel , M.L. Fardeau , P. Thomas , J.L. Crolet, J.L. Garcia, **Dethiosulfovibrio peptidovorans gen. nov., sp. nov., a new anaerobic, slightly halophilic, thiosulfate-reducing bacterium from corroding offshore oil wells**. International Journal of Systematic Bacteriology 47 (1997), 818 - 24.

E. Malard, D. Kervadec, O. Gil, Y. Lefevre, S. Malard, **Interactions between stainless steel and sulphide producing bacteria – Corrosion or carbon steels and low-alloy steels in natural sea water**. Electorchemica Acta, 54 (2008), 8-13.

A.K. Manohar, O. Bretschger, K. H. Nealson, F. Mansfeld, **The use of electrochemical impedance spectroscopy (EIS) in the evaluation of the electrochemical properties of a microbial fuel cell**. Bioelectrochemistry 72 (2) (2008), 149 -1 54.

F. Mansfeld, Z. Sun, Technical Note: **Localization Index Obtained from Electrochemical Noise Analysis**. Corrosion 55 (10) (1999), 915 - 918.

F. Mansfeld, **Electrochemical impedance spectroscopy (EIS) as a new tool for investigating methods of corrosion protection**. Electrochimica Acta 10 (35) (1990), 1533 - 1544.

F. Mansfeld, H. Xiao, Y. Wang, **Evaluation of localized corrosion phenomena with electrochemical impedance spectroscopy (EIS) and electrochemical noise analysis (ANA)**. Materials and Corrosion 1 (46) (1995), 3 - 12.

F. Mansfeld, **Simultaneous Determination of Corrosion Rates and Tafel Slopes from Polarization Resistance Measurements**. Journal of Electrochemical Society 120 (1973), 515 - 525.

F. Mansfeld, **Tafel Slopes and Corrosion Rates from Polarization Resistance Measurements**. Corrosion 29 (1973), 397 – 402.

F. Mansfeld, Z. Sun, C.H. Hsu, **Electrochemical noise analysis (ENA) for active and passive systems in chloride media.** Electrochimica Acta 46 (2001), 3651 - 3664.

K.C. Marshall, **Adhesion and growth of bacteria at surfaces in oligotrophic habitats, Canadian journal of microbiology**. 34 (1998), 503 - 506.

K.C. Marshall, **Adsorption and adhesion processes in microbial growth at interfaces**. Advance Colloid Interface Science, 25 (1) (1986), 59 - 86.

K.C. Marshall, R. Stout, R. Mitchell, **Mechanisms of the initial events in the sorption of marine bacteria to surfaces**. Journal of General Microbiology 68 (1971), 337 - 348.

W. F. McCoy, **Fouling biofilm formation**, In: **Biological Fouling of Industrial Water Systems: A Problem Solving Approach**. Water Micro Associates, Ed.: M.W. Mittelman, G.G. Geesey, San Diego, California, USA, 1987.

R.E. Melchers, R. Jeffrey, **The critical involvement of anaerobic bacterial activity in modeling the corrosion behavior of mild steel in marine environments**. Electrochimica Acta 54, Special Issue BIOCORROSION OF MATERIALS (2008), 80 - 85.

R.E. Melchers, **The relative influence of microbiological and abiotic processes in modelling longer-term marine corrosion of steel**. EUROCORR 2012, Paper no. 1128, Istanbul, Turkey (2012).

H. Men, J. Zhang, L. Zhang, S. Yang, Z. Xu, **Study on SRB induced corrosion based on electrochemical noise analysis and signal processing**. Proceedings of International Conference on Heat Exchanger Fouling and Cleaning/ 2011, Crete Island, Greece, 2011.

J. Messing, R. Crea, P.H. Seeburg, **A system for shotgun DNA sequencing**. Nucleic Acids Research 9 (1981), 309 - 314.

E. Miranda, M. Bethencourt, F.J. Botana, M.J. Cano,J.M. Sanchez-Amaya , A. Corzo , J. Garcı´a de Lomas , M.L. Fardeau, B. Ollivier, **Biocorrosion of carbon steel alloys by an hydrogenotrophic sulfate-reducing bacterium Desulfovibrio capillatus isolated from a Mexican oil field separator**. Corrosion Science 48 (2006), 2417 – 2431.

R.F. Mueller, W.G. Characklis, W.L. Jones, J.T. Sears, **Characterization of initial events in bacterial surface colonization by two Pseudomonas species using image analysis**. Biotechnology and Bioengineering 39 (1992), 1161 - 1170.

G. Muyzer, T. Brinkhoff, U. Nubel, C. Santegoeds, H. Schafer, C. Wawer, **Denaturing gradient gel electrophoresis (DGGE) in microbial ecology**. Molecular Microbial Ecology Manual (1998), 1 - 27.

N

A.Naguib, F. Mansfeld, **Evaluation of microbiologically influenced corrosion inhibition (MICI) with EIS and ENA**. Electorchemica Acta 47 (2002), 2319 - 2333.

M. Nemati, G. Voordouw, **Identification and Characterization of Sulfate-Reducing Bacteria involved in Microbially Influenced Corrosion in Oil Fields**. Paper no. 00125, Corrosion/ 2000, Paper no. 04579, NACE International, Orlando, FL, USA, 2000.

O

C.O. Obuekwe, D.W.S. Westlake, F.D. Cook, J.W. Costerton, **Surface changes in mild steel coupons from the action of corrosion-causing bacteria**. Applied Environmental Microbiology 41(3) (1981), 766 - 774.

M.E. Orazem, B. Tribollet, **Electrochemical impedance spectroscopy**. The electrochemical society series, John Wiley & sons, Inc., publication, USA, 2008.

P

N.R. Pace, **Time for a change**. Nature 441, 289 (2006)

A. Padilla-Viveros, E. Garcia-Ochoa, D. Alazard, **Comparative electrochemical noise study of the corrosion process of carbon steel by the sulfate-reducing bacterium Desulfovibrio alaskensis under nutritionally rich and oligotrophic culture conditions**. Electrochimica Acta 51 (2006), 3841 - 3847.

K. Pedersen, **Factors regulating microbial biofilm Development in a system with slowly flowing seawater**. Applied and Environmental Microbiology 44 (5) (1982), 1196 - 1204.

T.E. Perez, G. Echaniz, and C. Morales, **The Effect of Microstructure on the Kissc* Low Alloy Carbon Steels**. Corrosion/ 98, Paper no. 98120, NACE International San Diego, Ca, USA, 1998.

J.R. Postgate, L.L Campbell, **Classification of Desulfovibrio species, the nonsporulating sulfate-reducing bacteria**. Bacteriology Reviews 30 (4) (1966), 732 - 738.

Princeton Applied Research, 801 South Illinois Avenue, Oak Ridge, TN 37830, USA.

R

A. Rajasekar, B. Anandkumar, S. Maruthamuthu, Y.-P. Ting, P. K. S. M. Rahman, **Characterization of corrosive bacterial consortia isolated from petroleum-product-transporting pipelines**. Applied Microbiology and Biotechnology 85 (2010), 1175 - 1188.

A. Rauf, E. Mahedi, **Comparison Between Electrochemical Noise and Electrochemical Frequency Modulation Measurements during pitting corrosion**. Journal of New Materials for electrochemical systems 15 (2012), 107 - 112

A. Rauf, W.F. Bogaerts, **Employing electrochemical frequency modulation for pitting corrosion**. Corrosion Science 52 (2010) 2773 - 2785.

R.I. Ray, J.S. Lee, B.J. Little, **Iron-Oxidizing Bacteria: A Review of Corrosion Mechanisms in Fresh Water and Marine Environments**. Paper no. 10218, Corrosion/ 2010, San Antonio, TX, USA, 2010.

S.A. Reid, D.A. Eden, **Assessment of Corrosion**, patent no.: US 6.264.824 B1, United States Patent, USA, 2001.

S.A. Reid, G.E.C. Bell, G.L. Edgemon, **The Use of Skewness, Kurtosis and Neural Networks for Determining Corrosion Mechanism from Electrochemical Noise Data**. Corrosion/98, Paper no. 98176, NACE International, San Diego, CA, USA, 1998.

I. Ruseska, J. Robbins, J.W, Costerton, E.S. Lashen, **Biocide testing against corrosion causing oil-field bacteria helps control plugging**. Oil and Gas Journal 80 (1982), 253 - 264.

S

A. Salam Hamdy, M.A. Shoeib, A.G. Sa`eh and Y. Barakat, **The Electrochemical Behavior of Mild Steel in Sulfide Polluted NaCl at Different Velocities**. International Journal of Electrochemical Sciety, 3 (2008) 1142 - 1148.

F.K. Sahrani, Z. Ibrahim, M. Aziz & A. Yahya, **Electrochemical Impedance Spectroscopy and Surface Studies of Steel Corrosion by Sulphate-Reducing Bacteria**. Sains Malaysiana 38 (3) (2009), 359 - 364.

J. Sambrook, E.F. Fritsch, T. Maniatis, **Analysis and cloning of eukaryotic genomic DNA, Molecular cloning: a laboratory manual**. Cold Spring Harbor Laboratory Press, Cold Spring Harbor, NY, USA, 1989.

J.M. Sanchez-Amyay, R.A Cottis, F.J. Botana, **Shot noise and statistical parameters for the estimation of corrosion mechanisms**. Corrosion Science 47 (2005), 3280 - 3299.

P. Sigalevich, M. V. Baev, A. Teske, Y. Cohen, **Sulfate Reduction and Possible Aerobic Metabolism of the Sulfate-Reducing Bacterium *Desulfovibrio oxyclinae* in a Chemostat Coculture with *Marinobacter* sp. Strain MB under Exposure to Increasing Oxygen Concentrations**. Applied Environmental Microbiology, 66 (11) (2000), 5013 - 5018.

R.V. Skold, T. E. Larson, **Measurements of the Instantaneous Corrosion Rate By Means Of Polarization data**. Corrosion 2 (13) (1957), 139 - 142.

J.A. Skvaria, **Physico-chemical model of microbial adhesion**. Journal of the Chemical Society: Faradays transactions 15 (89) (1993), 1913 - 2921.

K. Sørensen, T.L. Skovhus, J. Larsen, **Techniques for Enumerating Microorganisms in Oilfields**. In: **Applied Microbiology and Molecular Biology in Oilfield Systems**, Ed.: C. Whitby, T.L. Skovhus, Springer, New York, USA, 2010.

C.R. Southwell, J.D. Buitman, and C.W. Hummer, Jr., **Influence of marine organisms on the life of structural steel in seawater**. Naval Research Laboratory Washington, D.C., 1974, National Technical Intonation Service, U. S. DEPARTMENT OF COMERCE, 5285 Port Royal Road, Springfield, Va. 22151.

K.R. Sreekumari, K. Nandakumar, Y. Kikuchi, **Bacterial attachment to stainless steel welds: Significance of substratum microstructure**. Biofouling 17 (2001), 303 - 316.

M. Stern, **A Method For Determining Corrosion Rates From Linear Polarization Data**. Corrosion 14 (9) (1958), 440 - 444.

M. Stern, A.L Geary, **Electrochemical Polarization. I. A Theoretical Analysis of the Shape of the Polarization Curves**. Journal of Electrochemical Society 104 (1957), 56 - 63.

P. Stoodley, I. Dodds, J.D. Boyle, H. M. Lappin-Scott, **Influence of hydrodynamics and nutrients on biofilm structure**. Journal of Applied Microbiology Symposium Supplement 85 (28) (1999), 19-28.

P. Stoodley, J.D. Boyle, H.M. Lappin-Scott, **Influence of flow on the structure of bacterial biofilms**. In: **Microbial Biosystems: New Frontiers**, Proceedings of the 8th International Symposium on Microbial Ecology, Ed.: C. R. Bell, R. Colin, M. Brylinsky, P. C. Johnson-Green, Atlantic Canada Society for Microbial Ecology, Canada, 2000, 263 - 269.

H. Stott, T. Richardson, R.A. Cottis, R. Lindsay, S. Lyon, D. Scantlebury, , M. Graham, **Shreir's corrosion 2010: Corrosion in microbial environments**, Volume 2, Elsevier, Oxford, U.K., 2010.

J.M. Suflita, D.F. Aktas, A.L. Oldham, B.M. Perez-Ibarra, K.E. Duncan, **Molecular tools to track bacteria responsible for fuel deterioration and microbiologically influenced corrosion**. Biofouling 28 (9) (2012), 1003 - 1010.

T. Suter, H. Bohni, **Microelectrodes for corrosion studies in microsystem**. Electorchemica Acta, 47 (2001), 191 - 199.

M. Sztyler, J. Doma, I.B. Beech and V.V. Zinkevich, **Oligonucleotide probes for detection of microbial genes implicated in biocorrosion in oil field environments**. EUROCORR 2012, Paper no. 1344, Istanbul, Turkey (2012).

M. Sztyler, **Ph.D. thesis**, In Press, University of Portsmouth, U.K. 2013.

Z. Szklarska-Smialowska, **Effects of environmental factors in pitting, Composition of the electrolyte in pitting corrosion of metals**. NACE International, Houston, TX, Chap. 9, p201 - 219, 1986.

T

W.S. Tait, J. A. Maier, **A Novel Corrosion Test Cell for Predicting the Long-Term Corrosion Behavior of Metal Aerosol Containers**. Corrosion, 10 (42) (1986), 622 - 628.

W. Teughels, N. Van Assche, I. Sliepen, M. Quirynen, **Effect of material characteristics and/or surface topography on biofilm development**. Clinical Oral Implants Research 17 (2006), 68 - 81.

V

M. Vainshtein, H. Hippe, R. M. Kroppenstedtm, **Cellular Fatty Acid Composition of Desulfovibrio Species and Its Use in Classification of Sulfate-reducing Bacteria**. Systematic and Applied Microbiology, 4 (15) (1992): 554 - 566.

Valhall Corrosion Events and Management - Learning Pack, 2009.

J. Verran, R.D. Boyd, **The relationship between substratum surface roughness and microbiological and organic soiling: a review**. Biofouling 17(1) (2001), 59 - 71.

H.A. Videla, L.K. Herrera, **Microbiologically influenced corrosion: looking to the future**. International Microbiology 8 (2005), 169 - 180.

H.A. Videla, L.K. Herrera, R.G. Edyvean, **An updated overview of SRB influenced corrosion and protection of carbon steel**. Corrosion/ 2005, Paper no. 05488, NACE International, Houston, TX, USA, 2005.

H.A. Videla, **Manual of biocorrosion**, CRC Press, Boca Raton, FL, USA, 1996.

H.A. Videla, **Prevention and control of biocorrosion**. International Biodeterioration and Biodegradation 49 (2002), 259 - 270.

H.A. Videla, W.G. Characklis, **Biofouling and microbially influenced corrosion**. International Biodeterioration and Biodegradation 29 (1992), 195 - 212.

C.A.H. Von Wolzogen, I. S. Van der Vlugt, **Graphication of cast iron as an electrochemical process in anaerobic soils**. Water (18) (1934), 14 7 - 165.

W

D. Walsh, **The implications of thermomechanical processing for microbiologically influenced corrosion**. Corrosion/99, Paper no 00188. NACE International, Houston, TX, USA, 1999.

G.W. Walter, **Problems arising in the determination of accurate corrosion rates from polarization resistance measurements**. Corrosion Science 12 (17) (1977), 983 - 993.

J. Wen, K. Zhao, T. Gu, S. Nesic, **Effects of mass transfer and flow conditions on SRB corrosion of mild steel**. Corrosion/ 2006, Paper no. 06666, NACE International, Houston, TX, USA, 2006.

J. Wen, T. Gu, S. Nesic, **Investigation of the effects of fluid flow on SRB biofilm**. Corrosion/ 2007, Paper no. 07516, NACE International, Nashville, TN, USA, 2007.

W.D. Whitney, B.E. Smith , **"titrimetry" The Century Dictionary and Cyclopedia**, The Century co. (1911), 6504 - 6512.

F. Widdel, G. W.Kohring, F.Mayer, **Studies on dissimilatory sulfate-reducing bacteria that decompose fatty acids, III. Characterization of the filamentous gliding Desulfonemalimicola**. Archives of Microbiology 134 (1983), 286 - 294.

K. Wiencek, M. Fletcher, **Effects of substratum wettability and molecular topography on the initial adhesion of bacteria to chemically defined substrata**. Biofouling **11** (4) (1997), 293 - 311.

J. Wingender, T.R. Neu, H.-C. Flemming, **What are bacterial extracellular polymeric substances? In Microbial Extracellular Polymeric Substances: Characterization, Structure and Function**. Ed.: J. Wingender, T. R. NeuH.-C. Flemming, Springer, New York, USA, 1999.

G. Wranglen, **Active sulfides and the pitting corrosion of carbon steels. International Conference on Localized Corrosion**, Williamsburg, Va, U.S.A., (1971), 462 - 476.

G. Wranglen, **Pitting and sulphide inclusions in steel**. Corrosion Science 4 (1974), 331 - 349.

Y

C.K. Yu, X.L. Chong, H.H.P. Fang, **Anaerobic electrochemical corrosion of mild steel in the presence of extracellular polymeric substances produced by a culture enriched in sulfate-reducing bacteria**. Environmental Science and Technology, 36 (2002), 1720 - 1727.

H.A. Yuehuei, R.J. Friedman, **Handbook of Bacterial Adhesion: Principles, Methods, and Applications**. Humana Press, Totowa, NJ, USA, 2000.

Z

V.V. Zinkevich, I.B. Beech, **Screening of sulfate-reducing bacteria in colonoscopy samples from healthy and colitic human gut mucosa**. FEMS microbiology ecology 34 (2000), 147 - 155.